Fatigue Flaw Growth Behavior
in Stiffened and Unstiffened Panels
Loaded in Biaxial Tension

February 1973

MARTIN MARIETTA

FATIGUE FLAW GROWTH BEHAVIOR
IN STIFFENED AND UNSTIFFENED PANELS
LOADED IN BIAXIAL TENSION

February 1973

Prepared by

E. J. Beck
Program Manager

(

NOTICE
_____

ii

FOREWORD

The work described in this report was performed by Martin Marietta
Corporation, under Contract NAS9-12439 for the Manned Spacecraft
Center of the National Aeronautics and Space Administration. This
work was administered under the technical direction of the Struc-
tures and Mechanics Division, with Mr. Royce Forman acting as
Project Manager.

Mr. Emory J. Beck served as Martin Marietta Program Manager. Mr.
Robert D. Keys was responsible for the experimental effort; Dr.
A. A. Holston for the theoretical stress analysis. The author
gratefully acknowledges the assistance of the following colleagues:
J. LeBeau, C. Fiftal, and C. Weld.

This report is submitted in compliance with the data requirements
list (DRL), line item 2, Report, Final of Exhibit A, T-748 of
the Contract.

ABSTRACT _____

The primary purpose of this contract was to determine the effect
of biaxial loading on the flaw growth rate of 2219-T87 aluminum
alloy that would be typical of Space Shuttle cryogenic tankage
design. In support of this general objective, the stress distri-
bution and stress concentration factors for several integrally
stiffened panels under various loading conditions were obtained.
The flaw growth behavior of both stiffened and unstiffened panels
under biaxial loading conditions was determined. The effect of
a complex stress state is studied by introducing flaws in fillet
areas of biaxially loaded stiffened panels.

iv

CONTENTS

Table _____

I. INTRODUCTION _____

The principal goal of this work was to determine the effect of biaxial loading and stress gradients on the fatigue crack growth behavior of 2219-T87 aluminum alloy panels that are typical of Space Shuttle tank hardware. In order to satisfy this goal, it was necessary to perform experimental and theoretical stress analyses in addition to the experimental fatigue flaw growth behavior work. The resulting total program, therefore, consisted of the following two-part activity:

1) Stress Analysis (theoretical and analytical)

2) Fatigue Flaw Growth Behavior (uniaxial and biaxial)

To satisfy the program objectives, the following specific tasks were performed:

1) Stress Analysis

- Theoretical stress analysis of integrally stiffened panels using two-dimensional and three-dimensional finite element techniques;

- Experimental stress analysis of stiffened panels using various loading conditions using photoelastic and strain gage techniques;

- Experimental stress analysis of unstiffened, welded panels to determine welding residual stresses.

2) Fatigue Flaw Growth Behavior

- Uniaxial flaw growth tests conducted to provide baseline data;

- Unstiffened and stiffened biaxially loaded panels tested to provide flaw growth data;

- Unstiffened, welded panels tested to provide flaw growth data under biaxial loading;

- Comparison of the data with other data using currently available flaw propagation analyses.

Phase B design studies for the Space Shuttle cryogenic tanks indicate that the tank walls will have integrally milled stiffener construction for both the longitudinal stiffeners and the circumferential ring stiffeners. The stiffener sizing is based on criteria that the tank walls will not buckle at a given percent of the limit design compression load. The tank walls will also be subjected to tension loads at particular times during a mission, and the so called "smeared thickness" of the tank walls will be based on criteria for carrying limit design tensile loads.

Extensive experience has been obtained on the design and testing of large integrally stiffened tanks from the Saturn and other booster programs; however, these tanks were basically designed and tested for carrying one-time launch loads and pressures. The fatigue behavior for these types of tanks resulting from multiple launches and aircraft-type gust and maneuver loads has not been adequately investigated. Even though integrally stiffened tanks may be reliably made for withstanding one-time ultimate loads or burst pressures, the ability to carry thousands of fatigue cycles at lower loads and pressures cannot now be confidently predicted.

Fatigue crack propagation testing is the most informative method for understanding the effects of different fatigue environments on structural designs. Extensive testing has been performed on small tensile loaded specimens to obtain basic fatigue crack propagation data for 2219-T87 aluminum alloy. Ability to directly use this data, however, for analyzing integrally stiffened tank walls with complex stress distributions has not been investigated.

As a result, the empirical approach used in this work was deemed best to permit a good engineering assessment of the capability of existing analytical methods for prediction of flaw growth behavior. The results of this program should aid in understanding the stress distribution in integrally stiffened tankage wall designs and the fatigue crack growth behavior in these designs. In addition, the stress analysis and crack propagation results should assist in improving the crack propagation analysis methods, and possibly uncover any significant fatigue or crack propagation problems that may exist in preliminary Shuttle tankage designs.

I-2

II. PROGRAM PLAN

The nature of the work performed under each program task is discussed in this chapter.

A. STRESS ANALYSIS

Theoretical – The initial theoretical stress analysis activity was used to provide assistance in panel and loading technique design. To predict the stress distribution throughout the panel and the deflections of the loading straps and grip plates, a finite element computer program was used.

Following finalization of the biaxial panel design, a detailed two-dimensional stress analysis was performed to provide displacements and rotations. The results of the two-dimensional analysis were used as inputs for the more refined and precise three-dimensional analysis conducted on two areas of the central bay in the vicinity of the stiffeners.

Experimental – Six stiffened panels (varying skin and stiffener thickness combinations) were subject to photoelastic stress analysis by Photolastic, Inc. This work performed at our facility included analyses at two stress levels and three loading conditions (biaxial ratios).

Following completion of the photoelastic evaluation, coatings were removed and sites for strain gage location were selected after a careful review of the photoelastic results. The strain gage evaluation was performed for two of the stiffened panels.

Two large biaxial panels containing a long weld through the center section were subjected to stress analysis using the technique of strain gaging and selective metal removal to relieve residual stresses.

B.   FATIGUE FLAW GROWTH BEHAVIOR

Uniaxial Testing - Uniaxially loaded surface flaw specimens were evaluated to provide information for cycles to initiate flaw extension from an EDM starter notch, and baseline flaw extension data suitable for comparison with other work. Twenty-seven parent metal and twelve welded specimens were used for this work.

Biaxial Testing (Unstiffened Panels) - Cyclic flaw testing was performed for twenty-two panels under balanced biaxial loading. Each specimen, containing four defects was tested with various crack shapes, depths, and stress levels.

Biaxial Testing (Stiffened Panels) - Cyclic flaw testing was performed for six panels under balanced biaxial loading. Each specimen contained ten defects placed in various locations selected on the basis of experimental stress analysis data.

Biaxial Testing (Welded Panels) - Cyclic flaw testing of weld panels was conducted at a 2:1 stress ratio to simulate the cylindrical portion of a propellant tank. Four panels, each containing four defects located in the heat affected zone and weld centerline, were evaluated.

III.   MATERIAL AND PROCESSING _____

Aluminum alloy sheet and plate (2219-T87) used in this program
were obtained in the fully heat-treated condition. Four thick-
nesses [1/8, 1/4, 1/2, and 1 in. (3.2, 6.4, 13, and 25 mm)] of
stock were used; material for each gage was from a single heat.

Parent metal panels were machined by mechanical and/or chemical
milling. The unstiffened biaxial panels were fabricated from
1/2-in. (13-mm) plate by mechanically milling the reduced section
to 1/4-in. (6.4-mm) thickness, and then chemically milling to
a final thickness of 1/16 or 1/8-in. (1.6 or 3.2-mm). This two-
step operation was required because of difficulties encountered
during mechanical milling. As material was removed, stiffness
decreased and the remaining material deflected sufficiently to
cause irregular cutting and loss of dimensional control.

Stiffened panels (pockets and grip holes) were mechanically milled
using numerically controlled equipment. Starting stock was 1-in.
(25-mm) thick.

Weld panels for biaxial testing were prepared from 1/2-in. (13-mm)
stock. Material was chemically milled to 1/4 in. (6.4 mm), welded,
and then mechanically milled to 1/8 in. (3.2 mm). The resulting
specimen was identical in appearance to parent metal unstiffened
panels, having a 1/2-in. (13-mm) thick border for gripping and a
central reduced thickness section measuring 1/8 in. (3.2 mm), but
contained a weld extending across the complete width of the speci-
men.

Panels were prepared for welding in the following manner. First,
the aluminum was degreased in trichlorethylene vapor, soaked in
an alkaline solution for 15 minutes, and deoxidized for 10 minutes.
Then the edges were filed and after the corners were broken slight-
ly, the region next to the edge was cleaned with a wire brush.
Welding was performed longitudinal to the grain direction using
a direct-current, straight polarity power source and automatic
equipment. A two-pass butt weld was used. Both passes were made
from the same side, 2319 filler rod was used for the second pass.
The weld schedule used for this work, considered typical for pro-
duction welding at our facility, is given in Table III-1.

Table III-1 Weld Schedule, 2219-T87

Welding Parameter	1st Pass	2nd Pass
Voltage, V	11.5	12.5
Current, amp	175	150
Torch speed, in./min	11	11
Wire feed, in./min	0	40
Helium gas coverage, cfh	70	70

Uniaxial test coupons were machined from 1/8-in. (3.2-mm) sheet stock for parent metal. For welded coupons, 1/4-in. (6.4-mm) stock was welded using the same schedule given above; specimens were then mechanically milled to 1/8 in. (3.2 mm) after welding.

IV. DESIGN AND STRESS ANALYSIS

The total effort associated with design, theoretical, and experimental stress analysis of the biaxial panels is described in this chapter. The design of the unstiffened biaxial panel was performed with the aid of finite element analytical techniques to establish uniformity of loading and to identify possible areas where malfunction might be anticipated during cyclic loading. Design and analysis of the attendent fixturing required to apply uniform loads was also included in this effort. The stiffened panel design was established as identical to the unstiffened design except for the incorporation of typical rib stiffening members. The preceding portion of this work is described in Section A of this chapter. The detailed two- and three-dimensional stress analyses of the stiffened panel is described in Section B. Experimental stress analyses using photoelastic stress analysis and strain gage analysis are given in Section C. The experimental analysis to determine residual stresses in a welded biaxial panel is also described in this section. A comparison of the analytical and experimental stress analyses is presented in Section D.

A. DESIGN

The biaxial specimen size was selected to provide stiffened regions simulating those used in actual construction. In order to provide a panel containing a rib-stiffened pocket of approximately 8 in. square (203 mm square) and introduce loads in a uniform manner, an overall size of 28 in. square (711 mm square) was selected.

The specimen was designed for stressing to 45.0 ksi (311 MN/m^2) which represents a maximum load of 157.5 kips (705 kN). Actually, the load required was assumed to be closer to 200 kips (896 kN) when the stiffened loading region is considered. Based on this analysis, the biaxial testing machine was designed to ensure 200 kips (896 kN) load capability.

Design and Analysis of Unstiffened Panel

The panel was analyzed with our in-house finite-element computer program. The panel and grip plate were modeled in the computer program as flat membranes of different materials and different thicknesses, and the load straps were modeled as axial members. The results of these computer runs are discussed in detail in the following paragraphs.

The basic problem is how to reduce the nonuniform stresses or strains in the panel's center region which arise from three conditions.

First, the grip plate experiences a slight amount of bending causing less load, and therefore less strain, along the sides than in the center of the panel. Second, if the outer two inches of the panel are thickened, the resulting strain in this region will be even further reduced in the direction parallel to the edge of the panel, due to the added stiffness. The third contribution to the nonuniform stresses across the center of the panel is that the loads are applied at points around the panel and the stresses along the panel edge are not uniform or biaxial. This condition turns out to produce the least significant effect upon the center region because the stresses redistribute themselves very quickly within a few inches of the panel edge. However, since the local stresses in this outer region are higher than the stresses in the center of the panel, fatigue loading could cause this area to fail prematurely.

There are three areas in the panel border region that must be watched for critical stresses: (1) the corner where the thin inner section meets the thick border sections, an area of high shear stress; (2) the bearing stress where the greatest load is applied by the loading straps; and (3) the concentrated tensile stress around the hole at the midspan of any one side of the panel. These three stresses have been studied in each model to be discussed.

A detailed description of the six models evaluated to select a final configuration is presented in the following paragraphs.

One-fourth of the test fixture and panel was modeled assuming symmetry about two axes. This was done to allow a finer element breakdown. Since the actual test fixture is basically symmetrical, this assumption is valid.

The first model considered, shown in Figure IV-1a, consisted of a panel of constant thickness with no stiffened section around the edge of the panel. The load on the straps varied from the average load by +1.72% at the center of the panel to -3.45% at the outer ends of the panel, a total of 5% variation. The stresses along the symmetrical center line of the panel in the direction perpendicular to the center line varied from the average stress by +0.28% at the center to -0.2% at the edge of the panel, a total variation of 0.5%. This would be an ideal panel configuration if it were not for bearing stresses.

t =0.060

4 - A

t =0.125/0.500

4 - B

t =0.125/0.500

4 - C

t =0.125/0.500

4 - D

t =0.120/0.500

4 - E

t =0.125/0.500
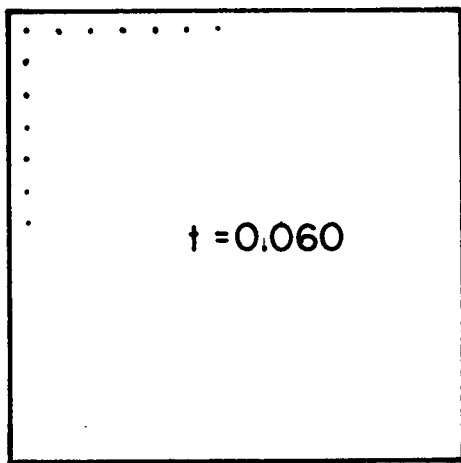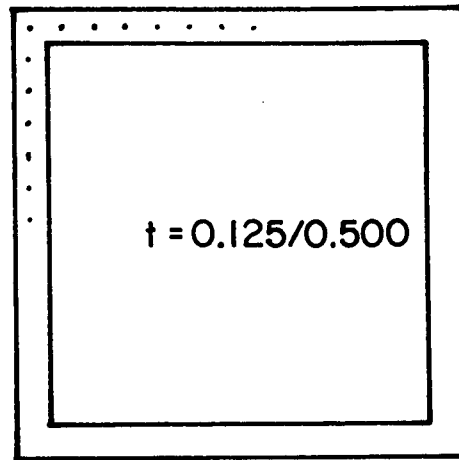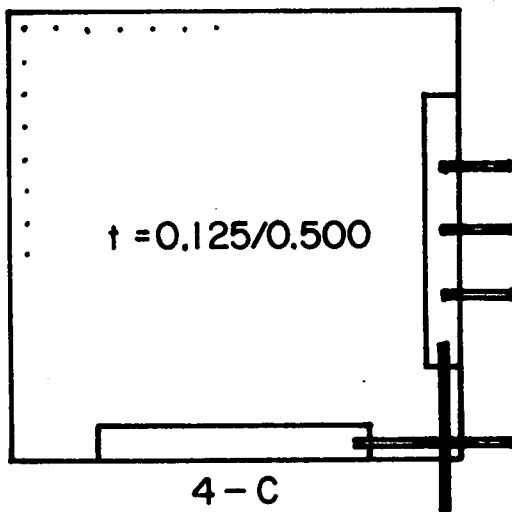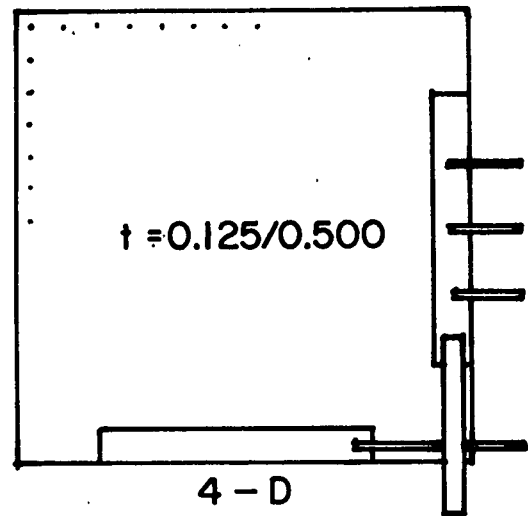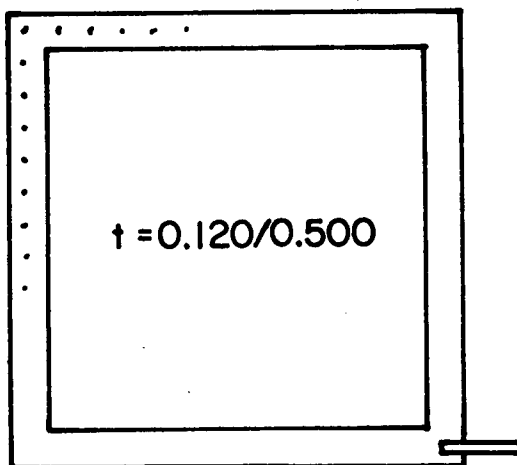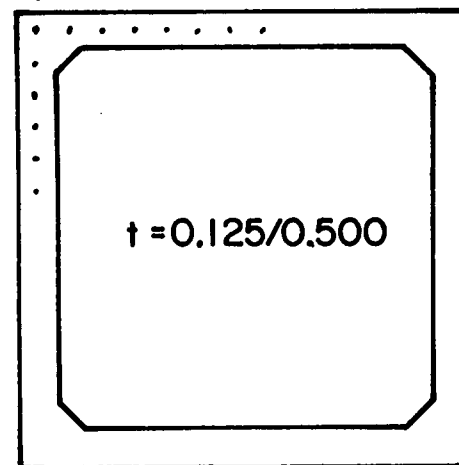
4 - F

Figure IV-1 Computerized Models, Schematic

The second panel configuration, Figure IV-1b, had a thickened border section around the edge like a picture frame. This was designed to provide sufficient bearing strength and tensile strength between holes, as discussed earlier in this report. The resulting load variance was +9.48% at the outer end of the panel and -5.36% at the center of the panel, a total of 15% due to the added stiffness of the picture frame. The stress variation was +3.0% at the center of the panel to -5.2% at four inches from the edge of the panel. This low stress near the edge was caused by the added stiffness of the thicker section along the edge of the panel. The peak stress in the corner of the thin section was 53.5 ksi (369 MN/m^2). The peak bearing stress was 54.5 ksi (375 MN/m^2) and the concentrated tensile stress was 60.0 ksi (413 MN/m^2), using a stress concentration factor of 1.67. The stress would be more uniform across the center line of symmetry if we could increase the loads at the ends of the panel into the stiffened edges. We are limited in the extent to which this may be done by peak bearing stresses that are already high, and concentrated tensile stresses being high at the edge of the attchment pin holes. It is desirable, however, to have these end loads as large as possible within those restraints to have more uniform stresses in the center of the panel. This idea tends to discredit the premise that the strap loads should be as nearly constant as possible to achieve more constant stresses in the center region.

The third and fourth panel configurations represented an attempt to use straps bonded along the edges to take out the bearing load (Fig. IV-1c and 1d). These straps were modeled as thickened elements along the edges of the panel. The thickened sections were not connected at the corners. On Model No. 3 the loading straps were all of the same thickness. The computer run predicted a stress of 78.3 ksi (540 MN/m^2) at the corner of the panel when the corresponding stress at the center of the panel was 42.0 ksi (289 MN/m^2). In an effort to reduce this stress, the thickness of the end loading straps in Model No. 4 were increased by three times the thickness of the other loading straps. This was done in Model No. 4. The peak stress in the corner was reduced to 51.3 ksi (353 MN/m^2). However, the bearing stress was increased from 49.1 ksi (338 MN/m^2) to 99.0 ksi (682 MN/m^2) for above desired levels.

Since the bearing stresses were so critical and it was desirable to dump a larger percentage of the load into the edges of the panel, we tried a thinner central panel section. Along with this change, the integral picture frame border was used to reduce high corner shear stresses. This was accomplished in Model No. 5

(Fig. IV-1e). The central section of the panel was 0.120 in.
(3.0 mm) thick, and constant thickness loading straps were used.
The resulting load variance was -41% at the outer edge to -10%
at the center. The stress variance was +2.9% at the center to
-3.1% at four inches from the outer edge. The peak corner stress
was 52.7 ksi (363 MN/m^2), the peak bearing stress was 70.2 ksi
(483 MN/m^2), and the peak concentrated tensile stress was 65.1 ksi
(448 MN/m^2). Comparing these stresses to Model No. 2 shows that
we have lowered the stress in the corner of the panel by 2.0 ksi
(13.8 MN/m^2), but we have raised the bearing stress by 16.0 ksi
(110 MN/m^2) and the peak tensile stress at the edge of the attach-
ment holes by 5.0 ksi (34 MN/m^2). Using a thinner central section
appears not to be the correct approach.

The final run, Model No. 6, had a 0.125-in. (3.2-mm) thick central
section with 0.5-in. (13-mm) thick x 2-in. (51-mm) border around
the edge (Fig. IV-1f). The corner was stiffened additionally with
a thickened triangualar element 1 x 1 in. (25 x 25 mm). The load-
ing straps were of constant thickness. The resulting loading
point variance $(L/L \text{ avg}^{-1})^{100}$ was +14.5% at the ends of the panel
to -8.1% at the middle of the panel. The stress variance $(\sigma/\sigma \text{avg}^{-1})$
^{100} was +5.5% at the center of the panel to -3.4% at four inches
(102 mm) from the edge of the panel.

The peak stress in the corner of the panel was 45.9 ksi (316 MN/m^2)
and the peak concentrated tensile stress was 60.8 ksi (418 MN/m^2),
using a stress concentration factor of 1.67. These stress values
are achieved at a central panel stress of approximately 40 ksi
(275 MN/m^2); balanced biaxial, and are shown in detail in Figure
IV-2. Although this final run had a high concentrated tensile
stress, it is very localized and yielding will reduce its value
after the first cycle.

There is a tradeoff between the three critical stresses. If the
bearing stress is increased at the corner of the panel to reduce
the shear stress in the adjacent thinner corner section, the
tensile stress around the hole increases. This tensile stress
around the hole increases if the bearing loads are left alone,
but the corner of the panel is stiffened to reduce the peak shear
stress. The increased tensile stress is due to a larger portion
of the bearing loads near the corner of the panel being carried
by shear through the stiffened corner section into the thickened
panel edge. The best choice seems to be the compromise obtained
in Model No. 6. The three critical stresses--bearing stress at
the loading holes, net-section tensile stress between holes, and
the peak stress at the panel corner, appear to be balanced so

168.0 kips

84.0 kips

11.0   11.0   11.1   11.4   12.2   13.6   13.7

1/2-in. Thick Panel

5.8
-4.2

24.4 12.7
11.7 -3.3

13.7

36.4 27.4 15.8
21.2   8.8 -2.0

1/8-in. Thick Panel

45.1 45.9 26.4 17.5
30.1 29.7 12.4 -2.3

13.6

44.8 45.2 45.7 27.0 21.6
32.0 31.8 30.9   8.8 -1.1

44.1   45.6 25.3 22.6
34.4   31.9 11.0 -0.7

12.2

43.3   45.0
35.8   33.6

42.6   44.7
36.9   34.5

11.4

41.9   44.3
37.9   35.7

41.4   44.2
38.5   36.2

11.1

40.8   43.8 27.6 24.6
40.8   36.7 10.4 -0.3

40.4   43.8 27.6 24.8
40.4   37.0 10.6 -0.3

11.0

40.2   43.7 27.8 24.8
40.2   37.2 10.5 -0.3

2 in.

40.0 40.1 40.2   40.7   41.5   42.4   43.3 43.7 27.8 24.8
40.0 39.9 39.8   39.3   38.6   38.0   37.4 37.3 10.5 -0.3

11.0

14 in.

2 in.

14 in.

Figure IV-2   Principal Stress and Load Distribution in Unstiffened 0.125-in.
(3.2 mm) Thick Biaxial Quarter-Panel from Finite Element
Analysis

that fatigue failure is equally possible at any one of the three locations. Detailed discussion of the situation at each of these three locations is given in the following paragraphs.

The final design for the unstiffened biaxial panel is given in Figures IV-3 and IV-4.

Design and Analysis of Loading Fixtures

The loading hardware consists of a plate, straps, and pins.

Loading Plate - The loading plate provides a load path from the single pin joint that attaches to the load train to the 14 pin joints that attach the loading straps to the panel. The loading plate design is shown in Figure IV-5. The A36 steel plate had the same hole configuration as the panel and was designed against bearing yield and net section yield using the fatigue endurance limit.

Loading Straps - The 4340 steel loading strap design is shown in Figure IV-6. As before, bearing stresses and net section stresses were considered.

Loading Pins - Grade 5 steel bolts were used for pins in order to meet the strength requirement for carrying a maximum antici- pated fatigue load of 13.7 kips (61 kN).

Design of Stiffened Panel

The stiffened panel is identical with the unstiffened panel except for the introduction of the rib stiffener members. The stiffener dimensions were arbitrarily selected to be typical of hardware. Various combinations of membrane and rib thicknesses were used for the six panels. Three rib thicknesses [0.060, 0.125 and 0.250 in. (1.5, 3.2, and 6.4 mm)], and two membrane thicknesses [0.060 and 0.125 in. (1.5 and 3.2 mm)] were used. Figures IV-7 and IV-8 give the specifications for the stiffened panel configurations.

B.   THEORETICAL STRESS ANALYSIS

A finite element stress analysis of the stiffened panel was per- formed to provide calculated stresses for comparison with the test results and to predict the critical locations for flaws.

B .012

-B-

See Typical Panel Quadrant Detail, Sheet 2

26.000 Ref

28.00

Remove Burrs and Break All Edges.

26.000 Ref

28.00

-C-

SECTION

C .012

-001
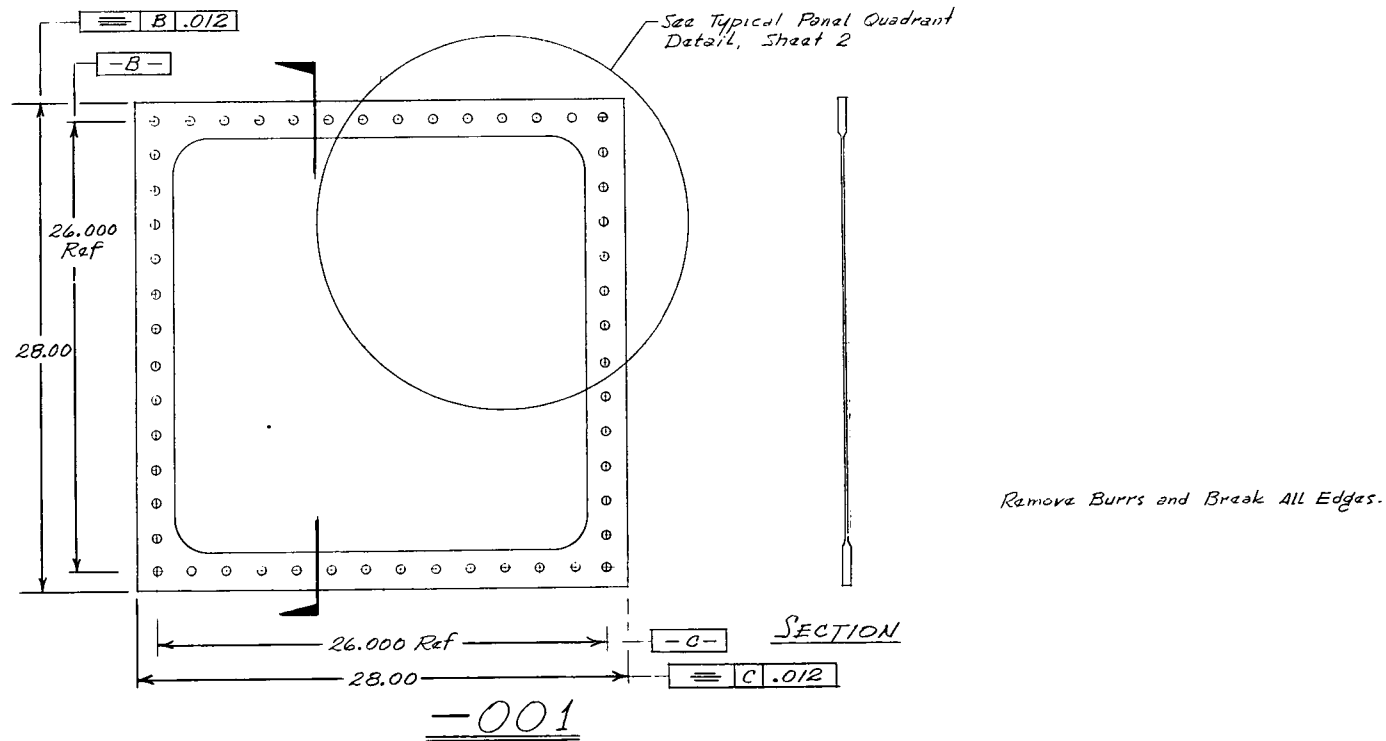
						-001		Panel			Alum Alloy R.	2219-T87			
	QUANTITY/DASH NO.			PART NO.	ZONE	REQ SYM	DESCRIPTION		STOCK SIZE		MATERIAL OR VENDOR	ISSUE COND	MATERIAL SPECIFICATION	FINISH OR MFR CODE	CHG
ODD DASH NO SHOWN			EVEN DASH NO OPP					LIST OF MATERIAL							

Figure IV-3   Unstiffened Biaxial Fatigue Panel (Sheet 1) Specifications

See Other End View for Dims.

13.000 ±.002

11.000 ±.005

9.000 ±.005

7.000 ±.005

5.000 ±.005

3.000 ±.005

1.000 ±.005

0.500 +.005/-.000 Dia
Holes, 52 Places.

-A-

0.50 Stock Thickness

2.00 R

90° ±0.2°

-0.25 R. Typ.
-Avoid Undercutting
Gage Section at Fillet
Tangency Points

0.125 ±.005
Gage
Thickness

13.000 ±.002

11.000 ±.005

9.000 ±.005

11.75

7.000 ±.005

5.000 ±.005

3.000 ±.005

1.000 ±.005

⇌ | A | .004
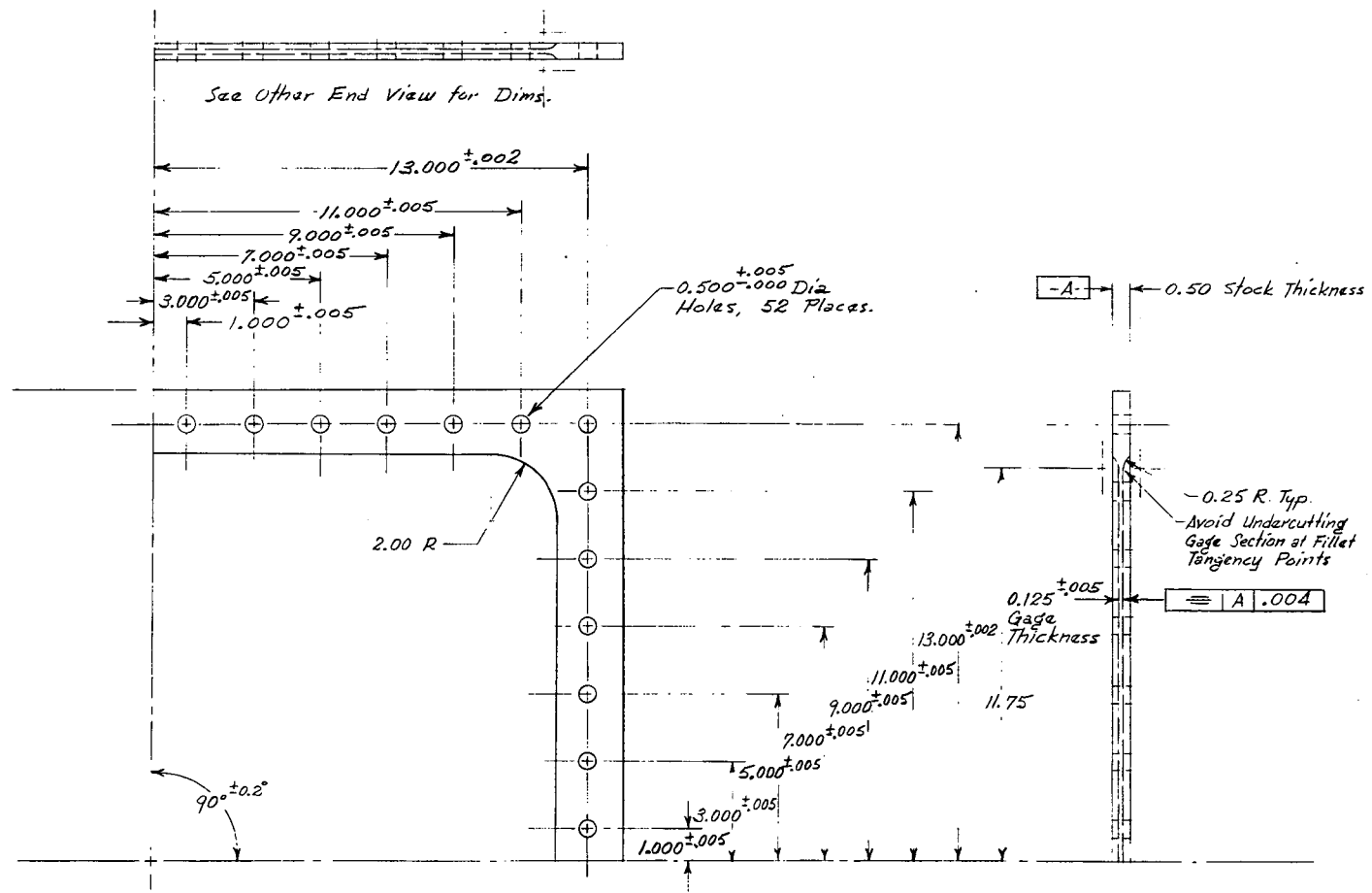
DETAIL - Typical Panel Quadrant

Figure IV-4   Unstiffened Biaxial Fatigue Panel (Sheet 2) Specification
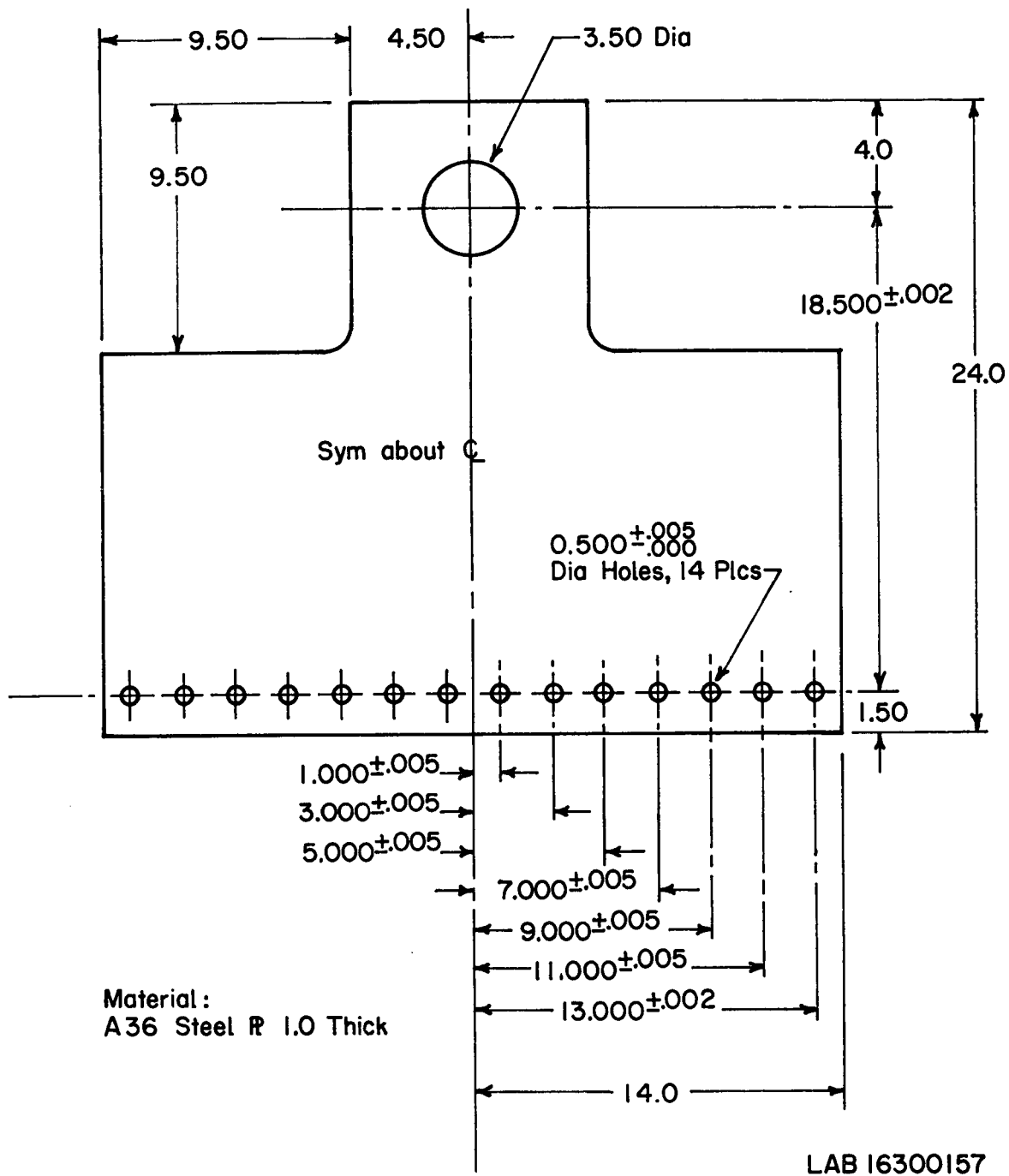
Figure IV-5 Loading Plate for Biaxial Fatigue Machine

LAB 16300157

Material:
A36 Steel ℞ 1.0 Thick

Figure IV-6   Loading Strap Design for Biaxial Panel Test

28 or Stock

⊟ | A | .012

-A-

26.0 Ref

8.00 Typ   4.00 Typ

See Typ Panel Quadrant Detail - Sheet 2

Stock 1.00

0.50

28 or Stock

V Typ See L/M

8.00 Typ

S See L/M

4.00 Typ

T See L/M

26.0 Ref

H Typ See L/M

2.00 R Typ

Remove Burrs & Break All Edges

-B-

Rolled Direction

SECTION

⊟ | B | .012

Variable Dimensions		S	V	H	T			
-006	Panel	0.125	0.125	0.250	0.188	2219-T87 Alum Alloy		
-005		0.125	0.060	0.125	0.188			
-004		0.125	0.060	0.060	0.188			
-003		0.060	0.125	0.125	0.220			
-002		0.060	0.060	0.125	0.220			
-001	Panel	0.060	0.060	0.060	0.220	2219-T87 Alum Alloy		

| QUANTITY/DASH NO | | PART NO | ZONE | REG QTY | DESCRIPTION | | MATERIAL OR VENDOR | ISSUE CODE | MATERIAL SPECIFICATION | FINISH OR MFR CODE | CHG |

LIST OF MATERIAL

Figure IV-7   Stiffened Biaxial Fatigue Panel (Sheet 1) Specifications

0.50   1.00 Stock

4.00 Ref   8.00 Ref

0.25 R Typ

13.000 ±.002

0.500 +.005 −.000 Dia
Holes, 52 Plcs

1.000   3.000   5.000   7.000   9.000   11.000   13.000 ±.002

C

V Typ
See L/M

0.25 R
Typ

13.000 ±.002

11.000

2.00 R
Ref

9.000

S - See L/M

T - See L/M

SECTION D-D
Scale 2/1

7.000

0.25 R
Typ

5.000

D   D

3.000

90° ±0.2°

H Typ
See L/M

0.25 R
Typ

1.000

C

DETAIL - TYPICAL PANEL QUADRANT
Scale 1/2

S - See L/M

T - See L/M

SECTION C-C
Scale 2/1

Avoid Undercutting Skin & Stiffener
Sections at Fillet Tangency Points.

Figure IV-8   Stiffened Biaxial Fatigue Panel
      (Sheet 2) Specifications

The stiffened panel was first modeled in two dimensions with plate elements. This step was necessary to reduce the magnitude of the problem before making a model in three dimensions with tetrahedral elements. Modeling initially with tetrahedrons would have made the finite element model too large to handle on the computer if a reasonable mesh size were used; or if the model were made to fit the computer, then the mesh size would be too large to show any meaningful results. More detailed descriptions of the two-dimensional and three-dimensional models follow.

A finite element model of the stiffened biaxially loaded panel is shown in Figure IV-9. Symmetry of the panel made it possible to model only one-quarter of the complete assembly. The node point mesh was developed to give a large number of elements near the center of the panel. The 1/8-in. (3.2 mm) (thin rib) and 1/4-in. (6.5 mm) (thick rib) stiffeners were modeled as plate elements standing on edge. The seven load fingers that connect to each side of the quarter panel are modeled as axial elements linked to the fixture arms. Again by symmetry, it was possible to model half of one load fixture arm. The fixture model was collapsed to a stiffness matrix for the seven node points common to the load fingers and one node point for the load application point. The collapsed stiffness matrix was then renumbered to fit the load finger node points along both edges of the panel model.

Node points on the X-axis line of symmetry were fully restrained against deflection in the Y direction and rotation about the X-axis. Node points on the Y-axis line of symmetry were fully restrained against deflection in the X direction and rotation about the Y-axis. The stiffeners were fully restrained against rotation about the Z-axis at the lines of symmetry. The thin rib was fully restrained against deflection in the Y direction at the X-axis; the thick rib was fully restrained against deflection in the X direction at the Y-axis. The node point at the origin was also fully restrained against deflection in the Z direction, thus making all other node point deflections relative to the node point at the origin.

Formulation of the elements used in modeling the stiffened panel was based on references 1 thru 4.

All plate elements used in the model have five degrees of freedom per node point, or 15 degrees of freedom for each triangular plate element, and 20 degrees of freedom for each rectangular plate element.
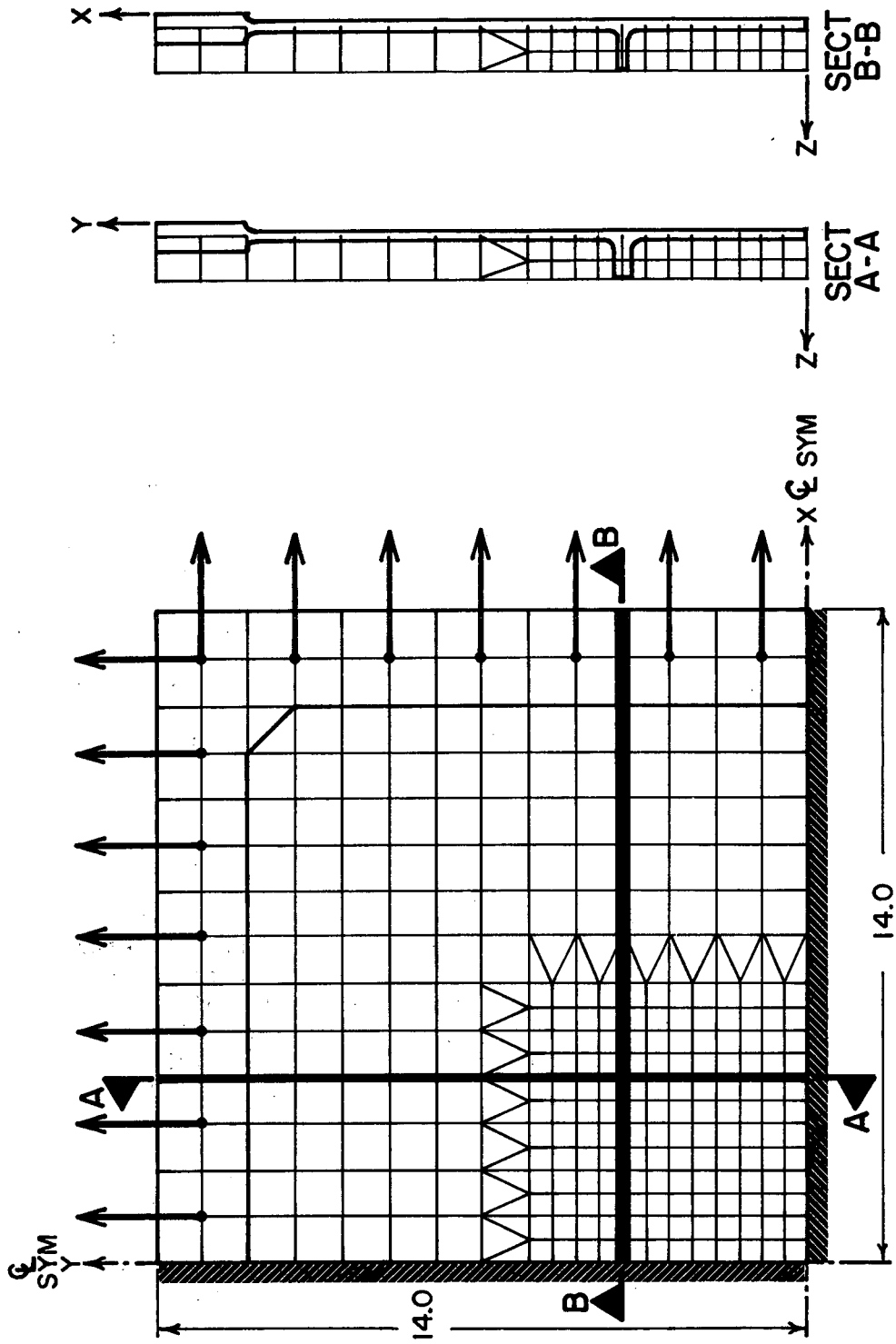
Figure IV-9 Finite Element Model of Stiffened Biaxial Panel

A balanced biaxial stress of 30 ksi (207 MN/m^2) at the mid-surface of the plate was expected from the loading arrangement shown in Figure IV-10. The stress analysis showed a biaxial stress of about 28 ksi (193 MN/m^2) on the stiffener side of the plate and 32 ksi (220 MN/m^2) on the opposite side. The stiffeners, therefore, caused a bending stress of 2 ksi (14 MN/m^2) at the center of the panel. Biaxial stresses for each element within the central bay of the panel balance within ± 1%. Principal stresses were computed for each plate element; their directions are shown for some elements in Figure IV-10. Distribution of the principal stresses through the stiffener is shown in Figure IV-11.

The cross-hatched areas in Figure IV-10 illustrate the locations of the segments selected for the more detailed three-dimensional analysis using tetrahedral elements. One segment designated the "thin-rib" model, cuts across the 1/8-in. (3.2 mm) thick stiffener; the other segment designated the "thick-rib" model, cuts across the 1/4-in. (6.5 mm) thick stiffener. Each segment was chosen to minimize the effect on that segment of the boundary conditions for the panel model and the other stiffener. The basis for the boundary conditions on the three-dimensional model was the displacement (deflection and rotation) calculated in the panel model computer run for node points common to the two- and three-dimensional models. Deflections for node points on the boundary of the three-dimensional model, but not common to the two-dimensional model, were calculated by straight-line interpolation.

Formulation of the tetrahedral element is covered in a report by A. Holston, Jr., *A Three Dimensional Finite Element*, Martin Marietta Corporation R-71-48637-001, 1971. The element has four node points with three translational degrees of freedom at each node point, or twelve degrees of freedom for each element. It is a constant strain element with thermal strains included. It is essentially an extension of the *In Plane Triangular Plate Element* mentioned earlier from two to three dimensions.

Each segment to be analyzed using tetrahedral elements was subdivided into "bricks" (parallelepipeds) and "wedges." The wedges were used in modeling the fillets only. Each brick was composed of five tetrahedral elements; wedges were composed of three tetrahedrons (Fig. IV-12). The thin-rib model had 800 node points and 2592 tetrahedral elements; the thick-rib model had 750 node points and 2432 tetrahedral elements. The material properties for aluminum alloy 2219-T87 (given in Section A) were used. The mesh size in the Y direction (thin-rib model) was constant. It was also constant in the Z direction for the plate portion of the model,
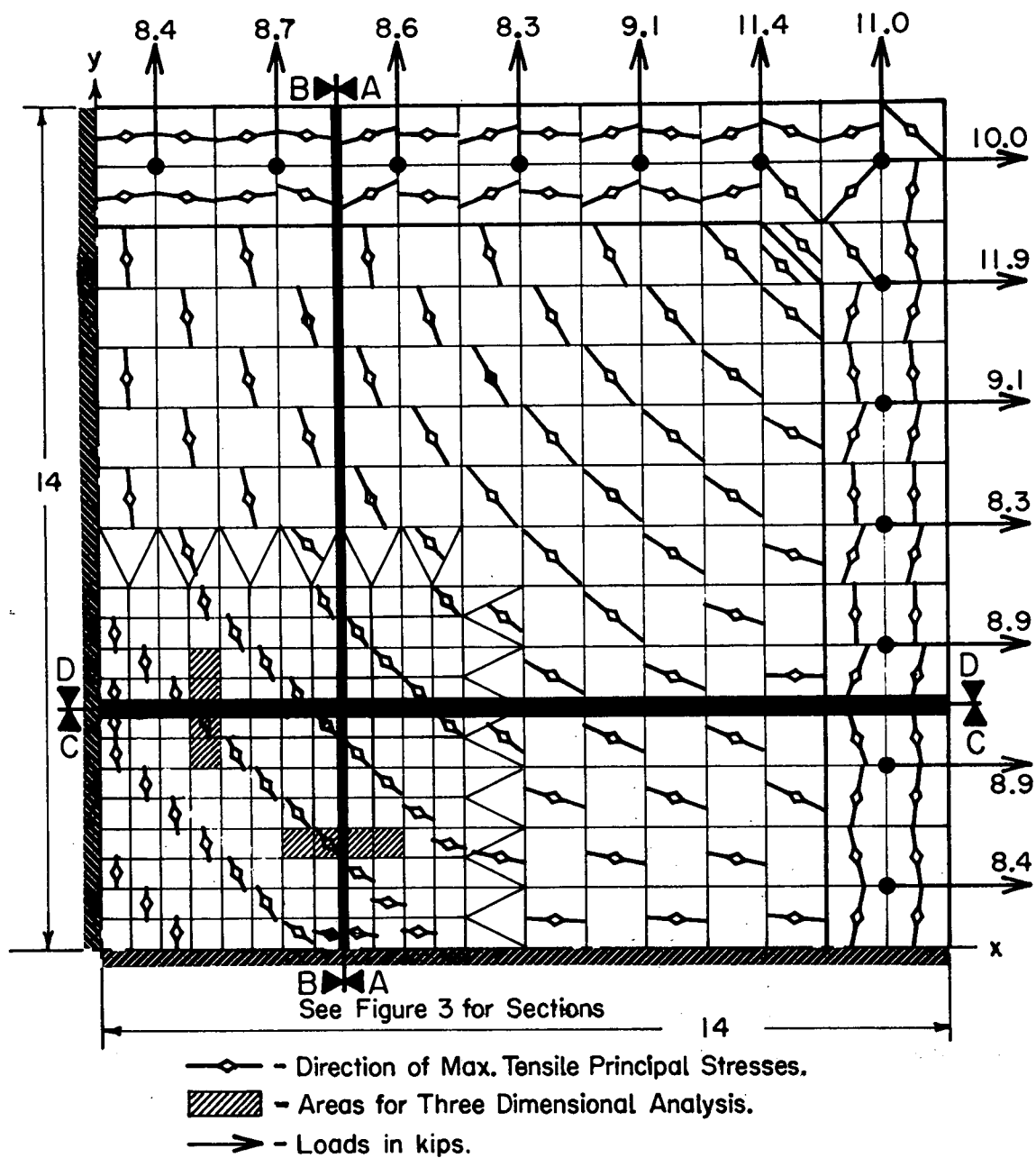
*Figure IV-10 Principal Stress Directions and Load Distribution in 0.125-in.
(3.2 mm) Biaxial Stiffened Quarter Panel from Finite Element
Analysis*

SECTIONS

B-B		A-A		D-D		C-C	
-0.1 2.3		-0.2 2.8		-0.2 2.3		0 1.2	
-1.5 4.6		-1.8 4.7		-1.5 2.9		-0.8 2.6	
0 12.9		-0.1 12.6		0 9.5		-0.2 10.0	
-0.1 13.1		-0.1 13.1		-0.1 10.1		-0.1 10.2	
0 13.1		0 13.1		0 10.2		0 10.3	
0 13.0		0 13.0		0 10.3		0 10.3	
-0.1 12.9		-0.1 12.9		-0.1 10.3		-0.1 10.4	
0 15.0		-0.1 15.0		-0.4 12.9		-0.1 12.7	
-0.8 20.1	0.6 10.9	0.5 11.0	-0.8 20.2	-0.1 18.5	0.2 8.3	0.5 7.9	-1.1 18.3
-0.5 17.5	-0.1 8.0	-0.1 8.1	-0.6 17.5	-0.6 16.2	-0.2 4.6	-0.1 4.5	-0.5 16.3
0 17.0	-0.1 8.1	-0.1 8.2	-0.1 16.9	0.2 15.5	0.1 4.8	0.2 4.7	0.3 15.5
0 16.5	0.1 8.0	-0.1 8.2	0.2 17.1	-0.6 14.5	-0.4 5.1	-0.3 4.9	-0.5 14.5
0 16.5	0.6 8.6	-0.7 7.8	-0.4 16.2	1.2 22.4	0.8 11.2	0.8 11.3	1.3 22.3
0.1 16.8	0.6 8.6	-0.7 7.9	-0.6 15.8	-0.4 14.3	-0.4 5.0	-0.4 5.1	-0.4 14.4
0 16.2	0.1 8.1	0.1 8.3	0.1 16.8	0.2 15.0	0.2 4.9	0.2 4.9	0.2 15.0
0 16.6	0 8.2	0 8.3	0 16.4	0 15.1	0 4.9	0 4.9	0 15.1
0 16.4	0 8.3	0 8.3	0 16.5	0 15.1	0 4.9	0 4.9	0 15.1
0 16.4	0 8.3	0 8.3	0 16.4	0 15.1	0 4.9	0 4.9	0 15.1
0 16.4	0 8.3	0 8.3	0 16.4	0 15.1	0 4.9	0 4.9	0 15.1
0 16.4	0 8.3	0 8.3	0 16.4	0 15.1	0 4.9	0 4.9	0 15.1
0 16.3	0 8.3	0 8.3	0 16.4	0 15.1	0 4.9	0 4.9	0 15.1

B-B   A-A   D-D   C-C

Figure IV-11 Principal Stress Distribution through Stiffeners

IV-18
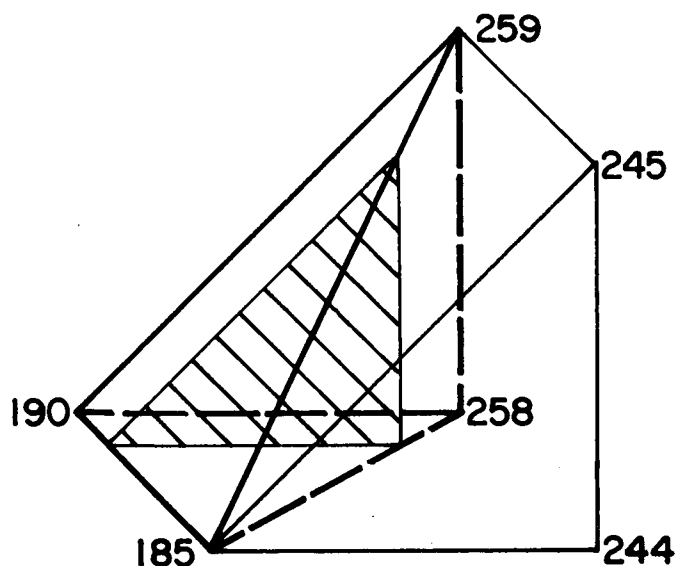
ELEMENT NUMBER 2324
185, 190, 258, 259
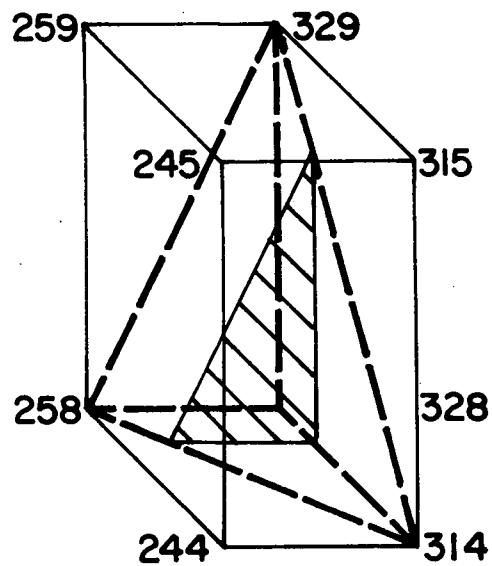
ELEMENT
NUMBER 729
258, 314, 328, 329
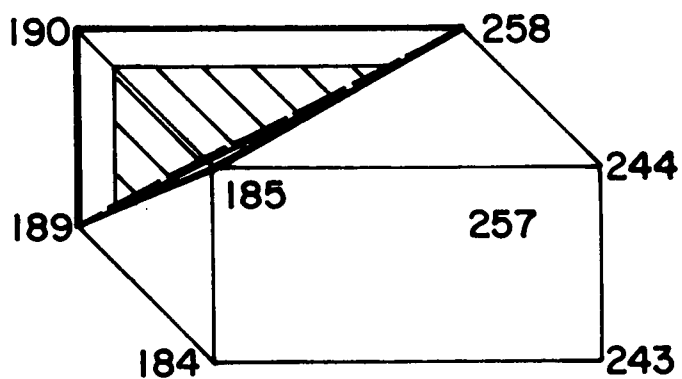
ELEMENT NUMBER 597
185, 189, 190, 258

$\overline{Y} = \frac{7}{32}$ Plane

Figure IV-12   Tetrahedral Modeling Elements

but it varied from fine to coarse in the stiffener. The mesh
size in the X direction (thin-rib model) varied from coarse at
the plate edges to fine at the juncture of the plate and stiffener
(Figure IV-13 and Figure IV-14). Data for elements in the plate and
stiffener portion of the model were produced automatically with a
data generation computer program modified to accommodate the model.
Element data for one fillet on the thin-rib model were generated
by hand. These elements were also renumbered to fit the other
fillet on the thin-rib model and both fillets on the thick-rib
model. The models were plotted to verify that no errors existed.
Deflections and rotations for the 14 node points on the mid-sur-
face of the plate and stiffener common to the two-dimensional
model and the three-dimensional segments were used to calculate
the deflections of node points on the cut faces of the segments.
Rotations of a node point on the mid-surface were converted to
deflections for node points at a distance from and normal to the
mid-surface. Deflections for intermediate node points on the cut
faces of the segments were calculated by straight line interpola-
tion between the node points common to both two- and three-dimen-
sional models.

The two problems (thin-rib and thick-rib models) were solved by
displacing the boundary node points to the calculated deflections
and computing the stresses thus induced. Output from the com-
puter program included six values each of stress and strain, plus
three principal stresses with their associated principal directions
for each tetrahedral element in each model. In addition, a value
known as the distortion energy ratio (DER) was calculated for
each element. The DER is the ratio of distortion energy in the
stress state to the distortion energy at yield. It is based on
the von Mises (J_2) theory of plasticity. One computes an effective-
stress level using the normal and shear stress components and
then divides by a yield stress. This gives the DER and is a con-
venient way to compare stress levels among elements.

An examination of the normal stresses and DERs indicated that ele-
ments away from the boundaries where node points had been dis-
placed initially did, in fact, behave independently of the plate
action enforced at the boundaries. Stresses in the middle tetra-
hedron and an "outside" tetrahedron for selected bricks were com-
pared and found to differ only slightly. Figure IV-15 illustrates
middle and outside tetrahedrons. Normal stresses and DERs were
nearly symmetric with respect to the rib centerline and also with
respect to a plane at Y = 1/4 in. (6.4 mm) for the thin-rib model
(X = -1/4 in. (6.4 mm) for the thick-rib model). A cutting plane

Figure IV-13   Thin-Rib Segment of Stiffened Panel
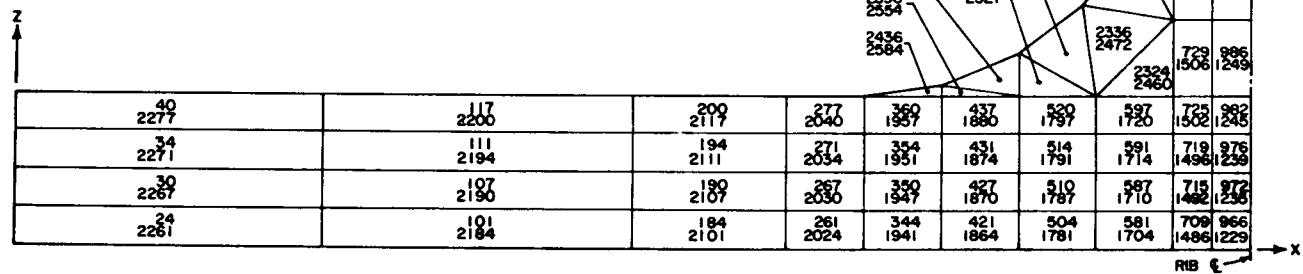
Figure IV-14   Thin-Rib Model Elements

Typical "Outside" Tetrahedron

"Middle" Tetrahedron
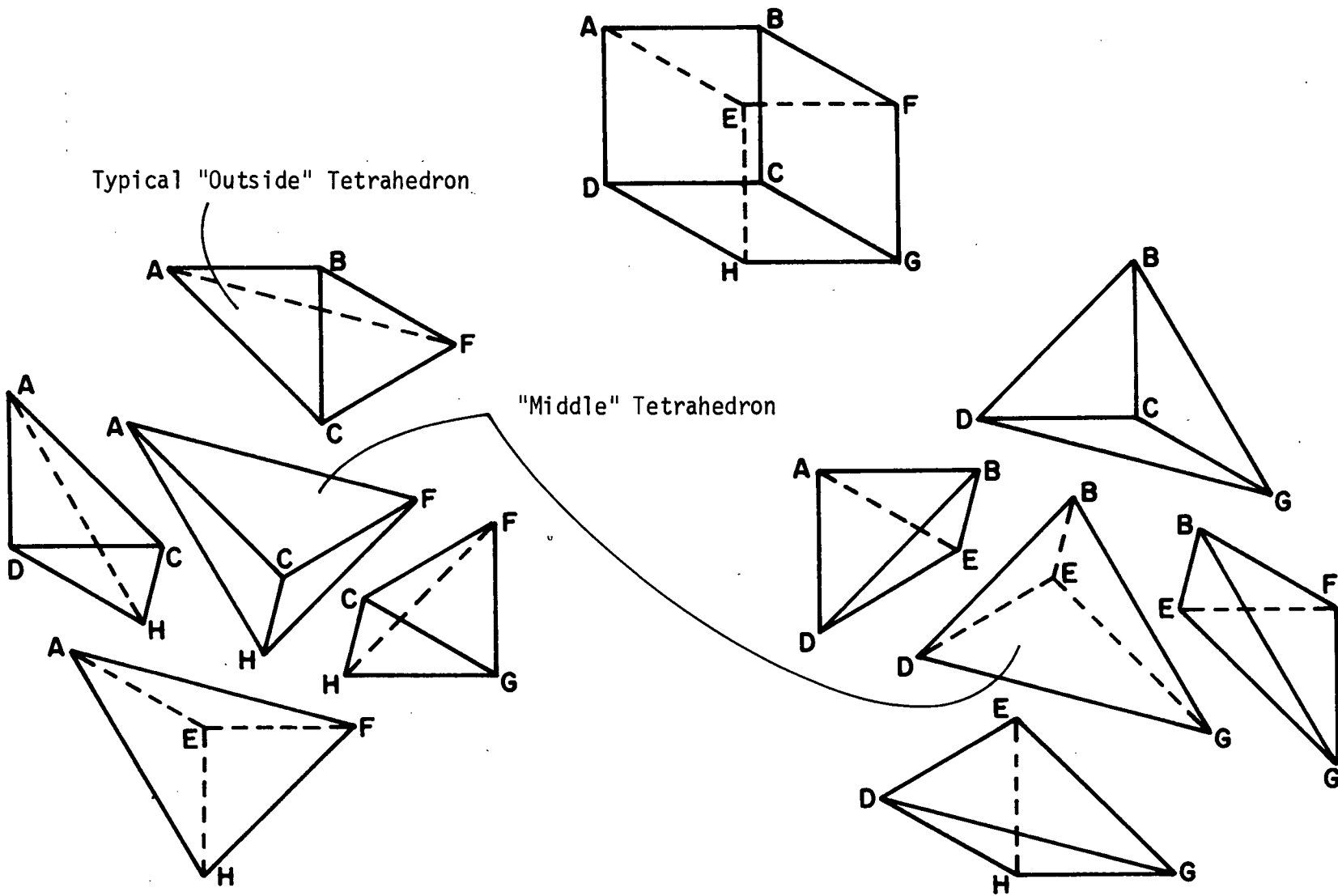
Figure IV-15   Segments of Tetrahedral Element

was passed through the thin-rib model at Y = 7/32 in. (5.7 mm) and the thick-rib model at X = -5/32 in. (4.1 mm) (See Figures IV-13 and IV-16). Elements selected as typical for the thin-rib model had a Y centroid equal to 7/32-in. (5.7 mm). For the thick-rib model, typical elements had a X centroid equal to -5/32 in. (4.1 mm). These elements in the thin-rib model also had the same X centroids (Y centroids in the thick-rib model) in each "stack" of bricks when viewed in the Z direction. Figure IV-12 illustrates the elements at the corner of the fillet in the thin-rib model.

DERs for elements selected from the thin- and thick-rib models are tabulated in Figures IV-17 and IV-18. Normal stress (σ_{xx}) variation in the X direction is plotted in Figure IV-19; normal stress (σ_{yy}) variation in the X direction is plotted in Figure IV-20. All normal and shear stresses for the selected elements are tabulated in Appendix A, Table A-1. Further examination of the DERs indicated that the critical elements were at the toe of the fillets. These are shown as shaded areas in Figures IV-17 and IV-18.

The stress distribution through the plate thickness at selected distances from the stiffener centerline is shown in Figures IV-19 and IV-20. These may be compared with data theory as follows. Two types of classical plate analyses could be performed: one in which the stiffeners were neglected and the panel analyzed as an isotropic plate; another approach would be to "smear" the stiffeners and use orthotropic plate theory. The former would produce constant stress through the thickness; the latter would show a linear variation. Thus, deviations from isotropic and orthotropics plate analyses are shown by deviations from constant and linear distributions, respectively. Figures IV-19 and IV-20 and Table A-1 of Appendix A show a peak stress of 41.1 ksi, and the isotropic plate theory would give 30 ksi and thus underestimate the peak by 37% at the toe of the fillet. Also note that the deviation in σ_{xx} is greater than that in σ_{yy} which is to be expected since this stiffener is oriented in the Y direction.

Figures IV-21 and IV-22 are plots of stresses that occurred in elements on the front surface of the thin- and thick-rib segment models, respectively. Rear surface plots are given in Figures IV-23 and IV-24.

In summary, a two-dimensional macroanalysis of the stiffened panel was used to establish node point deflections and rotations that were used as boundary conditions for a three-dimensional micro-analysis of small segments of the stiffened panel. The selected

Figure IV-16   Thick-Rib Segment of Stiffened Panel

Thin Rib - Inboard
No. - Number of Element whose $\bar{y}$ = 7/32 Plane
DER - Distortion Energy Ratio

No.	DER	No.	DER	No.	DER	No.	DER	No.	DER	No.	DER	No.	DER	No.	DER	No.	DER	No.	DER
																769	.019	1026	.019
																765	.019	1022	.019
																759	.048	1016	.048
																755	.048	1012	.048
																749	.073	1006	.073
														2448	.085	745	.072	1002	.072
														2418	.089	739	.105	996	.104
														2420	.098				
														2385	.137	735	.111	992	.107
														2360	.135				
								2436	.565	2400	.339	2348	.232	2336	.227	729	.220	986	.216
										2398	.467	2373	.322	2324	.234				
40	.326	117	.345	200	.386	277	.438	360	.494	437	.402	520	.288	597	.281	725	.229	982	.228
34	.415	111	.439	194	.481	271	.484	354	.436	431	.414	514	.406	591	.401	719	.356	976	.356
30	.415	107	.439	190	.478	267	.482	350	.434	427	.415	510	.402	587	.397	715	.350	972	.351
24	.405	101	.423	184	.486	261	.456	344	.394	421	.387	504	.408	581	.414	709	.458	966	.460

₵ of Rib ⟶

Figure IV-17 (Sheet 1) Distortion Energy Ratios for Thin-Rib Model

No.	DER	No.	DER	No.	DER	No.	DER	No.	DER	No.	DER	No.	DER	No.	DER	No.	DER	No.	DER
1289	.019	1546	.019																
1285	.019	1542	.019																
1279	.048	1536	.048																
1275	.048	1532	.048																
1269	.073	1526	.073																
1265	.073	1522	.073	2572	.086														
1259	.105	1516	.107	2534	.086														
				2536	.100														
1255	.109	1512	.113	2509	.154														
				2484	.149														
1249	.207	1506	.209	2472	.190	2496	.214	2556	.335	2584	.565								
				2460	.180	2521	.313	2554	.467										
1245	.220	1502	.221	1720	.286	1797	.294	1880	.401	1957	.493	2040	.439	2117	.387	2200	.345	2277	.326
1239	.355	1496	.354	1714	.409	1791	.415	1874	.415	1951	.437	2034	.483	2111	.480	2194	.438	2271	.414
1235	.349	1492	.348	1710	.403	1787	.409	1870	.416	1947	.434	2030	.481	2107	.478	2190	.438	2267	.414
1229	.463	1486	.461	1704	.421	1781	.415	1864	.391	1941	.398	2024	.454	2101	.484	2184	.421	2261	.403

Thin Rib - Outboard
No. - Number of Element whose $\bar{y}$ = 7/32 Plane
DER - Distortion Energy Ratio

← ℄ of Rib

Figure IV-17 (Sheet 2) (concl)

Thick Rib - Inboard
No. - Number of Element whose $\bar{y}$ = 5/32 Plane
DER - Distortion Energy Ratio

No.	DER	No.	DER	No.	DER	No.	DER	No.	DER	No.	DER	No.	DER	No.	DER	No.	DER
																686	.004	949	.005
																682	.005	945	.005
																676	.024	939	.026
																672	.024	935	.025
																666	.046	929	.049
														2290	.047	662	.046	925	.047
														2259	.072	656	.080	919	.073
														2261	.087				
														2224	.092	652	.087	915	.072
														2201	.091				
										2239	.500	2189	.267	2178	.191	646	.261	909	.170
								2278	.522	2241	.428	2212	.354	2166	.268				
40	.311	117	.330	200	.411	277	.468	360	.339	437	.283	520	.248	642	.237	905	.167
34	.328	111	.349	194	.418	271	.408	354	.374	431	.359	514	.358	636	.349	899	.301
30	.330	107	.351	190	.417	267	.407	350	.373	427	.359	510	.349	632	.339	895	.292
24	.400	101	.418	184	.457	261	.429	344	.382	421	.377	504	.404	626	.405	889	.419

¢ of Rib ⟶

Thick Rib - Outboard
No. - Number of Element whose $\bar{y}$ = 5/32 Plane
DER = Distortion Energy Ratio

No.	DER	No.	DER	No.	DER	No.	DER	No.	DER	No.	DER	No.	DER	No.	DER	No.	DER
1206	.005	1469	.004														
1202	.005	1465	.004														
1196	.026	1459	.024														
1192	.025	1455	.024														
1186	.049	1449	.046														
1182	.047	1445	.046	2414	.048												
1176	.073	1439	.083	2375	.073												
				2377	.090												
1172	.072	1435	.091	2348	.097												
				2325	.095												
1166	.170	1429	.269	2314	.198	2337	.266	2395	.486	2426	.513						
				2302	.272	2360	.343	2397	.414								
1162	.166	1425	.241	1637	.250	1720	.274	1797	.328	1880	.463	1957	.407	2040	.334	2117	.312
1156	.301	1419	.351	1631	.358	1714	.359	1791	.372	1874	.407	1951	.417	2034	.352	2111	.329
1152	.293	1415	.340	1627	.348	1710	.359	1787	.371	1870	.406	1947	.416	2030	.354	2107	.331
1146	.418	1409	.406	1621	.405	1704	.379	1781	.383	1864	.430	1941	.458	2024	.420	2101	.401

⟵ ¢ of Rib

THIN RIB - INBOARD

Y = $\frac{7}{32}$ TYPICAL (X, Y, & Z IN INCHES)
( ) - ELEMENT NUMBER

NORMAL STRESS, σ_{XX}, KSI

σ_{XX}, KSI
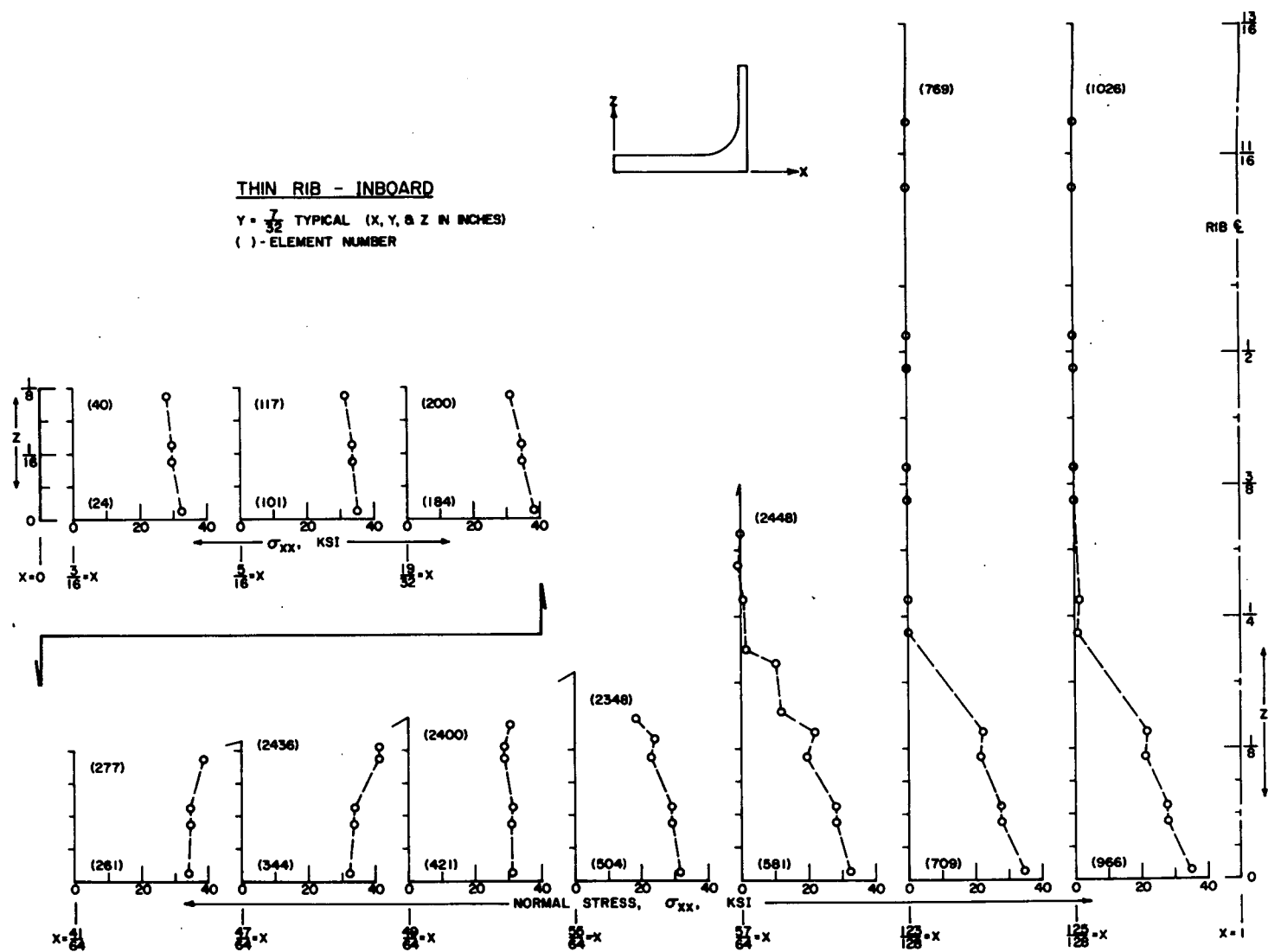
Figure IV-19 Plot of Normal Stress (σ_{xx})

THIN RIB - INBOARD

$Y = \frac{7}{32}$ TYPICAL (X, Y, & Z IN INCHES)

( ) - ELEMENT NUMBER
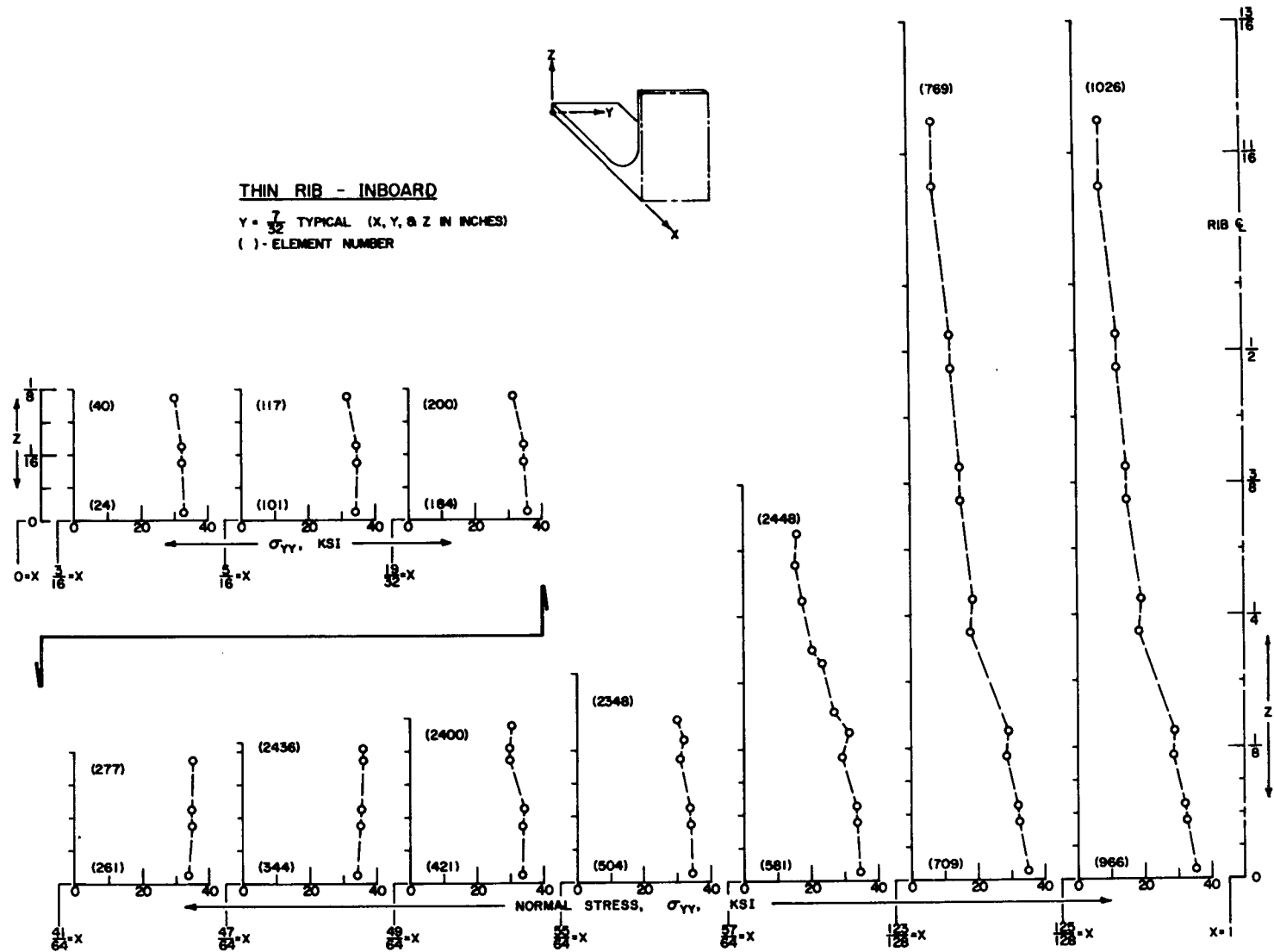
Figure IV-20   Plot of Normal Stress (σ_{yy})
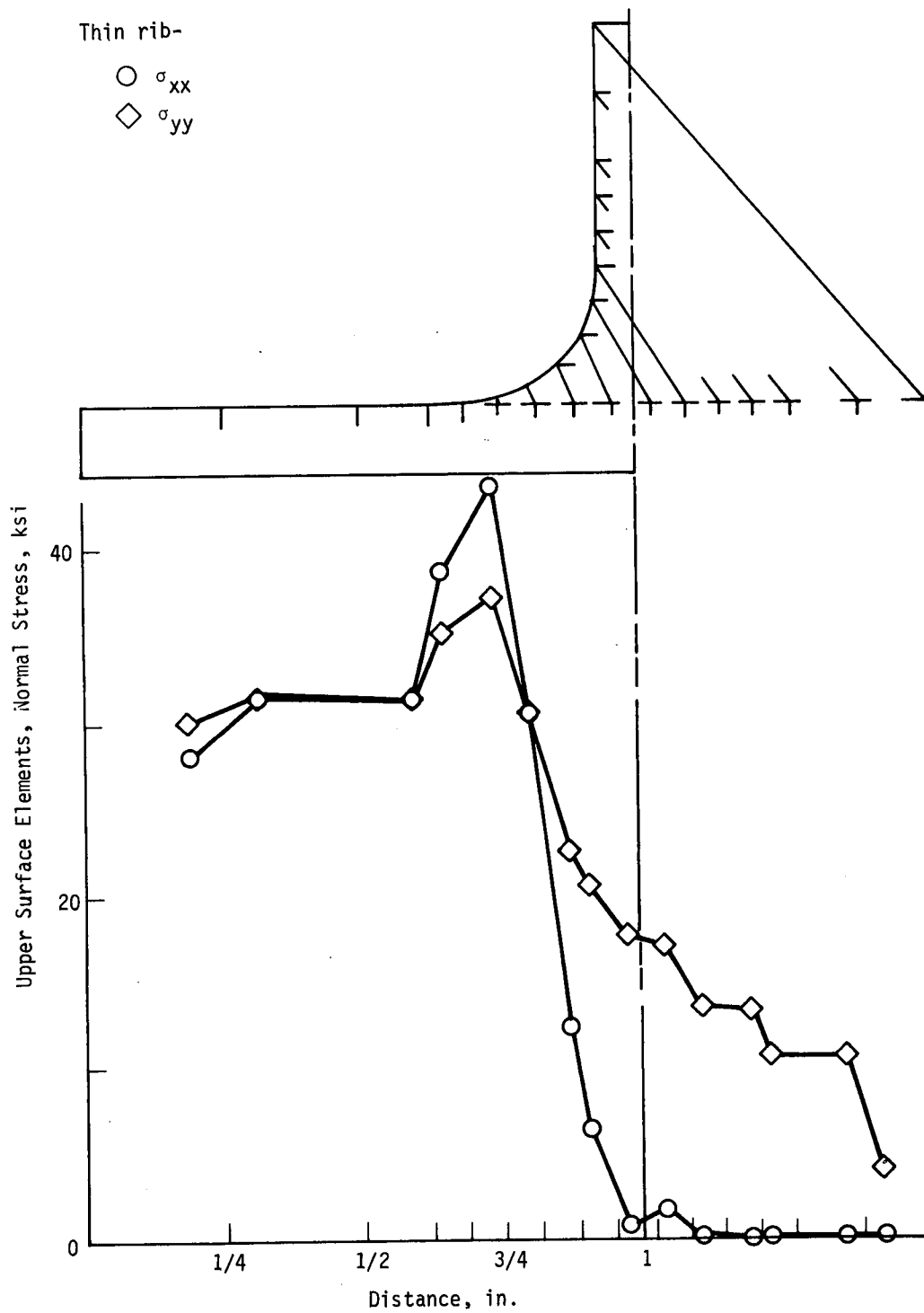
Figure IV-21 *Surface Element Stresses (Front Face) for Thin-Rib Model*
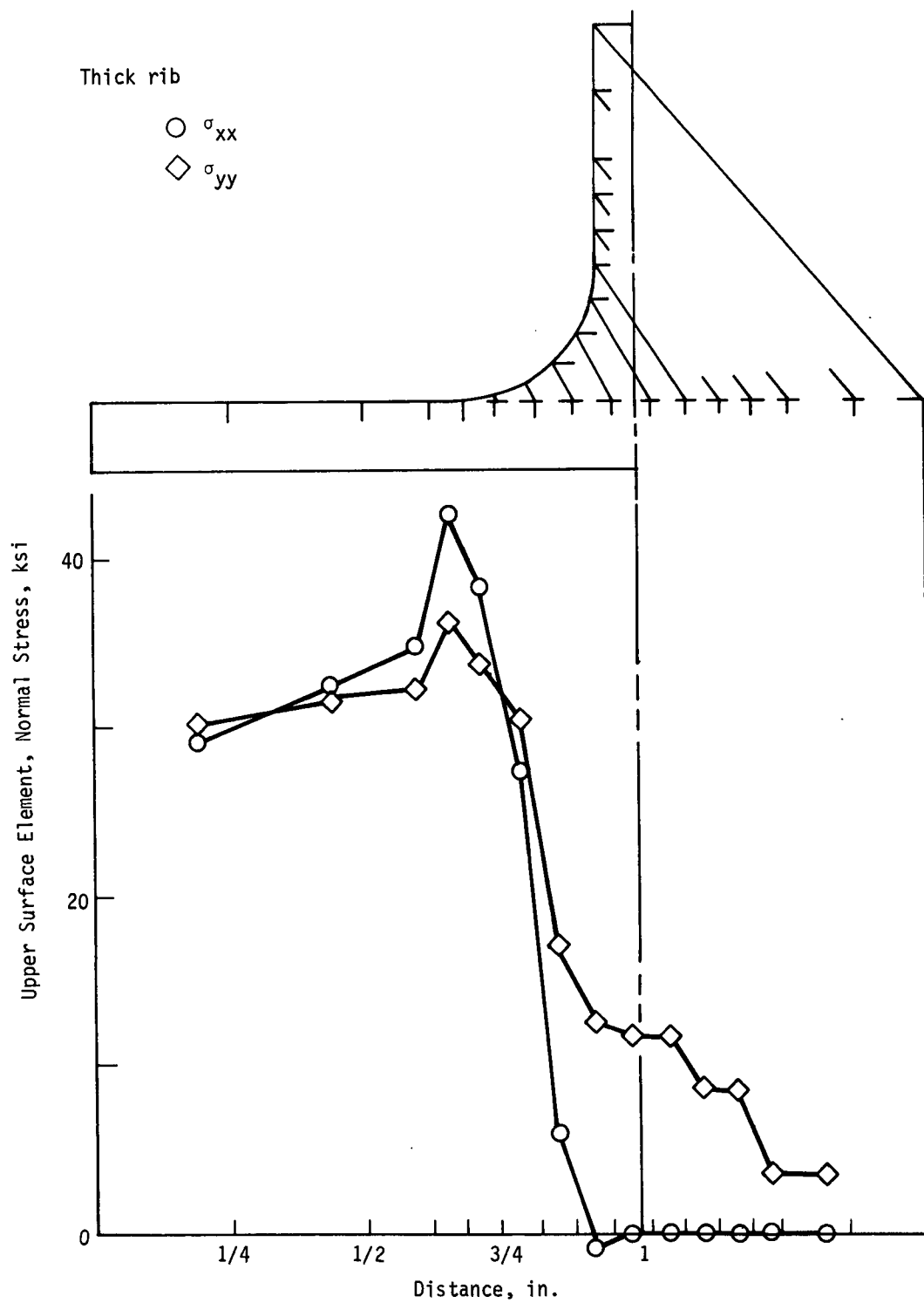
Figure IV-22 Surface Element Stresses (Front Face) for Thick-Rib Model
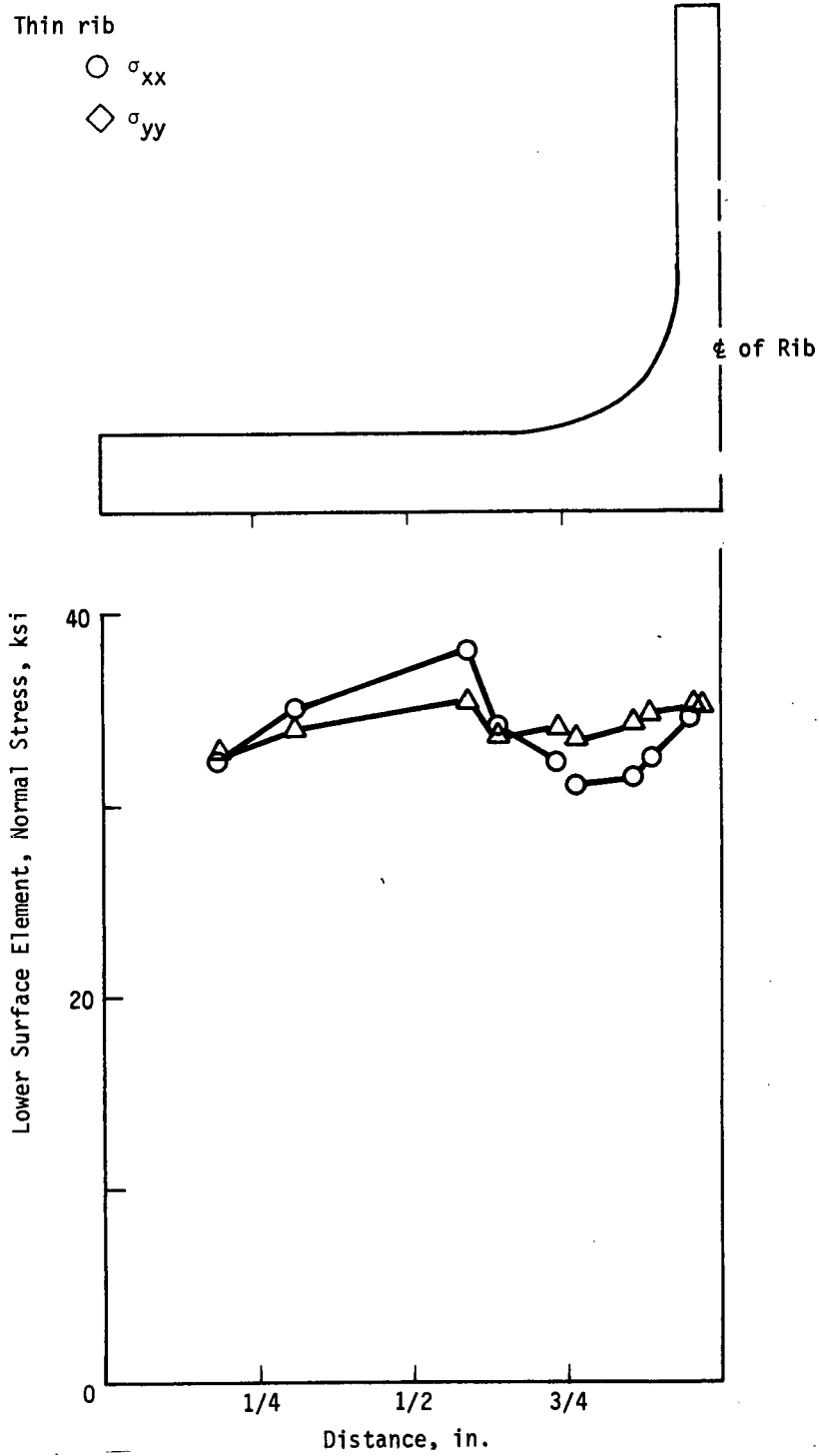
Figure IV-23 Surface Element Stresses (Rear Face) for Thin-Rib Model
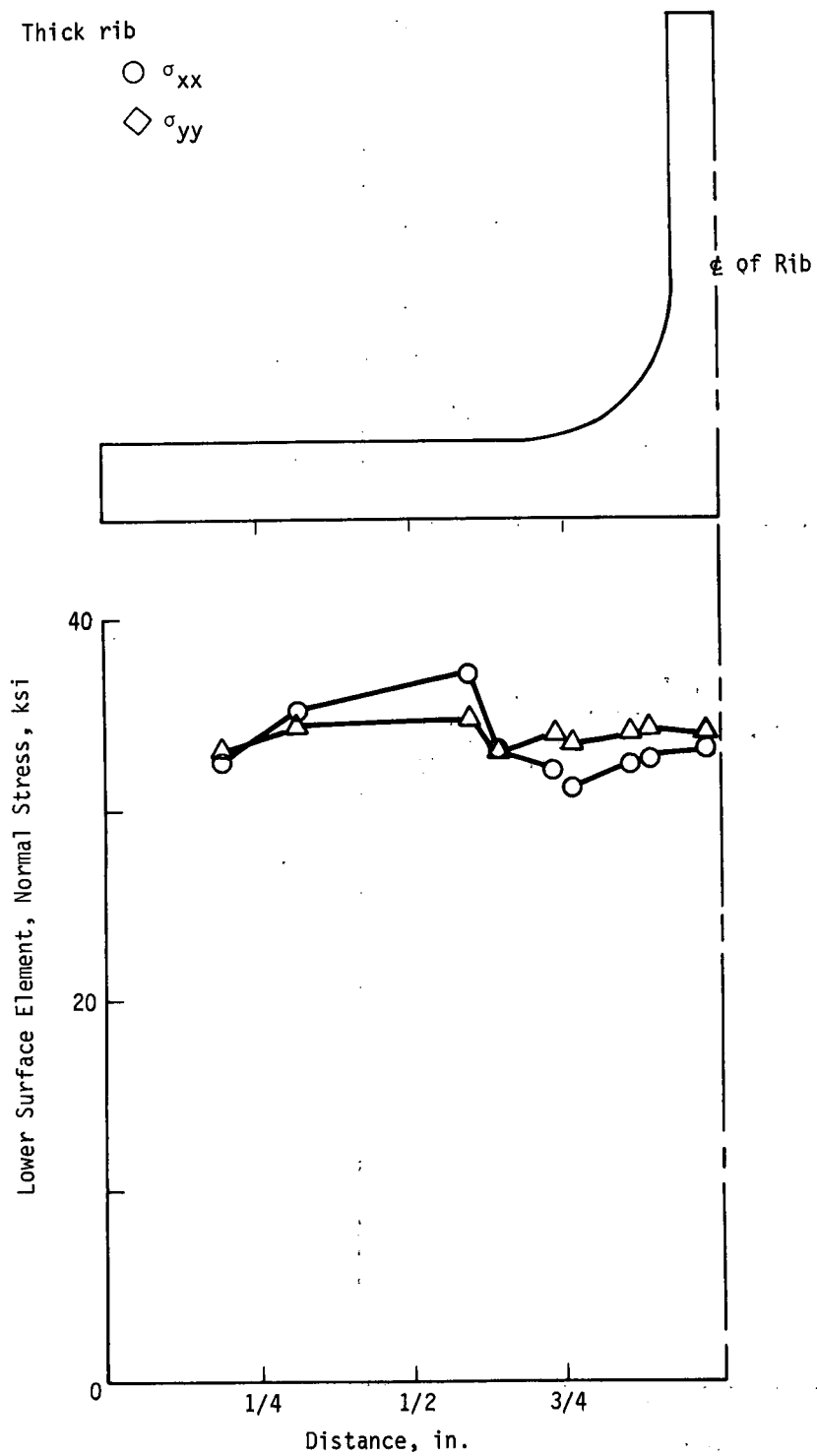
Figure IV-24 Surface Element Stresses (Rear Face) for Thick-Rib Model

segments included portions of the thin rib and thick rib. A ratio
(DER) relating the distortion energy level in a given state of stress
to the distortion energy level at yield stress was introduced as
a means of interpreting the voluminous data available from the
three-dimensional analysis. Based on the DER, it was evident that
normal stresses were nearly symmetric, but not exactly, in both the
X and Y directions. Tabulation of the DERs for typical sections
cut through each model indicated little difference in the magnitude
of the stresses nor location of the critical elements in the two
models. The critical stress point in each model was shown to be
the elements at the toe of the fillets adjacent to the plate por-
tion of the panel. Plots of the normal stress confirmed the need
for the three-dimensional analysis around the fillets and the
juncture of the plate and stiffener. The maximum deviation from
isotropic plate theory, wherein the stiffeners are neglected, was
37% at the fillet toe for the configuration shown. This deviation
diminished to 9% at three stiffener-widths away from stiffener
centerline.

EXPERIMENTAL STRESS ANALYSIS

Three distinct experimental stress analyses were conducted in this
portion of the program. These were (1) photoelastic stress anal-
ysis of stiffened biaxial panels; (2) strain gage stress analysis
of stiffened biaxial panels; (3) strain gage residual stress anal-
ysis of unstiffened, welded biaxial panels. All three experimental
analyses were conducted on full size panels. The strain gage and
photoelastic analyses were performed using the biaxial test fixture
shown in Figure IV-25 and the stiffened panel (Fig. IV-7).

Photoelastic Stress Analysis

All six stiffened panels were analyzed by the photoelastic tech-
nique. This work was subcontracted to Photoelastic, Inc., of
Malvern, Pennsylvania, who are recognized experts in this field.
A summary of their work is included in this subsection. Detailed
descriptions of their work and findings are given in Appendix B.

The purpose of this work was to provide determination of (1) stress
distribution in the center bay of each panel on both the front and
rear surfaces; (2) level of stress concentration in the corners
and fillet radii adjacent to the center bay; (3) stress distribu-
tion in the stiffener ribs.
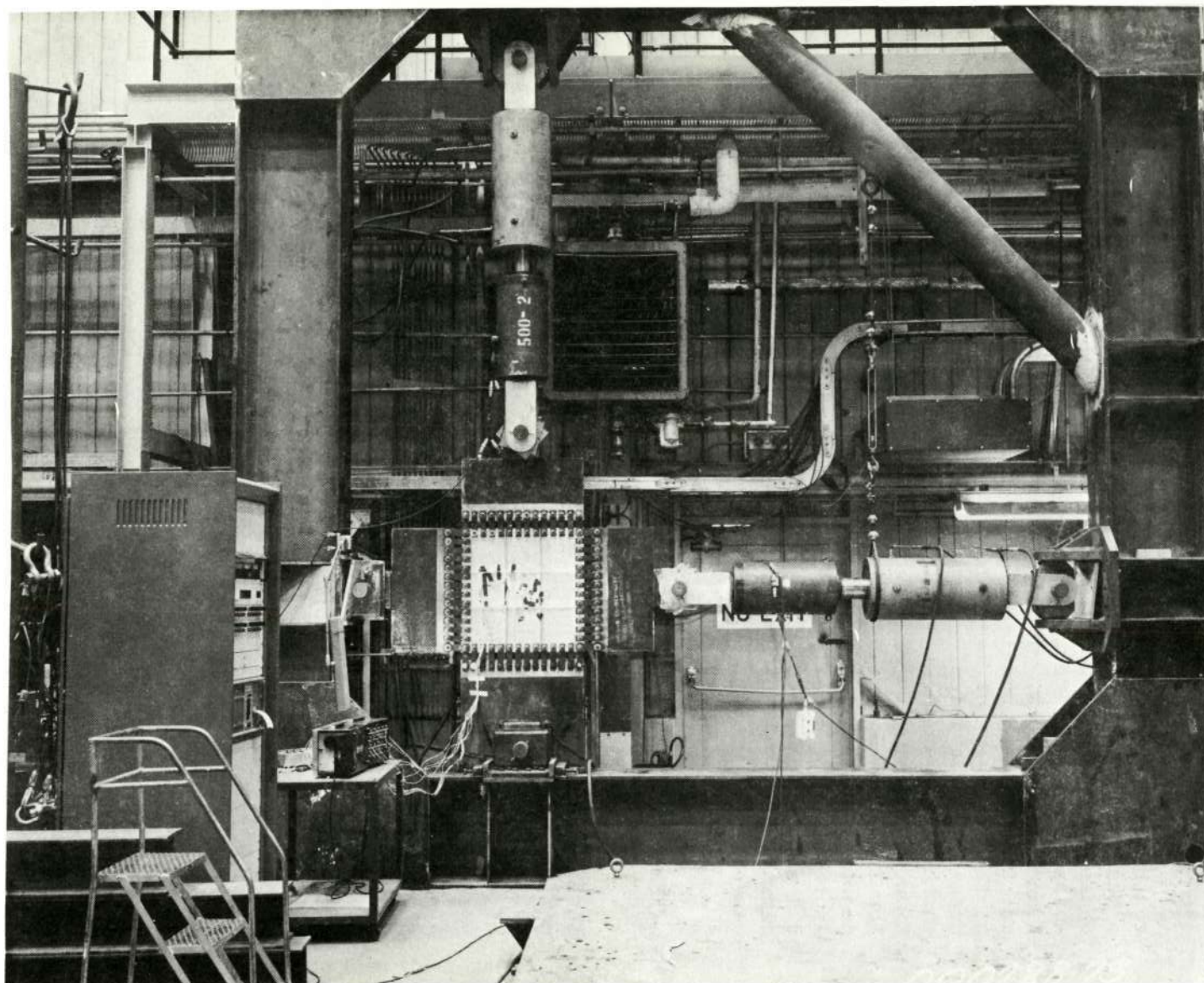
Figure IV-25   Biaxial Testing Machine with Strain Gaged,
                Stiffened Panel

The above information was obtained for each panel for three loading conditions: 1:0 uniaxial loading, 1:1 biaxial loading and 2:1 biaxial loading.

Application of the coating was made by Photolastic at their Malvern facility. The coated specimens were returned to Denver and stressed in the same equipment used for the cyclic flaw growth work. (A description of the testing machine is included in Chapter V.) Martin Marietta applied the loads and Photolastic performed the stress analysis measurements.

The following observations were made on the basis of the photoelastic study:

1) A stress concentration of about 15-30% was noted on the back smooth face of the panel directly behind the ribs in a direction perpendicular to the rib length. This stress concentration was highest directly behind the point of rib intersection;

2) The central bay section of all panels is essentially an area of plane stress indicating good biaxiality and the absence of large bending stresses through the thickness;

3) Although the corners of intersecting ribs showed steep gradients, the stresses were much less than the nominally applied membrane stresses;

4) Rib thickness did not appear to influence the magnitude of the localized stress disturbance, but did affect the extent of the disturbance.

Results for the photoelastic analysis of panels 1 and 6 have been extracted from Table I, Appendix A, and are summarized in Figures IV-26 and IV-27.

Strain Gage Stress Analysis

Using the results from the photoelastic analysis, appropriate locations and types and sizes of strain gages were selected to obtain complementary strain gage data for comparison of these two experimental analysis methods. The photoelastic coating was removed before strain gage installation.

Plan -
Quadrant of Panel

Typical
Section
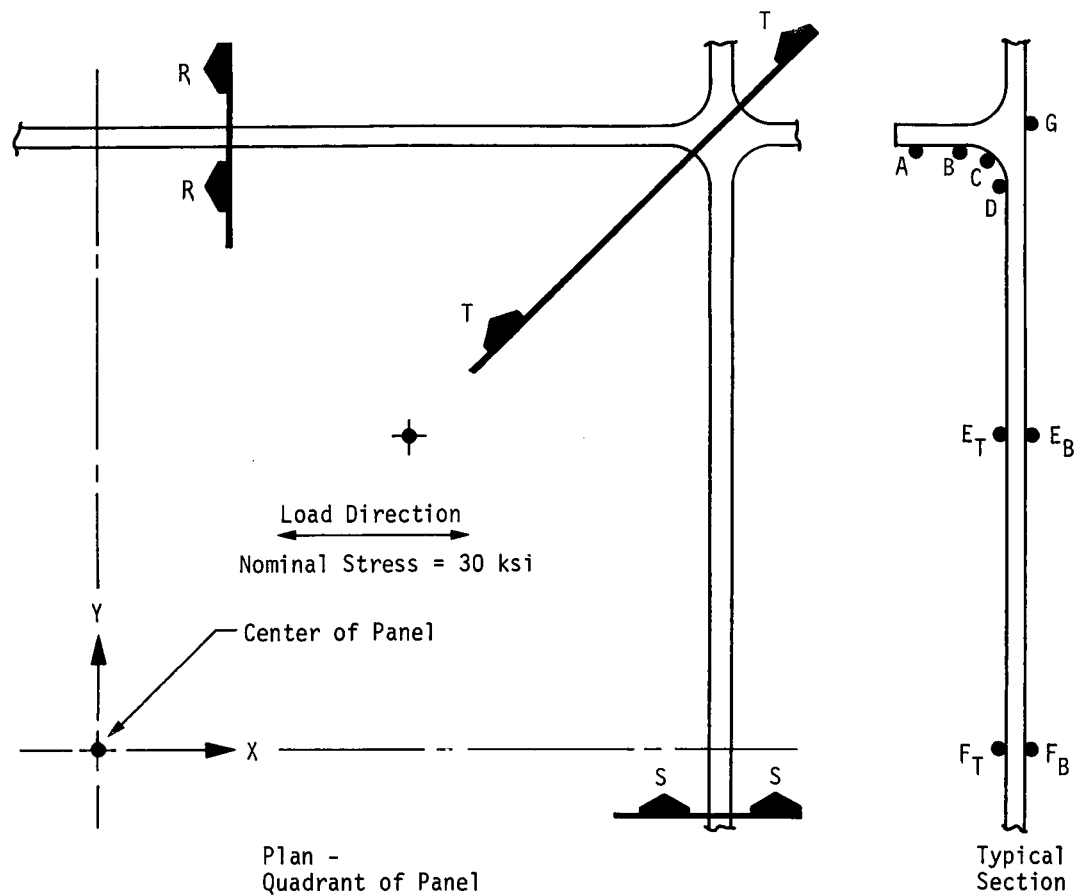
Photoelastic Results									
Section	Top or Bottom	Coordinate Direction	Stress (ksi) at Indicated Location						
			A	B	C	D	E	F	G
R	Top	X	35.0	36.0	34.0				
	Bottom	X							33.0
S	Top	X			5.0	24.0			
	Bottom	X							45.0
T	Top	X	15.0*	9.0*	21.0*		34.0		
	Bottom	X					36.0		47.0
Strain Gage Results									
R	Top	X			20.4	32.3		34.9	
	Bottom	X						34.9	35.2
S	Top	X			-6.1	38.2		34.9	
	Bottom	X						34.9	35.2
T	Top	X			27.3*	33.3	34.9	34.9	
	Bottom	X					34.9	34.9	41.7
*Stress perpendicular to section.									

Figure IV-26   Selected Stress Data from Photoelastic and Strain Gage
Analyses (Panel No. 1, 1:0 Stress Ratio)

Plan -
Quadrant of Panel

Typical
Section

Photoelastic Results									
			Stress (ksi) at Indicated Location						
Section	Top or Bottom	Coordinate Direction	A	B	C	D	E	F	G
R	Top	X	29.0	29.0	26.0	27.0			
	Bottom	X							27.0
S	Top	X			15.0	27.0			
	Bottom	X							34.0
T	Top	X					29.0		
	Bottom	X					29.0		34.0
Strain Gage Results									
R	Top	X	30.2		26.5	28.6		31.0	
	Bottom	X						31.0	24.8
S	Top	X			-2.9	17.9		31.0	
	Bottom	X						31.0	34.7
T	Top	X				37.3	28.8	31.0	
	Bottom	X						31.0	32.2

Figure IV-27   Selected Stress Data from Photoelastic and Strain Gage
Analyses (Panel No. 6, 1:0 Stress Ratio)

A prime consideration in gage selection was the stress gradient found from the photoelastic results. Large rosette gages were used in areas of relatively uniform strain, such as the membrane regions of the central bay. Small stacked rosettes were used at the fillet junction of the two stiffener ribs to determine principal directions. Small uniaxial gage pairs were placed in the fillet areas of the stiffener rib and behind the ribs. Uniaxial gages were orthogonally oriented.

Approximately 28 strain gages were applied to each panel. Gage sizes varied from 1/4 to 1/32-in. (6.4 to 0.8 mm) grid length. All were 120-ohm resistance and were compensated for the thermal expansion of aluminum material. A cyanoacrylate room-temperature curing adhesive was used to bond all strain gages. Customary application procedures were used which include careful surface preparation by chemically cleaning and etching before gage installation. A typical panel gage installation is shown before test in Figure IV-28. Note that all gages are located in the center bay of the panel.

The instrumented stiffened panel was placed in the biaxial test fixture for application of uniaxial and biaxial loads. Each panel was exercised to the maximum required load level to seat the various linkage and pinhole loading points before data acquisition.

Using a B&F digital acquisition system, strain gage outputs were recorded. The strain gage readings were taken as the panel was step loaded to predetermined load levels. (The same loads were used in the previous photoelastic study conducted on the same panels.) The linearity of readings was thus established by having several strain-versus-applied-load points for each unique state of loading.

Loads were applied to achieve a nominal 30 ksi (207 MN/m^2) stress level in both uniaxial and balanced biaxial tension. Strain gage output data was recorded, reduced, and plotted for each gage versus load. A best-fit curve was then drawn through these points to eliminate zero shift effects. The strains obtained were then used to compute principal stresses using rosette and rectangular analysis methods.

Strain gage data for panels 1 and 6 are presented for 1:0 and 1:1 load ratios in Figures IV-26 and IV-27, and IV-28, IV-29 and IV-30, respectively.
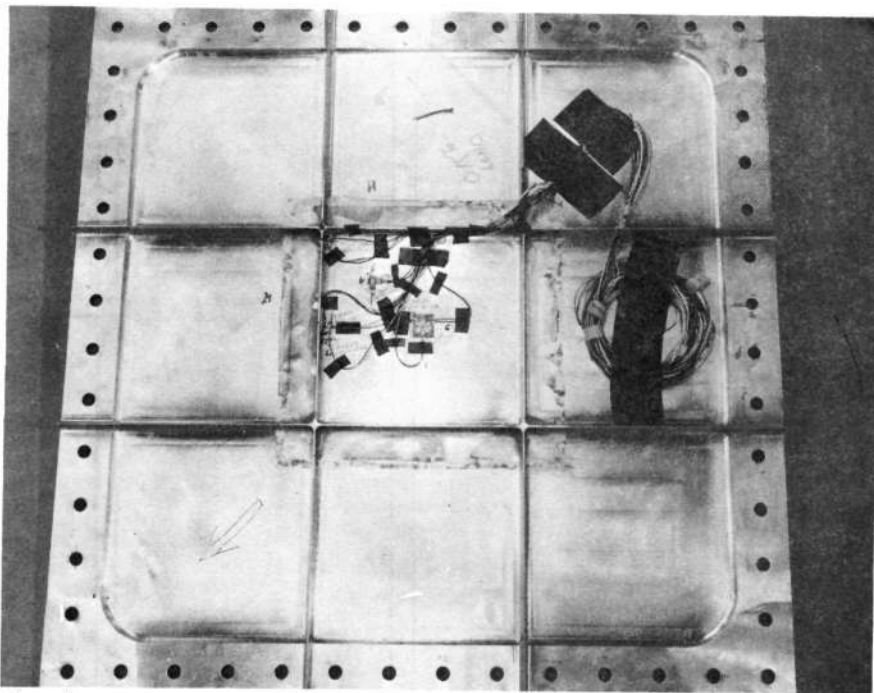
Front
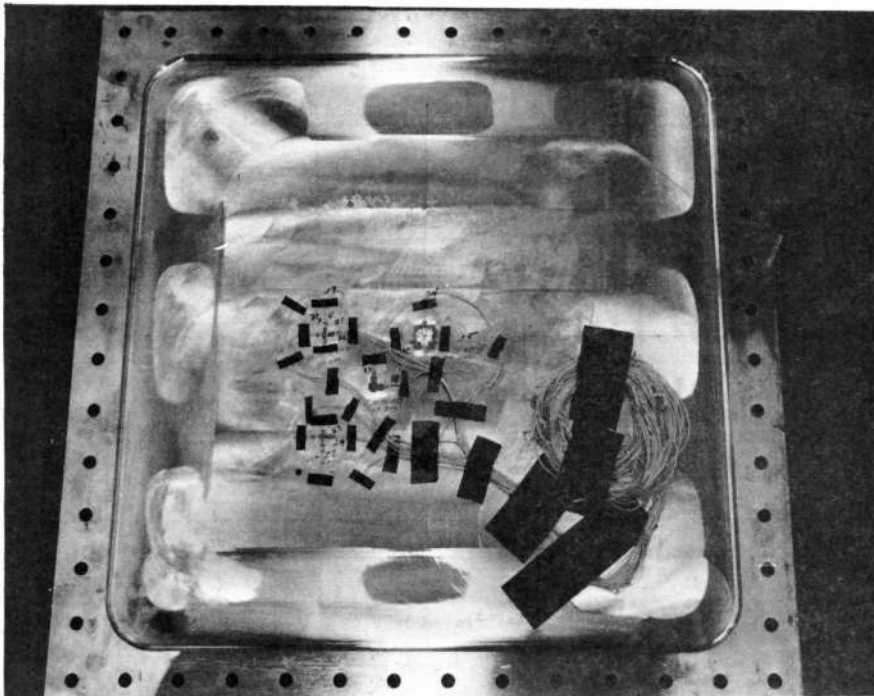
Back

Figure IV-28   Typical Strain Gage Installation
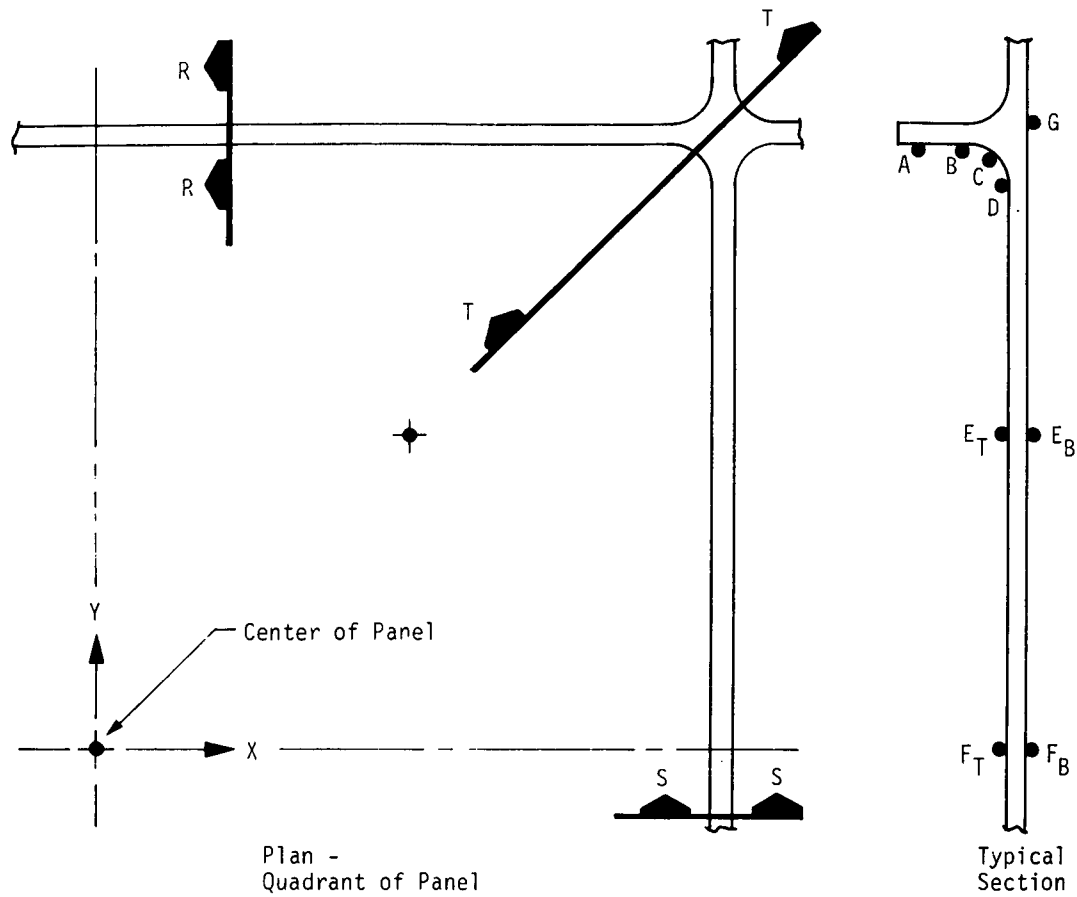
			Stress (ksi) at Indicated Location						
Section	Top or Bottom	Coordinate Direction	A	B	C	D	E	F	G
R	Top	X			9.4	37.4		34.7	
		Y			-9.6	45.2		34.7	
	Bottom	X						34.7	36.1
		Y						34.7	37.8
S	Top	X			-9.6	45.2		34.7	
		Y			9.4	37.4		34.7	
	Bottom	X						34.7	37.8
		Y						34.7	36.1
T	Top	X			20.0*	42.0	34.7	34.7	
		Y			-7.1†	30.4	34.7	34.7	
	Bottom	X					34.2	34.7	30.7
		Y					34.2	34.7	28.5
*Stress perpendicular to section.									
†Stress parallel to section.									

Figure IV-29   Stress Data from Strain Gage Analysis
(Panel No. 1, 1:1 Stress Ratio)
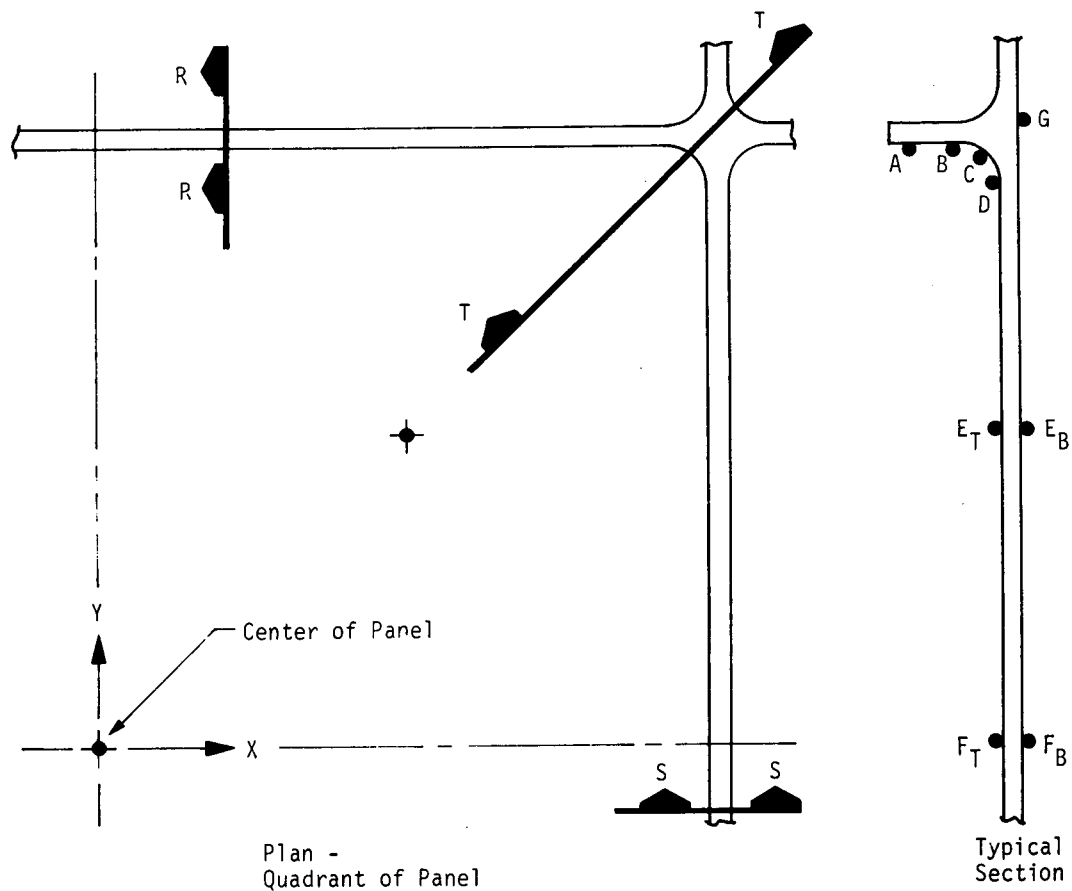
Plan -
Quadrant of Panel

Typical
Section

Section	Top or Bottom	Coordinate Direction	Stress (ksi) at Indicated Location						
			A	B	C	D	E	F	G
R	Top	X	21.3			22.1		27.5	
		Y				9.2		29.0	
	Bottom	X						27.5	25.9
		Y						29.0	
S	Top	X			-3.8	18.2		27.5	
		Y			17.1	19.0		29.0	
	Bottom	X						27.5	31.6
		Y						29.0	28.8
T	Top	X			8.5*	38.5	27.0	27.5	
		Y			-4.9†			29.0	
	Bottom	X						27.5	25.6
		Y						29.0	25.6

*Stress perpendicular to section.

†Stress parallel to section.

Figure IV-30   Stress Data from Strain Gage Analysis
(Panel No. 6, 1:1 Stress Ratio)

Analysis of the data shows that an area of high stress concentration appears to be on the rib side of the panel in the fillet region (location D in the four schematic diagrams cited previously). The maximum stress concentration was approximately 40%. A second region that exhibited some stress concentration was behind the rib on the smooth surface of the panel (location G). Although this region did not show concentration in all cases, a concentration of 20% was shown for panel No. 1 under 1:0 loading.

Biaxial stresses in the central region of the panel (location F) were quite consistent with a small variation in stress through the thickness of the material of Panel No. 6 under 1:1 loading.

Residual Stress Measurement

Residual stresses were determined on two welded biaxial panels. These panels were processed in the same manner as those used for welded flaw growth data. As noted earlier, these panels were prepared from 1/2-in. plate that was chem-milled to 1/4 in., welded, and then mechanically milled to 1/8 in.

The technique used for this work was to remove metal surrounding miniature strain gages and determine the change in strain attendant with the relief of residual stresses. Strain gages with a 1/32-in. grid size were bonded in both the longitudinal and transverse directions (with respect to welding direction) at the weld and heat affected zone regions. These gages are sufficiently small to characterize strain distribution in the region of the weld without significantly masking or averaging peak reading, which would occur if larger gages were used.

After application of strain gages to the selected areas and strain measurement (Fig. IV-31), the panel was coated with a chemical milling maskant. The maskant was then carefully stripped from the region surrounding each gage to allow chemical attack. After sufficient material is chem-milled from the region surrounding each gage, the process is halted, the coating removed, and the strain is again measured. Temperature is carefully monitored at the time of each reading.* The chemical milling technique allows material to be removed from around the strain gage without introducing mechanical stresses or damage to the gages and yet achieves the degree of isolation or separation from the surrounding metal necessary to obtain accurate residual measurements.

---

*Although the strain gages were temperature-compensated for aluminum, the precise nature of the work required additional correction.
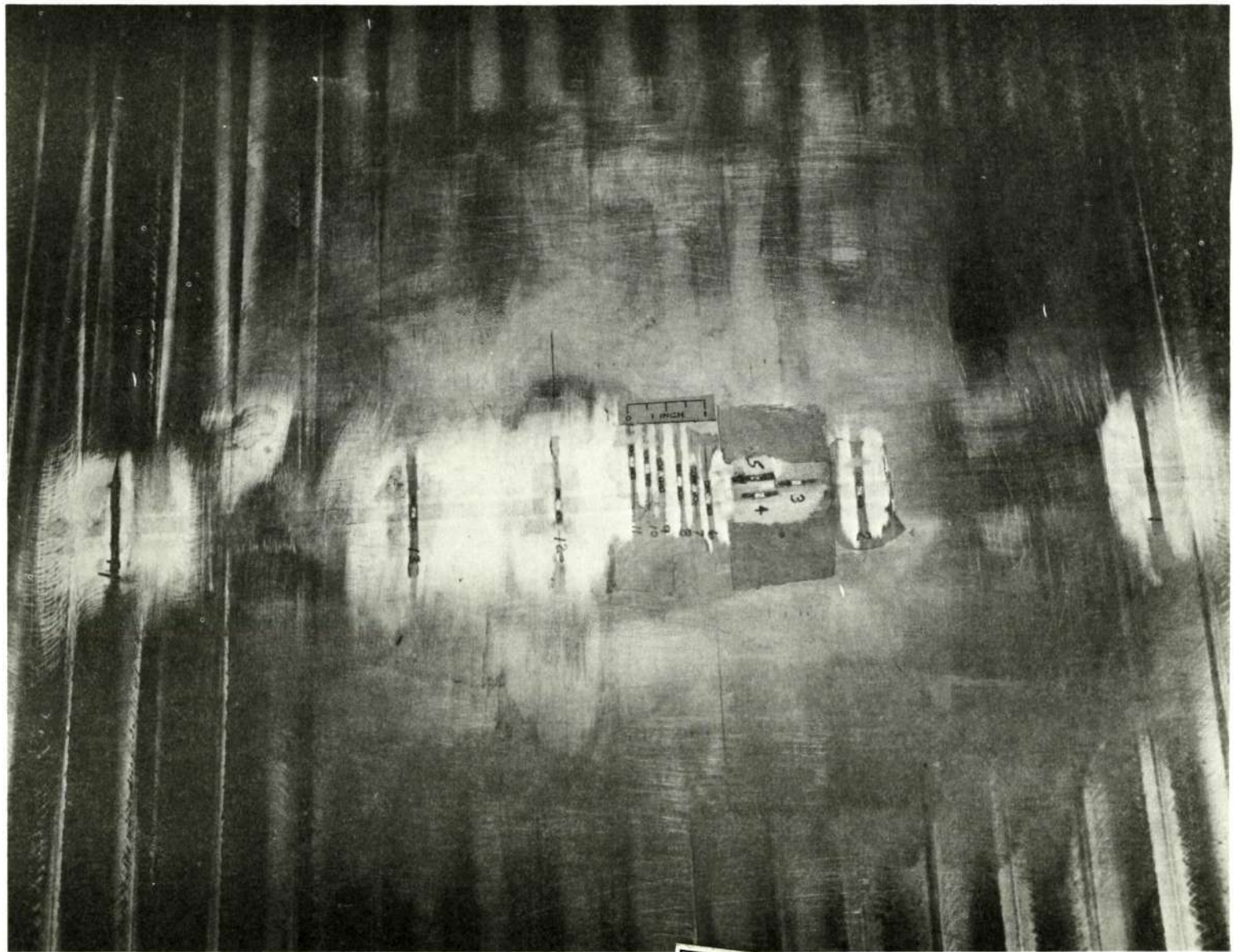
Figure IV-31   Strain Gaged Weld Panel

Experimental data from both panels are summarized in Figure IV-32. The data is graphically presented as a function of gage location in Figure IV-33. The longitudinal data shows a residual stress level of 7.8 ksi (54 MN/m²) at the weld centerline. Residual stress increases to a peak of over 29 ksi (200 MN/m²) and then starts to decrease. These findings are not typical of the results we have obtained in other work on aluminum alloys, where the longitudinal residual stress is constant (at a peak level of approximately 20 ksi [138 MN/m²]) across the weld zone and into the heat affected zone and then starts to decrease. However, in our past work, we have measured residual stresses on as-welded material where the only material removal has been bead shaving. In this work, removal of half of the weld thickness would be expected to reduce residual stresses. It is interesting to note that although the residual stress in the weld centerline was low, the residual stress 0.3 in. (7.6 mm) from the centerline (heat affected zone) was surprisingly high. A more uniform decrease of residual stress would have been anticipated as a result of material removal. The longitudinal residual stress along the centerline of the weld was uniform in the central portion of the panel, decreasing with proximity to the ends of the panel, as expected (Fig. IV-33B).

The transverse residual stress was compressive (-11 ksi [-76 MN/m²]) at the weld centerline, increasing to approximately 20 ksi (138 MN/m²) tension at a distance of 0.3-in. (7.6 mm) from the weld centerline.

The residual strains measured were used to compute stresses in both longitudinal and transverse directions. The effect of the biaxial state of stress was considered in these computations. All data for the plots in Figure IV-33A were obtained from gages placed within the central portion of the weld panel where the longitudinal residual stress appeared to be constant. A backside strain reading obtained in the center of the panel showed a very small bending stress through the thickness which was ignored in computations.

D.   COMPARISON AND DISCUSSION

A comparison of the theoretical and experimental stress analyses showed rather good agreement. Although some of the very sharp gradients predicted by the theoretical analysis could not be found experimentally, the agreement in some cases (i.e., Panel No. 1, 1:0 loading ratio and Panel No. 6, 1:0 loading ratio) was remarkably good.
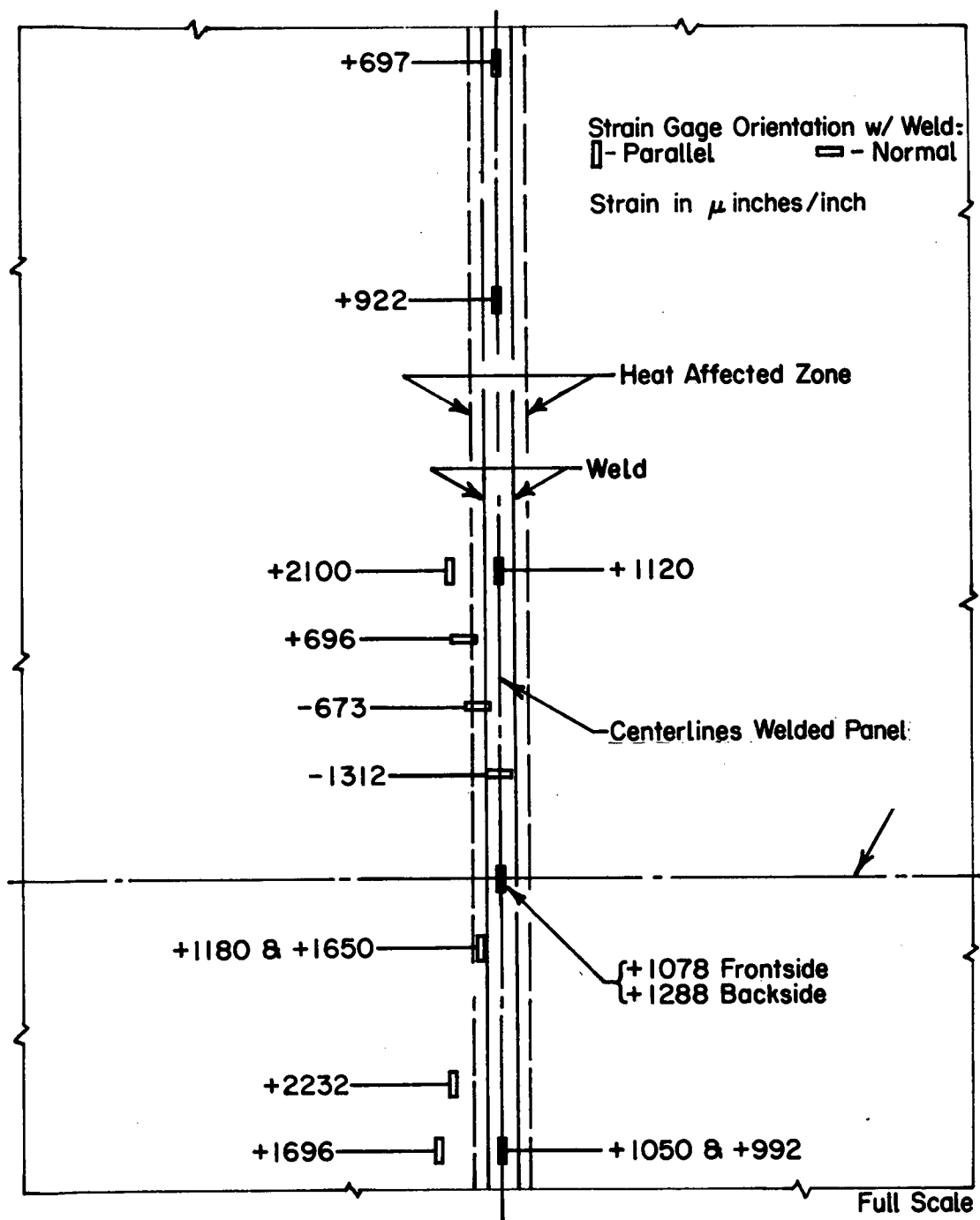
Figure IV-32   Strain Gage Location and Residual Strain Readings
for Welded 2219-T87 Aluminum Residual Stress
Measurement
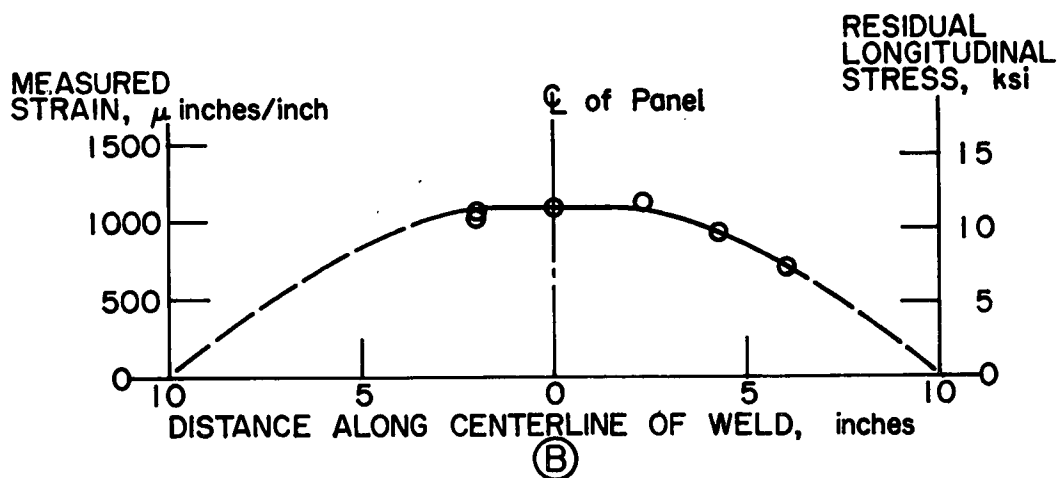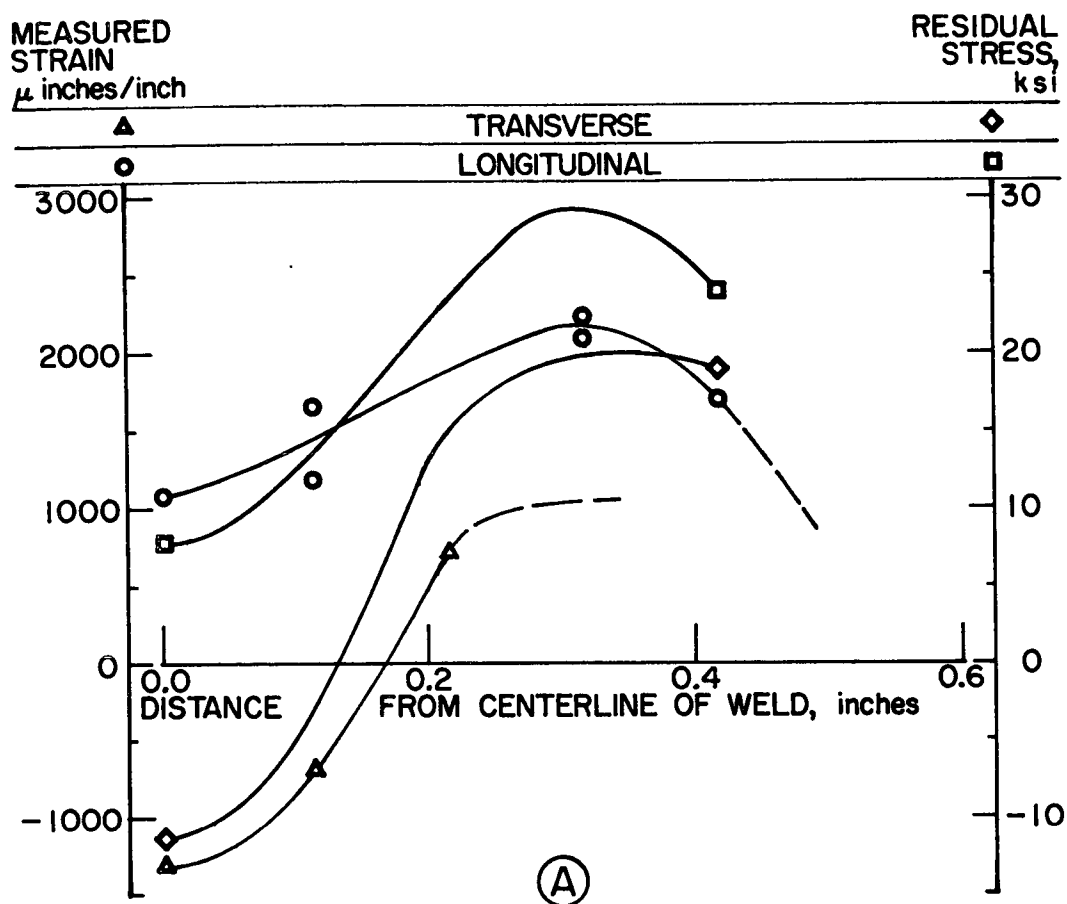
Figure IV-33 Residual Stresses in Welded 2219-T87 Aluminum

The 1:0 loading ratio data are summarized in Figures IV-34 and IV-35 for the two experimental techniques. These comparisons are restricted to the photoelastic and strain gage methods since the theoretical analysis was performed only for biaxial loading.

Figure IV-34 (Panel No. 1) shows similar behavior in the membrane area. The stress perpendicular to the rib decreases sharply at the fillet from both strain gage and photoelastic measurements.

The stress parallel to the rib shows no variation with respect to location according to photoelastic stress measurements; however, the strain gage curve shows a decrease in the fillet region. Note that the strain gage data are not measured over the same range of length as the photoelastic measurements; hence, the basic for comparison is limited.

Figure IV-35 (Panel No. 6) shows very good agreement for both methods with respect to both perpendicular and parallel stresses. The agreement for the parallel stresses is within 2 ksi (14 MN/m^2).

For the 1:1 (balanced biaxial) loading ratio, the comparison is restricted to the theoretical finite element analysis and strain gage analysis. A comparison with the photoelastic measurements cannot be made because this method does not resolve the stress values. The photoelastic technique establishes points of high stress gradient and principal stress directions; however, stress data is given in terms of stress difference ($\sigma_1 - \sigma_2$) only and cannot be used for comparison with the other two methods.

Data for Panels No. 1 and No. 6 are given in Figures IV-36 and IV-37, respectively. The former panel shows good agreement between the theoretical and experimental analyses, particularly for the magnitude of the peak stress and the gradient at the beginning of the fillet. For Panel No. 6, the strain gage analysis did not detect the peak at the beginning of the fillet as shown by the theoretical analysis.

In general, the strain gage measurements show lower stress values than the theoretical analysis predicted. Several reasons are apparent to explain this difference. First, even the smallest size strain gage, 1/32-in. (0.8 mm) grid, may miss or average sharp stress concentrations. Second, the strain gage analysis measures surface behavior, whereas the theoretical analysis actually yields subsurface data. The centroids of the finite elements closest to the surface are 1/64-in. (0.4 mm) from the actual surface. In addition, it should be noted that the theoretical two-dimensional analysis was performed only for Panel No. 6.
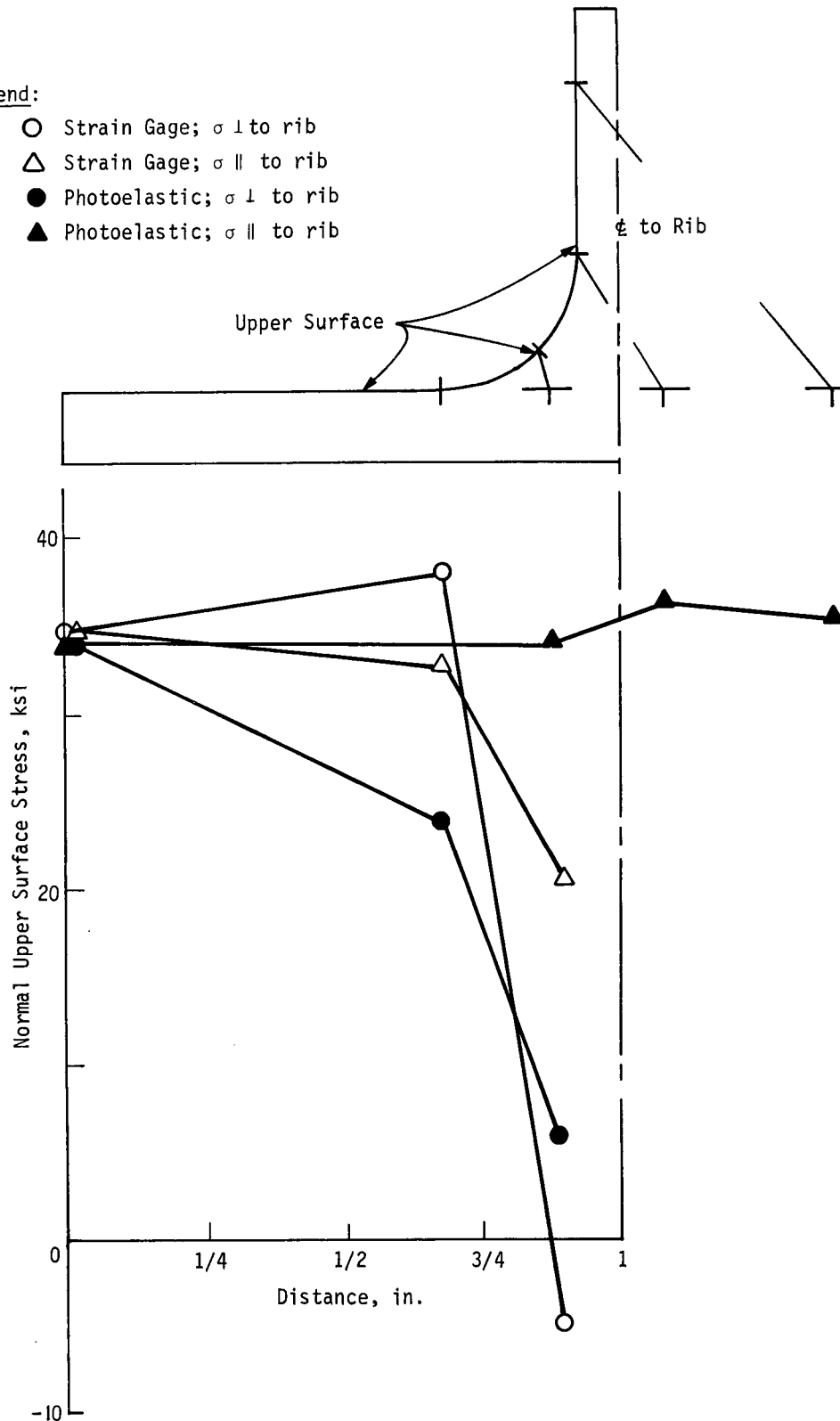
Figure IV-34 Comparison of Surface Stresses (Front Face) by Strain Gage and Photoelastic Measurements, Panel No. 1, 1:0 Loading

Legend:
○ Strain Gage, σ ⊥ to rib
△ Strain Gage, σ ∥ to rib
● Photoelastic, σ ⊥ to rib
▲ Photoelastic, σ ∥ to rib
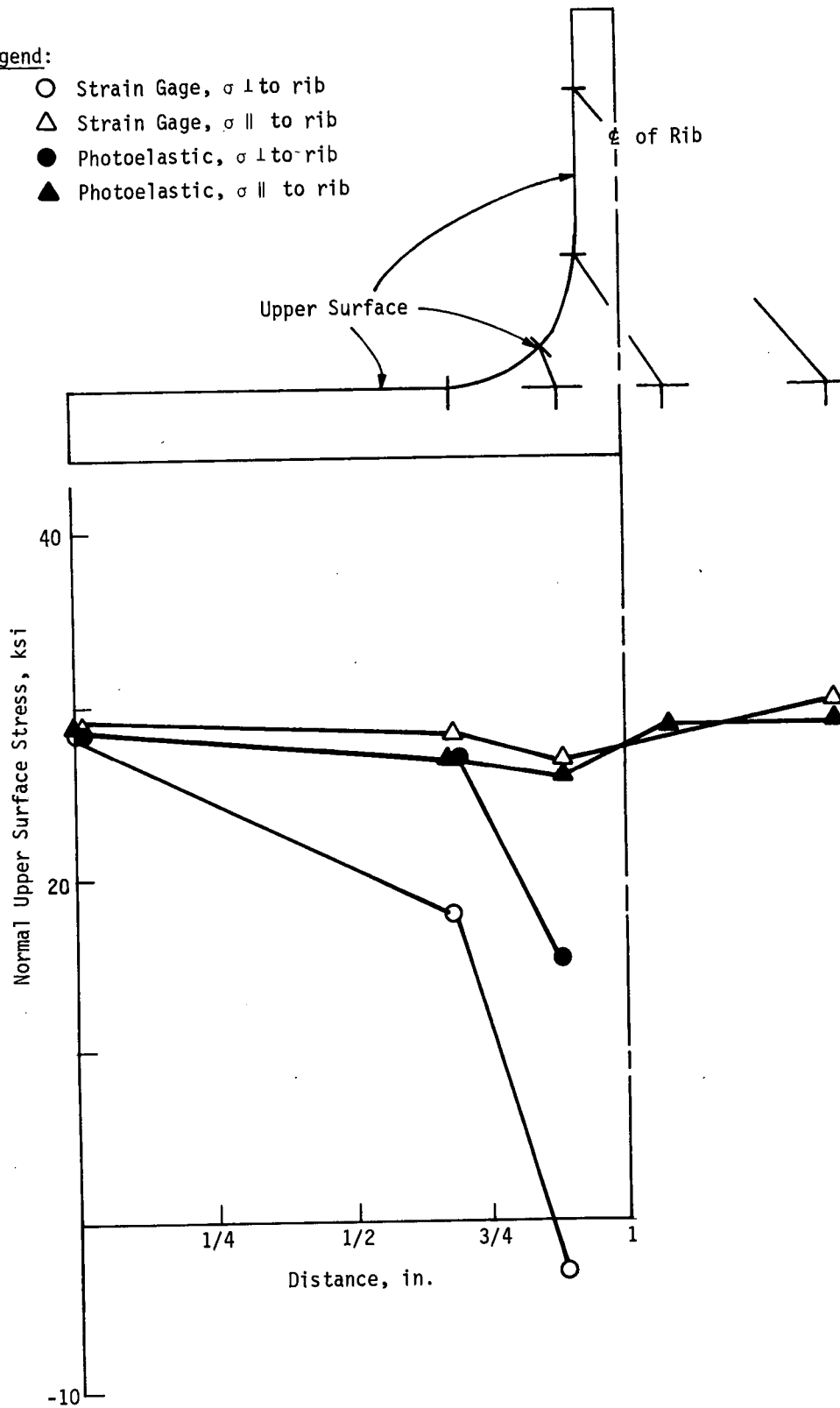
Figure IV-35 *Comparison of Surface Stresses (Front Face) by Strain Gage and Photoelastic Measurements, Panel No. 6, 1:0 Loading*
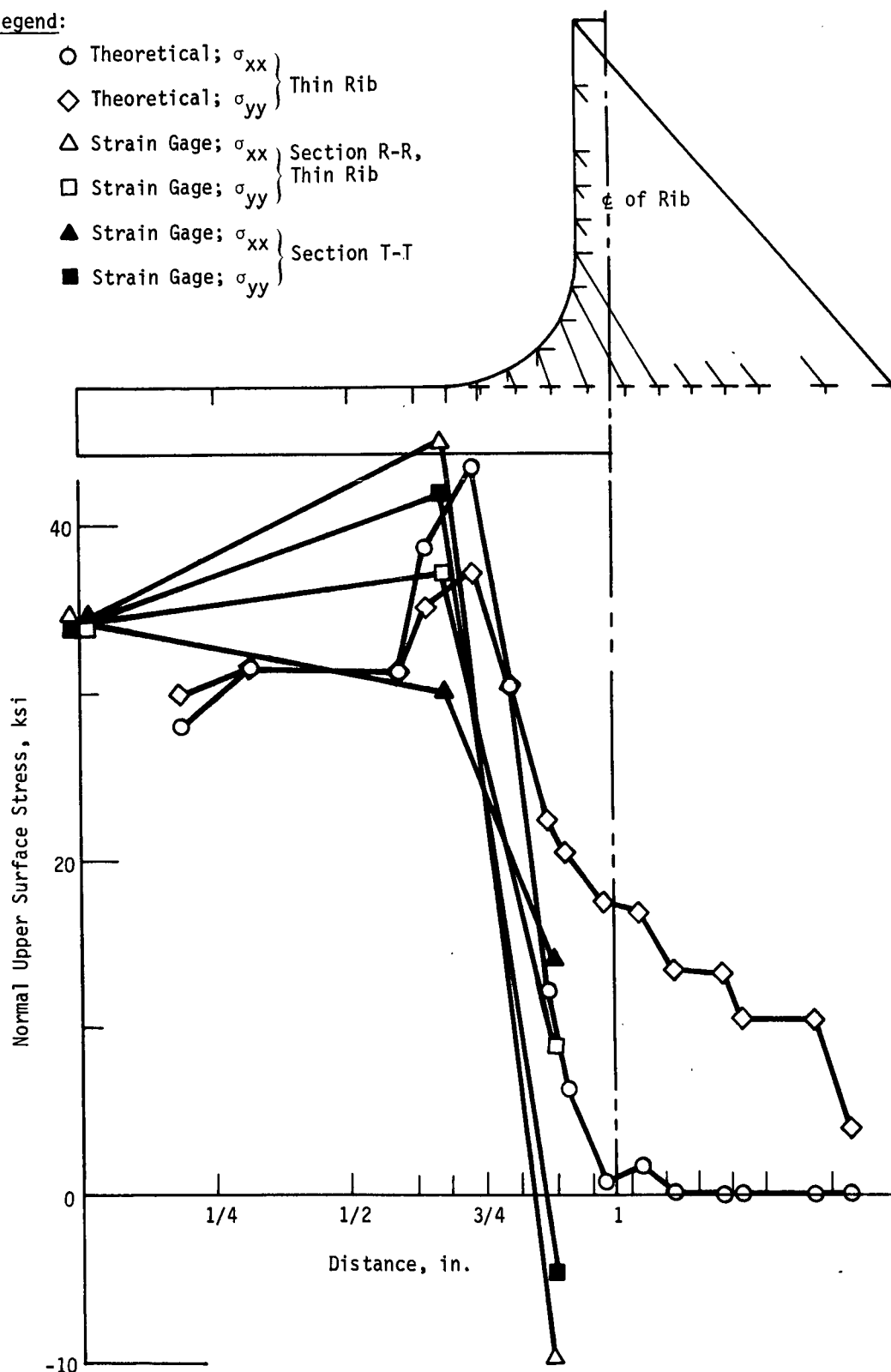
Figure IV-36   *Comparison of Surface Stresses (Front Face) by Theoretical and Strain Gage Analyses, Panel No. 1, 1:1 Loading*
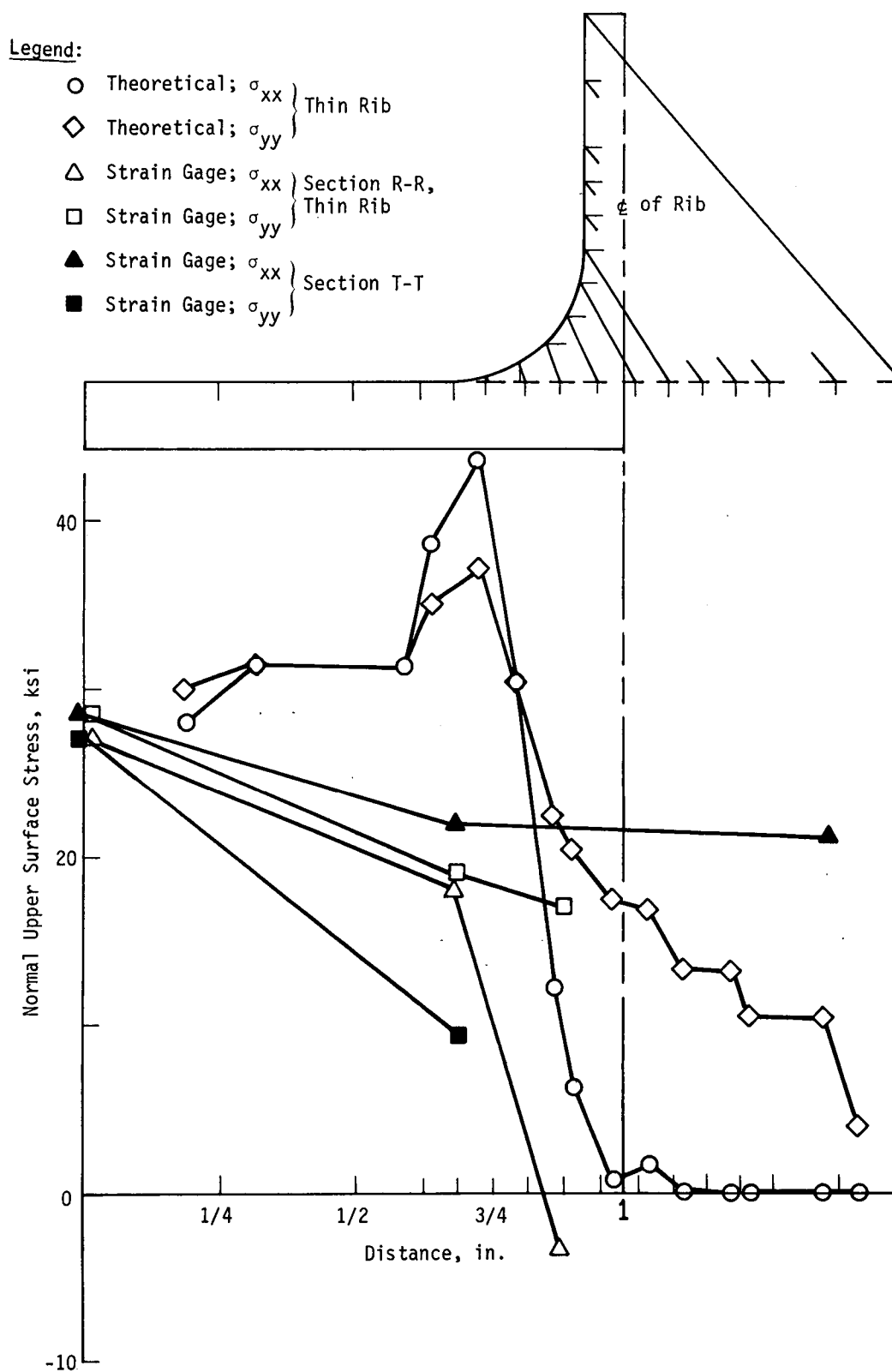
Figure IV-37   Comparison of Surface Stresses (Front Face)
by Theoretical and Strain Gage Analyses,
Panel No. 6, 1:1 Loading

In summary, for the 1:1 data, we find that the finite element re-
sults show a sharp stress gradient at the intersection of the fillet
and membrane. This result was confirmed in Panel No. 1 but not in
Panel No. 6. The finite element analysis shows the gradient to be
very narrow; the change in stress in a 1/32-in. (0.8 mm) region is
12 ksi (83 MN/m^2). Hence, it is easy to miss such a sharp gradient
using experimental techniques. Based on our success in finding
the gradient in one of our two attempts, we must conclude it does
occur and the magnitude (approximately 1.4 stress concentration
factor) is realistic. The gradient may actually be steeper than
the theoretical analysis predicts, since some of the strain gage
readings indicate compressive stresses at locations further along
the fillet. The other region that exhibits stress concentrations
is the back surface of the panel behind the rib. Both strain gage
and theoretical predictions show a region of concentration wider
than in the fillet, but of lower stress magnitude. In this re-
gion, concentration does not appear to exceed 20%.

The data from these analyses were used for selection of sites for
flaw growth measurements made on the six stiffened panels.

The finite element used is a compatible element; thus, convergence
of potential energy with decreasing element size is assured. The
element is a constant stress element, hence its calculated values
represent average stresses over the element volume. Comparisons
with other mesh sizes were not made but the agreement with measured
stress volumes indicates the mesh size was sufficiently fine to
establish trends for the configuration and loading considered. A
finer mesh or higher order element would provide a sharper defi-
nition of stress distribution but computer storage and economic
restraints must set limitations.

V. FLAW GROWTH BEHAVIOR

That part of the program dealing with cyclic flaw growth behavior for uniaxially and biaxially loaded specimens of both parent metal and welded material is presented in this chapter.

A. EQUIPMENT AND METHODS

A biaxial testing machine was designed and constructed for evaluation of 28-in. (711 mm) square panels at loads up to 200 kips (896 kN). The machine is a simple, welded 20-ft (6.1 m) square structure whose principal elements are 24-in. (61 cm) I-beams welded together with a 1-in (25 mm) thick gusset plates at each corner. Load train details are bolted to this framework.

The hydraulic system for the machine is closed loop servo controlled. Each channel is independently controlled to provide for variable loading ratios.

Alignment of each loading axis was performed by transit measurements and adjustment of the fixed grip ends. Orthogonality was also confirmed using the transit. Following alignment, an unstiffened panel strain gaged with four rosette and two unidirectional gages was installed in the machine and loaded to confirm uniformity of stresses in the central portion of the panel and to provide a load versus stress calibration.

The rosette gages were placed at the corners of an imaginary 4-in. (102 mm) square in the center of the panel to determine in-plane variations. These locations were those where defects would be subsequently introduced. The uniaxial gages were located on each surface at the panel center to detect bending.

The panel was incrementally loaded (1:1 stress ratio) in the stress range of 20-40 ksi (138-275 MN/m^2). The variation in applied load averaged less than ±1 percent. The resulting stress field showed biaxiality within ±2.3 percent. The principal stress variation through the thickness (each side of the panel) was ±2.5 percent. This outstanding result is indicative of the precautions taken in design, analysis, and fabrication of the machine and specimens.

The panel, previously loaded to prove biaxiality, was incrementally loaded to establish the necessary applied load to give a biaxial center panel applied stress of 30 and 40 ksi (207 and 276 MN/m^2). Stresses were computed from strain data using an elastic modulus value of 10.5×10^6 psi (721×10^3 MN/m^2).

Uniaxial crack growth testing was performed in a 100-kip (448 kN) MTS closed loop servo controlled testing machine. Each specimen contained two flaws located 3.0 in. (76 mm) apart to ensure freedom from interactions. The uniaxial test specimen configuration is shown in Figure V-1.

All flaws were introduced using electrodischarge machining (EDM). Because of the criticality of the number of cycles required to initiate growth in the biaxial panels, extreme care was taken to ensure reproducibility of the starter notches. All work was performed by a single operator using a single machine. A two-step process was used for electrodischarge machining. The initial machining was accomplished with a rather blunt tool to provide a sufficiently large cavity for fluid circulation and flushing action; for machining to final depth, the tool was sharpened to a fine tip and reinserted. Figure V-2 shows an example of the resulting starter defect.

It was originally planned to use uniaxial coupons to determine the number of cycles to cause crack initiation so that the biaxial panels could be tested without prior fatigue sharpening. The number of cycles required to cause initiation was subtracted from the total number of load cycles applied, and the net difference was used for growth rate determinations. As shown by the experimental data presented in the Section B, this technique was not sufficiently precise; therefore, it was necessary to mark the flaw. The technique of varying stress, frequency, and stress ratio for marking purposes could not be used for this work. Staining was selected as the only available technique. NaOH solution (10%) was used as the etchant to provide a subtle stain. In order to stain without removing specimens from the testing machine, small plastic reservoirs were attached to the flaws; the specimens were cycled several times in the presence of the staining solution to assure intimate contact with the crack front. After removal of the reservoir, the area was cleaned and heated until the flaw was dry. Subsequent flaw growth was then readily measured. This staining technique has been shown by NASA/MSC (Ref 5) and Lockheed (Ref 6) to have no effect on flaw growth rate.
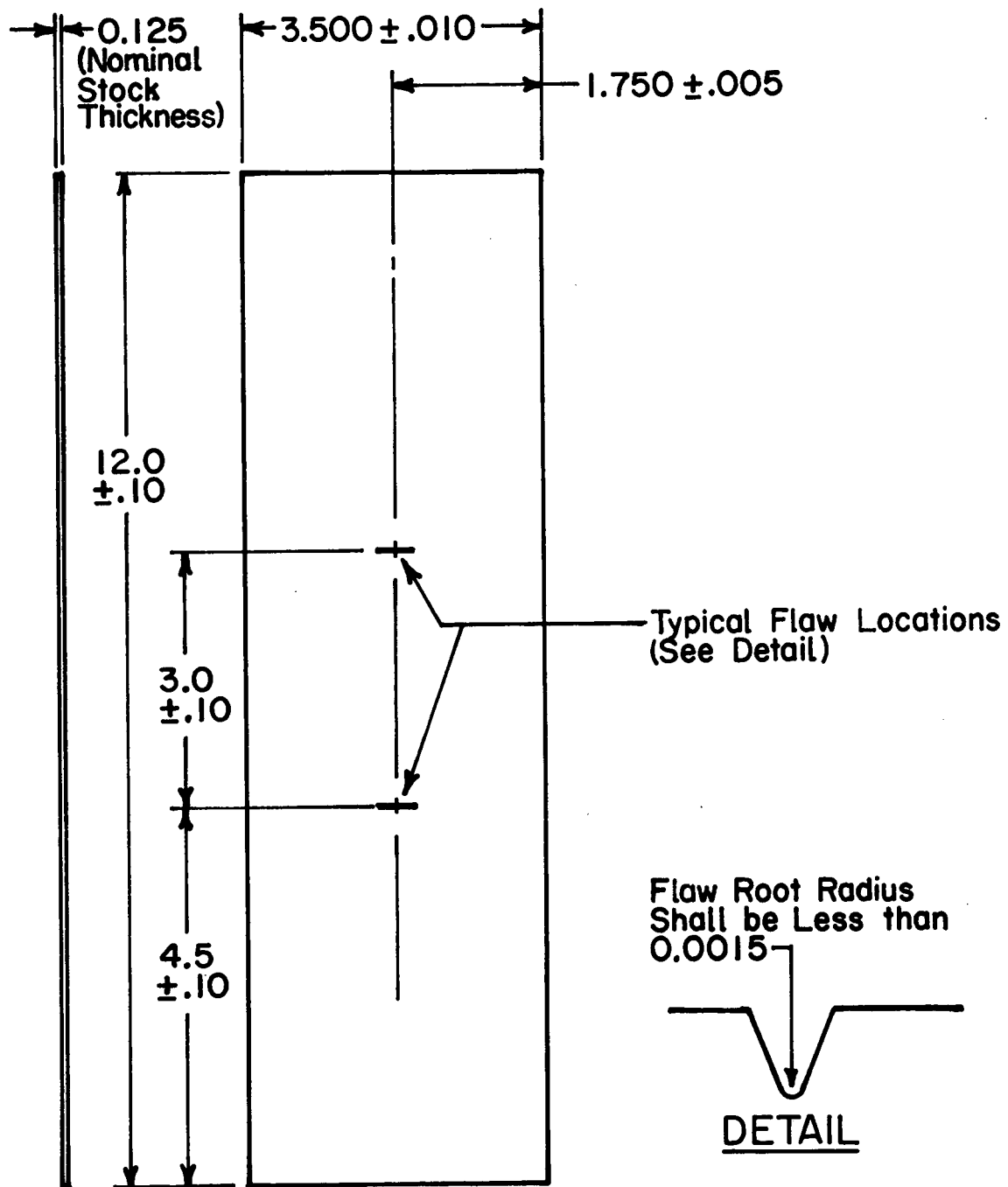
Figure V-1 Uniaxial Flaw Growth Sample Configuration
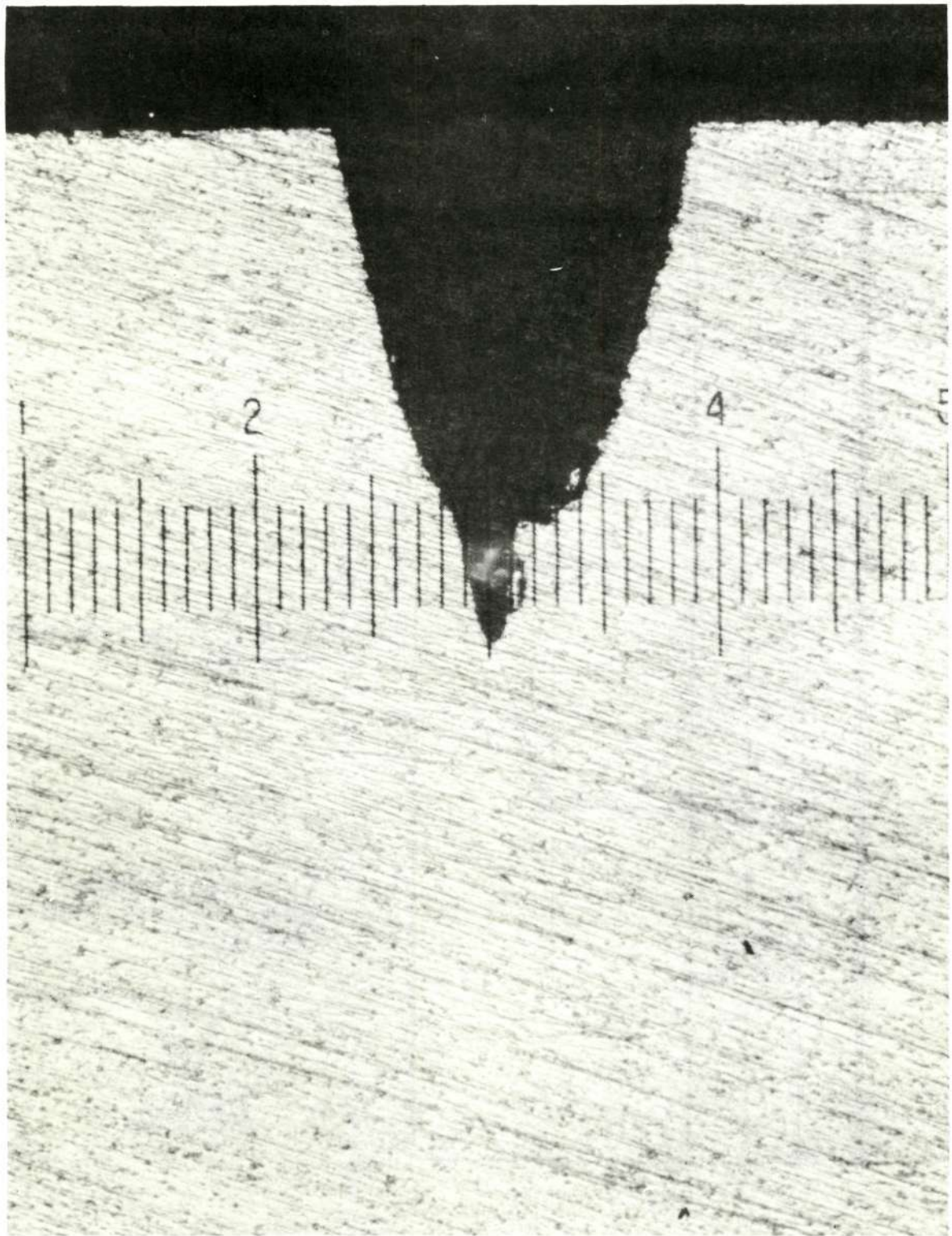
Figure V-2   Macrosection of Electrodischarge Machined Starter
             Defect [one division = 0.001 in. (0.025 mm)]

V-4

B.   UNIAXIAL FLAW GROWTH BEHAVIOR

Uniaxial flaw growth properties were determined for both parent metal and welded 2219-T87 material. Detailed data for both conditions are given in Appendix A, Tables A-2 and A-3.

Parent metal data are presented graphically in Figure V-3. With the exception of two data points, scatter was relatively small.

As noted in the preceding section uniaxial data was originally intended to provide information with respect to the number of cycles required for flaw initiation. The appropriate data, extracted from Appendix A-3, is presented graphically in Figure V-4. It is clearly shown that the scatter is too large to permit use of this method for predictive purposes.

Weld data are presented graphically in Figure V-5. In the latter, both weld orientations and both defect locations are used to construct a single curve since the effect of these variables is relatively small.

C.   BIAXIAL FLAW GROWTH BEHAVIOR-UNSTIFFENED PANELS

Biaxial flaw growth properties were determined for both parent metal and welded 2219-T87 material. Detailed data are given in Appendix A, Tables A-4 and A-5.

Parent metal data are presented graphically in Figures V-6 and V-7 for the longitudinal and transverse flaw orientations, respectively. The graphical presentations show least square fits for the data (1) plotting all points, and (2) by excluding several data points showing large scatter.

Welded data are presented graphically in Figure V-8. Figures V-9 and V-10 show the flaw locations in the welded panels.
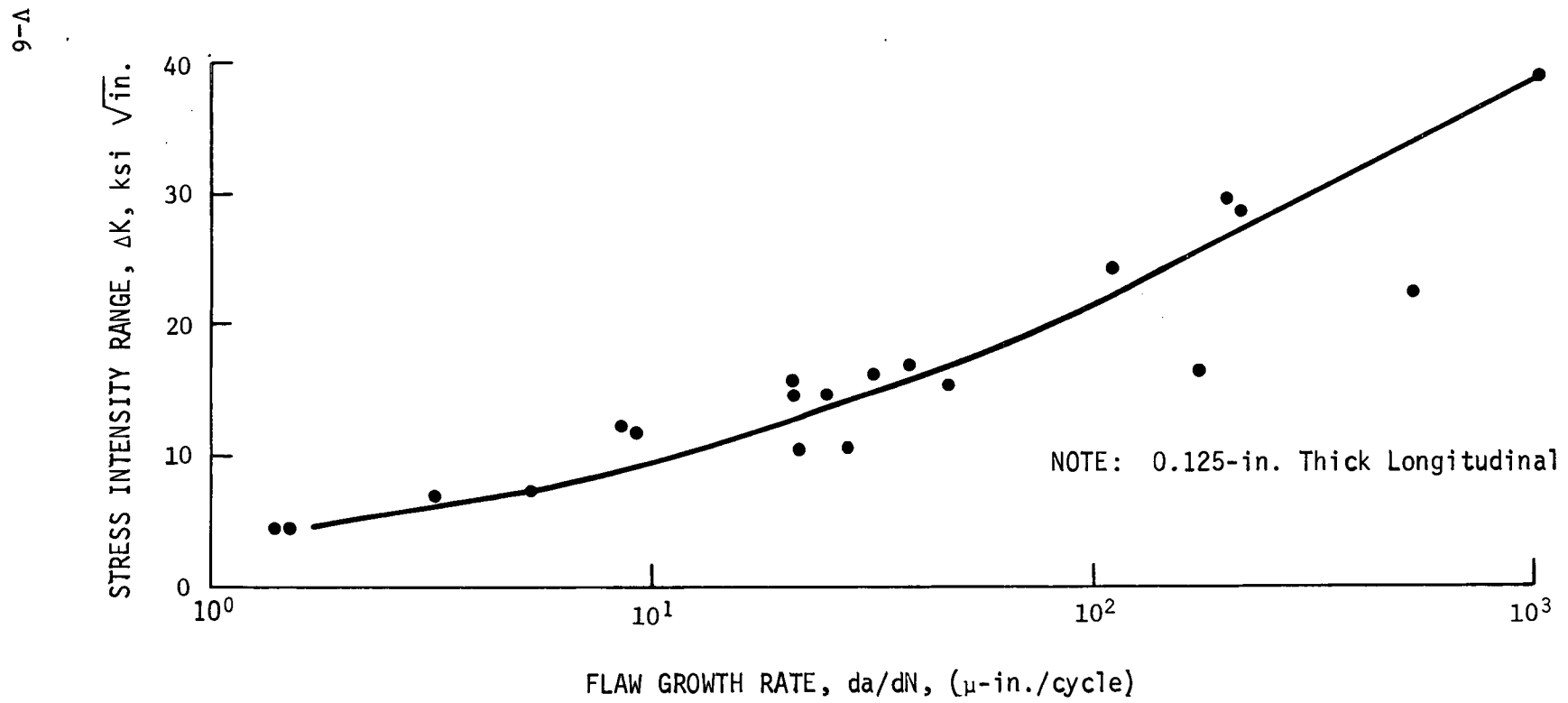
Figure V-3 · Uniaxial Flaw Growth Data for Parent Metal
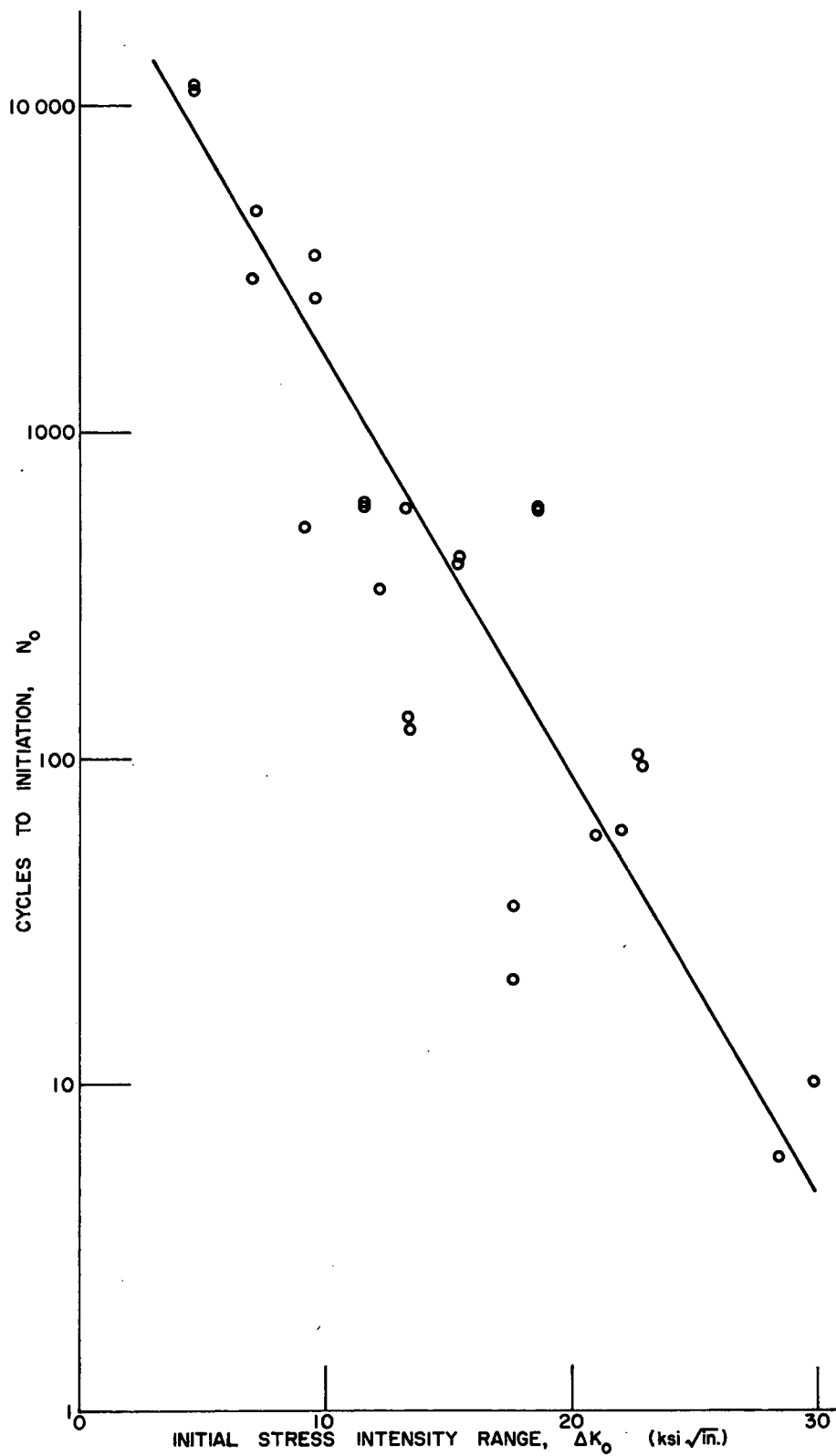
Figure V-4   Flaw Initiation Curve for Parent Metal
2219-T87 Aluminum
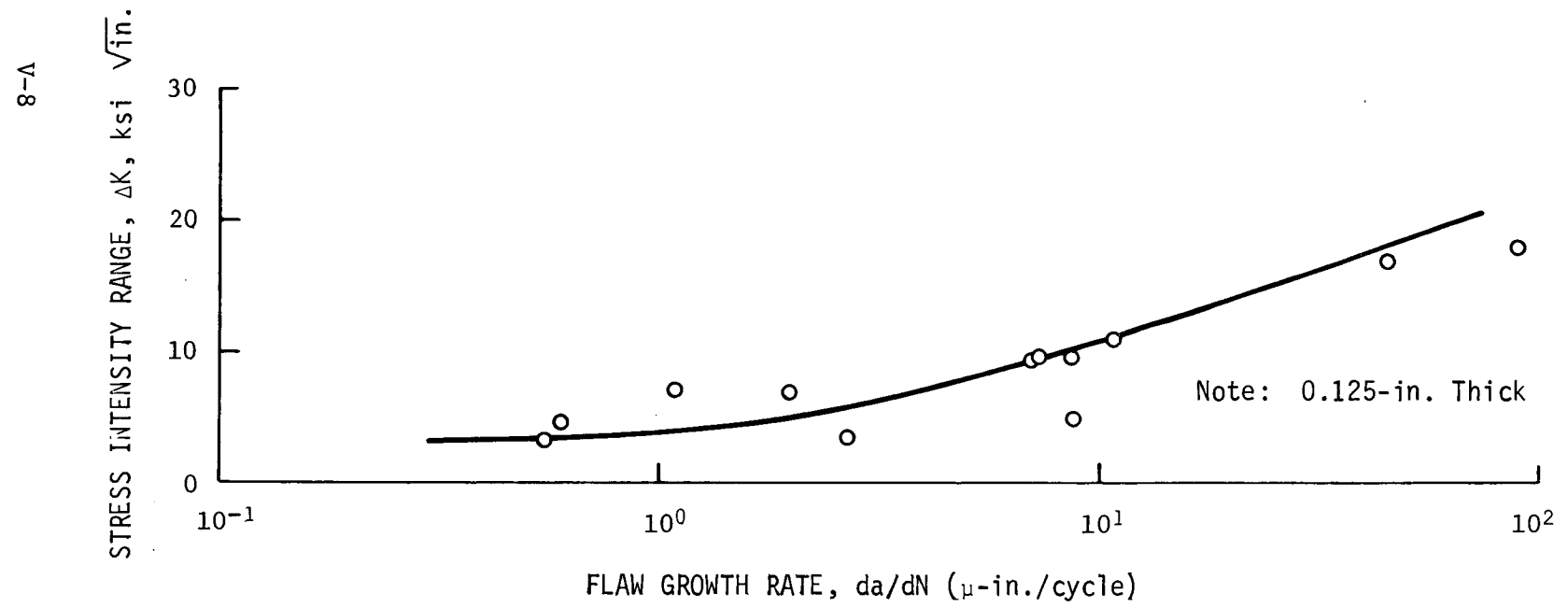
Figure V-5   *Uniaxial Flaw Growth Data for Welded Material*
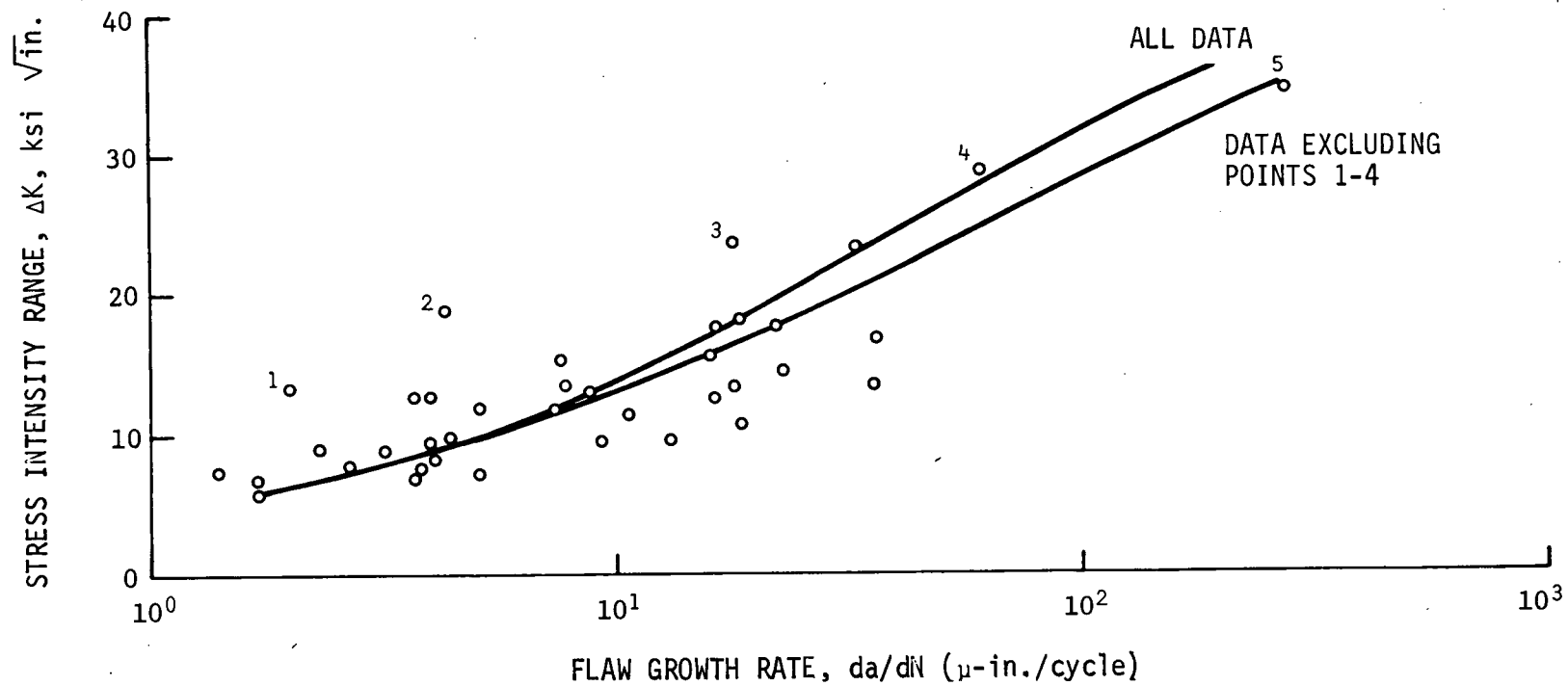
Figure V-6   *Biaxial Flaw Growth Data for Unstiffened Parent Metal Panels,*
            Longitudinal Flaws; 1:1 Stress Ratio
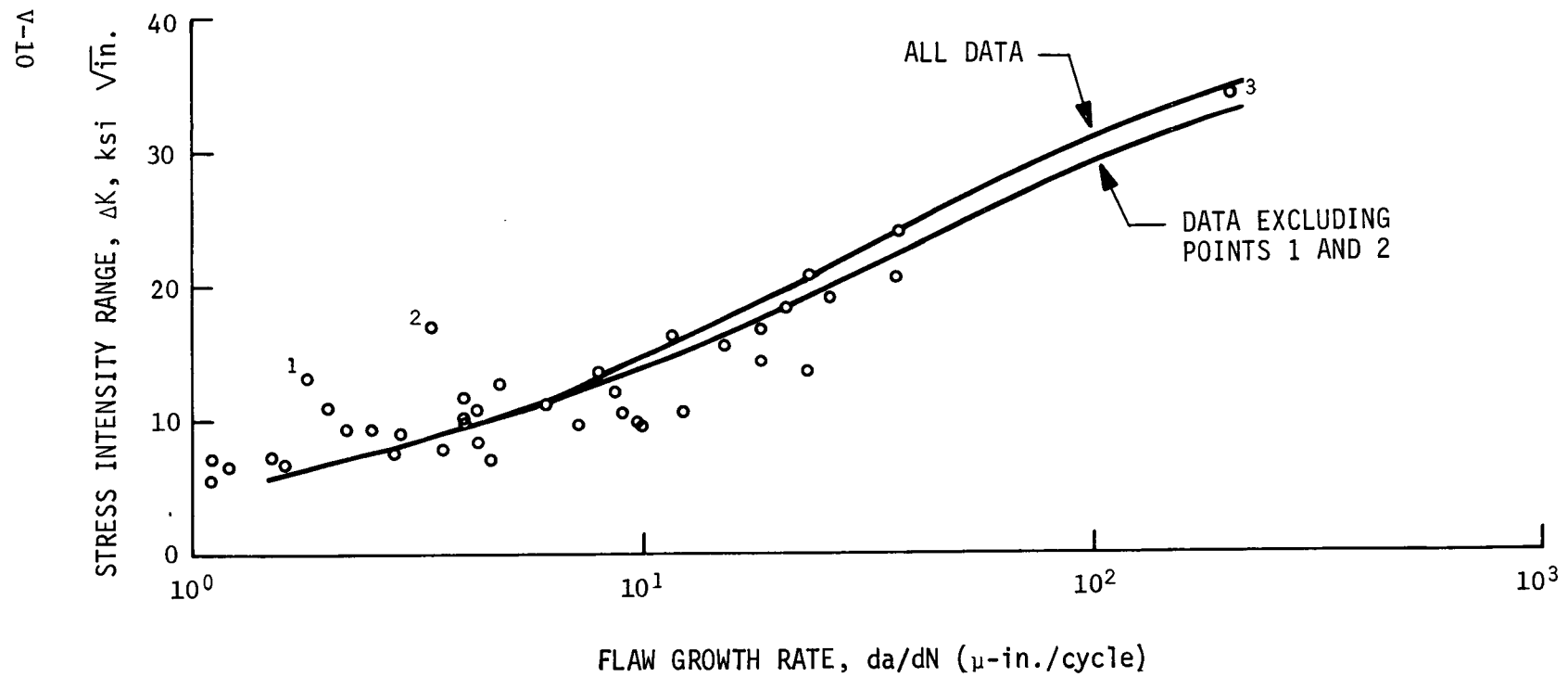
Figure V-7 Biaxial Flaw Growth Data for Unstiffened Parent Metal Panels, Transverse Flaws; 1:1 Stress Ratio
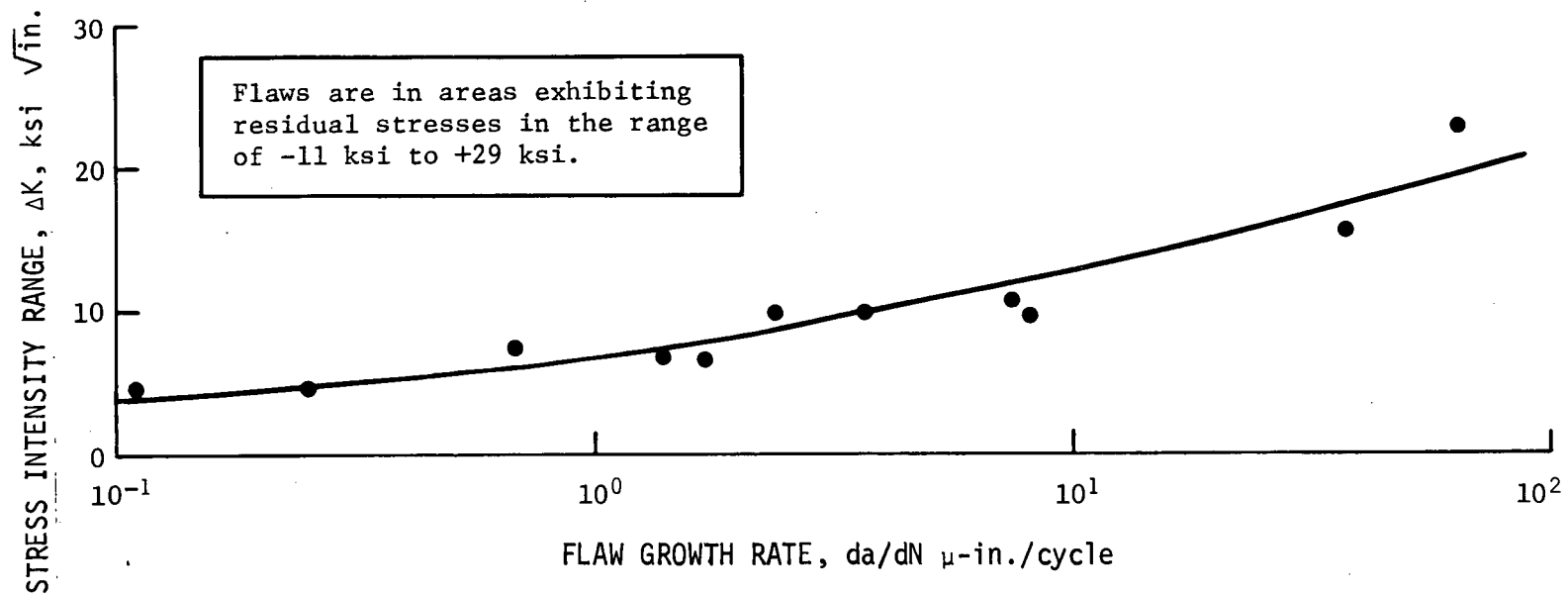
Figure V-8 Biaxial Flaw Growth Data for Unstiffened Weld Panels; 2:1 Stress Ratio

The chart shows STRESS INTENSITY RANGE, ΔK, ksi $\sqrt{in.}$ on the vertical axis versus FLAW GROWTH RATE, da/dN μ-in./cycle on the horizontal axis. A text box reads: "Flaws are in areas exhibiting residual stresses in the range of -11 ksi to +29 ksi."
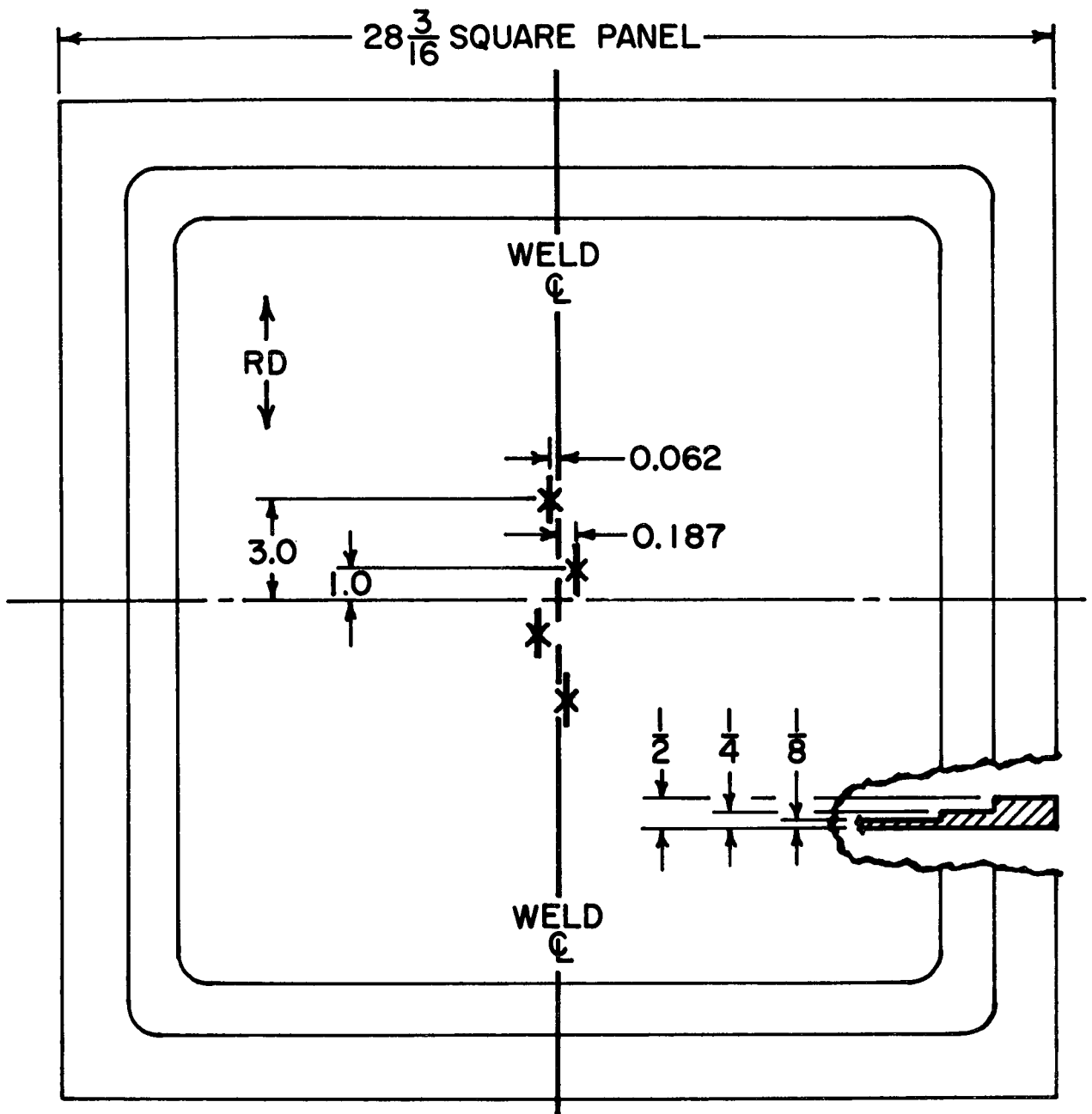
PREFLAW LOCATION DIMENSIONS: Sym about ₵'s
Tolerances. = ± 0.005

*Figure V-9   Flaw Locations in Welded Biaxial Fatigue Panels,
Longitudinal Flaws*

PREFLAW LOCATION DIMENSIONS: Sym about ℂ's

Tolerances = ± 0.005

Figure V-10   Flaw Locations in Welded Biaxial Fatigue Panels,
Transverse Flaws

D.   CRACK GROWTH BEHAVIOR OF STIFFENED PANELS

After the six integrally stiffened panels, designed in Chapter IV (Fig. IV-7) had been subjected to photoelastic and strain gage stress analyses, they were used for flawing and crack growth studies. The preceding analyses required that the panels be pre-loaded up to a load level corresponding to 30 ksi (207 MN/m^2) nominal stress in the biaxial test fixture. These nominal loading levels were used to develop flaw growth behavior in these same panels. All fatigue testing of the stiffened panels was performed under balanced biaxial tensile loading at a nominal 30 ksi (207 MN/m^2) stress level. This testing was performed at a cyclic stress ratio of R = 0 and at a rate of 30 cycles per second.

Starter flaws were placed in critical stress regions indicated by the preceding experimental analyses. These regions include fillet areas (both corners and along ribs) and areas in back of the ribs on the smooth surface. Flaws were also placed in the ribs them-selves, although analyses have indicated this to be a low stress region. All flaws were placed within the central bay area of the panel. No flaws were placed in the central membrane area because an extremely good balanced biaxial field was indicated to be pres-ent in this region, and the preceding unstiffened panel tests pro-vided sufficient data for such a state of loading.

Specific areas for flawing are shown in Figures V-11 and V-12. The slight modification between the two sets of figures was necessary to cover the cases of balanced and unbalanced rib thickness. All flaws within a given panel were of the same configuration, i.e., a/2C and a/t were constant. Four flaw configurations were used in these six panels, 2 a/2C ratios (0.15 and 0.5) and a single a/t ratio of 0.5, based on membrane thickness. Ten starter flaws were placed in each panel.

Six of the ten flaws were in regions of relatively constant stress, i.e., the stress is not likely to vary greatly across the flaw front. These six flaws are represented in sections 4, 5, 7, 8, 9, and 10 in Figures V-10 and V-12 and can be identified in subsequent tables and figures by these numbers, The growth data for these six locations, mentioned above, are given in Table A-6 of Appendix A. (See paragraph V-E.4.)
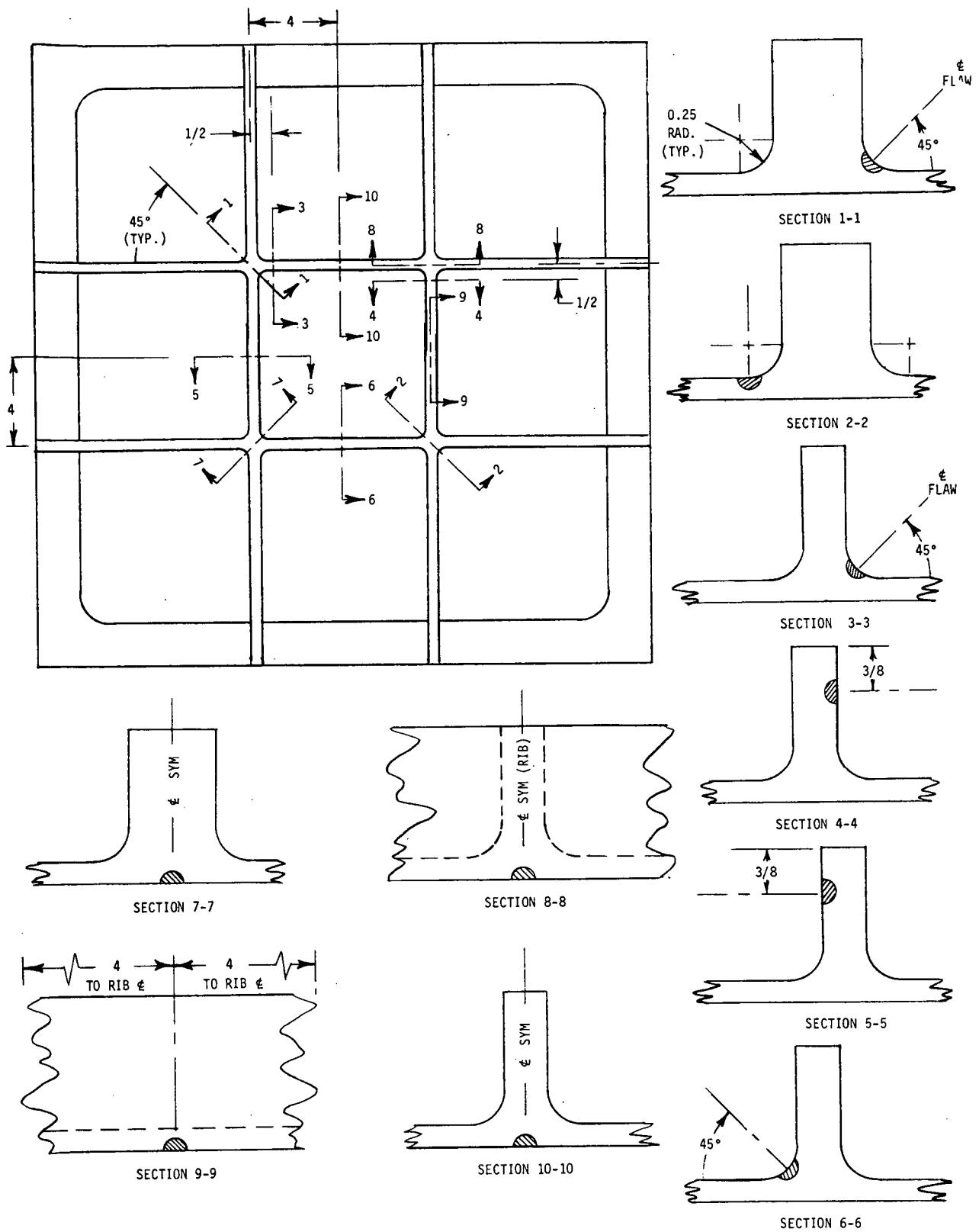
Figure V-11 Flaw Location Diagram for Stiffened Panels 1, 3 and 4

Figure V-12   Flaw Location Diagram for Stiffened Panels 2, 5 and 6

The flaws in position 1, 2, 3, and 6 are in fillet regions where the stress field is likely to be nonuniform on the basis of our stress analysis work. These data are given in Table A-7 of Appendix A. Some data presented in this table are based on measurements at points on the periphery of the flaw where maximum growth occurred. An estimated effective 2C was measured to correspond. Other flaws in fillet areas exhibited uniform growth and were measured in a normal manner. These areas normally showed lower growth rates, indicating subnominal stresses and no stress gradient.

An example of the type of nonuniform growth exhibited by flaws in fillet areas is shown by photograph in Figure V-13. All flaws in fillet areas always grew more rapidly in the membrane direction at the junction of the membrane and the fillet. This nonuniform growth was not obtained from any flaws placed on the smooth back face of the panel.
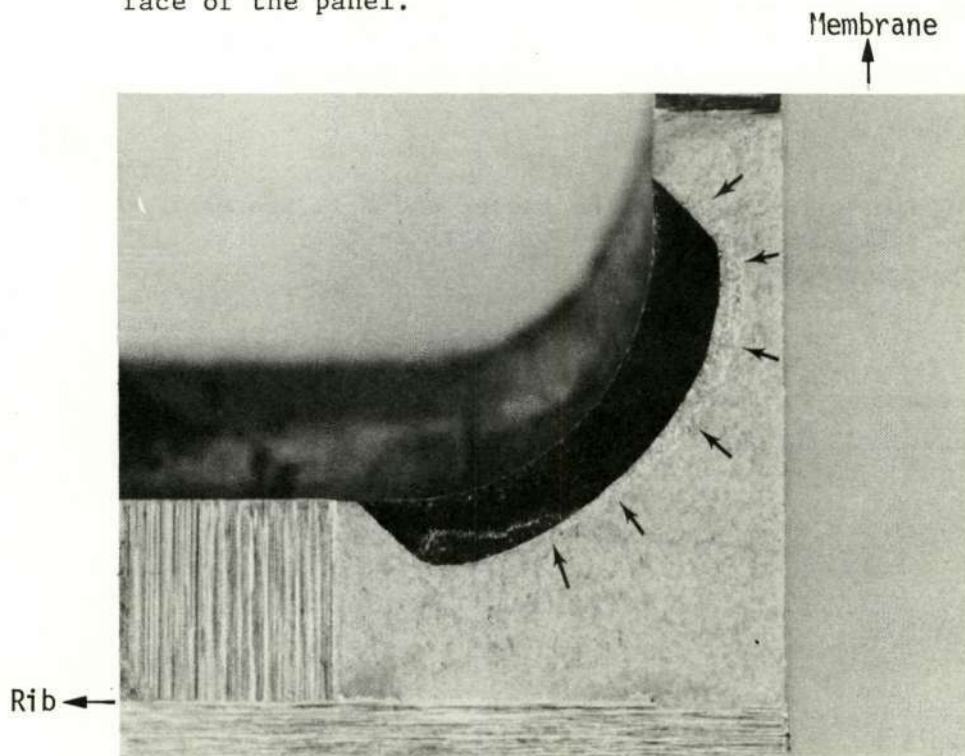
PANEL 6, POSITION 1

Figure V-13   Fillet Flaw Showing Nonuniform Growth

E.   DISCUSSION AND DATA COMPARISON

In this section, we will discuss the following:

1) Data analysis method;

2) Parent metal behavior of unstiffened panels;

3) Weld metal behavior;

4) Stiffened panel behavior.

1.   Data Analysis Method

In the following sections the analysis of the data is based on presenting the data as a plot of ΔK vs da/dN.   For this purpose the stress intensity range was computed using the equation

$$\Delta K = F\ M\ \Delta\sigma\ \sqrt{\pi a/Q} \qquad\qquad\qquad [1]$$

where F is the front surface correction factor and M is the back surface correction factor.   Figure V-14 illustrates the crack geometry under consideration.
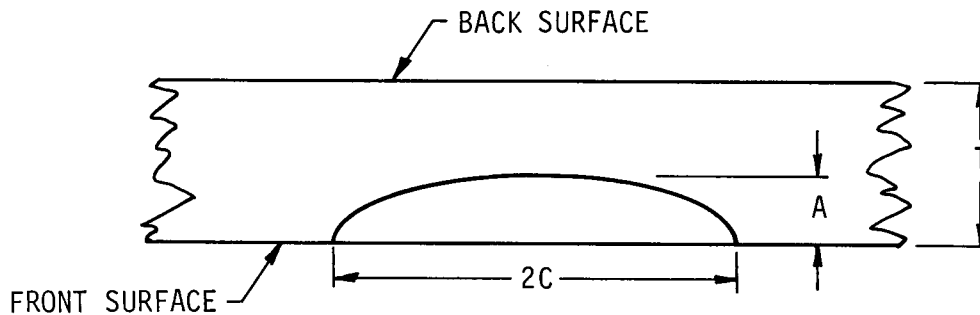
Figure V-14   Semielliptical Surface Flaw in a Plate

There have been numerous estimates of the factors F and M by several investigators that were reviewed in careful detail by Smith and by Shah and Kobayashi in a recent ASME special publication (Ref 7). For this work the estimates for F and M presented by Shah and Kobayashi were used in the calculations of ΔK. The detailed comparisons found by Shah and Kobayashi indicate that for most of the program, magnification factors compare well with the results of Smith (Ref 7) and represent a good estimate for design and testing purposes.

In the computation of ΔK using Equation [1] for the cases of biaxial loading, it is assumed that the stress component parallel to the crack surface has no influence on the stress intensity factor. This supposition is correct for cases in which linear fracture mechanics is applicable, but is probably not correct in a case where the effects of plasticity cannot be ignored. Since the stress levels being applied are about 50% of yield and in the absence of an analytical method to account for the effect of biaxial stress on ΔK in the presence of plasticity effects, Equation [1] was used in the data analysis.

Because each test specimen had cracks present with a/2C = 0.15 as well as a/2C = 0.50, different amounts of crack growth were experienced on the various cracks. An attempt was made to control the tests so that the more intense slender cracks did not have excessive growth, while trying to maintain an amount of growth on the round cracks which was not too small. · In fatiguing enough to produce accurately measurable crack growths in the round cracks, a comparatively large crack growth was induced in the slender cracks. Accordingly, the calculations of ΔK and da/dN for each test were done as follows.

A value of ΔK was computed for each crack, using Equation [1] based on the dimensions after sharpening which were indicated by staining. A second value of ΔK was computed based on the crack dimensions at the conclusion of the fatigue test. These two ΔK values were then averaged and used in preparing the ΔK vs da/dN plots. The crack growth rates, da/dN, were approximated by the ratio, Δa/ΔN, where Δa is the measured crack growth and ΔN is the number of cycles for each fatigue test.

The equations and procedures described here were programmed for the computer to reduce the data to the form of ΔK and Δa/ΔN.

The results of the uniaxial and biaxial fatigue flaw growth tests
were interpreted in terms of comparison with Forman's equation
(Ref 8) expressed in the form

$$da/dN = \frac{C(\Delta K)^n}{(1-R)K_{I_c} - \Delta K} \cdot$$

[2]

Wherever possible, a least square fit of Equation [2] to the data
was performed. For the tests done under this program, the stress
ratio, R, was zero, so the least square fits were done by rewriting
Equation [2] in the form

$$(K_{I_c} - \Delta K) \, da/dN = C(\Delta K)^n$$

and taking the natural log of both sides of the equation. This
produces a problem of least square fitting a straight line in the
log plane to the data to determine C and n. This was done using
standard procedures and was programmed for the CDC 6400 computer.
The following paragraphs present the results of the analyses and
their interpretations.

2. Behavior of Unstiffened Panels (Parent Metal)

As shown in Section C (Fig. V-6 and V-7), elimination of outlying
points does affect the shape of the flaw growth curves slightly.
For the longitudinal direction, elimination of points 1 through
4 decreases the slope of the curve. Point 5 grew through the plate
thickness, but its deletion produces no further change in the re-
sulting 36-point curve.

In order to least square fit a curve to the longitudinal data, it
was devided to select a value for K_{Ic} corresponding to the speci-
men orientation. These values were taken from a report by Engstrom
(Table V-1). To determine the sensitivity of the curve fit to the
K_{Ic} value selected, K_{Ic} was varied by plus or minus five percent
of the nominal value presented in the report. This much variation
in K_{Ic} produces a shift in the curves on Figure V-6 which is small
compared to the shift caused by deleting the outlying points.

The transverse data was treated in a similar way. The two curves shown in Figure V-7 demonstrate the effect of eliminating the outlying points 1 and 2. There is a total 40 data points for the transverse samples and the curve fitted to all the points is so indicated. The lower curve was fitted to the data remaining after deletion of points 1 and 2. Point 3 was subsequently deleted because the crack grew through the full thickness of the plate and accordingly the growth rate value for that crack is uncertain. The absence of this point, however, did not modify the 37-point curve any further.

A further interpretation of these results may be obtained from Table V-1 which summarizes the results of the least square fits to the data in terms of the parameters n and C of the Forman equation. It is noted that the greatest change in n occurs as a result of deleting the outlying points. The effect of the plus or minus five percent shange in K_{Ic} is seem to be small on n. It is also noted that a small change in n produces a fairly large effect on the value of C. In comparing the values for the transverse and longitudinal orientations, it is observed that there is not much difference in comparable values of n and C. This is born out by a comparison of the data of Figures V-6 and V-7 from which it is found that the data are indistinguishable from one another. The values of n and C found in Table V-1 for the two orientations produce ΔK vs da/dN curves that are virtually identical for purposes of design in the range of the experiments. Figure V-15 further shows the similarity of the two curves.

It is important to make comparison of these results with uniaxial fatigue data in order to assess the effects of biaxial fatigue. This may be done in part by reference to Figure V-16 in which ΔK vs da/dN is compared for the two types of loading. It is noted that while the data are similar in nature, the uniaxial data does fall below the biaxial results; that is, in this range of ΔK and da/dN, a crack subjected to uniaxial fatigue tends to grow faster than one in biaxial fatigue by as much as a factor of two or three.

For purposes of overall comparison, Table V-2 presents comparable n and C values from different sources to further establish the effects of biaxial stress on the fatigue of surface flaws. It is noted that the n coefficient is smaller for the biaxial case indicating the tendency for slower growth. Figure V-17 shows a graphical comparison of uniaxial data from three sources. Note that Forman's data and the Lockheed data (NAS9-11722) are identical.

Table V-1 *Crack Growth Parameters for Biaxial Flaw Growth*

Defect Orientation	Fracture Toughness, K_{Ic}, ksi $\sqrt{in.}$	n, for indicated number of points			C, for indicated number of points		
Longitudinal		40 pts	36 pts	35 pts	40 pts	36 pts	35 pts
	44.2	1.736	2.061	2.027	3.20	1.62	1.76
	(Avg)* 46.2	1.780	2.105	2.049	3.06	1.56	1.77
	48.2	1.818	2.141	2.069	2.97	1.52	1.79
Transverse		40 pts	38 pts	37 pts	40 pts	38 pts	37 pts
	39.3	1.702	1.923	2.003	2.56	1.66	1.38
	(Avg)* 41.3	1.776	2.001	2.039	2.32	1.49	1.36
	43.3	1.832	2.060	2.070	2.17	1.38	1.35

40 Points = All Data Points

For Transverse Specimens:

37 Pts = All Data - Pts 1 and 2
36 Pts = All Data - Pts 1, 2, and 3

For Longitudinal Specimens:

36 Pts = All Data - Pts 1, 2, 3, and 4
35 Pts = All Data - Pts 1, 2, 3, 4, and 5

Use of n and C values with K_{Ic} and ΔK units of ksi in. produces da/dN in μ-in./cycle

*W. L. Engstrom: *Determination of Design Allowable Properties - Fracture of 2219-T87 Aluminum Alloy.* NASA CR 115388, Prepared by The Boeing Company under Contract NAS9-10364, Task 24, 1972.

Table V-2 *Comparison of Biaxial and Uniaxial Fatigue Data for 2219-T87 at Room Temperature*

	Biaxial		Uniaxial					
			This work		Boeing (Ref. NAS9-10364)		Lockheed (Ref. NAS9-11722)	
	n	C	n	C	n	C	n	C
All Points	1.78	2.32-3.06	2.34	1.84	2.17-2.40	.71-.75	2.5	0.44
Outlying Points Deleted	2.0-2.1	1.49-1.56	2.18	2.36	--	--		
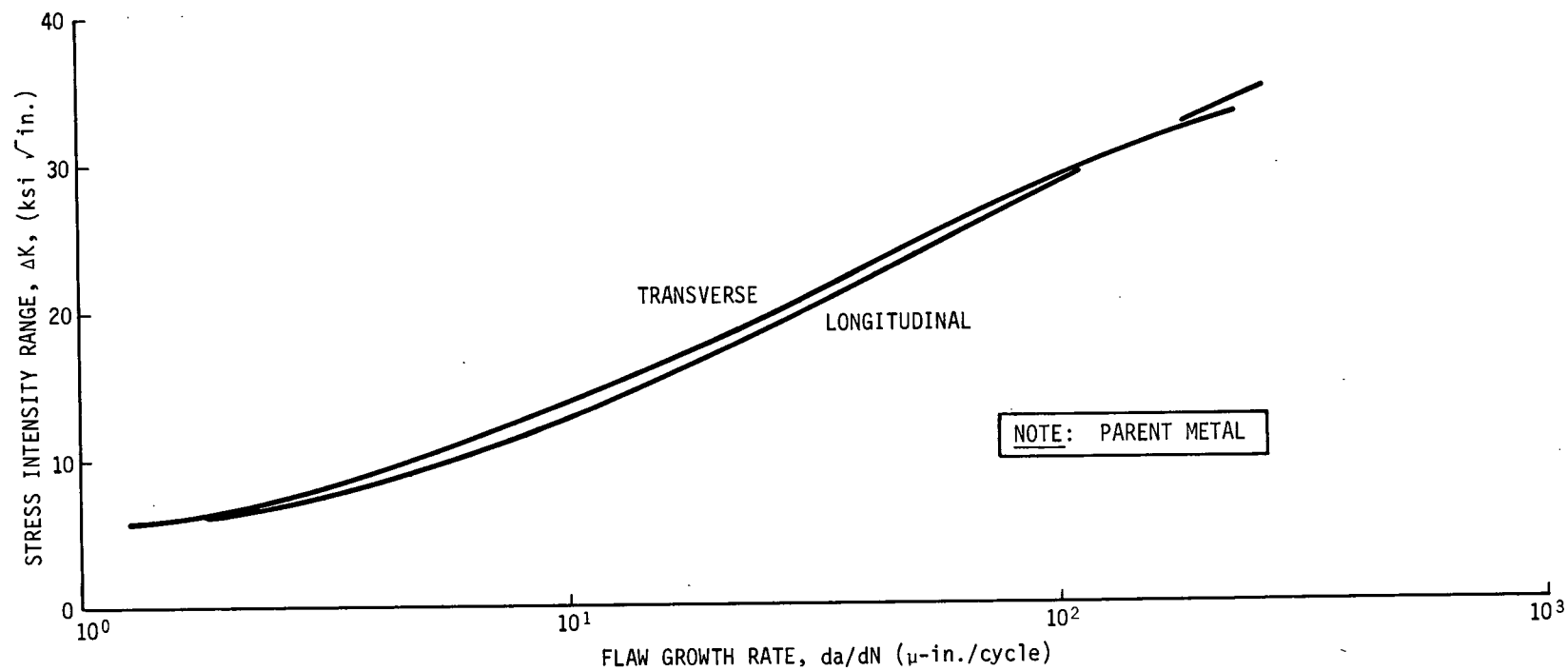
Figure V-15   Comparison of Defect Orientation on Flaw Growth Rate for Unstiffened, Biaxial Panels
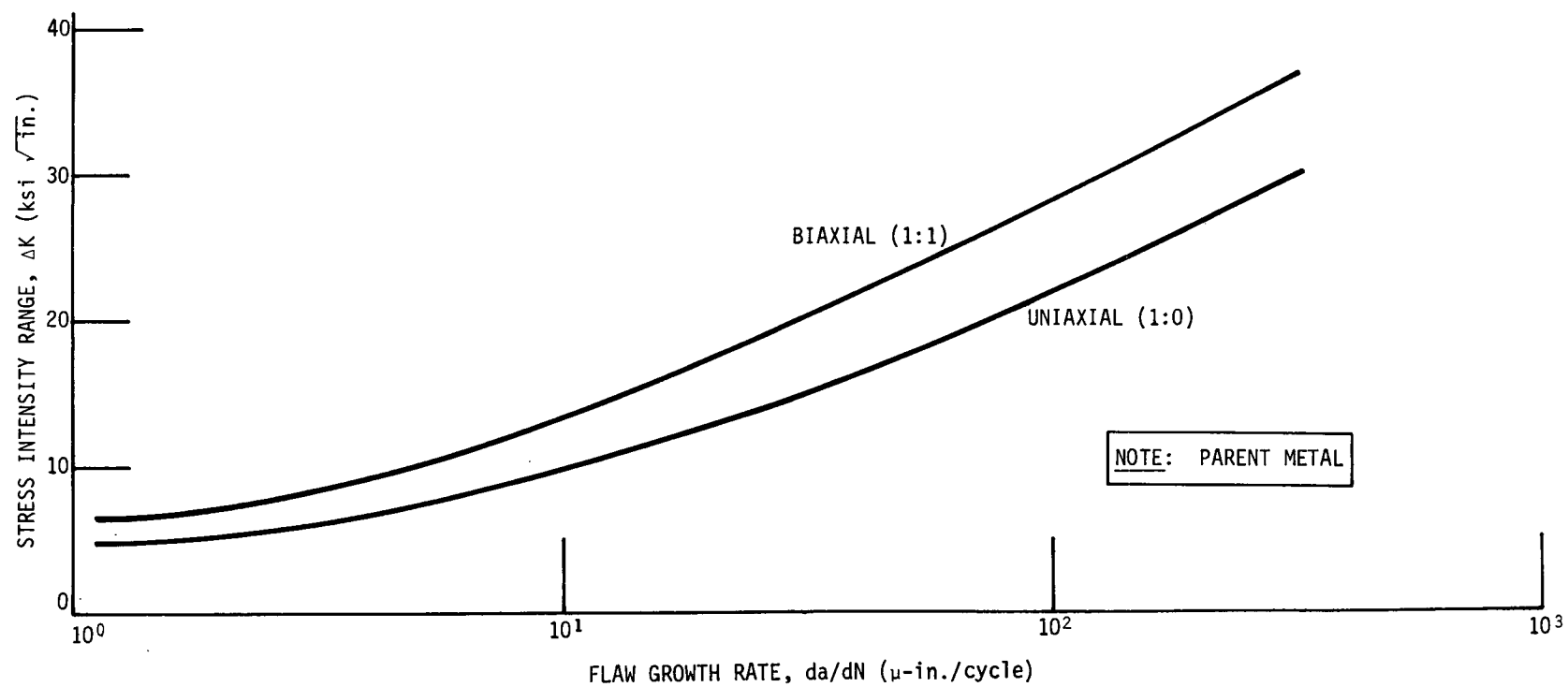
Figure V-16 Comparison of Stress Ratio on Flaw Growth Rate
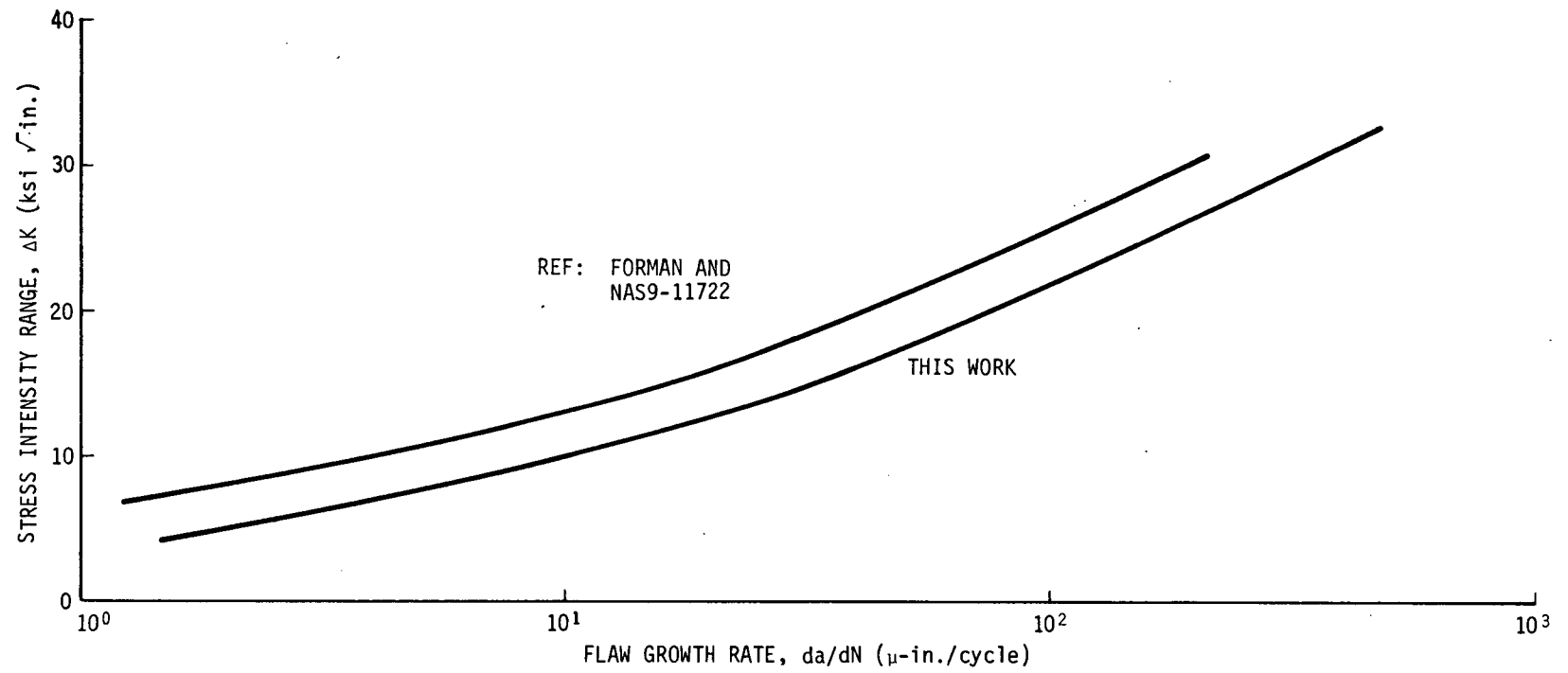
Figure V-17   Comparison of Uniaxial Flaw Growth Rate Data from Various Sources

3. Behavior of Welded Panels

Figure V-18 summarizes ΔK vs da/dN data for the uniaxial and bi-axial fatigue growth of surface cracks in or near a weld in a sheet of 2219-T87 aluminum. The data for cracks on the weld centerline and in the heat affected zone are all plotted together. In study-ing the data, it is difficult to discern any significant distinc-tions between the uniaxial and biaxial results for the minimal number of data points available.

In keeping with the work described earlier, an attempt was made to least square fit Forman's equation to these data. A difficulty arises in doing so because a value of K_{Ic} must be chosen and this data is not available because of the extremely tough behavior of the weld material. It was decided to select a value of 30 ksi-in.$^{\frac{1}{2}}$ for fitting the fatigue data, remembering that varying K_{Ic} does not overwhelmingly change the least square fit curve. Table V-3 shows the effect of K_{Ic} on n and C using the least square fitting technique. The curves given in Figures V-5 and V-8 are the results of this procedure, and it is noted that the cracks subjected to biaxial fatigue tend to grow more slowly until a crossover point is reached according to the curves. This is due to the higher value of n that was predicted for the biaxial data. Since there are not a large number of data points, it is inappro-priate to draw any conclusion based on the least square fit curves. There appears to be little distinction between the fatigue behav-ior of surface cracks in or near welds which depends directly on whether or not the loading is biaxial. As usual, the problem is complicated by the decreased yield strength of the weld material and the material in the heat affected zone, and also the presence of residual stresses parallel to the weld bead as well as residual stresses that vary in the thickness direction. The theoretical stress intensity predictions and stress analyses presently avail-able are inadequate to properly cope with these difficulties.

A comparison of the uniaxial data with Lockheed data from NAS9-11722 is given in Figure V-19.
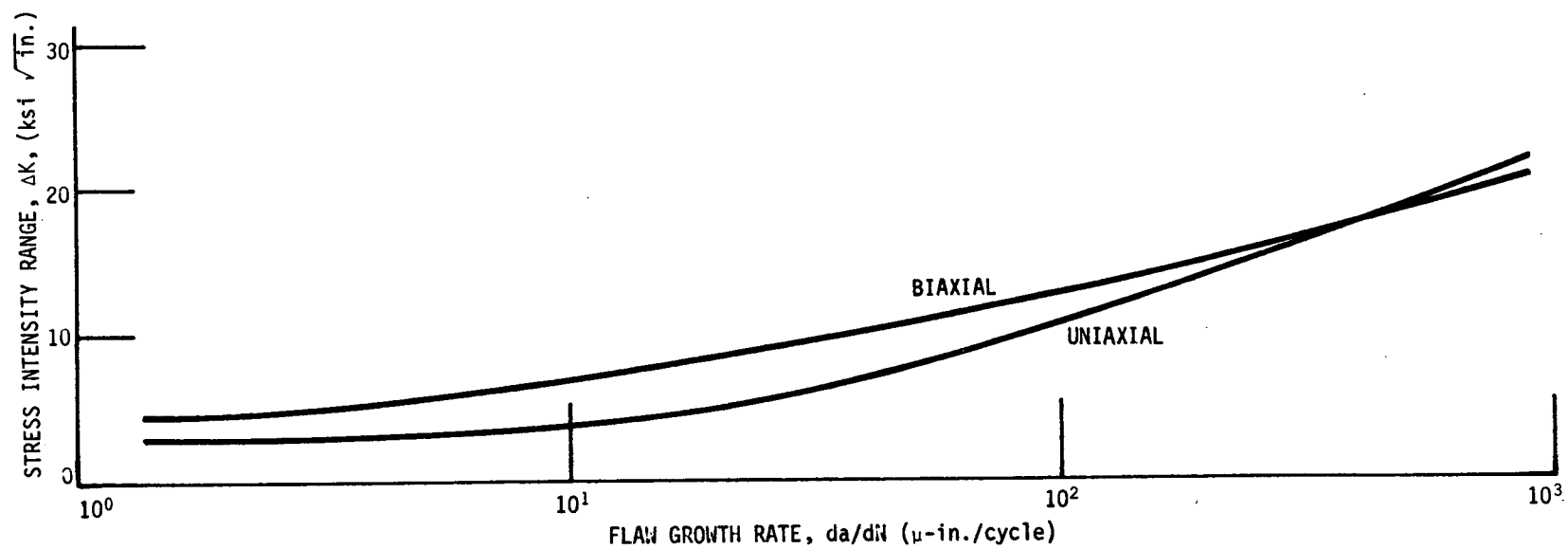
Figure V-18   Comparison of Uniaxial and Biaxial Flaw Growth Data for Welded Material
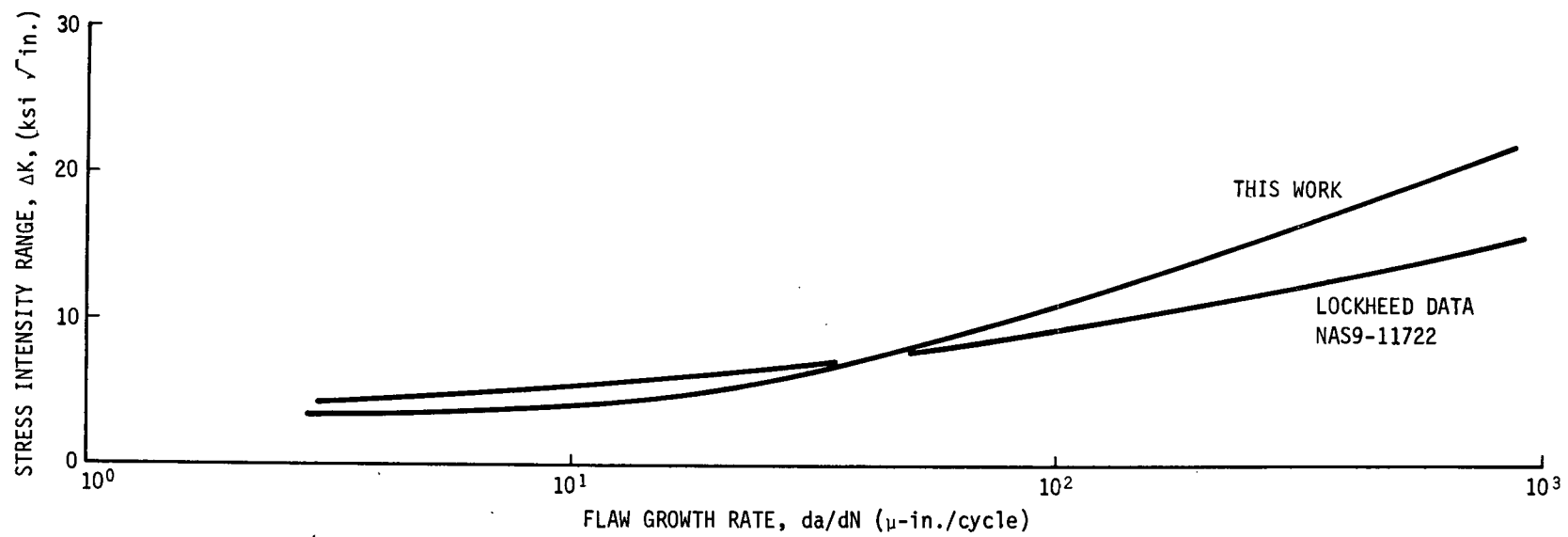
Figure V-19 Comparison of Uniaxial, Welded Flaw Growth Data

Table V-3 Effect of Fracture Toughness Level on Flaw Growth Parameters in Welded Material

Fracture Toughness, K_{Ic}, ksi $\sqrt{in.}$	Uniaxial Analysis*		Biaxial Analysis*	
	n	C	n	C
30	1.88	2.41	3.25	0.044
36	1.98	2.55	3.45	0.038
41.3	2.03	2.73	3.55	0.038
46.2	2.07	2.93	3.61	0.038
48.2	2.08	3.02	3.63	0.039
*Analysis using least square fitting technique				

4. Flaw Growth Behavior of Stiffened Panels

As described in the preceding Section, the ten flaws placed in each stiffened panel were analyzed in two different manners. Flaws contained in sections 4, 5, 7, 8, 9, and 10 of Figures V-11 and V-12 and Table A-6 were assumed to be in regions having a relatively constant stress field, which allowed reasonable uniform growth patterns to develop. Data from these flaws are presented in Figure V-20 with the average growth rate best fit curves obtained from biaxial and uniaxial tests and for parent material presented previously in this section. The points, as plotted, were computed using Forman's equation (Ref 8) and experimentally measured stress values obtained in the region where each flaw was located.

Note that in general points are within the two curves plotted for comparison from biaxial and uniaxial flaw growth data. Exceptions are at the lower end of the curve where growth rates were small and highly subject to errors from insufficient flaw growth. Data taken from these flaws would be expected to fall between biaxial and uniaxial data results as all points are in regions where stresses are either uniaxial or unbalanced biaxial.

Flaws in positions 1, 2, 3, and 6 (Figs. V-11 and V-12) were located in regions where the stress gradient was expected to be changing very rapidly, i.e., where stress concentrations had been indicated from experimental analysis.

C-2
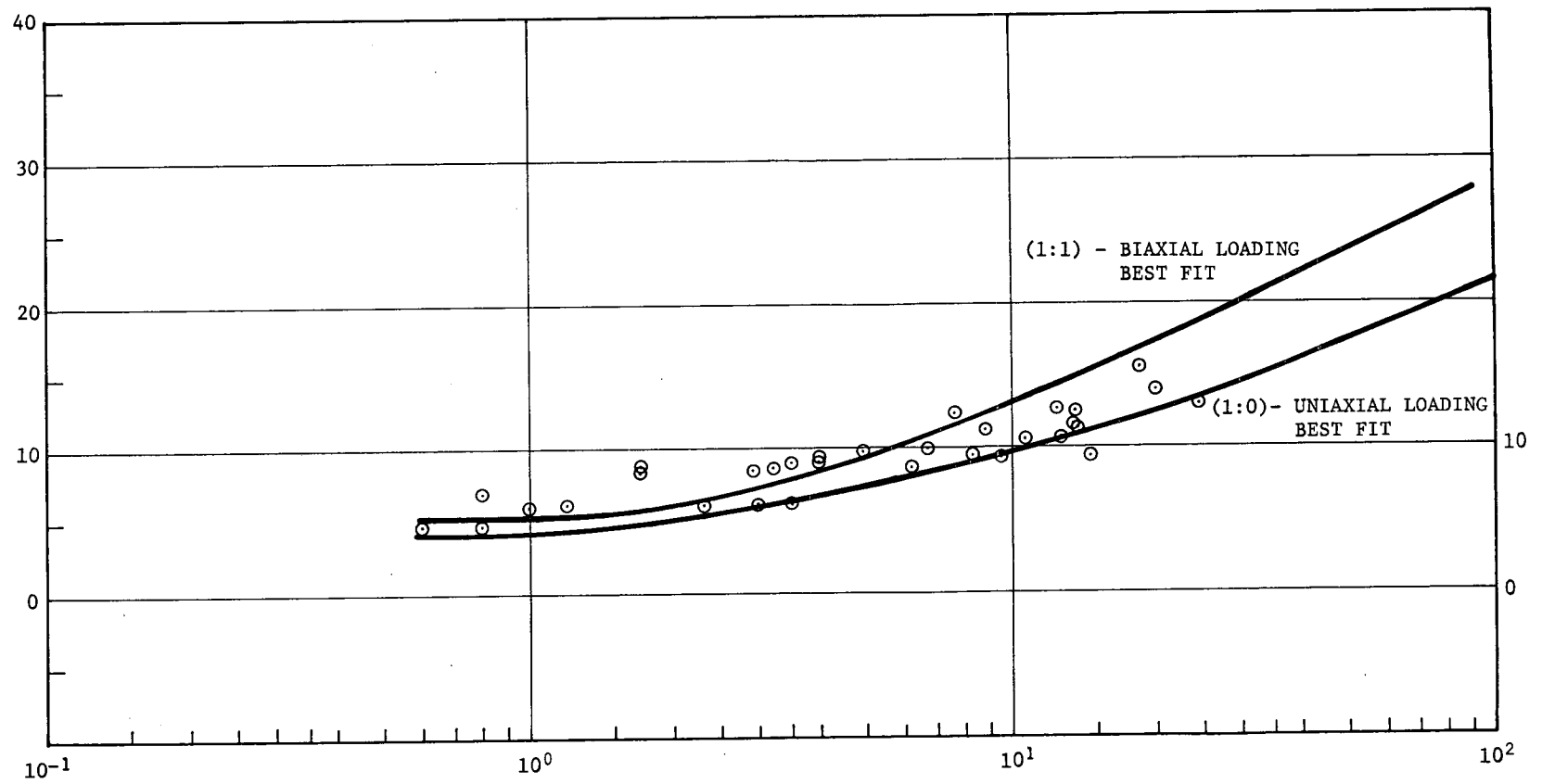
Figure V-20   Flaw Growth Data From Stiffened Panels (Uniform Stress Field)

The analysis of these data was conducted in the following manner. First, a maximum $\Delta a / \Delta N$ was measured from each flaw. Flaws that exhibited uniform growth or growth in a direction normal to the surface were also measured. The measured $\Delta a / \Delta N$ was then used with the average growth rate curve in Figure V-20 to obtain an average ΔK. This ΔK was then used to compute an indicated applied stress. Thus, the flaw growth rate is used to compute a maximum stress value that can be used to compare with values obtained by stress analysis methods previously employed. The resulting stresses are then divided by the nominal membrane stress to obtain stress concentration values, K_t, which are presented in Table V-4.

The table is divided into the four flaw positions that can be related from each panel. Flaws at positions 1 and 2 are in similar areas, i.e., the corner of the central bay where two fillets intersect, while flaws at positions 3 and 6 are in the fillet area adjacent to ribs. Flaws at positions 1, 3, and 6 are similar in that all are perpendicular to the fillet surface at 45° to the plane of the panel.

In general, flaws in positions 3 and 6 show a low stress field while flaws in positions 1 and 2 show considerable stress concentration. Stress analysis results indicate that a low stress field does occur in the fillet radius which agrees with Table V-4 results shown at positions 3 and 6. Analysis also shows a sharp stress concentration of about 40 percent corresponding very closely to flaws in position 2 from the tabulation.

Table V-4 Stress Concentration Factors Computed from Flaw Growth Data and Compared with Experimental and Analytical Values

	Flaw Position (Fig. V-11 and V-12)	K_t		
		Flaw Growth	Theoretical	Experimental
Panel 2	1	1.41		
Panel 6	1	0.91	<0.57*	0.29
Panel 5	1	1.34		
Panel 1	2	0.93	1.40*	1.40
Panel 3	2	1.35		
Panel 4	2	0.98		
Panel 2	2	1.57		
Panel 6	2	1.32	1.40*	1.29
Panel 5	2	1.45		
Panel 3	3	0.85		
Panel 4	3	0.77		
Panel 2	3	0.75		
Panel 6	3	0.88	0.57	0.57
Panel 5	3	1.16		
Panel 2	6	0.75		
Panel 6	6	0.76	0.67	0.71

*The theoretical analysis was not conducted at the corner of the panel, represented by flaw positions 1 and 2. Values shown are approximations based on analysis at other fillet locations in the panel where both a thin and thick rib was studied.

VI. SUMMARY AND CONCLUSIONS

The sample designs used in this program proved to be adequate in all respects. No failures of any samples occurred and all samples proved to be of adequate size and design to obtain required uniform stress fields of sufficient size in central regions of the sample. No delamination of any materials was noted.

Experimental and theoretical analyses of the stiffened panel configurations studied yield the following conclusions:

1) The highest stress concentration occurred on the stiffened side of the panel at positions where skin meets the fillet radius. The concentration appears to be in the order of 40%.

2) Another stress concentration, but of smaller magnitude, occurred on the smooth unstiffened side of the panel in back of the ribs but in skin thickness material. The stress concentration factor in this region was about 1.2.

The photoelastic stress analysis method provided a general picture of critical areas to be examined but did not detect the sharp stress gradient indicated by analytical and strain gage analysis. The uniformity of stress fields and principal stress directions were identified by photoelastic analysis. Approximate stress levels were obtained by this method in regions of low stress gradient.

Our finite element analysis (three-dimensional) has shown that two-dimensional analysis methods would be highly inaccurate for predicting critical stresses at geometric anomalies, e.g. fillet areas, in an integrally stiffened structure or panel.

Unfortunately, the analytical finite element analysis was not available before the strain gage analysis was conducted. If this additional input had been available, it would have aided strain gage placement and size selection to an even greater extent. The extremely sharp gradient in the fillet area was largely unsuspected. Nevertheless, sufficient strain gage results were obtained to verify the existence of the strain gradient predicted by analytical analysis.

A comparison of uniaxial fatigue flaw growth properties (room temperature) of 2219-T87 aluminum from several sources with the biaxial fatigue flaw growth data obtained in this study reveals that the presence of a biaxial state of stress tends to decrease flaw growth rate in 2219-T87 aluminum. The decrease is in the order of a factor of 2 to 3 in flaw growth rate.

Flaw growth data from biaxially loaded (2 to 1 stress ratio) 2219-T87 weld panels was not sufficient to determine whether this loading condition causes an increase or decrease from uniaxial loaded weldments.

The flaw growth behavior of stiffened panel configurations, in general, confirmed the presence of stress concentrations in those critical areas indicated by experimental and analytical analyses, namely at the skin-fillet junction. Areas directly behind ribs and in the ribs themselves or in the fillet itself were found to exhibit slower crack growth and were expected to have lower stress.

It appears that the current crack growth propagation analysis methods satisfactorily predict crack growth rates in complex stress states, such as in fillet areas and rib intersection in the stiffened panels studied.

VII. REFERENCES

1. In Plane Triangular Plate Element: Zienkiewicz, O. C., *The Finite Element Method in Engineering Science*. McGraw-Hill, 1971.

2. Bending Triangular Plate Element: Bazeley, C. P., *et al.*, "Triangular Elements in Plate Bending – Conforming and Non-conforming Solutions." *Air Force Conference on Matrix Methods in Structural Mechanics*, Dayton, Ohio, 1965.

3. In Plane Rectangular Plate Element: Batdorf, W. J., *Matrix Method for the Analysis of Complex Structures Using the Direct Stiffness Approach.* Martin Marietta Corporation SR-0530-63-12, 1963.

4. Bending Rectangular Plate Element: Melosh, Robert J., "A Stiffness Matrix for the Analysis of Thi Plates in Bending." *Journal of Aerospace Science*, 1961, pp 34–42.

5. R. G. Forman: *Fatigue Flaw Growth Behavior of 2219-T87 Aluminum at Cryogenic, Room and Elevated Temperatures*. Materials Technology Branch Report 71-ES5-1, September 1971.

6. Don E. Petit and David W. Hoeppner: *Fatigue Flaw Growth and NDI Evaluation for Preventing Through Cracks in Spacecraft Tankage Structures*. NAS9-11722, Lockheed-California Company, September 1972.

7. *The Surface Crack, The Physical Problem and Computation Solutions*. ASME Special Publication, Edited by J. Swedlow, November 1972.

8. Forman, R. G., Kearney, V. E., Engle, R. M.: "Numerical Analysis of Crack Propagation in Cyclic Loaded Structures." *ASME Trans., J. Basic Engineering*, September 1967.

APPENDIX A

TABULATED DATA

$a-1$

Element No.	DER	Normal Stress, ksi			Shear Stress, ksi		
		σ_{xx}	σ_{yy}	σ_{zz}	σ_{yz}	σ_{zx}	σ_{xy}
24	0.405	32.2	32.6	-0.6	-0.2	0.7	-0.4
30	0.415	29.4	32.1	-2.6	0	0.3	-0.2
34	0.415	29.4	32.1	-2.7	0	-0.2	-0.2
40	0.326	28.0	29.9	-0.7	0.1	-0.9	-0.3
101	0.423	35.0	34.0	0.7	-0.2	-1.1	-0.4
107	0.439	33.5	34.1	-0.6	0	0.5	-0.2
111	0.439	33.4	34.1	-0.7	0	0	-0.2
117	0.345	31.2	31.5	0.9	0	1.3	-0.3
184	0.486	38.1	35.5	0.7	-0.1	-0.8	-0.1
190	0.478	34.4	34.5	-1.4	0	1.4	0
194	0.481	34.3	34.4	-1.6	0	1.5	0
200	0.386	31.0	31.2	-1.1	-0.1	0.9	.4
261	0.456	34.0	33.4	-1.3	-0.1	0.6	-0.1
267	0.482	34.6	34.7	-1.3	-0.1	1.9	0
271	0.484	34.5	34.6	-1.5	0	2.0	0
277	0.438	38.6	34.9	2.6	-0.1	1.6	0.4
344	0.394	32.1	34.0	0.5	-0.2	0.8	0
350	0.434	33.5	34.9	0.2	-0.1	1.8	0.2
354	0.436	33.8	35.2	0.6	-0.1	3.3	0.2
360	0.494	41.0	34.9	3.6	-0.5	5.8	0.4
2436	0.565	41.1	36.0	3.7	-0.6	10.0	0.4
421	0.387	31.0	33.3	-0.1	-0.2	-0.1	0
427	0.415	30.9	33.6	-1.1	-0.1	0.7	0.2
431	0.414	31.1	33.9	-0.6	-0.1	2.2	0.2
437	0.402	28.7	29.8	-2.4	-0.5	5.2	0.5
2398	0.467	28.7	29.8	-2.4	-0.6	9.3	0.5
2400	0.339	30.5	30.4	3.8	-0.8	8.3	0.4
504	0.408	31.3	34.2	-0.3	-0.4	-0.2	0
510	0.402	29.1	34.0	-1.1	-0.4	0	0
514	0.406	29.0	33.9	-1.3	-0.4	0.6	0
520	0.288	22.9	30.8	0	-0.6	1.7	0.3
2348	0.232	18.4	30.1	2.6	-0.6	4.2	0.4
2373	0.322	24.0	31.9	2.2	-0.7	7.3	0.3
581	0.414	32.4	34.7	0.2	-0.4	-0.2	0
587	0.397	28.1	33.5	-1.6	-0.4	0	0
591	0.401	27.9	33.4	-1.9	-0.4	0.7	0
597	0.281	19.5	29.1	-1.7	-0.6	2.1	0.3
2324	0.234	21.8	31.4	3.0	-0.7	1.2	0.3
2336	0.227	11.9	26.9	-0.8	-0.7	3.5	0.3
2360	0.135	10.3	23.5	1.6	-0.9	0.3	0

Table A-1 Normal and Shear Stresses for Stiffened Panel, Panel No. 6, 1:1 Loading

Element No.	DER	Normal Stress, ksi			Shear Stress, ksi		
		σ_{xx}	σ_{yy}	σ_{zz}	σ_{yz}	σ_{zx}	σ_{xy}
2385	0.137	1.4	20.3	1.1	-0.8	1.2	0.1
2418	0.089	0.7	15.4	1.5	-1.2	1.1	0.1
2420	0.098	0.7	17.4	1.9	-1.3	-0.8	0.1
2448	0.085	-0.2	16.0	2.6	-1.2	0.5	0.1
709	0.458	34.5	35.0	-0.4	-0.3	-0.4	-0.2
715	0.350	27.6	32.0	-0.7	-0.3	-0.4	-0.3
719	0.356	27.4	31.8	-1.1	-0.3	-0.6	-0.3
725	0.229	21.6	28.6	1.0	-0.4	-0.7	-0.2
729	0.220	22.2	29.2	2.2	-0.4	1.5	-0.2
735	0.111	0.3	17.9	1.6	-1.0	1.4	0.1
739	0.105	0.9	18.5	2.8	-1.0	0.5	0.1
745	0.072	-0.1	15.0	2.7	-1.0	0.2	0.1
749	0.073	-0.2	14.8	2.5	-1.0	0.3	0.1
755	0.048	0.1	12.1	1.9	-0.9	0.1	0
759	0.048	0	12.0	1.6	-0.9	0.2	0
765	0.019	0	7.3	0.5	-0.8	0.2	0
769	0.019	0.1	7.4	0.6	-0.8	0.2	0
966	0.460	34.9	35.2	-0.2	-0.3	0	0.2
972	0.351	27.8	32.1	-0.6	-0.3	-0.1	-0.3
976	0.356	27.6	31.9	-1.0	-0.3	-0.3	-0.3
982	0.228	21.1	28.3	0.7	-0.4	-0.3	-0.2
986	0.216	21.7	28.9	2.0	-0.4	0.4	-0.2
992	0.107	0.8	18.2	1.9	-1.0	0.3	0.1
996	0.104	1.4	18.8	3.0	-1.0	-0.5	0.1
1002	0.072	-0.1	14.9	2.7	-1.0	-0.2	0.1
1006	0.073	-0.2	14.8	2.5	-1.0	-0.1	0.1
1012	0.048	-0.1	12.1	1.9	-0.9	-0.2	0
1016	0.048	0	12.0	1.6	-0.9	-0.1	0
1022	0.019	0	7.3	0.5	-0.8	-0.2	0
1026	0.019	0.1	7.4	0.6	-0.8	-0.2	0
1229	0.463	35.0	35.2	-0.2	-0.4	-0.1	-0.3
1235	0.349	27.7	32.1	-0.6	-0.4	-0.1	-0.2
1239	0.355	27.4	31.8	-1.1	-0.4	-0.2	-0.2
1245	0.220	20.3	28.1	0.9	-0.3	-0.4	-0.1
1249	0.207	21.0	28.8	2.2	-0.3	0	-0.1
1255	0.109	0.7	18.2	1.6	-0.9	-0.3	-0.1
1259	0.105	1.4	18.9	3.0	-0.9	-0.6	-0.1
1265	0.073	-0.1	15.0	2.7	-1.0	-0.2	0
1269	0.073	-0.2	14.8	2.4	-1.0	0	0
1275	0.048	0.1	12.1	1.9	-0.9	0.1	0
1279	0.048	-0.1	12.0	1.6	-0.9	0.1	0
1285	0.019	0.1	7.3	0.5	-0.9	0.2	0
1289	0.019	0.1	7.4	0.6	-0.8	0.2	0

Table A-1 (cont)

A-2

Element No.	DER	Normal Stress, ksi			Shear Stress, ksi		
		σ_{xx}	σ_{yy}	σ_{zz}	σ_{yz}	σ_{zx}	σ_{xy}
1486	0.461	34.7	35.1	-0.4	-0.4	0.3	-0.3
1492	0.348	27.4	31.9	-0.7	-0.4	0.2	-0.2
1496	0.354	27.2	31.7	-1.2	-0.4	-0.5	-0.2
1502	0.221	20.6	28.3	1.0	-0.3	-0.7	-0.1
1506	0.209	21.3	29.0	2.4	-0.3	-1.1	-0.1
1512	0.113	0.2	17.9	1.3	-0.9	-1.4	-0.1
1516	0.107	0.9	18.6	2.7	-0.9	-0.5	-0.1
1522	0.113	-0.1	14.9	2.7	-1.0	-0.2	0
1526	0.209	-0.2	14.9	2.5	-1.0	-0.3	0
1532	0.221	-0.1	12.1	1.9	-0.9	-0.1	0
1536	0.354	0	12.0	1.6	-0.9	-0.2	0
1542	0.348	0	7.2	0.5	-0.9	-0.2	0
1546	0.461	0.1	7.4	0.6	-0.8	-0.2	0
1704	0.421	32.7	34.8	0.1	-0.5	0.1	-0.5
1710	0.403	27.9	33.2	-2.1	-0.5	-0.2	-0.6
1714	0.409	27.8	33.0	-2.5	-0.5	-1.0	-0.6
1720	0.286	17.5	26.9	-3.7	-0.8	-3.1	-1.0
2460	0.180	20.2	28.1	3.2	-0.4	-0.9	-0.1
2472	0.190	8.0	22.1	-2.7	-0.3	-4.0	0
2484	0.149	8.26	23.3	0.6	-0.4	-1.0	0
2509	0.154	1.1	20.7	-0.1	-0.5	-1.5	0
2534	0.089	-0.7	15.6	1.4	-1.1	-1.0	0
2536	0.100	0.8	17.6	2.0	-1.1	0.6	-0.1
2572	0.086	-0.1	16.1	2.6	-1.1	-0.5	0
1781	0.415	31.7	34.3	-0.4	-0.5	0.2	-0.5
1787	0.409	29.2	33.8	-1.4	-0.5	0.1	-0.6
1791	0.415	29.0	33.6	-1.9	-0.5	-0.7	-0.6
1797	0.294	23.0	29.6	-1.0	-0.8	-1.8	-1.0
2496	0.214	18.8	29.6	3.1	-0.6	-3.8	-1.1
2521	0.313	24.6	31.2	2.2	-0.7	-7.0	-1.0
1864	0.391	31.2	33.5	-0.1	-0.2	0.1	-0.6
1870	0.416	31.0	33.6	-1.1	-0.2	-0.6	-0.7
1874	0.415	31.2	33.8	-0.7	-0.1	-2.1	-0.7
1880	0.401	28.6	29.6	-2.5	-0.5	-5.2	-1.0
2554	0.467	28.6	29.6	-2.4	-0.5	-9.3	-1.0
2556	0.335	30.3	30.1	3.7	-0.6	-8.2	-1.0
1941	0.398	32.3	34.0	0.4	-0.2	-0.8	-0.6
1947	0.434	33.6	34.9	0.2	-0.2	-1.7	-0.7
1951	0.437	33.8	35.1	0.6	-0.1	-3.2	-0.7
1957	0.493	41.0	35.7	3.6	-0.5	-5.8	-1.0
2584	0.565	41.0	35.7	3.6	-0.5	-9.9	-1.0

Table A-1 (cont)

Table A-1 (concl)

Element No.	DER	Normal Stress, ksi			Shear Stress, ksi		
		σ_{xx}	σ_{yy}	σ_{zz}	σ_{yz}	σ_{zx}	σ_{xy}
2024	0.454	34.0	33.3	-1.3	-0.1	-0.5	-0.4
2030	0.481	34.6	34.5	-1.3	0	-1.8	-0.6
2034	0.483	34.6	34.5	-1.5	0	-1.9	-0.6
2040	0.439	38.7	34.8	2.5	-0.1	-1.5	-0.9
2101	0.484	38.1	35.4	0.7	-0.1	-0.8	-0.4
2107	0.478	34.4	34.4	-1.4	0	-1.4	-0.6
2111	0.480	34.3	34.3	-1.6	0	-1.5	-0.6
2117	0.387	31.2	31.1	-1.1	-0.1	-0.9	-0.9
2184	0.421	35.0	33.7	0.7	-0.2	1.1	-0.2
2190	0.438	33.5	33.9	-0.6	0	-0.5	-0.3
2194	0.438	33.6	33.9	-0.7	0	0	-0.3
2200	0.345	31.4	31.3	0.9	0	-1.3	-0.2
2261	0.403	32.3	32.4	-0.6	-0.2	-0.7	-0.2
2267	0.414	29.6	31.9	-2.6	0	-0.3	-0.3
2271	0.414	29.6	31.9	-2.6	0	0.2	-0.3
2277	0.326	28.2	29.7	-0.7	0	0.9	-0.2

Sample (Flaw)* Number	σ (ksi)	σ/σ_{ys}	EDM PREFLAW					STAGE I GROWTH						STAGE II GROWTH						CYCLIC GROWTH VALUES		
			a_0 (in.)	$2C_0$ (in.)	$a/2C_0$	Q_0	$K\dagger_{I_0}$	a_1 (in.)	$2C_1$ (in.)	$a_1/2C_1$	Q_1	$K\dagger_{I_1}$	N_1 (cycles)	a_2 (in.)	$2C_2$ (in.)	$a_2/2C_2$	Q_2	$K\dagger_{I_2}$	N_2 or ΔN (cycles)	a_2-a_1 (in.)	$\frac{K_{I_1}+K_{I_2}}{2}$	$\frac{\Delta a}{\Delta N}$ $\left(\frac{\mu in.}{cycle}\right)$
15-25-30-1	30	0.58	0.0296	0.2010	0.15	1.13	9.5	0.0304	0.2020	0.15	1.13	9.5	4000	0.0580	0.2180	0.27	1.45	11.6	1000	0.0276	10.6	27.6
15-25-30-2	30	0.58	0.0293	0.2030	0.14	1.12	9.4	0.0332	0.2050	0.16	1.16	9.8	4000	0.0547	0.2060	0.27	1.44	11.2	1000	0.0215	10.5	21.5
15-25-40-1	40	0.77	0.0255	0.2000	0.13	1.03	12.3	0.0438	0.2060	0.21	1.23	14.5	1567	0.0668	0.2310	0.29	1.47	16.6	1100	0.0230	15.6	20.9
15-25-40-2	40	0.77	0.0298	0.1970	0.15	1.08	13.9	0.0459	0.2020	0.23	1.27	14.6	1567	0.0885	0.2730	0.32	1.59	19.3	1100	0.0426	17.0	38.7
15-50-30-1	30	0.58	0.0592	0.4070	0.15	1.12	13.9	0.0604	0.4070	0.15	1.13	14.0	221	0.0761	0.4100	0.19	1.22	15.6	750	0.0157	14.8	20.9
15-50-30-2	30	0.58	0.0604	0.3810	0.16	1.15	13.8	0.0617	0.3810	0.16	1.16	13.9	221	0.0803	0.3830	0.21	1.28	15.7	750	0.0186	14.8	24.8
15-50-40-1	40	0.77	0.0616	0.4110	0.15	1.08	19.4	0.0880	0.4240	0.21	1.22	23.2	770	0.0992	0.4330	0.23	1.28	25.3	100	0.0112	24.2	112.0
15-50-40-2	40	0.77	0.0611	0.0415	0.15	1.07	19.3	0.0862	0.4220	0.20	1.21	22.9	770	0.1009	0.4350	0.23	1.29	25.7	100	0.0147	24.3	147.0
15-75-40-1	40	0.77	0.0931	0.5810	0.16	1.10	26.5	0.1002	0.5830	0.17	1.13	28.3	114	0.1067	0.5850	0.18	1.15	30.6	32	0.0065	29.4	203.1
15-75-40-2	40	0.77	0.0920	0.6000	0.15	1.08	26.5	0.0960	0.6050	0.16	1.10	27.5	114	0.1030	0.6290	0.16	1.11	30.0	32	0.0070	28.7	218.8
15-75-45-1	51	0.98	0.0938	0.5930	0.16	1.02	35.5	0.1007	0.6020	0.17	1.04	38.0	14	0.1049	0.6090	0.17	1.05	40.1	4	0.0042	39.1	1050.0
15-50-45-2	45	0.87	0.0591	0.4070	0.15	1.03	21.7	0.0600	0.4070	0.15	1.04	21.8	64	0.0659	0.4070	0.16	1.07	22.7	11	0.0059	22.3	536.4
50-25-30-1	30	0.58	0.0296	0.0710	0.42	2.01	6.7	0.0373	0.0760	0.49	2.35	6.9	6000	0.0436	0.0820	0.53	2.25	7.1	2000	0.0063	7.0	3.2
50-25-30-2	30	0.58	0.0307	0.0720	0.43	2.05	6.8	0.0335	0.0790	0.42	2.04	7.1	6000	0.0440	0.0860	0.51	2.34	7.3	2000	0.0105	7.2	5.3
50-50-15-1	15	0.29	0.0627	0.1230	0.51	2.40	4.3	0.0666	0.1280	0.52	2.35	4.4	13900	0.0703	0.1300	0.54	2.27	4.4	2500	0.0037	4.4	1.5
50-50-15-2	15	0.29	0.0606	0.1230	0.49	2.41	4.4	0.0639	0.1290	0.50	2.43	4.5	13900	0.0675	0.1320	0.51	2.40	4.5	2500	0.0036	4.5	1.4
50-50-40-1	40	0.77	0.0602	0.1240	0.49	2.27	12.0	0.0625	0.1240	0.50	2.32	11.9	109	0.0717	0.1240	0.58	2.03	11.8	1000	0.0092	11.8	9.2
50-50-40-2	40	0.77	0.0602	0.1250	0.48	2.25	12.1	0.0626	0.1270	0.49	2.31	12.1	109	0.0711	0.1380	0.52	2.27	12.5	1000	0.0085	12.3	8.5
50-75-40-1	40	0.77	0.0901	0.1810	0.50	2.33	15.3	0.0935	0.1890	0.49	2.32	15.8	450	0.0983	0.1990	0.49	2.31	16.5	150	0.0048	16.2	32.0
50-75-40-2	40	0.77	0.0910	0.1800	0.51	2.31	14.3	0.0930	0.1860	0.50	2.34	15.6	450	0.1000	0.1980	0.51	2.32	15.0	150	0.0070	15.3	46.7
50-75-45-1	45	0.87	0.0932	0.1850	0.50	2.29	16.4	0.0942	0.1860	0.51	2.28	16.5	43	0.0968	0.1860	0.52	2.21	16.5	15	0.0026	16.5	173.3

*First two numbers indicate nominal aspect ratio, a/2C; next two numbers indicate nominal flaw-depth ratio, a/t; next two numbers represent nominal applied stress, ksi; two flaws in each sample.

†Minimum cyclic stress is zero, therefore $K = \Delta K = FM\sigma\sqrt{\pi a/Q}$, where $F = 1.0 + 0.12(1-a/2C)^2$, M is the back surface correction factor (Forman, R. G.: "Computer Analysis of Two-Dimensional Fatigue Flaw Growth Problem." NASA TMX-58086, Feb 1972); units of K are ksi $\sqrt{in.}$

Table A-2 Flaw Growth Data for Parent Metal 0.125-in. 2219-T87 Aluminum -- Uniaxial Loading

Sample** Number	σ (ksi)	σ/σ_ys †	EDM PREFLAW					STAGE I GROWTH						STAGE II GROWTH						CYCLIC GROWTH VALUES		
			a_o (in.)	$2C_o$ (in.)	$a/2C_o$	Q_o	$K^{\dagger\dagger}_{I_o}$	a_1 (in.)	$2C_1$ (in.)	$a_1/2C_1$	Q_1	$K^{\dagger\dagger}_{I_o}$	N_1 (cycles)	a_2 (in.)	$2C_2$ (in.)	$a_2/2C_2$	Q_2	$K^{\dagger\dagger}_{I_2}$	N_2 or ΔN (cycles)	a_2-a_2 (in.)	$\dfrac{K_{I_1}+K_{I_2}}{2}$ ††	$\dfrac{\Delta a}{\Delta N}$ $\left(\dfrac{\mu \text{ in.}}{\text{cycle}}\right)$
PU-WT-W-25-15																						
LT	15	0.86	0.0264	0.1778	0.15	1.04	4.6	0.0264	0.1809	0.15	1.04	4.6	420	0.0350	0.1809	0.19	1.15	5.0	1000	0.0086	4.8	> 8.6
LB	15	0.86	0.0265	0.0647	0.41	1.89	3.3	0.0265	0.0647	0.41	1.89	3.3	420	0.0290	0.0647	0.45	2.08	3.3	1000	0.0027	3.3	> 2.7
PU-WT-H-25-15																						
LT	15	0.52	0.0277	0.2063	0.13	1.11	4.6	0.0277	0.2063	0.13	1.11	4.6	400	0.0289	0.2063	0.14	1.12	4.7	2000	0.0012	4.6	> 0.6
LB	15	0.52	0.0245	0.0629	0.39	1.91	3.1	0.0245	0.0629	0.39	1.91	3.1	400	0.0256	0.0629	0.41	1.98	3.1	2000	0.0011	3.1	> 0.6
PU-WL-W-25-30																						
LT	30	0.92	0.0279	0.2006	0.14	1.00	9.7	0.0305	0.2058	0.15	1.02	10.1	2000	0.0523	0.2144	0.24	1.27	11.7	2000	0.0218	10.9	10.9
LB	30	0.92	0.0275	0.0643	0.43	1.95	6.6	0.0299	0.0707	0.42	1.93	6.9	2000	0.0321	0.0740	0.43	1.98	7.0	2000	0.0022	7.0	1.0
PU-WL-W-50-30																						
LT	30	0.92	0.0607	0.4103	0.15	1.02	14.8	0.0629	0.4128	0.15	1.03	15.0	400	0.1078	0.4183	0.26	1.31	20.6	500	0.0449	17.8	89.8
LB	30	0.92	0.0597	0.1269	0.47	2.15	9.2	0.0612	0.1345	0.46	2.07	9.5	400	0.0648	0.1375	0.47	2.15	9.7	500	0.0036	9.6	7.2
PU-WL-H-25-30																						
LT	30	0.58	0.0263	0.1909	0.14	1.10	9.0	0.0269	0.2034	0.13	1.09	9.2	1000	0.0340	0.2046	0.17	1.17	9.9	1000	0.0071	9.5	7.1
LB	30	0.58	0.0263	0.1909	0.14	1.10	9.0	0.0305	0.0738	0.41	2.00	6.9	1000	0.0325	0.0774	0.42	2.02	7.0	1000	0.0020	6.9	2.0
PU-WL-H-50-30																						
LT	30	0.58	0.0592	0.4073	0.15	1.12	13.9	0.0745	0.4158	0.18	1.20	15.5	600	0.0958	0.4388	0.22	1.30	18.2	475	0.0213	16.9	44.8
LB	30	0.58	0.0598	0.1281	0.47	2.24	9.1	0.0612	0.1381	0.44	2.13	9.4	600	0.0653	0.1452	0.45	2.16	9.7	455	0.0041	9.6	8.6
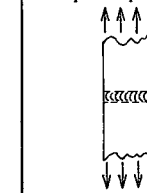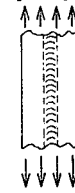
Transverse Weld – WT   Longitudinal Weld – WL

**Two flaws were placed in each sample: T = Top, B = Bottom: WT – weld transverse to loading direction, WL – weld parallel to loading direction: W means flaw placed in centerline at weld, H means flaw placed in heat affected zone: next two numbers in designation represent a/t ratio: last two numbers are applied stress in ksi.

±Note yield strength values were:
  17.5 ksi for weld zone, transverse to load
  32.5 ksi for weld zone, parallel to load
  28.7 ksi for heat affected zone, transverse to load
  52.0 ksi for heat affected zone, parallel to load (same as parent metal)

±†Minimum cycle stress is zero, therefore, $K = \Delta K = FM\sigma\sqrt{\pi a/Q}$, where $F = 1.0 + 0.12 (1 - a/2C)^2$, M is the back surface correction factor (Forman, R. G.: "Computer Analysis of Two-Dimensional Fatigue Flaw Growth Problems." NASA TMX-58086, Feb 1972), units of K are ksi $\sqrt{\text{in}}$.

*No stain apparent, hence actual rate is greater than measurements indicate.

Table A-3   Flaw Growth Data for Welded 0.125-in. 2219-T87 Aluminum -- Uniaxial Loading

Panel[†] Number	σ (ksi)	σ/σ_{ys}	EDM PREFLAW					STAGE I GROWTH						STAGE II GROWTH						CYCLIC GROWTH VALUES		
			a_o (in.)	$2C_o$ (in.)	$a/2C_o$	Q_o	K_{I_o}[††]	a_1 (in.)	$2C_1$ (in.)	$a_1/2C_1$	Q_1	K_{I_1}[††]	N_1 (cycles)	a_2 (in.)	$2C_2$ (in.)	$a_2/2C_1$	Q_2	K_{I_2}[††]	N_2orΔN (cycles)	a_2-a_1 (in.)	$\frac{K_{I_1}+K_{I_2}[††]}{2}$	$\frac{\Delta a}{\Delta N}$ ($\frac{\mu in.}{cycle}$)
060-25-40-1																						
TLT	40	0.77	0.0160	0.1004	0.16	1.10	9.4	0.0180	0.1004	0.18	1.15	9.7	760	0.0390	0.1200	0.33	1.59	12.5	3440	0.0210	11.1	6.1
BLL	40	0.77	0.0157	0.0960	0.16	1.11	9.2	0.0180	0.0990	0.18	1.15	9.7	760	0.0435	0.1357	0.32	1.58	14.0	3440	0.0255	11.8	7.4
TRT	40	0.77	0.0155	0.0390	0.40	1.87	6.7	0.0162	0.0400	0.41	1.91	6.8	760	0.0215	0.0480	0.45	2.09	7.5	3440	0.0053	7.2	1.5
BRL	40	0.77	0.0150	0.0370	0.41	1.91	6.6	0.0160	0.0395	0.41	1.91	6.8	760	0.0203	0.0467	0.43	2.04	7.4	3440	0.0043	7.1	1.3
060-25-40-2																						
TLL	40	0.77	0.0154	0.0920	0.17	1.12	9.1	0.0225	0.0994	0.23	1.27	10.2	3550	0.0457	0.1330	0.34	1.66	13.5	4550	0.0232	11.9	5.1
BLT	40	0.77	0.0152	0.0897	0.17	1.12	9.0	0.0184	0.0962	0.19	1.18	9.6	3550	0.0380	0.1144	0.33	1.62	11.9	4550	0.0196	10.8	4.3
BRT	40	0.77	0.0140	0.0320	0.44	2.04	6.1	0.0184	0.0398	0.46	2.16	6.8	3550	0.0234	0.0490	0.48	2.23	7.5	4550	0.0050	7.1	1.1
TRL	40	0.77	0.0140	0.0340	0.41	1.94	6.3	0.0170	0.0406	0.42	1.97	6.9	3550	0.0235	0.0514	0.46	2.14	7.7	4550	0.0065	7.3	1.4
060-35-30-1																						
TLL	30	0.58	0.0195	0.1474	0.13			0.0200	0.1474	0.14			350	0.0504	0.1730				6350			
BLT	30	0.58	0.0204	0.1443	0.14			No Growth					350	0.0475	0.1620				6350			
BRT	30	0.58	0.0196	0.0419	0.47			No Growth					350	0.0232	0.0470				6350			
TRL	30	0.58	0.0200	0.0454	0.44			No Growth					350	0.0244	0.0600				6350			
060-35-30-2																						
BLL	30	0.58	0.0180	0.1342	0.13	1.10	7.5	0.0240	0.1450	0.17	1.17	8.4	4600	0.0470	0.1575	0.30	1.55	11.0	1750	0.0230	9.7	13.1
TLT	30	0.58	0.0195	0.1500	0.13	1.09	7.9	0.0250	0.1575	0.16	1.16	8.7	4600	0.0425	0.1605	0.26	1.44	10.7	1750	0.0175	9.7	10.0
BRL	30	0.58	0.0195	0.0470	0.41	2.00	5.5	0.0215	0.0508	0.42	2.04	5.7	4600	0.0245	0.0535	0.46	2.20	5.8	1750	0.0030	5.8	1.7
TRT	30	0.58	0.0197	0.0460	0.43	2.06	5.4	0.0220	0.0480	0.46	2.20	5.5	4600	0.0240	0.0505	0.48	2.28	5.7	1750	0.0020	5.6	1.1
060-35-40-1																						
BLT	40	0.77	0.0190	0.1450	0.13	1.04	10.7	0.0260	0.1495	0.17	1.13	12.0	1100	0.0323	0.1628	0.27	1.39	15.1	750	0.0174	13.5	23.2
TLL	40	0.77	0.0200	0.1450	0.14	1.05	10.9	0.0235	0.1510	0.16	1.09	11.6	1100	0.0358	0.1595	0.22	1.27	13.7	750	0.0123	12.6	16.4
BRT	40	0.77	0.0200	0.0470	0.43	2.00	7.4	0.0225	0.0500	0.45	2.10	7.6	1100	0.0252	0.0540	0.47	2.18	7.9	750	0.0027	7.8	3.6
TRL	40	0.77	0.0195	0.0480	0.41	1.91	7.5	0.0215	0.0515	0.42	1.96	7.8	1100	0.0235	0.0540	0.43	2.04	7.9	750	0.0020	7.9	2.7
060-35-40-2																						
BLL	40	0.77	0.0202	0.1325	0.15	1.08	10.7	0.0290	0.1430	0.20	1.21	12.4	1350	0.0380	0.1506	0.25	1.35	14.0	500	0.0090	13.2	18.0
TLT	40	0.77	0.0143	0.1188	0.12	1.02	9.3	0.0175	0.1205	0.15	1.07	10.0	1350	0.0220	0.1220	0.18	1.15	10.8	500	0.0045	10.4	9.0
BRL	40	0.77	0.0210	0.0440	0.48	2.23	7.1	0.0233	0.0380	0.49	2.27	7.4	1350	0.0252	0.0520	0.48	2.27	7.8	500	0.0019	7.6	3.8
TRT	40	0.77	0.0195	0.0440	0.45	2.08	7.2	0.0216	0.0472	0.46	2.14	7.4	1350	0.0230	0.0520	0.46	2.14	7.6	500	0.0014	7.5	2.8
060-50-30-1																						
TLL	30	0.58	0.0296	0.2112	0.14	1.11	9.9	0.0426	0.2120	0.20	1.26	12.0	2100	0.0605*	0.2600	0.23	1.34	18.7	2350	0.0179	15.3	7.6
BLT	30	0.58	0.0272	0.2015	0.13	1.10	9.4	0.0393	0.2030	0.19	1.24	11.2	2100	0.0580	0.2200	0.26	1.44	15.4	2350	0.0187	13.3	8.0
TRL	30	0.58	0.0304	0.0634	0.48	2.30	6.4	0.0319	0.0686	0.47	2.23	6.6	2100	0.0360	0.0760	0.47	2.27	7.0	2350	0.0041	6.8	1.7
BRT	30	0.58	0.0304	0.0650	0.47	2.24	6.4	0.0315	0.0665	0.47	2.27	6.5	2100	0.0352	0.0760	0.46	2.22	7.0	2350	0.0037	6.8	1.6

[†]First two letters orient flaw in relation to sample number on panel (T = top, B = bottom, L = left, R = right); last letter shows flaw orientation with respect to grain direction (T = transverse, L = longitudinal).

[††]First number represents material thickness in thousandths of an inch; second number represents nominal a/t ratio; third number indicates stress level in ksi. Minimum cyclic stress is zero, therefore, $K = \Delta K = FM\sigma\sqrt{\pi a/Q}$, where $F = 1.0 + 0.12(1-a/2C)^2$, M is the back surface correction factor (Forman, R. G.: "Computer Analysis of Two-Dimensional Fatigue Flaw Growth Problem." NASA TMX-58086, Feb 1972); units of K are ksi $\sqrt{in}$.

*Indicates thru flaw.

Table A-4 Fatigue Flaw Growth Data for Parent Metal 0.125-in. 2219-T87 Aluminum—Balanced Biaxial Loading, Unstiffened Panels

Panel† Number	σ (ksi)	σ/σ_{ys}	EDM PREFLAW a_o (in.)	$2C_o$ (in.)	$a/2C_o$	Q_o	$K_{I_o}^{\dagger\dagger}$	STAGE I GROWTH a_1 (in.)	$2C_1$ (in.)	$a_1/2C_1$	Q_1	$K_{I_1}^{\dagger\dagger}$	N_1 (cycles)	STAGE II GROWTH a_2 (in.)	$2C_2$ (in.)	$a_2/2C_2$	Q_2	$K_{I_2}^{\dagger\dagger}$	N_2 or ΔN (cycles)	CYCLIC GROWTH VALUES a_2-a_1 (in.)	$\frac{K_{I_1}+K_{I_2}^{\dagger\dagger}}{2}$	$\frac{\Delta a}{\Delta N}\left(\frac{\mu in.}{cycle}\right)$
060-50-30-2																						
BLL	30	0.58	0.0280	0.2130	0.13	1.09	9.7	0.0370	0.2206	0.17	1.17	11.3	2400	0.0515	0.2344	0.22	1.31	14.8	1650	0.0145	13.0	8.8
TLT	30	0.58	0.0275	0.2190	0.13	1.08	9.7	0.0334	0.2233	0.15	1.13	10.6	2400	0.0478	0.2325	0.21	1.27	13.4	1650	0.0144	12.0	8.7
BRL	30	0.58	0.0278	0.0625	0.44	2.14	6.3	0.0295	0.0658	0.45	2.15	6.5	2400	0.0316	0.0704	0.45	2.15	6.8	1650	0.0021	6.6	1.3
TRT	30	0.58	0.0260	0.0610	0.43	2.05	6.3	0.0270	0.0635	0.43	2.05	6.4	2400	0.0290	0.0660	0.44	2.11	6.5	1650	0.0020	6.5	1.2
060-50-40-1																						
TLL	40	0.77	0.0301	0.2055	0.15	1.07	13.5	0.0426	0.2152	0.20	1.19	16.0	1050	0.0565	0.2351	0.24	1.31	20.2	750	0.0139	18.1	18.5
BLT	40	0.77	0.0283	0.2320	0.13	1.04	13.2	0.0426	0.2055	0.21	1.22	15.6	1050	0.0582	0.2492	0.23	1.29	20.8	750	0.0156	18.2	20.8
BRT	40	0.77	0.0300	0.0695	0.43	2.02	9.0	0.0320	0.0730	0.48	2.05	9.3	1050	0.0374	0.0822	0.46	2.13	10.0	750	0.0054	9.6	7.2
TRL	40	0.77	0.0295	0.0640	0.46	2.15	8.6	0.0320	0.0698	0.46	2.14	9.1	1050	0.0350	0.0766	0.46	2.14	9.6	750	0.0030	9.3	4.0
060-50-40-2																						
BLL	40	0.77	0.0295	0.2175	0.14	1.05	13.5	0.0314	0.2175	0.14	1.06	13.9	500	0.0474	0.2292	0.21	1.22	17.2	1000	0.0160	15.5	16.0
TLT	40	0.77	0.0280	0.2170	0.13	1.03	13.2	0.0298	0.2200	0.14	1.05	13.6	500	0.0450	0.2300	0.20	1.19	16.9	1000	0.0152	15.3	15.2
BRL	40	0.77	0.0284	0.0653	0.43	2.04	8.8	0.0295	0.0670	0.44	2.06	8.9	500	0.0318	0.0720	0.44	2.07	9.2	1000	0.0023	9.0	2.3
TRT	40	0.77	0.0290	0.0660	0.44	2.06	8.8	0.0308	0.0680	0.45	2.12	8.9	500	0.0330	0.0740	0.45	2.09	9.4	1000	0.0022	9.2	2.2
125-25-30-1																						
TLT	30	0.58	0.0278	0.2186	0.13	1.08	9.4	0.0316	0.2285	0.14	1.11	9.9	4400	0.0650	0.2345	0.28	1.48	12.2	1640	0.0334	11.0	20.4
TRL	30	0.58	0.0274	0.2092	0.13	1.09	9.3	0.0310	0.2161	0.14	1.12	9.7	4400	0.0615	0.2220	0.28	1.48	11.8	1640	0.0305	10.8	18.6
BLT	30	0.58	0.0284	0.0620	0.46	2.20	6.3	0.0323	0.0715	0.45	2.17	6.7	4400	0.0364	0.6765	0.05	0.97	11.7	1640	0.0041	9.2	2.5
BRL	30	0.58	0.0285	0.0625	0.46	2.19	6.3	0.0324	0.0705	0.46	2.20	6.7	4400	0.0384	0.0785	0.49	2.34	7.0	1640	0.0060	6.9	3.7
125-25-30-2																						
TRL	30	0.58	0.0320	0.2210	0.14	1.12	9.9	0.0580	0.2520	0.23	1.34	12.1	6250	0.0940	0.2900	0.32	1.64	14.8	1000	0.0360	13.5	36.0
TLT	30	0.58	0.0275	0.2062	0.13	1.10	9.2	0.0335	0.2128	0.16	1.15	9.9	6250	0.0458	0.2150	0.21	1.29	10.9	1000	0.0123	10.4	12.3
BRL	30	0.58	0.0298	0.0697	0.43	2.06	6.7	0.0343	0.0795	0.43	2.08	7.1	6250	0.0394	0.0850	0.46	2.22	7.3	1000	0.0051	7.2	5.1
BLT	30	0.58	0.0278	0.0674	0.41	2.00	6.5	0.0314	0.0750	0.42	2.02	6.9	6250	0.0360	0.0806	0.47	2.14	7.2	1000	0.0046	7.0	4.6
125-25-40-1 (No data Sample not Stained)																						
125-25-40-2																						
BLT	40	0.77	0.0271	0.2048	0.13	1.04	12.6	0.0330	0.2092	0.16	1.09	13.5	1030	0.0462	0.2104	0.22	1.25	14.8	720	0.0132	14.1	18.3
TLL	40	0.77	0.0311	0.2140	0.15	1.07	13.3	0.0340	0.2185	0.16	1.10	13.7	1030	0.0505	0.2220	0.23	1.27	15.4	720	0.0165	14.5	22.9
TRL	40	0.77	0.0315	0.0660	0.48	2.23	8.7	0.0327	0.0680	0.48	2.25	8.9	1030	0.0350	0.0716	0.49	2.29	9.1	720	0.0023	8.9	3.2
BRT	40	0.77	0.0300	0.0640	0.47	2.19	8.6	0.0325	0.0684	0.48	2.22	8.9	1030	0.0346	0.0735	0.47	2.20	9.2	720	0.0021	9.0	2.9

†First two letters orient flaw in relation to sample number on panel (T = top, B = bottom, L = left, R = right); last letter shows flaw orientation with respect to grain direction (T - transverse, L = longitudinal).

††First number represents material thickness in thousandths of an inch; second number represents nominal a/t ratio; third number indicates stress level in ksi. Minimum cyclic stress is zero, therefore, $K = \Delta K = FM\sigma\sqrt{\pi a/Q}$, where $F = 1.0 + 0.12(1-a/2C)^2$, M is the back surface correction factor (Forman, R. G.: "Computer Analysis of Two-Dimensional Fatigue Flaw Growth Problem." NASA TMX-58086, Feb 1972); units of K are ksi $\sqrt{in}$.

*Indicates thru flaw.

Table A-4 (cont)

Panel[†] Number	σ (ksi)	σ/σ_{ys}	EDM PREFLAW a_o (in.)	$2C_o$ (in.)	$a/2C_o$	Q_o	K_{I_o}[††]	STAGE I GROWTH a_1 (in.)	$2C_1$ (in.)	$a_1/2C_1$	Q_1	K_{I_1}[††]	N_1 (cycles)	STAGE II GROWTH a_2 (in.)	$2C_2$ (in.)	$a_2/2C_2$	Q_2	K_{I_2}[††]	N_2 or ΔN (cycles)	CYCLIC GROWTH VALUES a_2-a_1 (in.)	$\frac{K_{I_1}+K_{I_2}}{2}$[††]	$\frac{\Delta a}{\Delta N}\left(\frac{\mu in.}{cycle}\right)$
125-35-30-2																						
TLT	30	0.58	0.0465	0.2905	0.16	1.15	11.8	0.0490	0.2957	0.17	1.17	12.0	2700	0.0770	0.3072	0.25	1.40	14.1	1600	0.0280	13.1	17.5
BLL	30	0.58	0.0410	0.2904	0.14	1.11	11.3	0.0490	0.2935	0.17	1.17	12.0	2700	0.0810	0.3075	0.26	1.44	14.4	1600	0.0320	13.2	20.0
TRT	30	0.58	0.0390	0.0980	0.40	1.93	7.9	0.0413	0.1025	0.40	1.95	8.1	2700	0.0482	0.1100	0.44	2.11	8.4	1600	0.0069	8.2	4.3
BRL	30	0.58	0.0382	0.0940	0.41	1.97	7.7	0.0402	0.1000	0.40	1.95	8.0	2700	0.0468	0.1085	0.43	2.08	8.3	1600	0.0066	8.2	4.1
125-35-40-1																						
TLT	40	0.77	0.0395	0.2750	0.14	1.06	15.1	0.0420	0.2802	0.15	1.08	15.5	1050	0.0692	0.2874	0.24	1.31	18.2	800	0.0272	16.9	34.0
BLL	40	0.77	0.0400	0.2775	0.14	1.06	15.2	0.0525	0.2960	0.18	1.14	16.9	1050	0.0870	0.3280	0.27	1.39	21.0	800	0.0345	18.9	43.1
TRT	40	0.77	0.0382	0.0972	0.39	1.86	10.7	0.0420	0.1030	0.41	1.92	11.0	1050	0.0490	0.1145	0.43	2.01	11.6	800	0.0070	11.3	8.8
BRL	40	0.77	0.0382	0.1000	0.38	1.80	10.8	0.0410	0.1060	0.39	1.83	11.1	1050	0.0495	0.1175	0.42	1.98	11.7	800	0.0085	11.4	10.6
125-50-30-1																						
BLL	30	0.58	0.0616	0.4161	0.15	1.13	14.1	0.0900	0.4255	0.21	1.28	17.0	1600	0.0990	0.4416	0.22	1.32	18.4	400	0.0090	17.7	22.5
TLT	30	0.58	0.0710	0.4355	0.16	1.16	15.3	0.1010	0.4560	0.22	1.31	19.4	1600	0.1103	0.4786	0.23	1.34	21.6	400	0.0093	20.5	23.3
TRT	30	0.58	0.0627	0.1358	0.46	2.21	9.3	0.0653	0.1442	0.45	2.17	9.7	1600	0.0692	0.1521	0.46	2.18	10.0	400	0.0039	9.8	9.8
BRL	30	0.58	0.0620	0.1335	0.46	2.23	9.3	0.0647	0.1400	0.46	2.22	9.5	1600	0.0684	0.1467	0.47	2.23	9.8	400	0.0037	9.6	9.3
125-50-30-2																						
TLL	30	0.58	0.0605	0.4197	0.14	1.12	14.1	0.0815	0.4330	0.19	1.22	16.4	1650	0.0987	0.4483	0.22	1.31	18.8	1050	0.0172	17.6	16.4
BLT	30	0.58	0.0600	0.4178	0.14	1.12	14.0	0.0860	0.4317	0.20	1.25	16.7	1650	0.1134	0.4665	0.24	1.38	21.3	1050	0.0274	19.0	26.1
TRL	30	0.58	0.0605	0.1357	0.45	2.14	9.4	0.0658	0.1425	0.46	2.21	9.6	1650	0.0704	0.1529	0.46	2.21	10.0	1050	0.0046	9.8	4.4
BRT	30	0.58	0.0670	0.1360	0.49	2.36	9.3	0.0660	0.1425	0.46	2.22	9.6	1650	0.0702	0.1546	0.45	2.18	10.1	1050	0.0042	9.8	4.0
125-50-40-1																						
TRL	40	0.77	0.0590	0.4155	0.14	1.06	19.2	0.0782	0.4355	0.18	1.15	22.4	140	0.1170*	0.4960	0.24	1.30	35.2	630	0.0388	28.8	61.6
TLT	40	0.77	0.0560	0.4046	0.14	1.05	18.6	No Growth					140	0.0792	0.4130	0.19	1.18	21.9	630	0.0232	20.3	>36.9
LRL	40	0.77	0.0590	0.1210	0.49	2.28	11.9	0.0637	0.1328	0.48	2.24	12.5	140	0.0660	0.1384	0.48	2.23	12.8	630	0.0023	12.7	3.7
LLT	40	0.77	0.0606	0.1255	0.48	2.26	12.1	0.0640	0.1310	0.49	2.29	12.4	140	0.0670	0.1385	0.48	2.26	12.8	630	0.0030	12.6	4.8
125-50-40-2																						
TLT	31	0.77	0.0600	0.4125	0.15	1.07	14.5	0.0680	0.4125	0.16	1.11	20.2	1345	0.0798	0.4205	0.19	1.17	16.8	1000	0.0118	16.2	11.8
BLL	40	0.77	0.0612	0.4180	0.15	1.07	19.3	0.0810	0.4300	0.19	1.17	22.1	1345	0.0990	0.4504	0.22	1.25	25.3	1000	0.0180	23.7	18.0
TRT	31	0.77	0.0564	0.1360	0.41	1.95	9.85	0.0580	0.1392	0.41	1.96	12.8	1345	0.0620	0.1475	0.42	1.97	10.2	1000	0.0040	10.1	4.0
BRL	40	0.77	0.0594	0.1375	0.43	2.02	12.7	0.0620	0.1430	0.43	2.03	13.0	1345	0.0698	0.1575	0.44	2.07	13.8	1000	0.0078	13.4	7.8
125-75-30-1																						
TLT	30	0.58	0.0910	0.6000	0.15	1.14	18.6	0.0945	0.0604	0.16	1.15	19.2	200	0.1320*	0.6205	0.21	1.29	28.7	1000	0.0375	23.9	37.5
BLL	30	0.58	0.0930	0.6041	0.15	1.14	18.7	0.0970	0.6094	0.16	1.15	19.3	200	0.1300*	0.6314	0.21	1.27	27.1	1000	0.0330	23.2	33.0
TRT	30	0.58	0.0921	0.1900	0.48	2.32	11.5	0.0930	0.1917	0.49	2.32	11.6	200	0.0970	0.1992	0.49	2.33	12.0	1000	0.0040	11.8	4.0
BRL	30	0.58	0.0926	0.2075	0.45	2.14	12.2	0.0945	0.2098	0.45	2.16	12.4	200	0.0985	0.2195	0.45	2.15	12.8	1000	0.0040	12.6	4.0

[†]First two letters orient flaw in relation to sample number on panel (T = top, B = bottom, L = left, R = right); last letter shows flaw orientation with respect to grain direction (T = transverse, L = longitudinal).

[††]First number represents material thickness in thousandths of an inch; second number represents nominal a/t ratio; third number indicates stress level in ksi. Minimum cyclic stress is zero, therefore, $K = \Delta K = FM\sigma \sqrt{\pi a/Q}$, where $F = 1.0 + 0.12(1-a/2C)^2$, M is the back surface correction factor (Forman, R. G.: "Computer Analysis of Two-Dimensional Fatigue Flaw Growth Problem." NASA TMX-58086, Feb 1972); units of K are ksi $\sqrt{in.}$

*Indicates thru flaw.

Table A-4 (cont)

Panel[†] Number	σ (ksi)	σ/σ_ys	EDM PREFLAW					STAGE I GROWTH						STAGE II GROWTH						CYCLIC GROWTH VALUES		
			a_0 (in.)	$2C_0$ (in.)	$a/2C_0$	Q_0	$K_{I_0}^{++}$	a_1 (in.)	$2C_1$ (in.)	$a_1/2C_1$	Q_1	$K_{I_1}^{++}$	N_1 (cycles)	a_2 (in.)	$2C_2$ (in.)	$a_2/2C_2$	Q_2	$K_{I_2}^{++}$	N_2 or ΔN (cycles)	a_2-a_1 (in.)	$\dfrac{K_{I_1}+K_{I_2}^{++}}{2}$	$\dfrac{\Delta a}{\Delta N}$ $\left(\dfrac{uin.}{cycle}\right)$
125-75-40-2																						
TLT	40	0.77	0.0955	0.6260	0.15	1.08	27.6	0.0996	0.6293	0.16	1.10	28.6	125	0.1255*	0.6438	0.19	1.19	39.6	125	0.0259	34.1	207.2
BLL	40	0.77	0.0900	0.6010	0.15	1.08	26.1	0.1024	0.6064	0.17	1.12	29.8	125	0.1234*	0.6300	0.20	1.19	39.2	75	0.0210	34.5	280.0
TRT	40	0.77	0.0930	0.1935	0.48	2.25	16.2	0.0937	0.2000	0.47	2.19	16.5	125	0.0960	0.2043	0.47	2.19	16.8	125	0.0023	16.7	18.4
BRL	40	0.77	0.0913	0.1945	0.47	2.19	16.2	0.0934	0.2015	0.46	2.17	16.6	125	0.0980	0.2060	0.48	2.22	17.0	125	0.0046	16.8	36.8

[†]First two letters orient flaw in relation to sample number on panel (T = top, B = bottom, L = left, R = right); last letter shows flaw orientation with respect to grain direction (T - transverse, L - longitudinal).

[††]First number represents material thickness in thousandths of an inch; second number represents nominal a/t ratio; third number indicates stress level in ksi. Minimum cyclic stress is zero, therefore, K = ΔK = FMσ $\sqrt{\pi a/Q}$, where F = 1.0 + 0.12(1-a/2C)^2, M is the back surface correction factor (Forman, R. G.: "Computer Analysis of Two-Dimensional Fatigue Flaw Growth Problem." NASA TMX-58086, Feb 1972); units of K are ksi $\sqrt{in.}$

*Indicates thru flaw.

Table A-4 (concl)

Panel† Number	σ (ksi)	σ/σ_ys	EDM PREFLAW					STAGE I GROWTH						STAGE II GROWTH						CYCLIC GROWTH VALUES		
			a_o (in.)	$2C_o$ (in.)	$a/2C_o$	Q_o	K_{I_o}††	a_1 (in.)	$2C_1$ (in.)	$a_1/2C_1$	Q_1	K_{I_1}††	N_1 (cycles)	a_2 (in.)	$2C_2$ (in.)	$a_2/2C_2$	Q_2	K_{I_2}††	N_2 or ΔN (cycles)	a_2-a_1 (in.)	$\frac{K_{I_1}+K_{I_2}††}{2}$	$\frac{\Delta a}{\Delta N}$ ($\frac{\mu\ in.}{cycle}$)
PB-WL-25-FL																						
15W	15	0.86	0.0295	0.1931	0.15	1.05	4.9	0.0295	0.1931	0.15	1.05	4.9	7000	0.0295	0.1931	0.15	1.05	4.9	3000	N.G.	4.9	
50W	15	0.86	0.0280	0.0654	0.43	1.98	3.3	0.0280	0.0654	0.43	1.98	3.3	7000	0.0280	0.0654	0.43	1.98	3.3	3000	N.G.	3.3	
15H	15	0.52	0.0282	0.1945	0.14	1.13	4.6	0.0282	0.1945	0.14	1.13	4.6	7000	0.0282	0.1945	0.14	1.13	4.6	3000	N.G.	4.6	
50H	15	0.52	0.0280	0.0640	0.44	2.12	3.2	0.0280	0.0640	0.44	2.12	3.2	7000	0.0280	0.0640	0.44	2.12	3.2	3000	N.G.	3.2	
PB-WL-25-FT																						
15W	30	0.92	0.0296	0.1990	0.15	1.02	9.9	0.0325	0.1995	0.16	1.05	10.2	1800	0.0423	0.2073	0.20	1.15	11.1	1300	0.0098	10.6	7.5
50W	30	0.92	0.0292	0.0654	0.45	2.03	6.6	0.0307	0.7000	0.44	2.00	6.8	1800	0.0325	0.0725	0.44	2.04	7.0	1300	0.0018	6.9	1.4
15H	30	0.58	0.0286	0.1960	0.15	1.12	9.3	0.0309	0.1960	0.16	1.15	9.5	1800	0.0357	0.2012	0.18	1.20	10.0	1300	0.0048	9.8	3.7
50H	30	0.58	0.0298	0.0640	0.47	2.23	6.4	0.0310	0.0660	0.47	2.25	6.5	1800	0.0332	0.0704	0.47	2.26	6.7	1300	0.0022	6.6	1.7
PB-WL-50-FL																						
15W	15	0.86	0.0563	0.4025	0.14	1.02	7.1	0.0575	0.4025	0.14	1.03	7.2	1250	0.0594	0.4025	0.15	1.04	7.3	2750	0.0019	7.2	0.7
50W	15	0.86	0.0578	0.1310	0.44	2.03	4.7	0.0578	0.1310	0.44	2.03	4.7	1250	0.0581	0.1310	0.44	2.04	4.7	2750	0.0003	4.7	0.1
15H	15	0.52	0.0605	0.4195	0.14	1.13	7.8	0.0605	0.4195	0.15	1.13	7.8	1250	0.0605	0.4195	0.14	1.13	7.8	2750		7.8	
50H	15	0.52	0.0575	0.1276	0.45	2.17	4.6	0.0575	0.1276	0.45	2.17	4.6	1250	0.0582	0.1276	0.46	2.20	4.6	2750	0.0070	4.6	0.3
PB-WL-50-FT																						
15W	30	0.92	0.0581	0.4050	0.14	1.01	14.6	0.0593	0.4200	0.14	1.00	14.9	300	0.0672	0.4200	0.16	1.04	15.8	210	0.0079	15.3	37.6
50W	30	0.92	0.0595	0.1320	0.45	2.05	9.5	0.0595	0.1340	0.44	2.02	9.6	300	0.0600	0.1380	0.43	1.98	9.8	210	0.0005	9.7	2.4
15H	30	0.58	0.0566	0.4280	0.13	1.10	14.8	0.0730	0.4520	0.16	1.16	19.0	300	0.0865	0.5340	0.16	1.16	26.3	210	0.0135	22.7	64.3
50H	30	0.58	0.0587	0.1300	0.45	2.16	9.2	0.0595	0.1350	0.44	2.12	9.4	300	0.0612	0.1495	0.41	1.98	9.9	210	0.0017	9.6	8.1

**Four flaws were placed in each panel, WL indicated weld was always oriented parallel to nominal 30 ksi loading direction, next two numbers, represent a/t ratio, FL means flaw oriented parallel to loading direction and FT means flaw is transverse to loading; flaw numbers show nominal aspect ratio of 0.15 or 0.50 and flaw location H for heat affected zone, W for weld zone.

†Note yield strength values were:
    17.5 ksi for weld zone, transverse to load
    32.5 ksi for weld zone, parallel to load
    28.7 ksi for heat affected zone, transverse to load
    52.0 ksi for heat affected zone, parallel to load (same as parent metal)

Table A-5 Flaw Growth Data for 0.125-in. Welded 2219-T87 Aluminum - 2:1 Biaxial Loading

Panel (flaw*) Number	σ (ksi)	σ/σ_ys	EDM PREFLAW a_o (in.)	2C_o (in.)	a/2C_o	Q_o	K_I_o†	STAGE I GROWTH a_1 (in.)	2C_1 (in.)	a_1/2C_1	Q_1	K_I_1†	N_1 (cycles)	STAGE II GROWTH a_2 (in.)	2C_2 (in.)	a_2/2C_2	Q_2	K_I_2^T	N_2 or ΔN (cycles)	CYCLIC GROWTH VALUES a_2-a_1 (in.)	(K_I_1+K_I_2†)/2	Δa/ΔN (μin./cycle)
1S-060-50-30																						
-4	28	0.54	0.0295	0.0667	0.44	2.12	6.0	0.0297	0.0667	0.45	2.14	6.0	3524	0.0328	0.0693	0.47	2.27	6.1	876	0.0031	6.1	3.5
-5	28	0.54	0.0316	0.0670	0.47	2.26	6.0	0.0320	0.0680	0.47	2.25	6.0	3524	0.0340	0.0685	0.50	2.38	6.1	876	0.0020	6.1	2.3
-7	31	0.60	0.0304	0.0681	0.45	2.14	6.2	0.0315	0.0711	0.44	2.13	6.8	3524	0.0322	0.0728	0.44	2.12	7.0	876	0.0007	6.9	0.8
-8	31	0.60	0.0323	0.0695	0.46	2.23	6.8	0.0323	0.0695	0.46	2.23	6.8	3524	0.0323	0.0695	0.46	2.23	6.8	876	0.0000	6.8	0.0
-9	36	0.69	0.0305	0.0650	0.47	2.25	8.1	0.0323	0.0685	0.46	2.21	8.3	3524	0.0338	0.0700	0.56	2.14	8.3	876	0.0015	8.3	1.7
-10	36	0.69	0.0305	0.0650	0.47	2.25	8.1	0.0325	0.0693	0.47	2.25	8.3	3524	0.0350	0.0712	0.49	2.36	8.3	876	0.0025	8.3	2.9
2S-060-50-30																						
-4	26	0.50	0.0310	0.1913	0.16	1.16	9.0	0.0332	0.1925	0.17	1.18	9.2	2650	0.0370	0.1938	0.19	1.23	9.5	950	0.0038	9.4	4.0
-5	26	0.50	0.0350	0.1953	0.18	1.20	8.4	0.0356	0.1953	0.19	1.23	8.5	2650	0.0386	0.1953	0.20	1.25	8.7	950	0.0030	8.6	3.2
-7	28	0.54	0.0296	0.2190	0.14	1.10	8.8	0.0327	0.2190	0.15	1.13	9.2	2650	0.0406	0.2190	0.19	1.22	9.8	950	0.0079	9.5	8.3
-8	29	0.56	0.0290	0.2231	0.13	1.09	9.4	0.0318	0.2255	0.14	1.11	9.7	2650	0.0382	0.2276	0.17	1.17	10.3	950	0.0064	10.0	6.7
-9	31	0.60	0.0294	0.2052	0.14	1.12	9.3	0.0330	0.2090	0.16	1.15	9.7	2650	0.0450	0.2110	0.21	1.29	10.6	950	0.0120	10.1	12.6
-10	35	0.67	0.0297	0.2041	0.15	1.12	12.9	0.0343	0.2085	0.16	1.16	10.6	2650	0.0531	0.2185	0.24	1.37	14.7	950	0.0188	14.0	19.8
3S-060-50-30																						
-4	23	0.44	0.0272	0.0630	0.43	2.08	4.7	0.0272	0.0630	0.43	2.08	4.7	3000	0.0285	0.0640	0.45	2.14	4.8	2300	0.0013	4.8	0.6
-5	23	0.44	0.0305	0.0642	0.48	2.28	4.8	0.0305	0.0642	0.48	2.28	4.8	3000	0.0323	0.0650	0.50	2.38	4.8	2300	0.0018	4.8	0.8
-7	28	0.54	0.0561	0.1405	0.40	1.94	8.8	0.0587	0.1440	0.41	1.97	9.0	3000	0.0668	0.1513	0.44	2.12	9.2	2300	0.0081	9.1	3.5
-8	28	0.54	0.0291	0.0689	0.42	2.04	6.2	0.0312	0.0710	0.44	2.11	6.3	3000	0.0335	0.0717	0.47	2.2	6.2	2300	0.0023	6.3	1.0
-9	35	0.67	0.0290	0.0700	0.41	2.00	8.0	0.0305	0.0732	0.42	2.01	8.1	3000	0.0344	0.0805	0.43	2.1	8.4	2300	0.0039	8.3	1.7
-10	35	0.67	0.0526	0.1427	0.37	1.81	11.7	0.0546	0.1473	0.37	1.82	11.9	3000	0.0721	0.1773	0.41	2.0	12.4	2300	0.0175	12.3	7.6
4S-125-50-30																						
-4	20	0.38	0.0600	0.1332	0.45	2.16	8.6	0.0600	0.1367	0.44	2.11	8.7	2000	0.0600	0.1709	0.35	1.74	8.8	1500	N.G.	8.8	N.G.
-5	20	0.38	0.0600	0.1103	0.54	2.20	7.6	0.0600	0.1103	0.54	2.20	7.8	2000	0.0600	0.1547	0.39	1.89	8.0	1500	N.G.	8.0	N.G.
-7	29	0.56	0.0644	0.1435	0.45	2.15	9.0	0.0650	0.1445	0.45	2.16	9.1	2000	0.0792	0.1566	0.51	2.37	9.4	1500	0.0142	9.2	9.5
-8	29	0.56	0.0590	0.1395	0.42	2.04	9.0	0.0600	0.1414	0.42	2.04	9.1	2000	0.0660	0.1571	0.42	2.03	9.4	1500	0.0060	9.2	4.0
-9	32	0.62	0.0545	0.1421	0.38	1.87	10.4	0.0565	0.1482	0.38	1.86	10.6	2000	0.0769	0.1801	0.43	2.06	11.6	1500	0.0204	11.1	13.6
-10	32	0.62	0.0582	0.1388	0.42	2.02	10.3	0.0610	0.1428	0.43	2.06	10.4	2000	0.0742	0.1902	0.39	1.90	11.9	1500	0.0132	11.2	8.8
5S-125-50-30																						
-4	20	0.38	0.0630	0.1300	0.48	2.32	5.9	0.0635	0.1318	0.48	2.31	6.0	3700	0.0645	0.1330	0.48	2.32	6.0	828	0.0010	6.0	1.2
-5	20	0.38	0.0600	0.1306	0.46	2.20	5.9	0.0610	0.1315	0.46	2.22	6.0	3700	0.0635	0.1352	0.47	2.25	6.0	828	0.0025	6.0	3.0
-7	27	0.52	0.0580	0.1456	0.40	1.93	8.5	0.0594	0.1500	0.40	1.92	8.7	3700	0.0645	0.1516	0.43	2.05	8.7	828	0.0051	8.7	6.2
-8	28	0.54	0.0574	0.1430	0.40	1.94	8.5	0.0632	0.1525	0.41	2.00	8.8	3700	0.0754	0.1-95	0.42	2.02	9.7	828	0.0122	9.3	14.7
-9	32	0.62	0.0530	0.1450	0.37	1.80	10.5	0.0595	0.1470	0.40	2.00	10.6	3700	0.0684	0.1500	0.46	2.20	10.7	828	0.0089	10.6	10.7
-10	32	0.62	0.0560	0.1434	0.39	1.90	10.3	0.0680	0.1655	0.41	2.00	11.1	3700	0.0790	0.1800	0.44	2.10	11.6	828	0.0110	11.4	13.3
6S-125-50-30																						
-4	21	0.40	0.0650	0.3760	0.17	1.18	9.0	0.0694	0.3800	0.18	1.20	9.3	2200	0.0791	0.3917	0.20	10.0	14.5	2000	0.0097	9.7	4.9
-5	21	0.40	0.0617	0.3061	0.20	1.26	8.3	0.0624	0.3061	0.20	1.27	8.6	2200	0.0658	0.3061	0.21	9.2	13.0	2000	0.0034	8.8	1.7
-7	26	0.50	0.0710	0.4462	0.16	1.15	12.0	0.0735	0.4462	0.16	1.17	12.1	2200	0.0982	0.4462	0.22	13.2	15.9	2000	0.0247	12.4	12.4
-8	26	0.50	0.0602	0.4456	0.14	1.09	11.4	0.0620	0.4456	0.14	1.11	11.5	2200	0.0890	0.4456	0.20	13.5	15.5	2000	0.0270	12.4	13.5
-9	32	0.62	0.0580	0.4332	0.13	1.09	14.3	0.0599	0.4385	0.14	1.10	14.5	2200	0.0964	0.4490	0.21	16.7	15.8	2000	0.0365	15.6	18.3
-10	26	0.50	0.0588	0.4268	0.14	1.10	11.5	0.0605	0.4302	0.14	1.11	11.6	2200	0.1098	0.4516	0.24	14.4	16.4	2000	0.0493	13.0	24.6

*Flaw number relates to flaw location in Figure V-11 and V-12.

†Minimum cyclic stress is zero; therefore $K = \Delta K = FM\sigma \sqrt{\pi a/Q}$, where $F = 1.0 + 0.12(1-a/2C)^2$, M is the back surface correction factor (Forman – NASA TM X-58086): units of K are $ksi\sqrt{in.}$

Table A-6 Tabular Listing of Flaw Growth Data for Biaxially Loaded Stiffened Panels (Uniform Stress Field)

Panel (Flaw*) Number	a_0 (in.)	$2C_0$ (in.)	a_1 (in.)	$2C_1$ (in.)	a_2 (in.)	$2C_2$ (in.)	$\Delta a/\Delta N$ (μ-in./cycle)	ΔK† (ksi $\sqrt{\text{in.}}$)	σ** (ksi)
1S-060-50-30									
-1	0.0298	0.0680	N.G.††	N.G.	N.G.	N.G.	--	--	--
-2	0.0317	0.0674	0.0426	0.1019	0.0464	0.1125	4.3	9.0	32.4
-3	0.0320	0.0705	N.G.	N.G.	N.G.	N.G.	--	--	--
-6	0.0280	0.0695	N.G.	N.G.	0.0285	0.0704	>0.6	--	--
2S-060-50-30									
-1	0.0330	0.1450	0.0358	0.1460	0.0460	0.1480	10.7	13.6	42.5
-2	0.0316	0.1584	0.0395	0.1800	0.0583	0.2060	19.7	17.3	47.2
-3	0.0338	0.1995	0.0354	0.2000	0.0382	0.2050	2.9	7.4	22.4
-6	0.0360	0.2050	0.0370	0.2060	0.0400	0.2060	3.1	7.6	22.6
3S-060-50-30									
-1	0.0320	0.0635	N.G.	N.G.	N.G.	N.G.	--	--	--
-2	0.0342	0.0635	0.0373	0.0680	0.0521	0.0880	6.4	10.8	40.6
-3	0.0324	0.0658	0.0325	0.0658	0.0350	0.0680	1.1	5.5	25.4
-6	0.0437	0.0628	N.G.	N.G.	N.G.	N.G.	--	--	--
4S-125-50-30									
-1	0.0660	0.1350	N.G.	N.G.	N.G.	N.G.	--	--	--
-2	0.0585	0.1310	0.0690	0.1500	0.0785	0.2010	6.3	10.8	29.3
-3	0.0616	0.1355	0.0624	0.1365	0.0665	0.1370	2.7	7.1	23.1
-6	0.0630	0.1370	N.G.	N.G.	0.0641	0.1370	>0.7	--	--
5S-125-50-30									
-1	0.0631	0.1312	0.0638	0.1335	0.0711	0.1382	8.8	12.5	40.3
-2	0.0611	0.1330	0.0680	0.1590	0.0815	0.1900	16.3	16.2	43.7
-3	0.0606	0.1373	0.0626	0.1395	0.0681	0.1430	6.6	11.0	34.7
-6	0.0580	0.1358	0.0588	0.1364	0.0603	0.1375	1.9	6.0	19.5
6S-125-50-30									
-1	0.0692	0.4165	0.0778	0.4165	0.0963	0.4165	9.2	12.8	25.6
-2	0.0605	0.4020	0.0635	0.4020	0.1130	0.4020	24.7	18.8	37.0
-3	0.0786	0.4148	0.0800	0.4148	0.0970	0.4148	8.5	12.3	24.6
-6	0.0600	0.4120	0.0733	0.4120	0.0845	0.4120	5.6	10.2	21.2

*Flaw numbers reflect location as shown in Figs. V-11 and V-12.

†ΔK from average biaxial growth rate curve and using obtained $\Delta a/\Delta N$.

**σ computed from $\Delta K = FM\ \sigma\ \sqrt{\pi a/Q}$.

††No Growth.

Table A-7 Tabular Listing of Flaw Growth Data for Stiffened Panels, Panels, - Nonuniform Stress Field

APPENDIX B

PHOTOELASTIC ANALYSIS REPORT

B-1

REPORT TO: MARTIN MARIETTA
WATERTON, COLORADO

"PHOTOELASTIC COATING ANALYSIS
OF ALUMINUM PANELS"

REFERENCE: MARTIN P.O. RC2-370203

DATE: DECEMBER 27, 1972

BY: PHOTOLASTIC, INCORPORATED
67 LINCOLN HIGHWAY
MALVERN, PENNSYLVANIA   19355

B-1 - a

1.0 INTRODUCTION

The purpose of the photoelastic coating analysis of the aluminum panels was oriented to:

1. Establish and define the stress distribution in the center bays of six aluminum panels. The stress distribution on both the front and rear sides was analyzed.

2. Determine the level of stress concentration in the corners and fillet radii adjacent to the center bay.

3. Determine the stress distribution in the stiffeners.

Determination of the above information was accomplished on each of the six panels for three loading conditions:

    1. 1:0 Uniaxial loading

    2. 1:1 Biaxial loading

    3. 2:1 Biaxial loading

Application of plastic and photoelastic coating measurements were conducted by Photolastic, Incorporated. Martin-Marietta constructed the test facility and applied the loads per their specifications.

2.0 INSTRUMENTATION

2.1 Plastic Application

Type PL-1* photoelastic coating was applied to the entire central bay of the six test panels defined on Martin dwgs. 163-72-027 sheets 1 and 2. In general, particular attention was given to the fillet and corner areas of the panels. Figure 1 shows the area which was coated. Preparation of the contour sheets was in accordance with Photolastic, Incorporated's bulletin IB-P-310 (Instructions for Molding and Contouring Photoelastic Sheets, See Appendix).

*Photolastic, Inc., Malvern, Pa.

Calibration of the individual plastic sheets established
the photoelastic strain sensitivity. Bonding of the plastic
to the panels was accomplished using type PC-1 reflective
adhesive*. Figure 2 shows pertinent dimensions for each
of the six test panels.

2.2 Polariscope

Photoelastic measurements were made using an 031 Reflective
Polariscope and the Oblique Incidence Attachment*. Photo-
graphic recordings of the resulting strain patterns were
made with a Nikon camera.

3.0 TEST PROCEDURE

The panels were installed in the loading fixture as shown in
Figures 3A and 3B. Once a panel was installed, it was loaded in:

Uniaxial Tension (Vert.: Horiz.:: 1:0)

Biaxial Tension (Vert.: Horiz.:: 1:1)

Biaxial Tension (Vert.: Horiz.:: 2:1)

The chronological sequence of testing was:

Spec No.	Dates Tested
5	11/14/72 - 11/15/72
6	11/16/72
4	11/17/72
2	11/17/72 - 11/18/72
1	11/18/72 - 11/20/72
3	11/21/72

The first test panel (#5) was subjected to uniaxial loads of
130, 86.6 and 43.3 kips. Experimental data showed that the
specimen's response to external load was essentially linear.

*Photolastic, Inc., Malvern, Pa.

The following table summarizes the kips load when photoelastic measurements were made:

PANEL	LOAD CONDITION (KIPS)		
	1:0	1:1	2:1
1	V = 65 & 25 H = 0 & 0	V = 65 & 25 H = V	V = 65 & 25 H = 1/2 V
2	V = 65 & 25 H = 0 & 0	V = 65 & 25 H = V	V = 65 & 25 H = 1/2 V
3	V = 65 & 25 H = 0 & 0	V = 65 & 25 H = V	V = 65 & 25 H = 1/2 V
4	V = 130 & 43.3 H = 0 & 0	V = 100 & 43.3 H = V	V = 130 & 43.3 H = 1/2 V
5	V = 130, 86.6 & 0 H = 0, 0, & 0	V = 130, 86.6 & 43.3 H = V	V = 130 & 43.3 H = 1/2 V
6	V = 130 & 43.3 H = 0 & 0	V = 130 & 43.3 H = V	V = 130 & 65 H = 1/2 V

The load induced photoelastic signal (ΔN) was obtained as the difference between measurements (N) taken at the tabulated upper and lower load levels. For example, on panels 1 through 3 (1:0 loading):

$$\Delta N = N_{65k} - N_{25k}$$

Here ΔN represents the signal induced by a 40 kip load. Martin's interest was to determine stress values induced by 130 kip on specimens 4, 5, and 6 and 91.6 kips on specimens 1, 2, and 3. All experimentally determined stresses were simply extrapolated linearly from the actual test load induced values to stress values corresponding with the expressed 130 kip and 91.6 kip levels. Data was collected at specific points designated by the coordinate system of Figure 4. The origin (HO, VO) was defined by the intersection of the horizontal and vertical ribs. Points of measurement (H2, V3 for example) were described in terms of inches from the horizontal rib axis and vertical rib axis (that is 2 in. in a direction parallel to the horizontal rib and 3 in. parallel to

the vertical rib). Further definition of points of measurement
are illustrated by the lower sketch of Figure 4. Lines identified
as "A", "B", "C" and "D" define:

    "A" the top edge of the ribs

    "B" the tangent line between ribs and fillet

    "C" the center (45°) of the fillet

    "D" the tangent line between the central bay and the fillet

For example, a location 1 inch from the origin (HO, VO) along the
top edge of the vertical rib is designated as A1. Further, point
B 1/2 indicates a location on a point one half inch removed from
the corner along the "B" line. Similar reasoning is used for
lines "C" and "D".

4.0 DATA REDUCTION

The experimental photoelastic signals were reduced to stresses
using the following relationships:

$$\varepsilon_1 - \varepsilon_2 = N_n f \qquad\qquad (1)$$

where,

    ε_1 and ε_2 = Maximum and minimum principal strains

        f = Fringe value of coating (established by calibra-
            tion)

        N_n = Normal incidence fringe measurements

From Hooke's Law:

$$\sigma_1 - \sigma_2 = \frac{E}{1+\nu} (\varepsilon_1 - \varepsilon_2) \qquad\qquad (2)$$

where,

        E = Elastic modulus

        ν = Poisson's Ratio

then:

$$\sigma_1 - \sigma_2 = \frac{E}{1+\nu} (N_n f) \qquad\qquad (3)$$

where "f" is established by calibration and is a function of coating thickness at the points of measurement. In thin skin applications, one finds that it becomes necessary to apply a correction factor (C_1) which will account for the reinforcement effect influenced by the plastic coating. This correction was taken into account and all tabulated data presented in this report are in final form. Determination of separate values of principal stresses (σ_1 and σ_2) can be accomplished with an additional photoelastic reading. This is accomplished by utilizing an oblique incidence attachment which is readily attachable to the reflecting polariscope. Thus, the emerging light from the polariscope is passed obliquely through the plastic establishing an additional oblique incidence fringe order (N_0). In this investigation the oblique measurements were used only to check the degree of biaxiability of the stress field.

5.0   TEST RESULTS

Before entering a discussion of the resulting test data, one should become familiar with the coordinate system defined on Figure 4. Due to the symmetry of the problem a detailed analysis was conducted on one quadrant of the central bay.

5.1   Uniaxial Loading (1:0 Loading)

Figures 5A through 10B show the photoelastic coating pattern resulting from uniaxial loading. Tables IA, IB, and IC show the experimental results for the required vertical loads.

5.2   Biaxial Loading (1:1 Loading)

The photoelastic coating patterns are shown in Figures 11A through 16B and the experimental results are shown in Tables IIA, IIB, and IIC.

5.3 Biaxial Loading (2:1 Loading)

Figures 17A through 22B show the photoelastic coating patterns and Tables IIIA, IIIB, and IIIC show the experimental results.

6.0 DISCUSSION OF TEST RESULTS

6.1 Uniaxial Loading (Tables IA, through IC & Figs. 5A through 10B)

The test results, tabulated in Tables IA through IC, demonstrate negligible bending through the thickness of the central panel bays. The measured stress values at H2V2, H2V6, H6V2, and H6V6, on the front and back surfaces, show good agreement (approximately ± 1 ksi or ± 3% of the nominal applied tensile stress). Further, the experimental data showed negligible stress gradients between the panel front face and the outside edge (top) of the vertical rib. This was particularly true in the central portion of the vertical rib (locations A4 through D4, A3 through D3, and A2 through D2). Stress gradients near the corner, formed by the intersecting vertical and horizontal ribs, were very steep. The experimental results show the stress levels at AO, BO, and CO to be measurably less than the nominal vertical rib stresses at mid-span. Reductions of 25% to 60% were observed. Stresses at DO were comparable to the nominal values of tensile stress in the panel faces and vertical ribs. The horizontal ribs experienced a low compressive stress along lines A and B. Measurements were made along lines A and B on specimen 3 only. The experimentally determined stresses along line A (-10 ksi to -13 ksi) compared favorably with the predictable value -10 ksi. Stresses along line D

adjacent to the horizontal rib were comparable with the
nominal tensile stresses in the central bay. The horizontal
ribs generated a disturbance in the stress field on the <u>back</u>
face (see Figures 5 through 10) with a maximum value occurring
at location HOVO (approximately 30% higher than the nominal
tensile stress). Stresses along the VO line (H 1/2 VO
through H4VO) were 10 to 25% greater than the nominal tensile
stress values. The data indicate that the nominal vertical
panel stress (specimen to specimen) ranged between a high
of 35 ksi in specimen 1 to 29 ksi in specimens 3 and 6. The
following observations are in order:

   -The corner stresses (corner formed by intersection

    ribs) were lower than the nominal tensile stress through

    the panel.

   -Bending stress through the panel thickness was

    generally less than ± 3% of the applied membrane

    stress.

   -Back face stresses (immediately behind the horizontal

    ribs) were 10 to 25% greater than the nominal values

    measured in the central portion of the panel.

   -The maximum experimental stress was observed on the

    back face at coordinate HOVO and was approximately

    30% greater than the nominal tensile stress.

   -Oblique incidence measurements established the stress

    field at HOVO, H1/2VO, H1VO, and H4VO to be uniaxial.

6.2 <u>Equal Biaxial Loading</u> (Tables IIA to IIC, Figs. 11A to 16B)
Normal incidence measurements provide an immediate evalua-
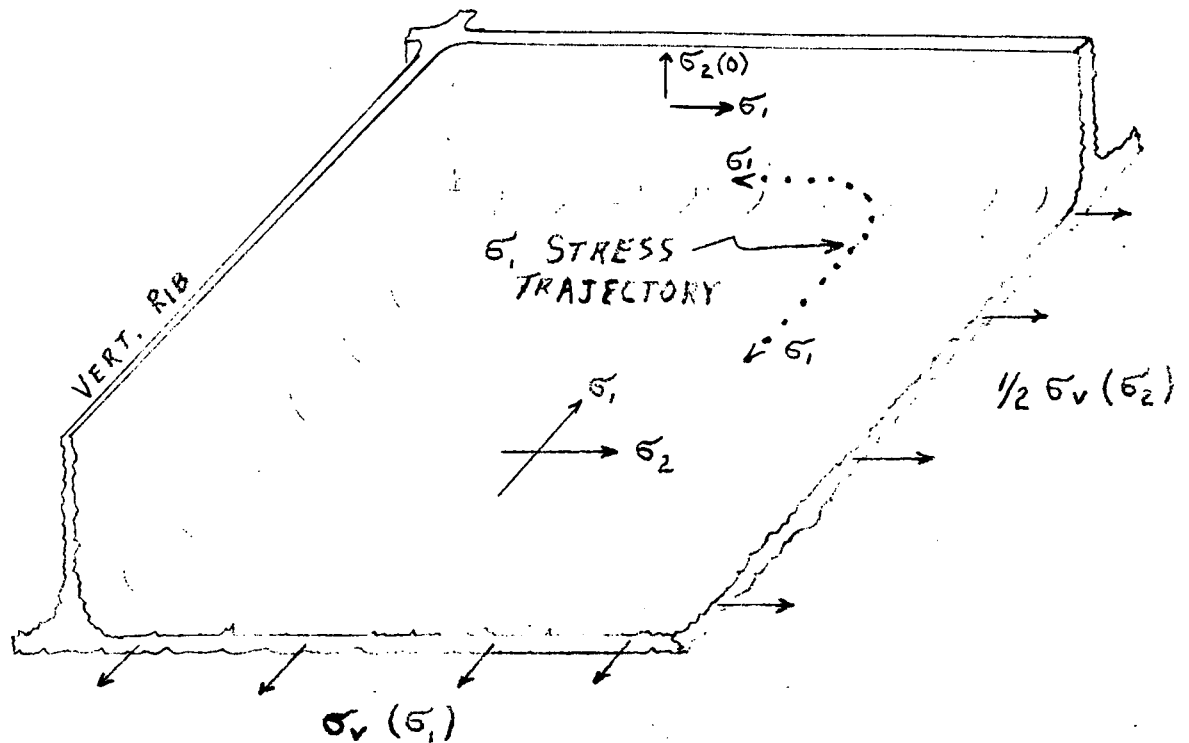tion of equal biaxial tension in the central panel. Deviation

from the zero fringe (black) indicates lack of symmetry between vertical (σ_v) and horizontal (σ_h) stress. Differences between σ_v and σ_h were generally less than 4 ksi or approximately 10% of the nominally applied stress. As in the uniaxial loadings, the stress gradients in the corner of the ribs were very steep. The data, in general, do not indicate a stress concentration in this area. Location CO of specimen 3 proved to be an exception to this general observation. No clear and obvious reason for this exception is postulated; however, it can be attributed to the general nonsymmetrical stress distribution, present in varying degrees of all specimens. Stresses along line A of the ribs (mid-span) were generally in the 20 to 25 ksi range. This is in qualitative agreement with the predictable value of $\frac{2}{3}$ the nominal membrane stress in the panel. The photoelastic patterns on the back face provided a simple indication of the nonsymmetrical stress system existing in the specimens. A pure biaxial load would necessarily produce a symmetrical strain distribution. None of the specimens exhibited a truly symmetrical pattern; however, the pattern of Specimen 3 (Figure 13B) approaches symmetry while the pattern on the back of Specimen 6 (Figure 16B) is a dramatic example of lack of symmetry. This 1:1 loading condition proved to be the most difficult to repeat. Further evidence of non-symmetrical loading was indicated by observed changes in the isoclinic angle (direction of principal stress) which occurred between the 25 kip and 65 kip load levels. In any event, the following observations are in order:

-The corner stresses (corner formed by intersecting
ribs) were lower in magnitude than the nominal mem-
brane stresses in the central section of the ribs.

-The ribs produced stress risers on the back face.
Stresses perpendicular to the rib directions were
generally 15. to 30% greater than the nominal panel
membrane stress.

6.3 Two to One Biaxial Load (σ_v: σ_h:: 2:1)

(Tables IIIA through IIIB, Figures 17A through 22B)

Measurements on the front and back faces (points H2V2,
H2V6, H6V2, and H6V6) again confirmed bending through
the panel thickness to be low (approximately $\pm$ 1.5 ksi).
Stresses in the central region of the vertical fillet
and rib were essentially uniform with an indication of
reduced stress levels at locations A0, B0, and C0. The
experimental stresses at D0 were generally comparable to
the membrane stresses in the panel faces and the strain
pattern indicated no stress concentration at the location.
Assuming that σ_v = 2 σ_h, it is possible to predict the
vertical and horizontal rib stresses as .84 σ_v and .17 σ_v
respectively*. The rib stresses along lines A & B are
seen to be in general agreement with these predictions.
There was a unique behavior along the fillet of the hori-
zontal rib which was not observed during the uniaxial and
equal biaxial loadings. The principal stress directions
were observed to be measurably different from vertical
and horizontal (tending towards 45°) along line C.

*E = 10(10)^6 and ν = .33 for aluminum

$\sigma_2(0)$ σ_1

σ_1

σ_1 STRESS TRAJECTORY

σ_1

VERT. RIB

σ_1

σ_2

$\frac{1}{2}\sigma_v\,(\sigma_2)$

$\sigma_v\,(\sigma_1)$

This behavior is reasonable and is illustrated here.
σ_1 in the horizontal rib is directed along the length of the rib while σ_1 (σ_v as applied) is vertical in the central bay of the panel. Clearly then, the σ_1 stress trajectory must experience a 90° rotation as it crosses through the fillet region and is illustrated above by the dotted line. This unique situation was not present in the other loading cases. As in the previous loading conditions the back face stresses were highest behind the horizontal rib along line VO with the vertical stresses 15 to 30% greater than the nominal applied membrane stress.

The following observations are in order:

    -Bending stress through the central portion of the panel was approximately $\pm$ 1 1/2 ksi.

    -The corner stresses (corner formed by intersecting ribs) at AO, BO and CO were lower in magnitude

than the nominal vertical membrane stress.

-The horizontal ribs produced stress risers on the back face (Line VO). Stresses perpendicular to the horizontal ribs were 15 to 30% greater than the nominal vertical membrane stress.

7.0 GENERAL OBSERVATIONS AND SUGGESTIONS

A. Analysis of the experimental findings indicates that the ribs create high stresses on the back face of the panel. The stress increase (up to 30%) occurs directly behind the ribs in a direction perpendicular to the rib length.

B. The results show that the stress field in the central section of the panel can be treated as plane stress. The bending component was generally less than $\pm$ 2 ksi for all loadings.

C. The stress gradients in the corners formed by intersecting ribs were very steep. In any case, the general conclusion derived from consideration of all tests is that the stresses at AO, BO, and CO are less than the nominally applied membrane stress.

D. The above observations are based on measurements made in one gradient of the specimen. Lack of loading symmetry most certainly produced different stress fields in each quadrant. However, observation of the overall photoelastic patterns suggests that the above are generally applicable to the entire panel.

E. An overall review of all test results leads to the observation that the fillet radii, rather than rib thickness, was the dominant factor influencing localized stress disturbances.

F. It is suggested that the above observations be confirmed by further strain gage studies. Figure 23 indicates locations where strain gage measurements would provide useful comparative data.

	V=91.6 KIPS ; H=0 KIPS									V=130 KIPS ; H=0 KIPS								
	#1			#2			#3			#4			#5			#6		
POINT	ΔN_n	$\varepsilon_1-\varepsilon_2$	$\sigma_1-\sigma_2$	ΔN_n	$\varepsilon_1-\varepsilon_2$	$\sigma_1-\sigma_2$	ΔN_n	$\varepsilon_1-\varepsilon_2$	$\sigma_1-\sigma_2$	ΔN_n	$\varepsilon_1-\varepsilon_2$	$\sigma_1-\sigma_2$	ΔN_n	$\varepsilon_1-\varepsilon_2$	$\sigma_1-\sigma_2$	ΔN_n	$\varepsilon_1-\varepsilon_2$	$\sigma_1-\sigma_2$
A0		1970	15.0		1630	12.0		1850	14.0	1.28	2020	15.0	1.55	2300	17.0	1.95	2750	21.0
A½		4460	34.0		5220	39.0		4380	33.0	3.15	4950	37.0	3.15	4650	35.0	3.37	5000	37.0
A1		4860	37.0		3880	29.0		4560	34.0	3.15	4680	35.0	3.00	4450	33.0	2.78	4100	31.0
A2		4340	33.0		4930	37.0		5550	42.0	3.23	4600	35.0	2.90	4300	32.0	2.40	3550	27.0
A3		4620	35.0		5050	38.0		4100	31.0	3.30	"	"	2.85	4200	31.0	2.34	3460	26.0
A4		4620	35.0		5000	38.0		3820	29.0	3.30	"	"	2.85	4200	31.0	2.62	3880	29.0
B0		1260	9.0		2380	18.0				0.83	1440	11.0	1.30	2180	16.0	2.18	3080	23.0
B½		4500	34.0		4700	35.0		4280	32.0	2.92	4600	35.0	2.45	3850	29.0	2.40	3560	27.0
B1		4560	34.0		4560	34.0		4160	32.0	3.15	4640	35.0	"	3650	27.0	2.62	3900	29.0
B2		4710	35.0		5080	38.0		3780	28.0	3.45	4950	37.00	"	"	"	2.40	3560	27.0
B3		4940	37.0		5250	39.0		3950	30.0	3.45	4800	36.0	"	"	"	2.70	4000	30.0
B4		4760	36.0		5150	39.0		3950	30.0	3.52	4900	37.0	"	"	"	2.62	3900	29.0
C0		2840	21.0		3460	26.0		1970	15.0	1.13	2200	17.0	1.30	2350	18.0	1.65	2780	21.0
C½		4560	34.0		4120	31.0		3660	28.0	2.56	4020	30.0	2.50	3900	29.0	2.40	3700	28.0
C1		4300	32.0		3740	28.0		3860	29.0	3.00	4180	31.0	2.70	4000	30.0	2.70	3740	28.0
C2		4420	33.0		4620	35.0		4120	31.0	3.38	4590	34.0	"	3700	28.0	2.50	3400	26.0
C3		4420	33.0		5140	38.0		4040	30.0	3.45	4660	34.0	"	"	"	2.50	"	"
C4		4460	34.0		5100	38.0		4040	30.0	3.52	4660	34.0	"	"	"	"	"	"
D0					4080	30.1		4000	30.0	2.25	3530	26.0	2.25	3600	27.0	2.18	3400	26.0
D½					3780	28.2		3740	30.0	2.40	3560	27.0	2.40	3800	28.0	2.18	3400	26.0
D1					4640	35.0		3820	29.0	2.92	4050	30.0	2.45	3600	27.0	2.62	3870	29.0
D2					4710	35.0		4440	33.0	3.38	4560	34.0	2.60	3850	29.0	2.55	3530	27.0
D3					5030	38.0		4000	30.0	3.30	4440	33.0	2.55	3800	29.0	2.62	3620	27.0
D4					4940	37.0		4140	31.0	3.30	4400	33.0	"	"	29.0	"	"	27.0

TABLE - IA   UNIAXIAL LOAD - VERT. RIB   * $\sigma_1-\sigma_2 \rightarrow$ KSI

Point	V=91.6 KIP ; H=0 KIP #1			#2			#3			V=130 KIP ; H=0 KIP #4			#5			#6		
	ΔN_n	$\varepsilon_1-\varepsilon_2$	$\sigma_1-\sigma_2$	ΔN_n	$\varepsilon_1-\varepsilon_2$	$\sigma_1-\sigma_2$	ΔN_n	$\varepsilon_1-\varepsilon_2$	$\sigma_1-\sigma_2$	ΔN_n	$\varepsilon_1-\varepsilon_2$	$\sigma_1-\sigma_2$	ΔN_n	$\varepsilon_1-\varepsilon_2$	$\sigma_1-\sigma_2$	ΔN_n	$\varepsilon_1-\varepsilon_2$	$\sigma_1-\sigma_2$
C 0													1.30	2350	18.0	1.65	2780	21.0
C ½		1180	9.0		2150	16.0		3260	24.0									
C 1		1180	9.0		3040	23.0		2700	24.0	1.20	1780	13.0	1.65	2230	17.0	1.50	1980	15.0
C 2		1180	9.0		3370	25.0		2880	22.0	1.28	1900	14.0	2.33	3080	23.0	"	"	"
C 3		673	5.0		3270	25.0		2880	22.0	1.35	2000	15.0				"	"	"
C 4		673	5.0		3200	24.0		2800	21.0	1.35	1870	14.0				"	"	"
D ½		3960	30.0		2860	21.0		4580	34.0	2.40	3560	27.0				2.25	3540	27.0
D 1		3480	26.0		3520	26.0		3950	30.0	2.70	4000	30.0				2.40	3550	27.0
D 2		3140	24.0		3760	28.0		3620	27.0	2.55	3800	29.0				2.55	3520	26.0
D 3		2960	22.0		3440	26.0		3680	28.0	2.40	3440	26.0				2.63	3560	27.0
D 4		3140	24.0		3880	29.0		3940	29.0	2.47	3400	25.0				2.63	3500	27.0
H2,V2		4500	34.0		4460	33.0		3790	28.0	3.22	4460	34.0	2.40	3500	26.0	2.80	3800	29.0
H2,V6		4700	35.0		−	−		3680	28.0	3.60	4780	36.0	2.30	3300	25.0	2.80	3800	29.0
H6,V2		4200	31.0		−	−		3620	27.0	3.00	4450	33.0				2.86	3770	28.0
H6,V6		4540	34.0		4720	35.0		4120	31.0	2.78	4350	33.0				2.80	3880	29.0

TABLE IB- UNIAXIAL LOAD- HORIZ. RIB & PANEL FACE

POINT	#1 ΔN_n	#1 $\varepsilon_1-\varepsilon_2$	#1 $\sigma_1-\sigma_2$	#2 ΔN_n	#2 $\varepsilon_1-\varepsilon_2$	#2 $\sigma_1-\sigma_2$	#3 ΔN_n	#3 $\varepsilon_1-\varepsilon_2$	#3 $\sigma_1-\sigma_2$	#4 ΔN_n	#4 $\varepsilon_1-\varepsilon_2$	#4 $\sigma_1-\sigma_2$	#5 ΔN_n	#5 $\varepsilon_1-\varepsilon_2$	#5 $\sigma_1-\sigma_2$	#6 ΔN_n	#6 $\varepsilon_1-\varepsilon_2$	#6 $\sigma_1-\sigma_2$
								V=91.6 KIPS	H=0 KIPS					V=130 KIPS	H=0 KIPS			
H0,V0		6320	47.0		5200	39.0		5200	39.0	4.50	5550	41.0	3.20	4450	33.0	3.52	4500	34.0
H0,V½		4080	30.0		3400	25.0		3060	23.0	3.23	3980	30.0	2.47	3420	26.0	2.40	3080	23.0
H0,V1		4150	31.0		3760	28.0		3600	27.0	3.23	3980	30.0	2.62	3620	27.0	2.55	3270	25.0
H0,V2		4320	32.0		4120	31.0		3660	28.0	3.38	4160	31.0	2.78	3800	29.0	2.70	3460	26.0
H0,V3		4500	34.0		4650	35.0		3820	29.0	3.52	4340	33.0				2.85	3650	27.0
H0,V4		4350	33.0		4650	35.0		3940	30.0	3.60	4430	33.0	2.86	3900	29.0	2.85	3650	27.0
H½,V0		5390	40.0		4000	30.0		3980	30.0	3.44	4220	32.0				4.64	6100	31.0
H1,V0		5540	42.0		4880	37.0		4340	33.0	4.05	4960	37.0	3.14	4350	33.0	4.80	6300	33.0
H2,V0		5770	43.0		5200	39.0		4480	34.0	4.20	5150	39.0	3.30	4570	34.0	4.95	6500	34.0
H3,V0		6150	46.0		5750	43.0		4620	35.0	4.20	5150	39.0				"	"	"
H4,V0		5960	45.0		5900	43.0		4860	36.0	4.12	5050	38.0	3.25	4500	34.0	"	"	"
H2,V2		4830	36.0		4380	33.0		3940	30.0	3.90	4700	35.0	3.10	4100	31.0	2.85	3890	29.0
H2,V6		4760	36.0		–	–		4000	30.0	3.90	4700	35.0				2.85	3890	29.0
H6,V2		4700	35.0		–	–		3940	30.0	3.23	4080	31.0				2.78	3800	28.0
H6,V6		4700	35.0		4320	33.0		3820	29.0	3.38	4260	32.0				2.62	3580	27.0

TABLE IC - UNIAXIAL LOAD - BACK FACE

POINT	V=H=91.6 KIPS						V=H=130 KIPS					
	#1		#2		#3		#4		#5		#6	
	$\varepsilon_1-\varepsilon_2$	$\sigma_1-\sigma_2$	$\varepsilon_1-\varepsilon_2$	$\sigma_1-\sigma_2$	$\varepsilon_1-\varepsilon_2$	$\sigma_1-\sigma_2$	$\varepsilon_1-\varepsilon_2$	$\sigma_1-\sigma_2$	$\varepsilon_1-\varepsilon_2$	$\sigma_1-\sigma_2$	$\varepsilon_1-\varepsilon_2$	$\sigma_1-\sigma_2$
A 0	2860	22.0	2150	16.6	3475	26.0			2025	15.0	1905	14.0
A ½	3420	25.6	3300	25.0	3250	24.0	3440	26.0	2775	21.0	2900	22.0
A 1	3660	27.6	2850	21.0	2970	22.0	3050	23.0	2670	20.0	2450	18.0
A 2	3700	27.8	3430	26.0	3060	23.0	2950	22.0	2670	20.0	2800	21.0
A 3	3620	27.2	3500	26.0	3060	23.0	2700	20.0			2800	21.0
A 4	3780	28.4	3430	26.0	3060	23.0	2700	20.0	2670	20.0	2800	21.0
B 0	1610	12.1	2690	20.0	2860	22.0	1785	13.0	1650	12.0	2220	17.0
B ½	3050	22.8	2780	21.0	3050	23.0	2890	22.0	2775	21.0	2670	20.0
B 1	2950	22.2	2700	20.0	2980	22.0	2890	22.0	2775	21.0	2670	20.0
B 2	3360	25.2	3100	23.0	2700	20.0	2970	22.0	2775	21.0	2550	19.0
B 3	3460	26.0	3040	23.0	2700	20.0	3030	23.0	2775	21.0	2670	20.0
B 4	3460	26.0	2810	21.0	2570	19.0	3030	23.0	2775	21.0	2670	20.0
C 0	2200	16.5	2030	15.0	4580	34.0	1990	15.0	1740	13.0	1890	14.0
C ½	2780	20.8	1970	15.0	2850	21.0	2340	18.0	2400	18.0	1890	14.0
C 1	2960	22.2	1930	15.0	3040	23.0	2060	15.0	2115	16.0	2400	18.0
C 2	3050	22.9	2070	16.0	2870	22.0	2170	16.0	1960	15.0	2550	19.0
C 3	3050	22.9	2170	16.0	2860	22.0	2340	18.0	1960	15.0	2550	19.0
C 4	3140	23.6	1960	15.0	2860	22.0	2590	19.0	1960	15.0	2550	19.0
D 0	218	1.6	203	2.0	1180	9.0	562	4.0	0	0	712	5.0
D ½	168	1.2	1255	9.0	437	3.0	680	5.0	0	0		
D 1	503	3.8	480	4.0	382	3.0	316	2.0	0	0	222	2.0
D 2	320	2.4	1060	8.0	512	4.0	620	5.0	0	0	0	0
D 3	456	3.4	1480	11.0	348	3.0	780	6.0	0	0	104	1.0
D 4	302	2.2	1160	9.0	178	1.0	610	5.0	0	0	104	1.0

TABLE II A - BIAXIAL LOAD (1:1), VERT. RIB

POINT	V=H=91.6 KIPS						V=H= 130 KIPS					
	1		2		3		4		5		6	
	$\epsilon_1-\epsilon_2$	$\sigma_1-\sigma_2$	$\epsilon_1-\epsilon_2$	$\sigma_1-\sigma_2$	$\epsilon_1-\epsilon_2$	$\sigma_1-\sigma_2$	$\epsilon_1-\epsilon_2$	$\sigma_1-\sigma_2$	$\epsilon_1-\epsilon_2$	$\sigma_1-\sigma_2$	$\epsilon_1-\epsilon_2$	$\sigma_1-\sigma_2$
A½	2860	22.0	2760	21.0	3960	30.0	3980	30.0	3000	23.0	2586	19.0
A1	3420	26.0	3760	28.0	3600	27.0	3770	28.0	3000	23.0	3000	23.0
A2	3140	24.0	3930	30.0	3650	27.0	3600	27.0	3000	23.0	3300	25.0
A3	3360	25.0	3190	24.0	3720	28.0	8790	28.0	3000	23.0	3500	26.0
A4	3460	26.0	2850	21.0	3520	26.0	4140	31.0	3000	23.0	3500	26.0
B½	2700	20.0	3240	24.0	3420	26.0	3840	29.0	2250	17.0	2790	21.0
B1	2880	22.0	3210	24.0	2960	22.0	3240	24.0	3000	23.0	3000	23.0
B2	3150	24.0	3570	27.0	2780	21.0	3430	26.0	3000	23.0	3180	24.0
B3	3160	24.0	2850	21.0	3190	24.0	3240	24.0	3000	23.0	3400	26.0
B4	3240	24.0	2680	20.0	2780	21.0	3420	26.0	3000	23.0	3400	26.0
C0							2230	17.0			2025	15.0
C½	2520	19.0	1070	8.0	3830	29.0	2690	20.0	3270	25.0	1785	13.0
C1	3210	24.0	800	6.0	3700	28.0	2740	21.0	2690	20.0	1990	15.0
C2	2700	20.0	480	4.0	3210	24.0	2890	22.0	2690	20.0	2100	16.0
C3	2700	20.0	0	0	3210	24.0	2390	18.0	2690	20.0	2100	16.0
C4	2790	21.0	456	3.0	2790	21.0	2060	15.0	2690	20.0	2100	16.0
D½	985	7.0	0	0	382	3.0	510	4.0			1110	8.0
D1	870	7.0	1120	8.0	162	1.0	1020	8.0			520	4.0
D2	870	7.0	156	1.0	0	0	850	6.0			407	3.0
D3	1040	8.0	1250	9.0	0	0	1140	9.0			407	3.0
D4	850	6.0	660	5.0	162	1.0	955	7.0				
H2,V2	320	2.0	149	1.0	1220	9.0	158	1.0	111	1.0	512	4.0
H2,V6	158	1.0			320	2.0			105	1.0	203	2.0
H6,V2	174	1.0			1145	4.0	170	1.0			198	2.0
H6,V6	0	0	149	1.0	665	5.0	357	3.0			109	1.0

TABLE IIB- BIAXIAL LOAD (1:1)- HORIZ. RIB & PANEL FACE

Point	V = H = 91.6 KIP						V = H = 130 KIP					
	1		2		3		4		5		6	
	$\epsilon_1-\epsilon_2$	$\sigma_1-\sigma_2$	$\epsilon_1-\epsilon_2$	$\sigma_1-\sigma_2$	$\epsilon_1-\epsilon_2$	$\sigma_1-\sigma_2$	$\epsilon_1-\epsilon_2$	$\sigma_1-\sigma_2$	$\epsilon_1-\epsilon_2$	$\sigma_1-\sigma_2$	$\epsilon_1-\epsilon_2$	$\sigma_1-\sigma_2$
H0,V0	185	1.0	360	3.0	179	1.0	142	10	615	5.0	675	5.0
H0,V½	740	6.0	740	6.0	1080	8.0	1700	13.0			1245	9.0
H0,V1	900	7.0	540	4.0	1260	10.0	1560	12.0	1545	12.0	1245	9.0
H0,V2	720	5.0	1080	8.0	870	7.0	1410	11.0	1440	11.0	1245	9.0
H0,V3	536	4.0	1080	8.0	1220	9.0	1410	11.0			1245	9.0
H0,V4	695	5.0	740	6.0	1400	11.0	1125	8.0	1125	8.0	1245	9.0
H½,V0	1110	8.0	1040	8.0	360	3.0	422	3.0			685	5.0
H1,V0	1110	8.0	1040	8.0	360	3.0	422	3.0	312	2.0	490	4.0
H2,V0	895	7.0	1040	8.0	540	4.0	422	3.0	312	2.0	390	3.0
H3,V0	1070	8.0	1040	8.0	540	4.0	562	4.0	312	2.0	390	3.0
H4,V0	1220	9.0	1040	8.0	540	4.0	562	4.0	312	2.0	490	4.0
H2,V2	174	1.0	149	1.0	720	5.0	277	2.0	203	2.0	308	2.0
H2,V6	0	0	174	1.0	522	4.0	415	3.0	198	2.0	204	2.0
H6,V2	170	1.0	0	0	360	3.0	290	2.0	312	2.0	308	2.0
H6,V6	0	0	305	2.0	174	1.0	290	2.0	207	2.0	99	1.0

TABLE IIC - BIAXIAL LOAD (1:1) - BACK FACE

POINT	V=91.6 KIPS ; H=45.8 KIPS						V=130 KIPS ; H=65 KIPS					
	#1		#2		#3		#4		#5		#6	
	$\varepsilon_1-\varepsilon_2$	$\sigma_1-\sigma_2$	$\varepsilon_1-\varepsilon_2$	$\sigma_1-\sigma_2$	$\varepsilon_1-\varepsilon_2$	$\sigma_1-\sigma_2$	$\varepsilon_1-\varepsilon_2$	$\sigma_1-\sigma_2$	$\varepsilon_1-\varepsilon_2$	$\sigma_1-\sigma_2$	$\varepsilon_1-\varepsilon_2$	$\sigma_1-\sigma_2$
A 0	1820	14.0	1440	11.0	1860	14.0	2720	20.0	1650	12.0	1540	10.0
A ½	3600	27.0	3830	29.0	3660	28.0	3900	29.0	3300	25.0	4000	30.0
A 1	4000	30.0	3200	24.0	3560	27.0	3650	27.0	3200	24.0	3400	26.0
A 2	4050	31.0	3450	26.0	3830	29.0	3650	27.0	3200	24.0	3280	25.0
A 3	3950	30.0	3690	28.0	3610	27.0	3720	28.0			3400	26.0
A 4	3790	29.0	3600	27.0	3825	29.0	3800	29.0	3200	24.0	3280	25.0
B 0	1260	10.0	1980	15.0	2240	17.0	1700	13.0	1650	12.0	2400	18.0
B ½	4500	34.0	2960	22.0	3660	28.0	3900	29.0	3200	24.0	3260	24.0
B 1	4360	33.0	3030	23.0	3360	25.0	3900	29.0	3200	24.0	2960	22.0
B 2	4380	33.0	3130	24.0	3410	26.0	3270	29.0	3200	24.0	3120	23.0
B 3	4600	35.0	3360	25.0	3600	27.0	3960	30.0	3200	24.0	3260	24.0
B 4	4600	35.0	3130	24.0	3760	28.0	4260	32.0	3200	24.0	3260	24.0
C 0	2620	20.0	2450	18.0	3270	25.0	2175	16.0	1700	13.0	2700	20.0
C ½	4150	31.0	4850	36.0	3450	26.0	3160	24.0	3400	26.0	3600	23.0
C 1	3950	30.0	3130	24.0	3680	28.0	3525	26.0	3000	23.0	3200	24.0
C 2	3960	30.0	3130	24.0	3600	27.0	3765	28.0	2800	21.0	3240	24.0
C 3	4260	32.0	3050	23.0	3540	26.0	3870	29.0	2800	21.0	3120	23.0
C 4	4170	31.0	2680	20.0	3540	26.0	3765	28.0	2800	21.0	3260	24.0
D 0	2630	20.0	1830	14.0	3540	27.0	1770	13.0	2010	15.0	1420	11.0
D ½	2190	16.0	1080	8.0	1750	13.0	1890	14.0	1770	13.0	1100	8.0
D 1	2430	18.0	1920	14.0	1910	14.0	2075	16.0	1770	13.0	2080	16.0
D 2	2730	21.0	2130	16.0	2230	17.0	2450	18.0	1770	13.0	1800	14.0
D 3	2600	20.0	2240	17.0	2090	16.0	2550	19.0	1770	13.0	1940	15.0
D 4	2600	20.0	2040	15.0	1980	15.0	2400	18.0	1770	13.0	1940	15.0

TABLE III A - BIAXIAL LOAD (2:1), VERT. RIB

POINT	V=91.6 KIPS H=45.8 KIPS						V=130 KIPS H=65 KIPS					
	1		2		3		4		5		6	
	$\epsilon_1-\epsilon_2$	$\sigma_1-\sigma_2$	$\epsilon_1-\epsilon_2$	$\sigma_1-\sigma_2$	$\epsilon_1-\epsilon_2$	$\sigma_1-\sigma_2$	$\epsilon_1-\epsilon_2$	$\sigma_1-\sigma_2$	$\epsilon_1-\epsilon_2$	$\sigma_1-\sigma_2$	$\epsilon_1-\epsilon_2$	$\sigma_1-\sigma_2$
A½	720	5.0	372	3.0	900	7.0	1410	11.0	1070	8.0	680	5.0
A1	720	5.0	1080	8.0	900	7.0	825	6.0	1070	8.0	680	5.0
A2	740	6.0	1440	11.0	955	7.0	1290	10.0	1070	8.0	820	6.0
A3	990	7.0	1510	11.0	1120	8.0	1170	9.0	1070	8.0	820	6.0
A4	820	6.0	1350	10.0	930	7.0	1290	10.0	1070	8.0	960	7.0
B½	542	4.0	765	6.0	900	7.0	1005	8.0	430	3.0	960	7.0
B1	360	3.0	540	4.0	1220	9.0	1180	9.0	855	6.0	1500	11.0
B2	742	6.0	900	7.0	870	7.0	1180	9.0	855	6.0	820	6.0
B3	1162	9.0	515	4.0	840	6.0	1180	9.0	855	6.0	820	6.0
B4	820	6.0	842	6.0	695	5.0	1290	10.0	855	6.0	680	5.0
C0												
C½	845	6.0	0	0	0	0	825	6.0	606	5.0	396	3.0
C1	1180	9.0	320	2.0	0	0	990	7.0	495	4.0	660	5.0
C2	505	4.0	160	1.0	0	0	990	7.0	495	4.0	396	3.0
C3	845	6.0	0	0	0	0	1220	9.0	495	4.0	264	2.0
C4	1020	8.0	154	1.0	0	0	1245	9.0	495	4.0	264	2.0
D½	1980	15.0	845	6.0	2480	19.0	1890	14.0			1680	13.0
D1	1570	12.0	640	5.0	2140	16.0	1440	11.0			1180	9.0
D2	1920	14.0	785	6.0	1960	15.0	1440	11.0			1400	10.0
D3	1570	12.0	0	0	2090	16.0	1110	8.0			1500	11.0
D4	1800	14.0	940	7.0	2140	16.0	1340	10.0			1200	9.0
H2,V2	2400	18.0	1490	11.0	1805	14.0	2090	16.0	1560	12.0	1640	12.0
H2,V6	2450	18.0			1760	13.0			1530	12.0	1640	12.0
H6,V2	2440	18.0			2140	16.0	2220	17.0	1890	14.0	1600	12.0
H6,V6	2525	19.0	1350	10.0	1810	14.0	2240	17.0	1680	13.0	1800	13.0

TABLE III B - BIAXIAL LOAD (2:1) - HORIZ. RIB & PANEL FACE

POINT	V = 91.6 KIP ; H = 45.8 KIP						V = 130 KIP ; H = 65 KIP					
	1		2		3		4		5		6	
	$\epsilon_1-\epsilon_2$	$\sigma_1-\sigma_2$	$\epsilon_1-\epsilon_2$	$\sigma_1-\sigma_2$	$\epsilon_1-\epsilon_2$	$\sigma_1-\sigma_2$	$\epsilon_1-\epsilon_2$	$\sigma_1-\sigma_2$	$\epsilon_1-\epsilon_2$	$\sigma_1-\sigma_2$	$\epsilon_1-\epsilon_2$	$\sigma_1-\sigma_2$
HO,VO	2980	22.0	2150	16.0	2340	18.0	2400	18.0	1840	14.0	1540	12.0
HO,V½	1670	13.0	1080	8.0	895	7.0	1380	10.0			128	1.0
HO,V1	1260	10.0	900	7.0	1260	10.0	1380	10.0	930	7.0	520	4.0
HO,V2	1980	15.0	1260	10.0	1390	10.0	1470	11.0	1040	8.0	640	5.0
HO,V3	2160	16.0	1260	10.0	1390	10.0	1660	12.0			900	7.0
HO,V4	2100	16.0	1260	10.0	1570	12.0	1760	13.0	1230	9.0	1020	8.0
H½,VO	2800	21.0	2610	20.0	2340	18.0	2760	21.0			1960	15.0
H1,VO	3160	24.0	2430	18.0	2340	18.0	2940	22.0	2370	18.0	2240	17.0
H2,VO	2880	22.0	2780	21.0	2680	20.0	3050	23.0	2560	19.0	2360	18.0
H3,VO	3240	24.0	2960	22.0	2880	22.0	3120	23.0	4650	35.0	2500	19.0
H4,VO	3300	25.0	2960	22.0	720	5.0	2950	22.0	4650	35.0	2360	18.0
H2,V2	2450	18.0	1650	12.0	2160	16.0	2180	16.0	1725	13.0	1780	13.0
H2,V6	2130	16.0	1930	14.0	2090	16.0			1890	14.0	1780	13.0
H6,V2	2360	18.0	1720	13.0	2160	16.0	1980	15.0	1725	13.0	1360	10.0
H6,V6	2200	16.0	1840	14.0	2260	17.0	2090	16.0	1770	13.0	1500	11.0

TABLE III C — BIAXIAL LOAD (2:1) - BACK FACE

Coating

Approx
1 in.
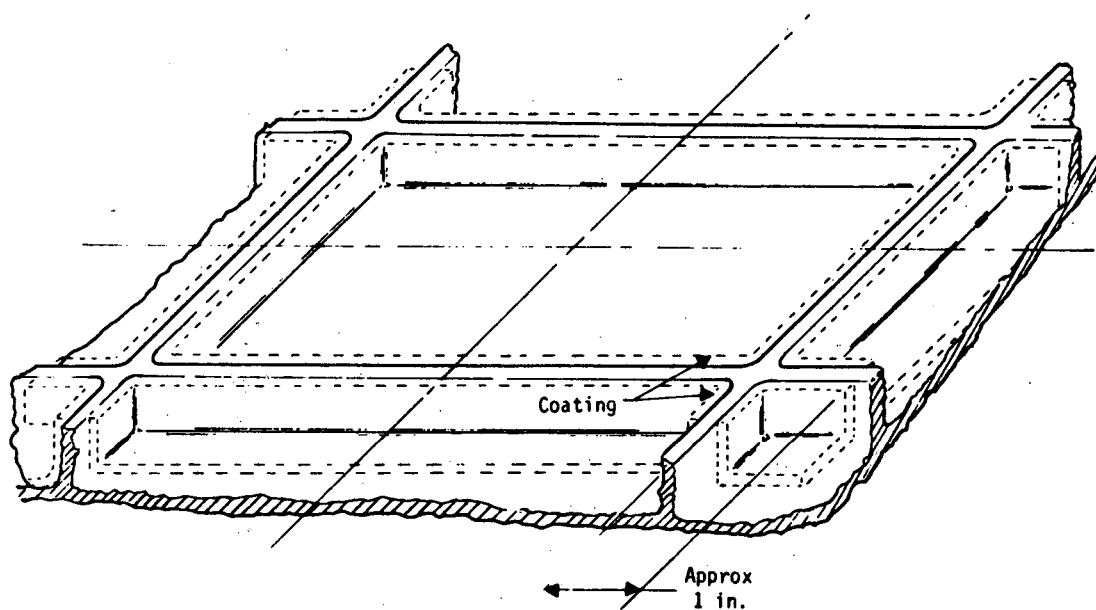
FIGURE I Typical Photoelastic Coating around Central Panel
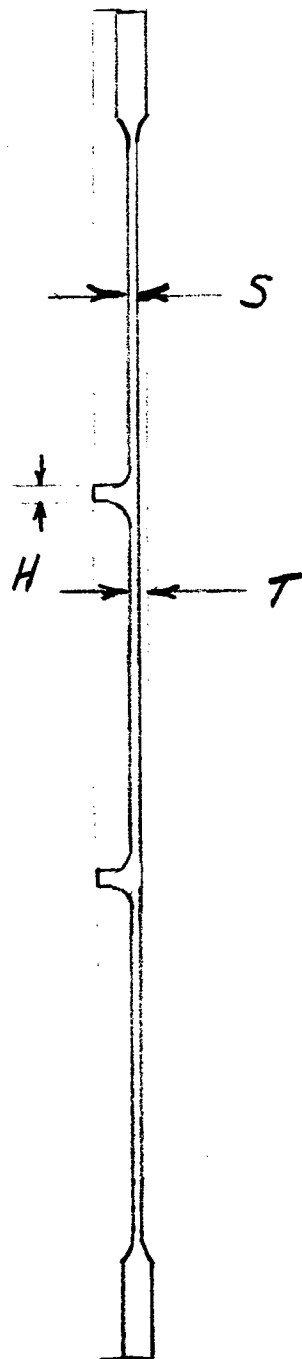
PANEL	VARIABLE DIMENSIONS			
	S	V*	H	T
1	0.060	0.060	0.060	0.220
2	0.060	0.060	0.125	0.220
3	0.060	0.125	0.125	0.220
4	0.125	0.060	0.060	0.188
5	0.125	0.060	0.125	0.188
6	0.125	0.125	0.250	0.188

* VERTICAL RIB THICKNESS

FIGURE 2 - PANEL DIMENSIONS
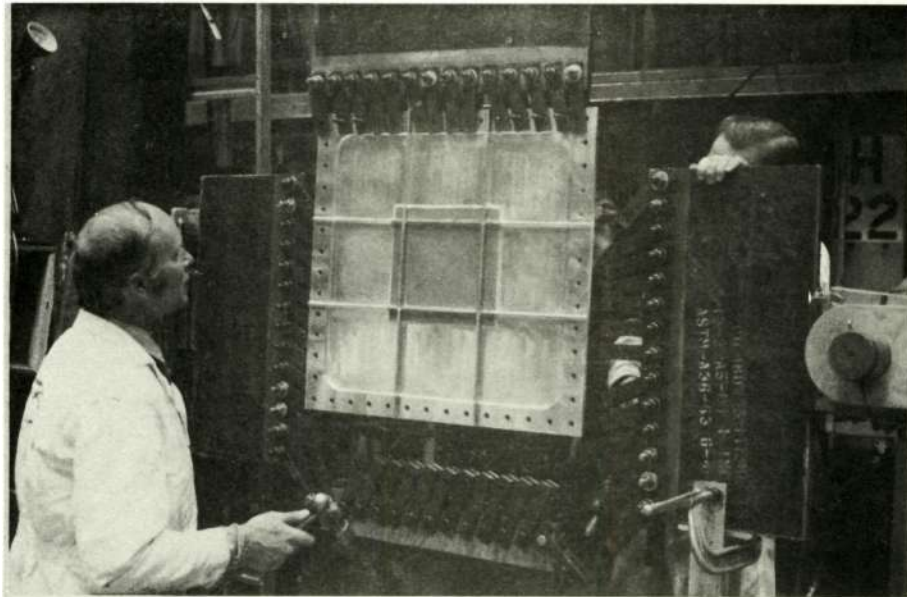
FIGURE 3A PANEL IN TEST FIXTURE
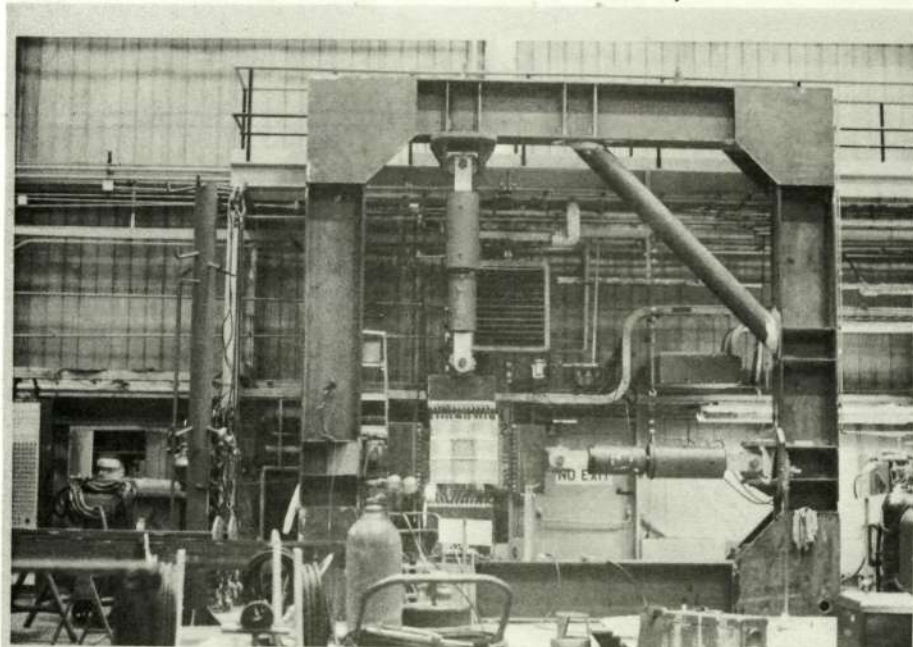
FIGURE 3B OVERALL VIEW OF TEST FIXTURE
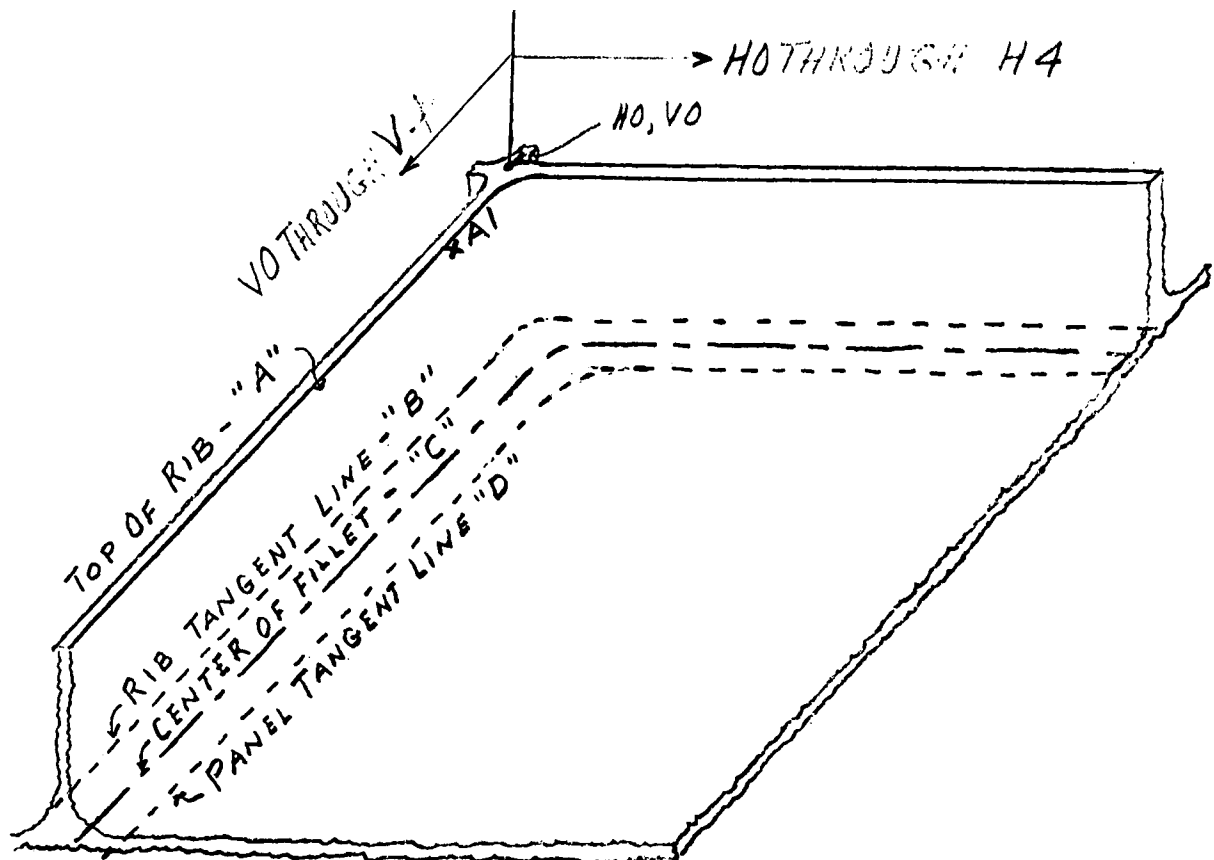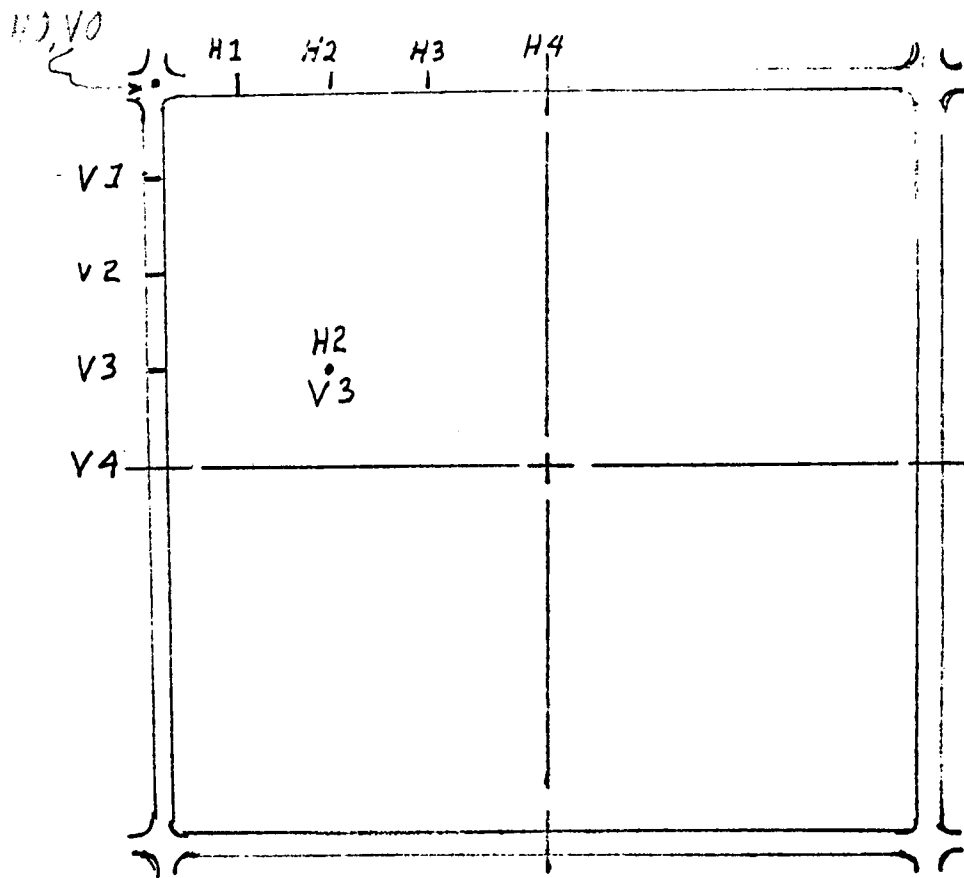
FIGURE 4 - POINTS OF MEASUREMENT ON CENTRAL PANEL QUADRANT
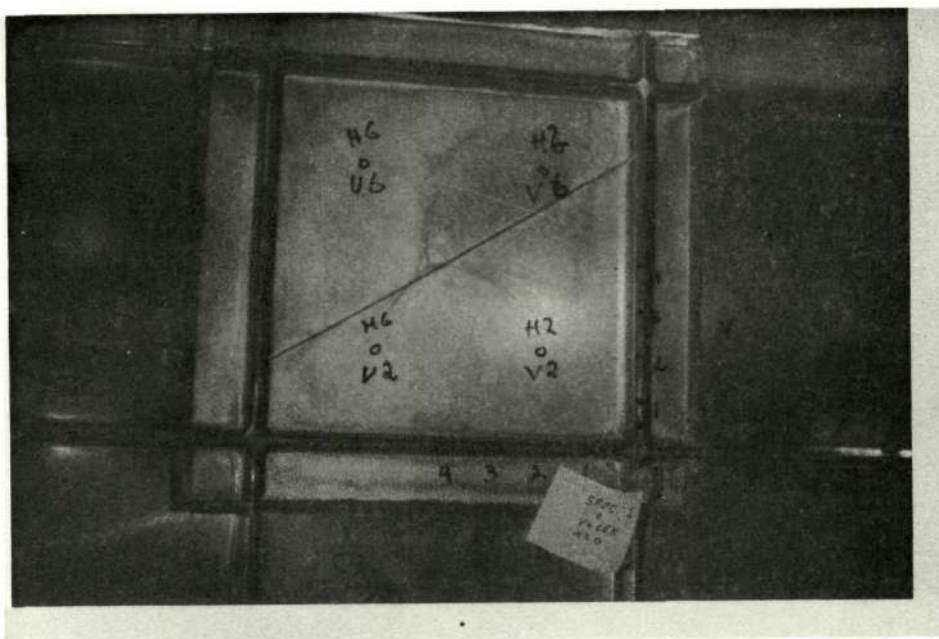
FIGURE 5A-PANEL 1, UNIAXIAL LOAD
FRONT SURFACE
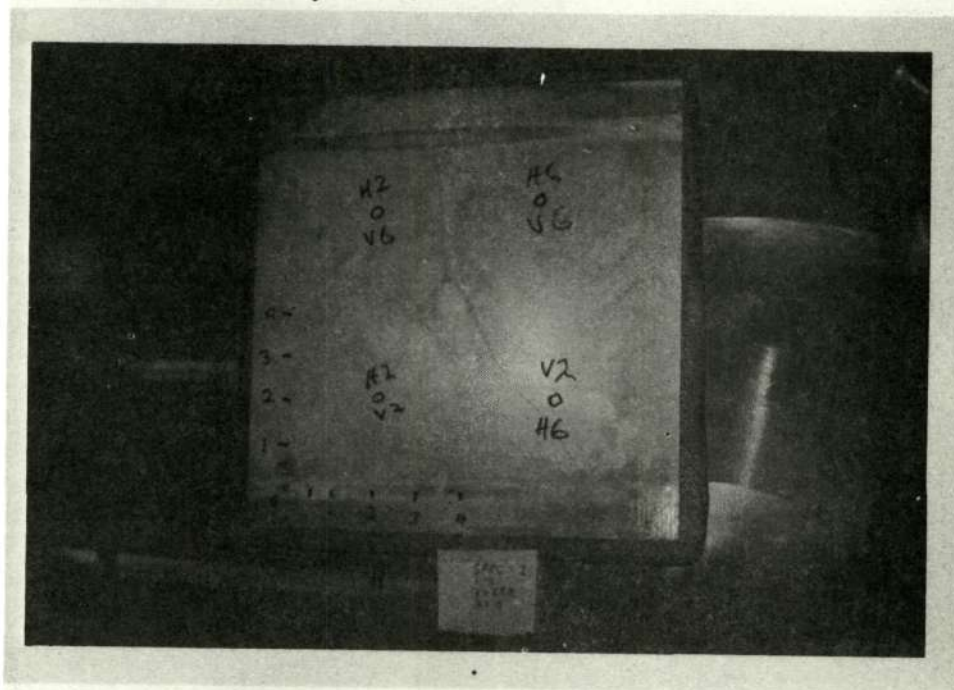
FIGURE 5B-Panel 1, UNIXIAL LOAD
REAR SURFACE
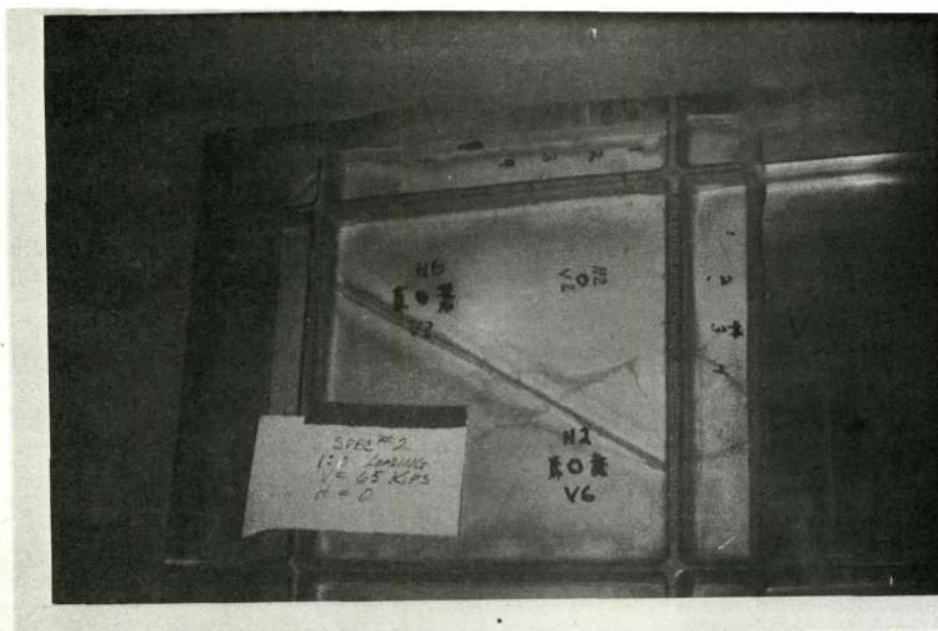
FIGURE 6A-PANEL 2 UNIAXIAL LOAD
FRONT SURFACE
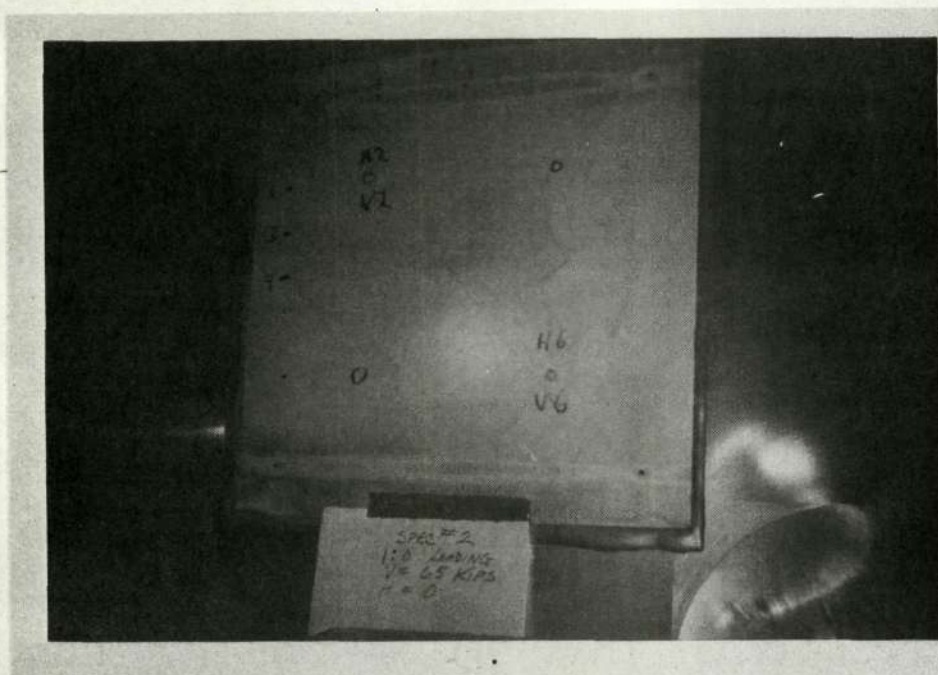
FIGURE 6B-PANEL 2 UNIAXIAL LOAD
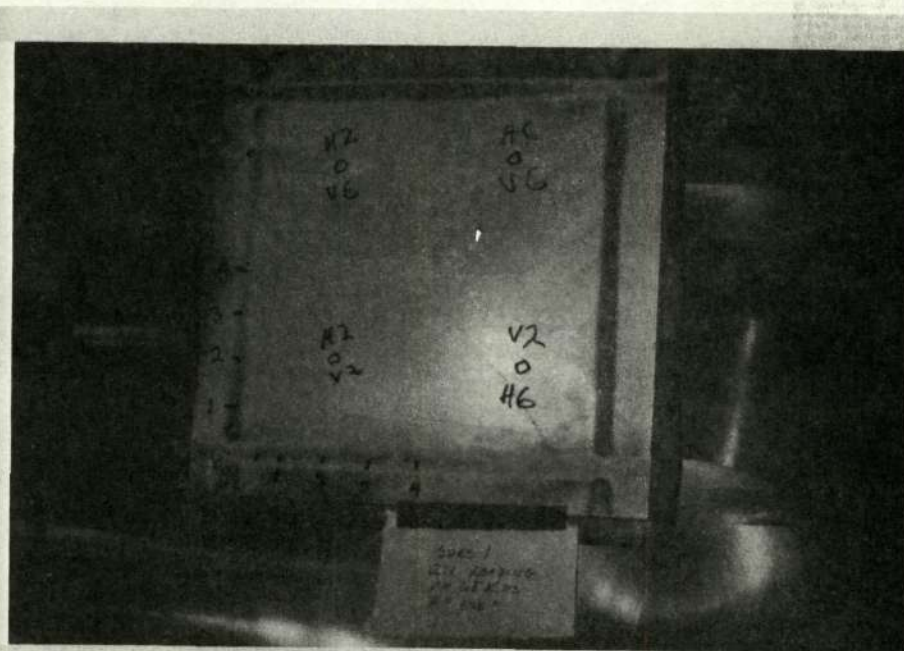REAR SURFACE
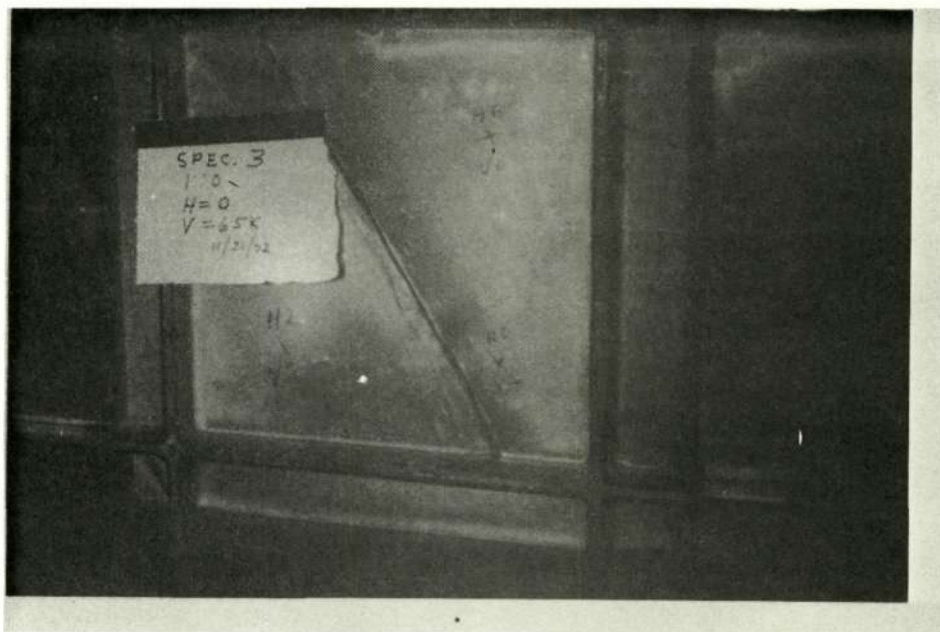
FIGURE 7A-PANEL 3 UNIAXIAL LOAD
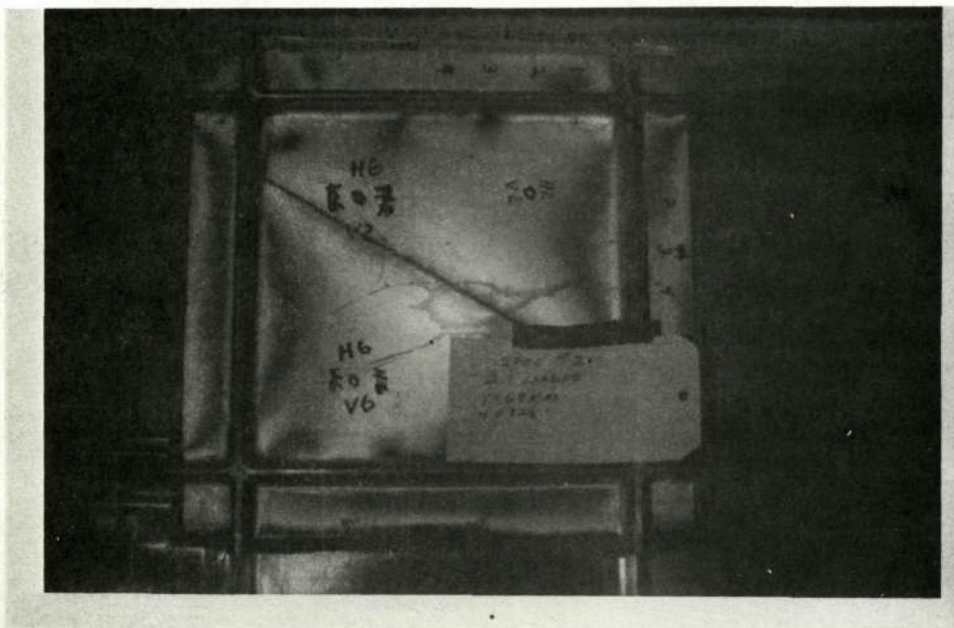FRONT SURFACE
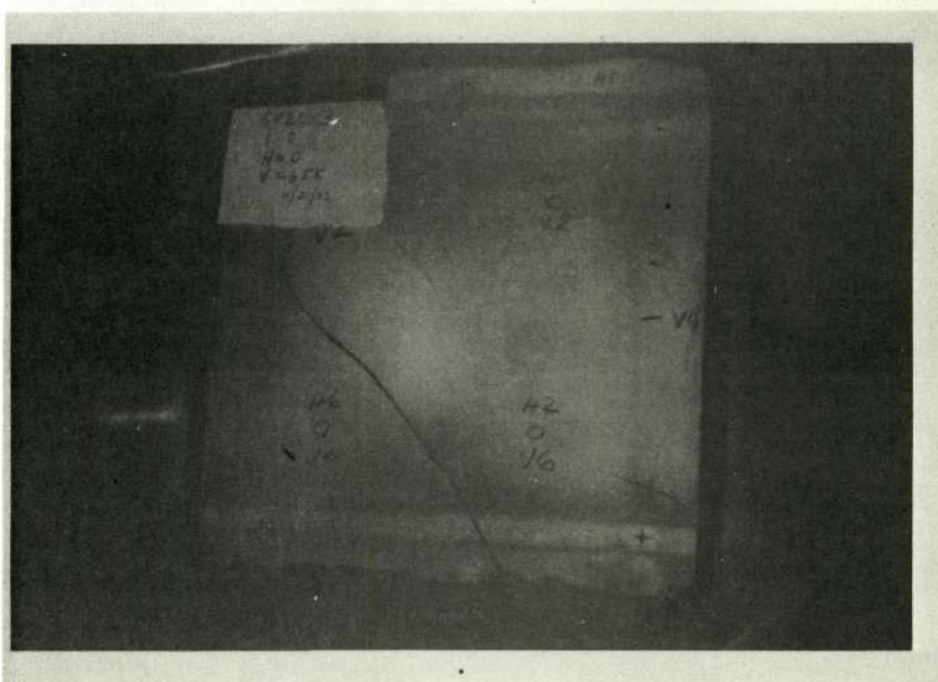
FIGURE 7B PANEL 3 UNIAXIAL LOAD
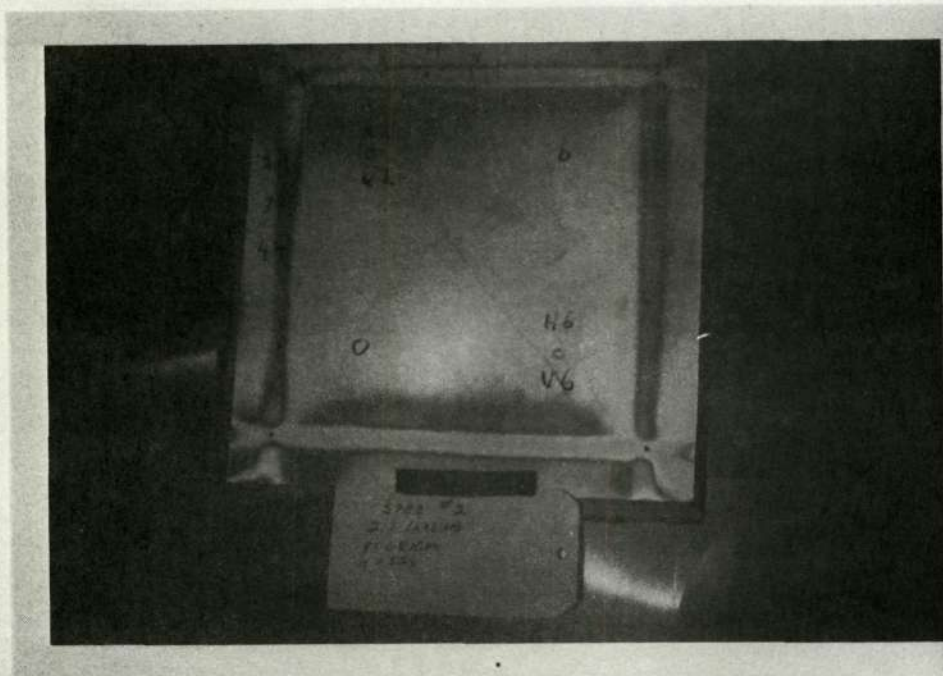REAR SURFACE
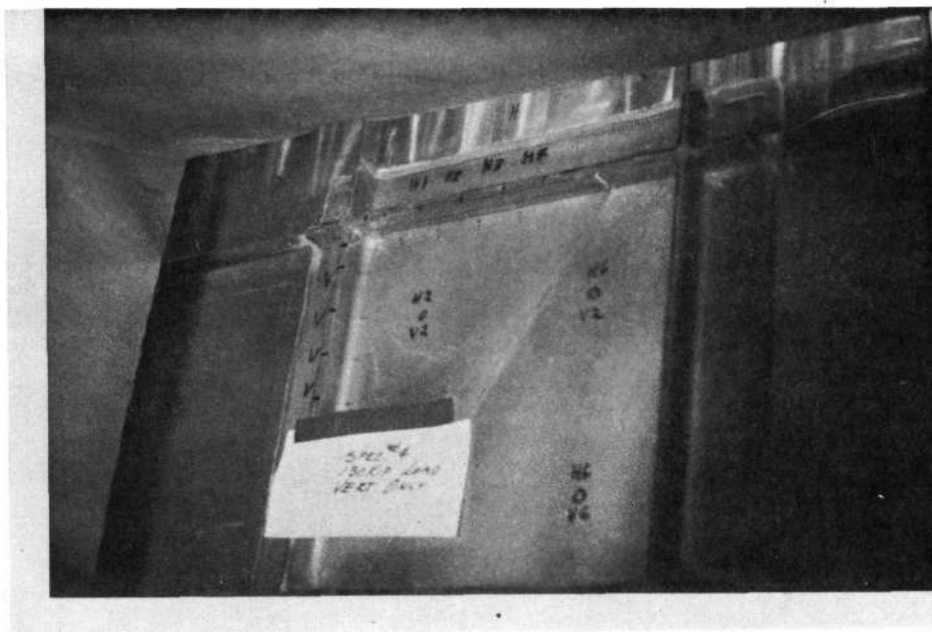
FIGURE 8A- PANEL 4 UNIAXIAL LOAD
FRONT SURFACE
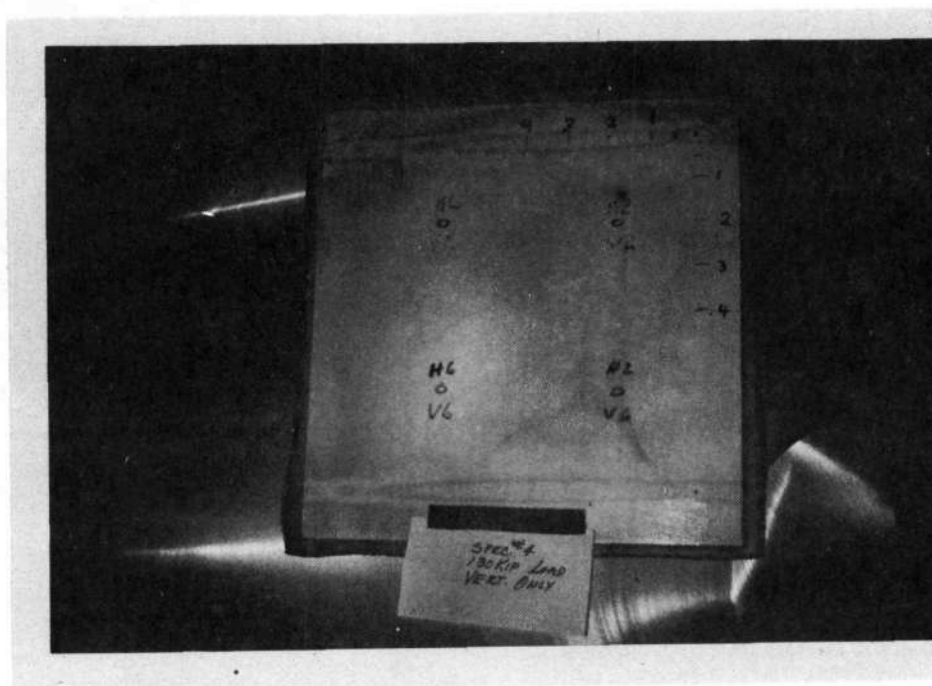
FIGURE 8B-PANEL 4 UNIAXIAL LOAD
REAR SURFACE
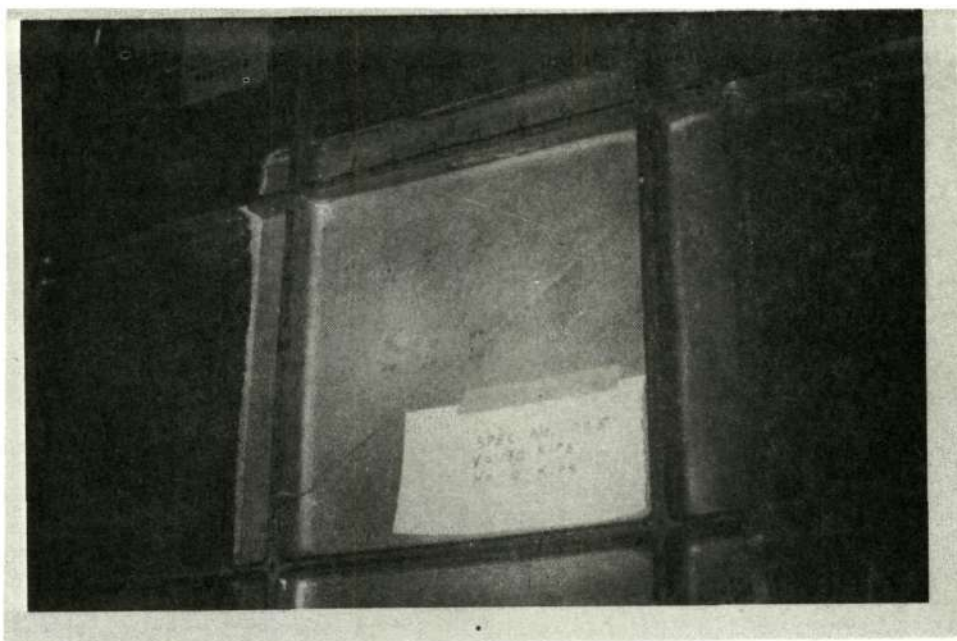
FIGURE 9A-PANEL 5 UNIAXIAL LOAD
FRONT SURFACE
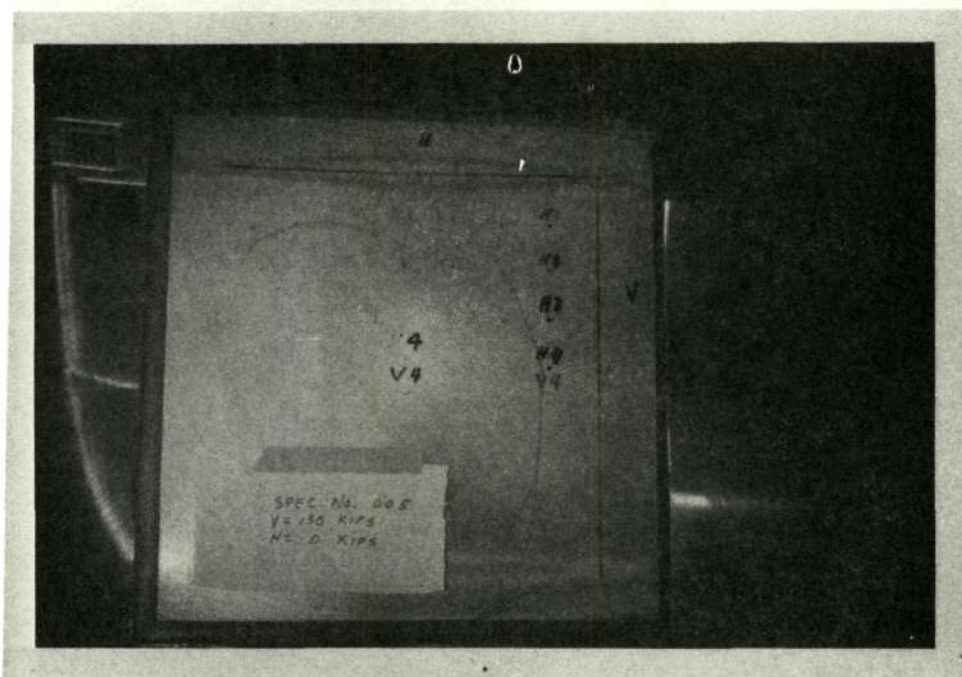
FIGURE 9B-PANEL 5 UNIAXIAL LOAD
REAR SURFACE
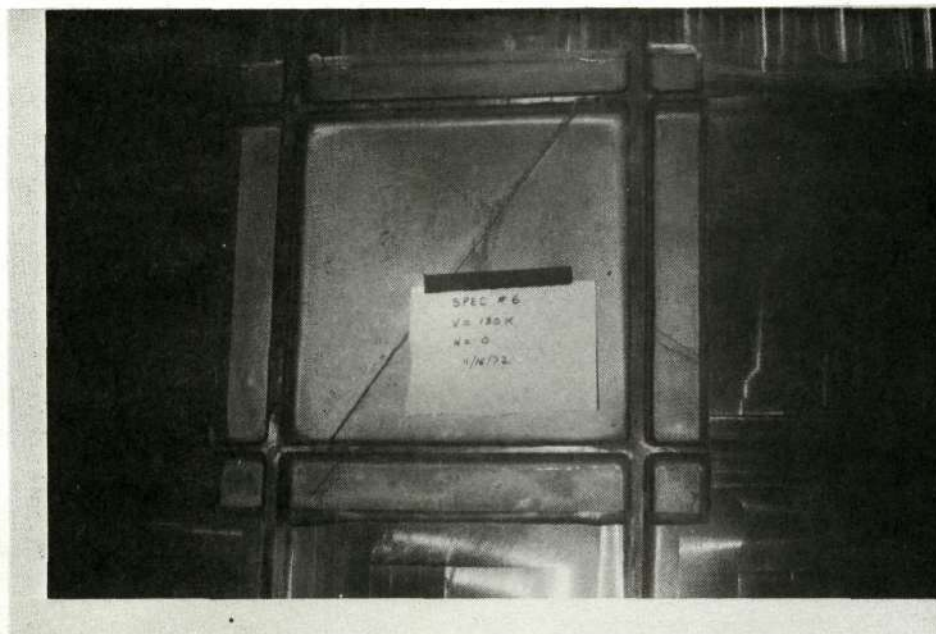
FIGURE 10-A PANEL 6 UNIAXIAL LOAD
FRONT SURFACE
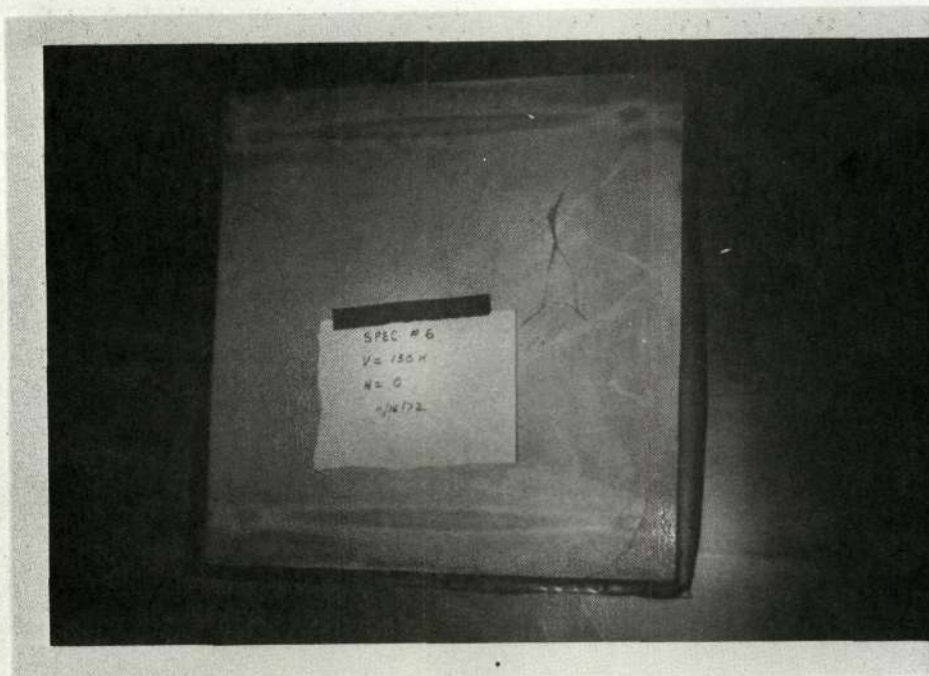
FIGURE 10-B PANEL 6 UNIAXIAL LOAD
·REAR SURFACE
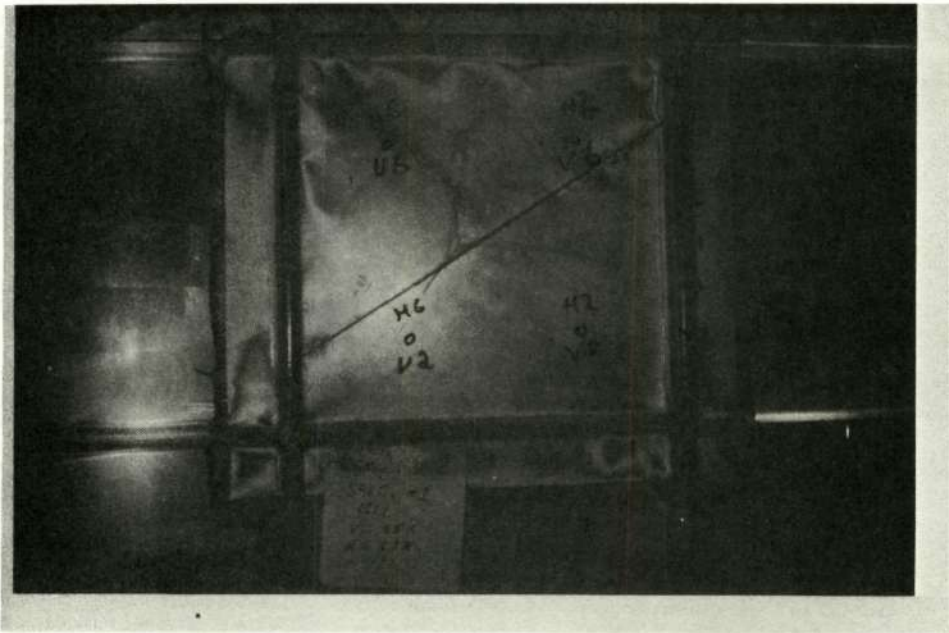
FIGURE 11A- PANEL 1-BIAXIAL LOAD (1:1)
FRONT SURFACE
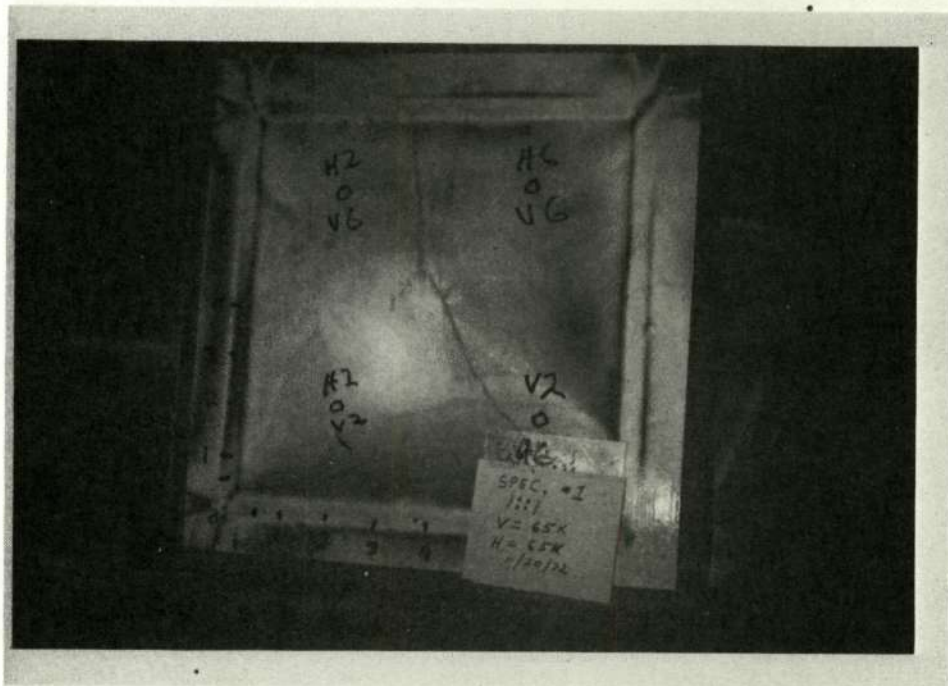
FIGURE 11B-PANEL 1-BIAXIAL LOAD(1:1)
REAR SURFACE
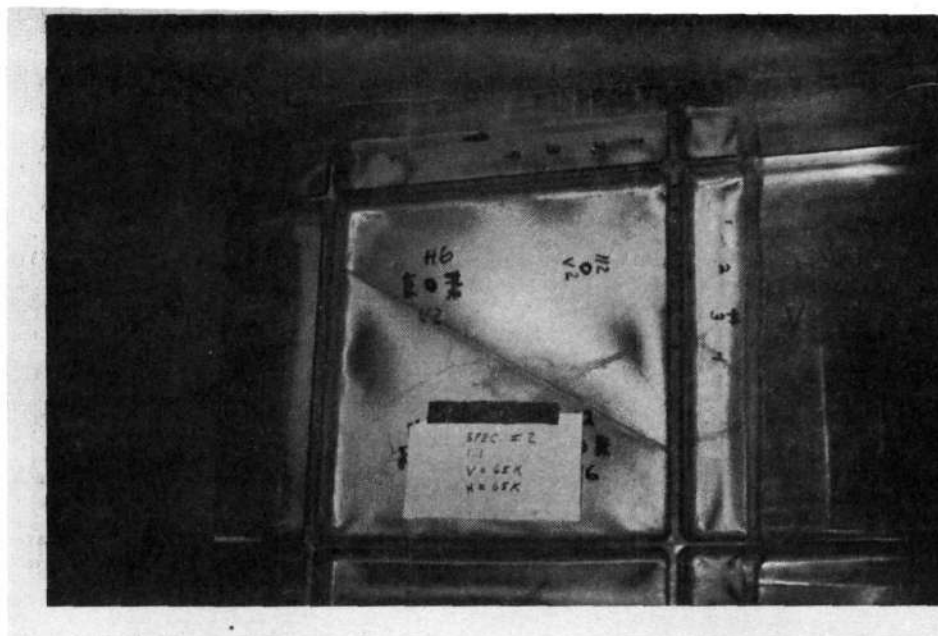
FIGURE 12A- PANEL 2 BIAXIAL LOAD (1:1)
FRONT SURFACE
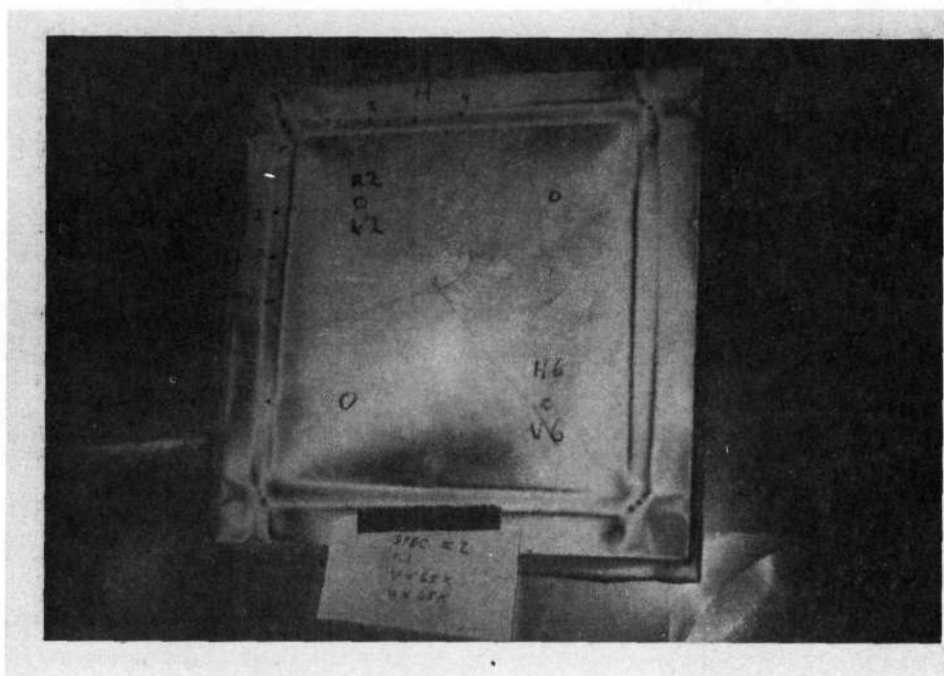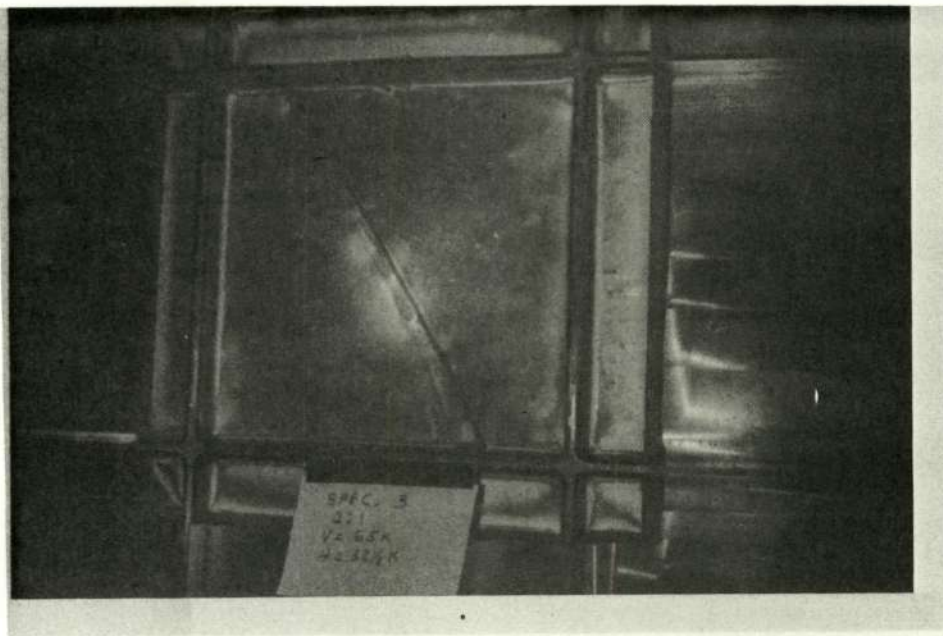

FIGURE 12B- PANEL 2 BIAXIAL LOAD (1:1)
REAR SURFACE
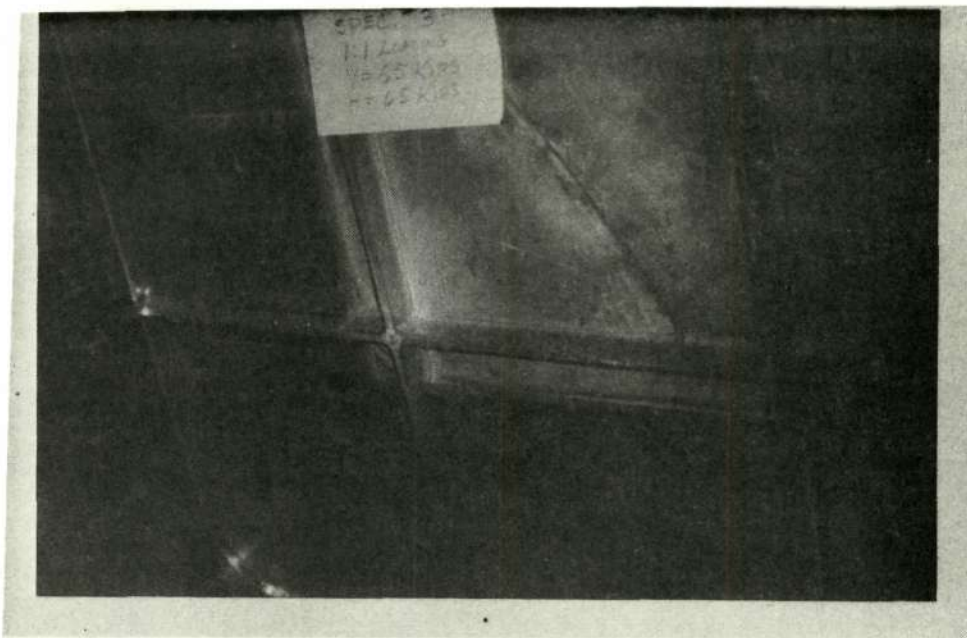
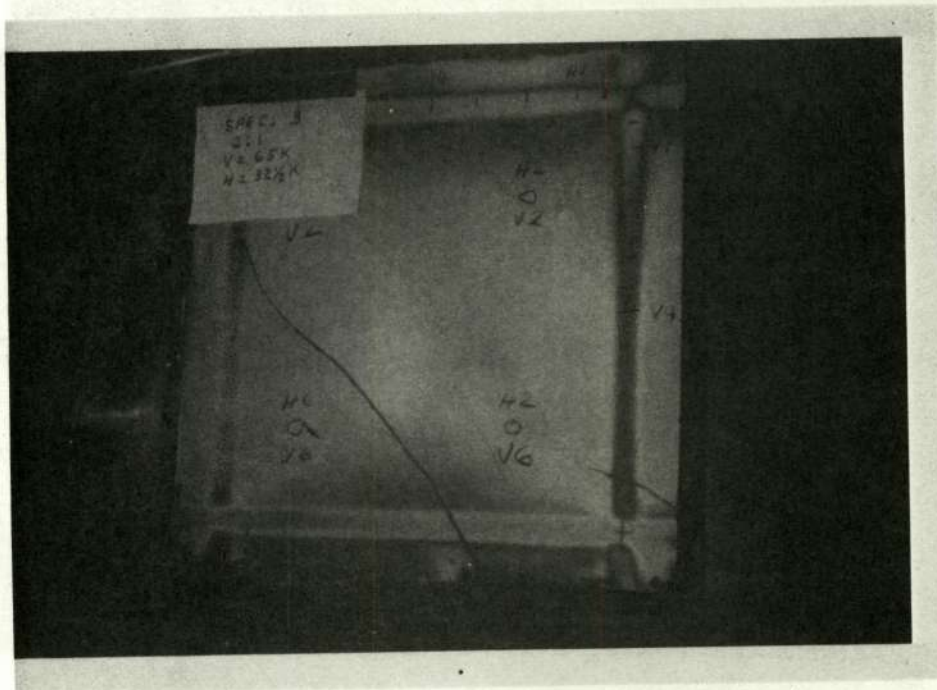FIGURE 13A- PANEL 3 BIAXIAL LOAD (1:1)
FRONT SURFACE
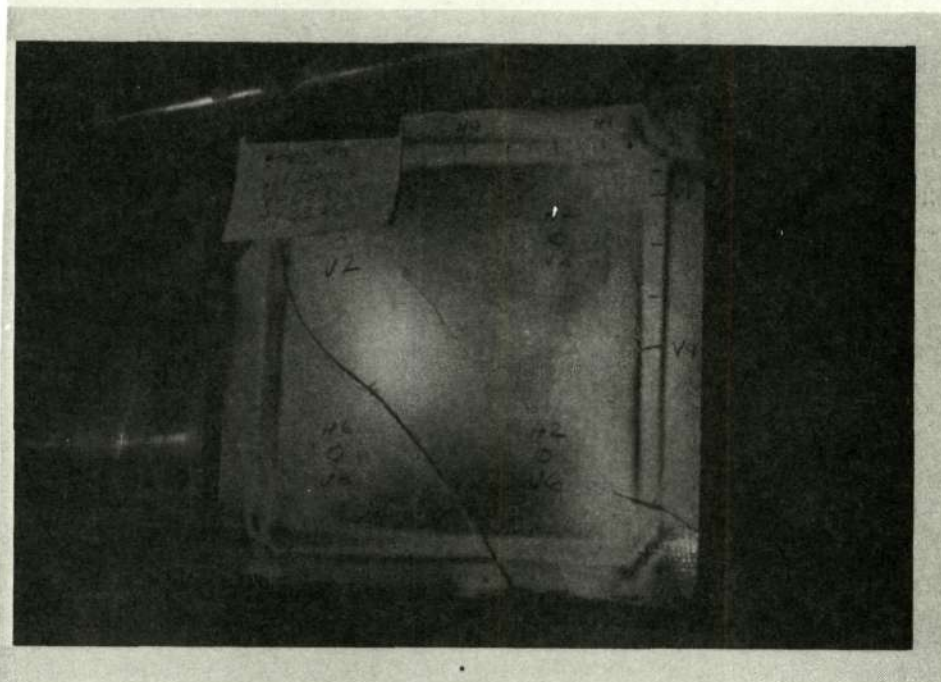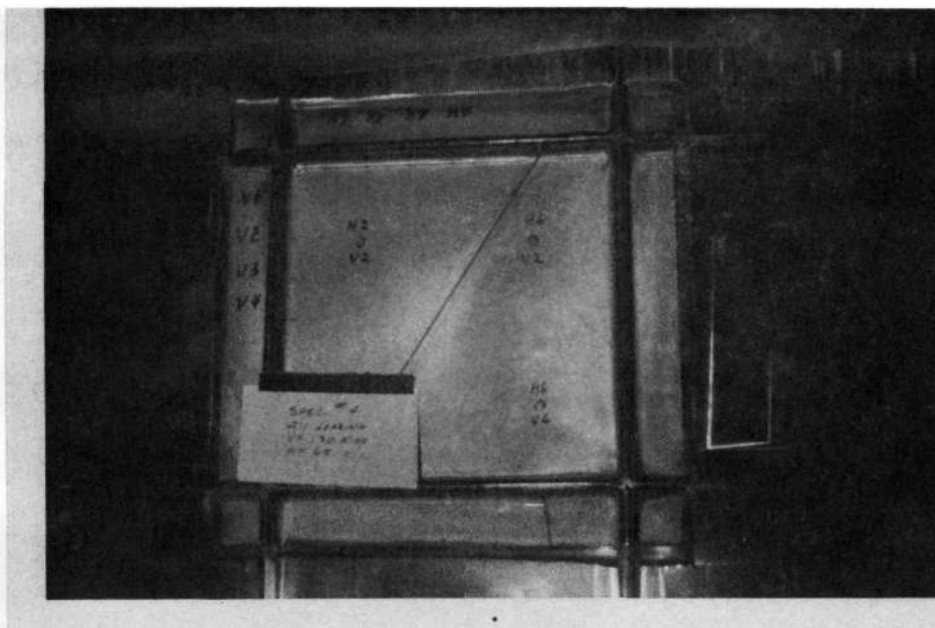

FIGURE 13B- PANEL 3 BIAXIAL LOAD (1:1)
REAR SURFACE
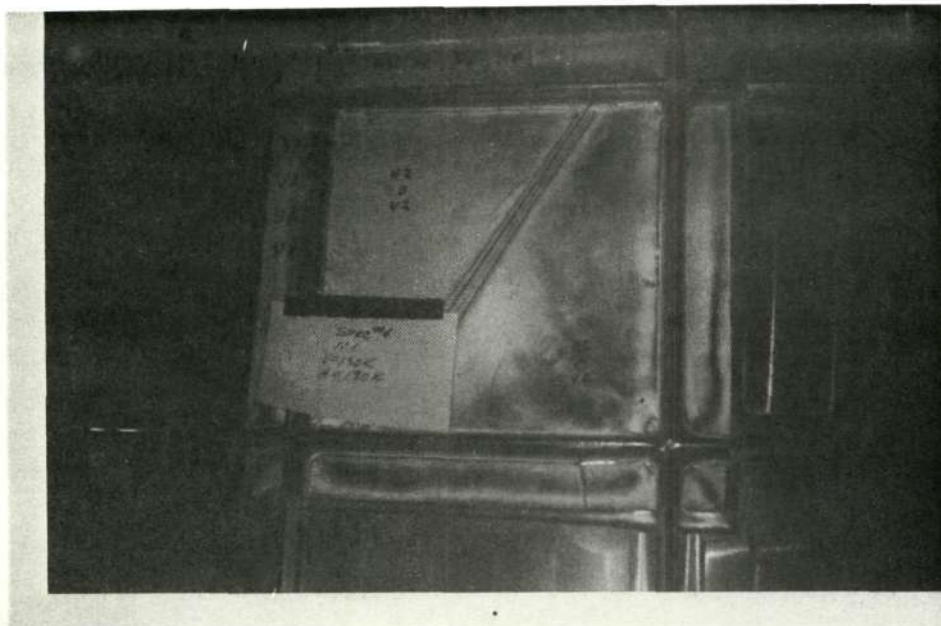
FIGURE 14A- PANEL 4 BIAXIAL LOAD (1:1)
FRONT SURFACE
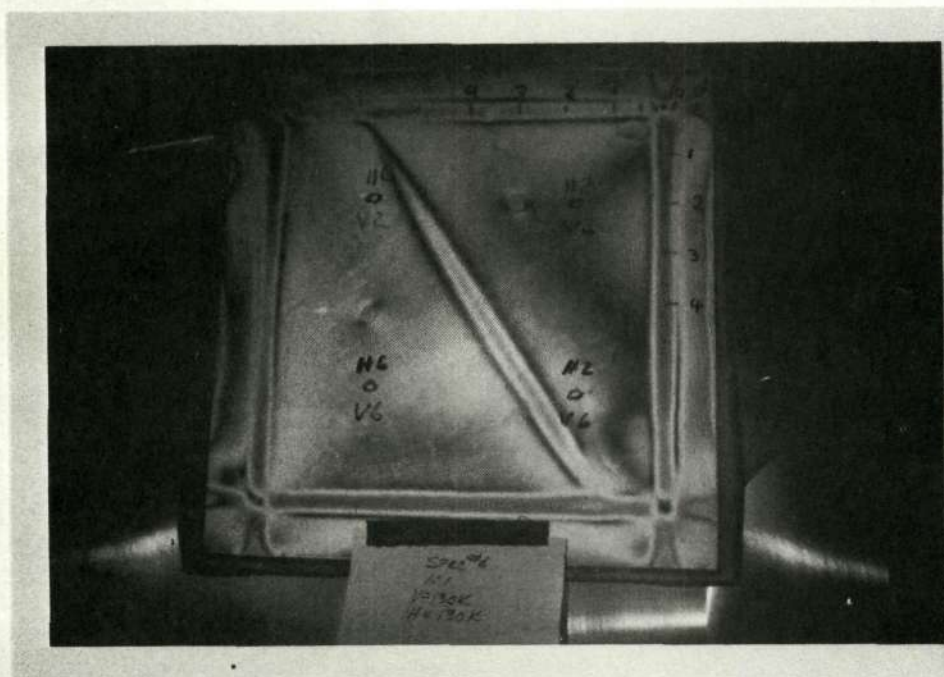
FIGURE 14B-PANEL 4 BIAXIAL LOAD (1:1)
REAR SURFACE
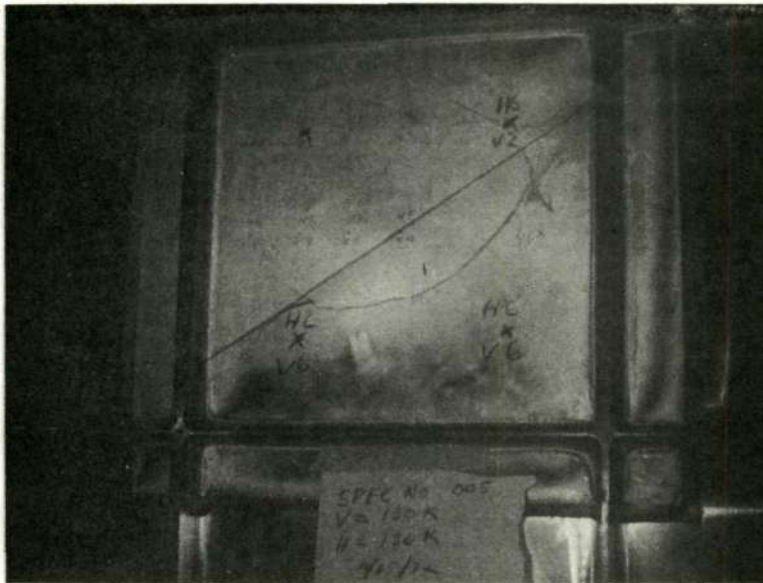
FIGURE 15A
PANEL 5
BIAXIAL LOAD (1:1)
FRONT SURFACE
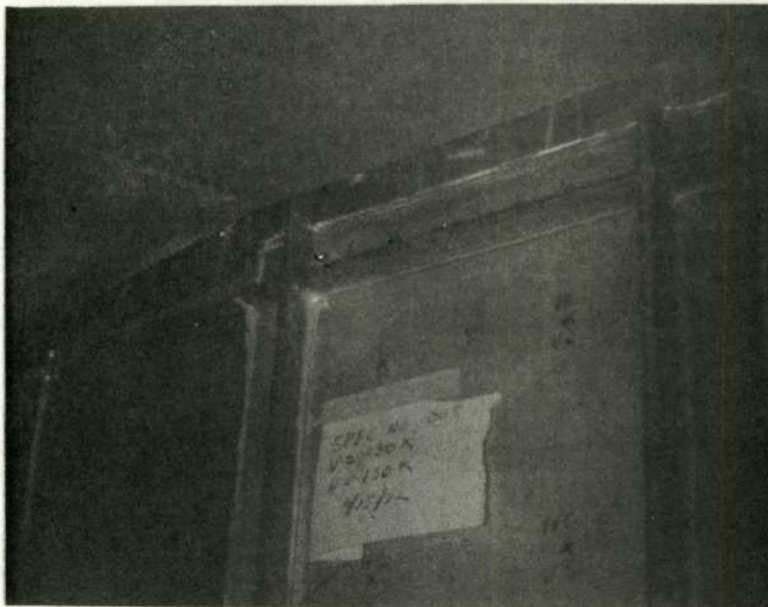
FIGURE 15B
PANEL 5
BIAXIAL LOAD (1:1)
CORNER VIEW
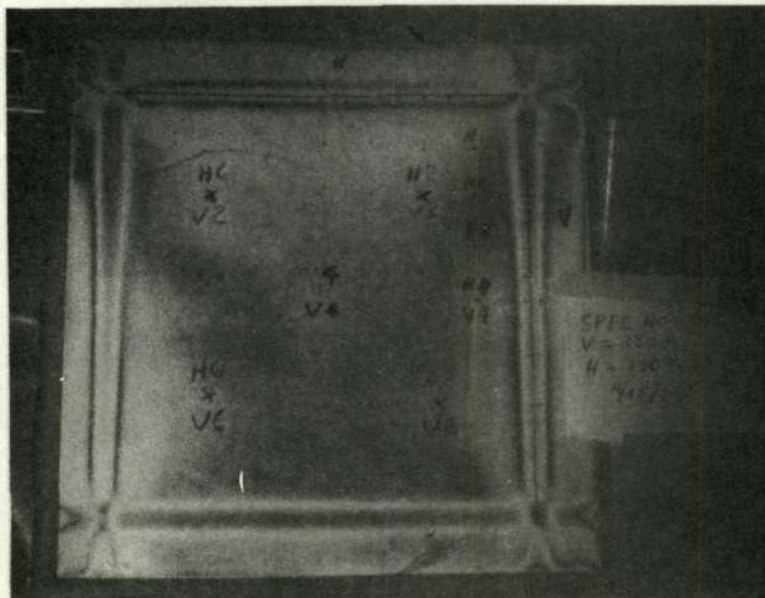
FIGURE 15C
PANEL 5
BIAXIAL LOAD (1:1)
REAR VIEW
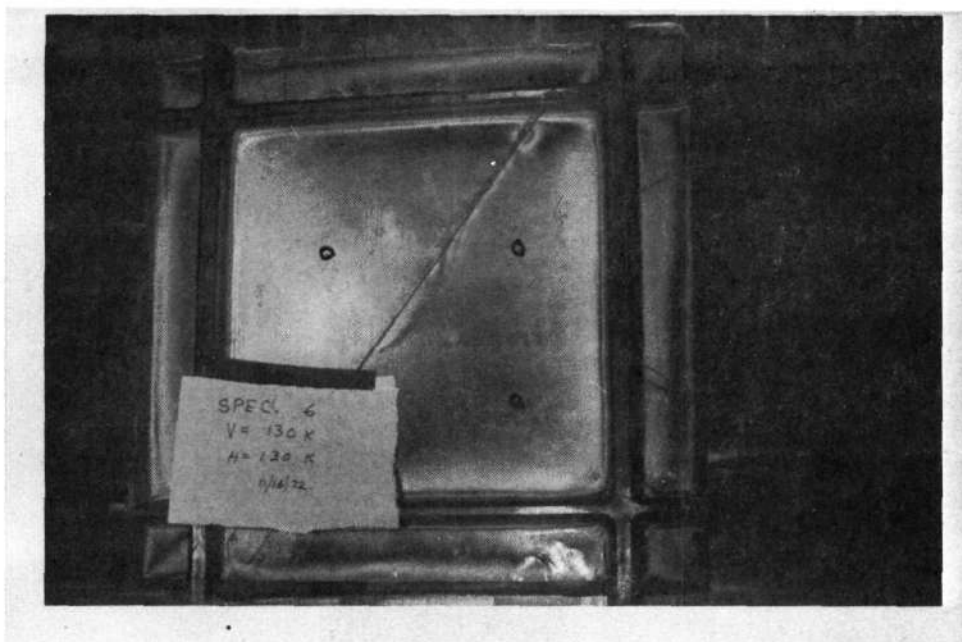
FIGURE 16A- PANEL 6 BIAXIAL LOAD (1:1)
FRONT SURFACE
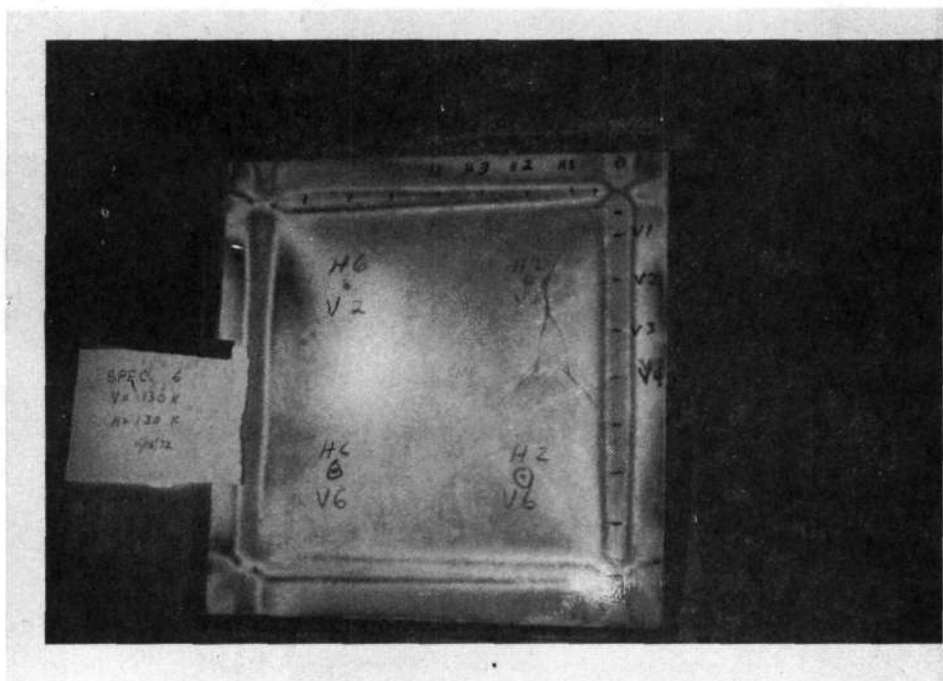
FIGURE 16B- PANEL 6 BIAXIAL LOAD (1:1)
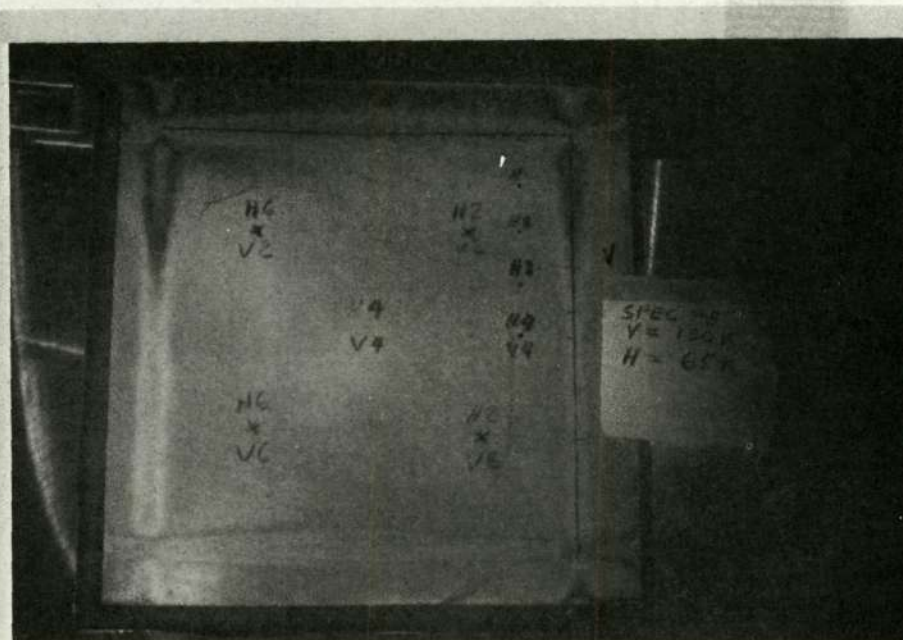REAR SURFACE
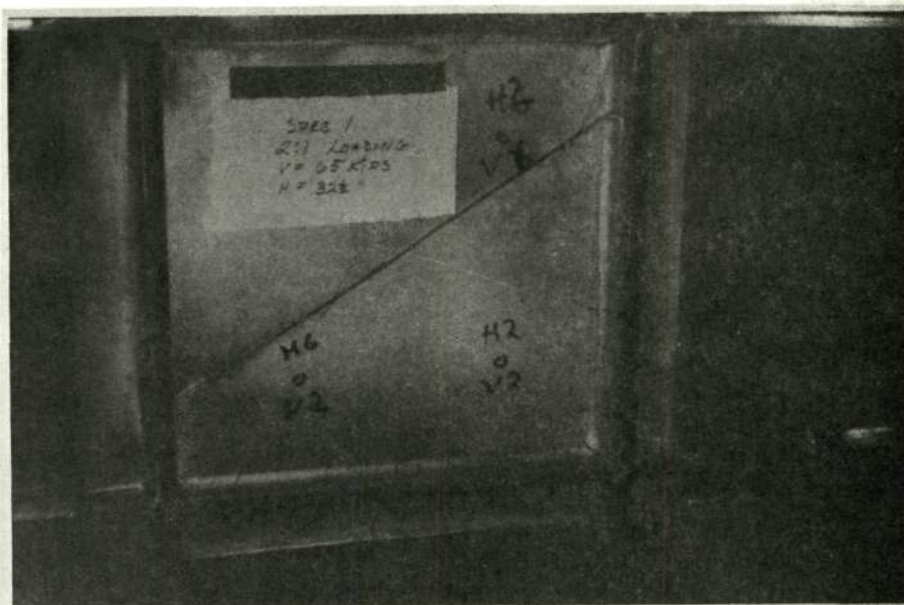
FIGURE 17A PANEL 1 BIAXIAL LOAD (2:1)
FRONT SURFACE

FIGURE 17B PANEL 1 BIAXIAL LOAD (2:1)
REAR SURFACE

FIGURE 18A- PANEL 2 BIAXIAL LOAD (2:1)
FRONT SURFACE

FIGURE 18B PANEL 2 BIAXIAL LOAD (2:1)
REAR SURFACE

FIGURE 19A PANEL 3 BIAXIAL LOAD (2:1)
FRONT SURFACE

FIGURE 19B- PANEL 3 BIAXIAL LOAD (2:1)
REAR SURFACE

FIGURE 20A- PANEL 4 BIAXIAL LOAD (2:1)
FRONT SURFACE

FIGURE 20B- PANEL 4 BIAXIAL LOAD (2:1)
REAR SURFACE

FIGURE 21A -PANEL 5 BIAXIAL LOAD (2:1)
FRONT SURFACE

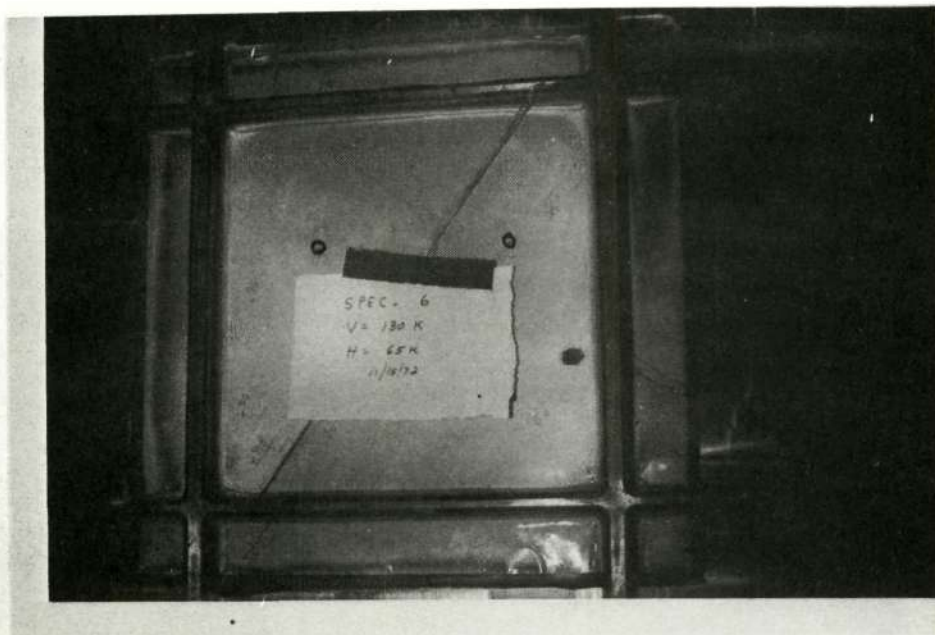FIGURE 21B- PANEL 5 BIAXIAL LOAD (2:1)
REAR SURFACE

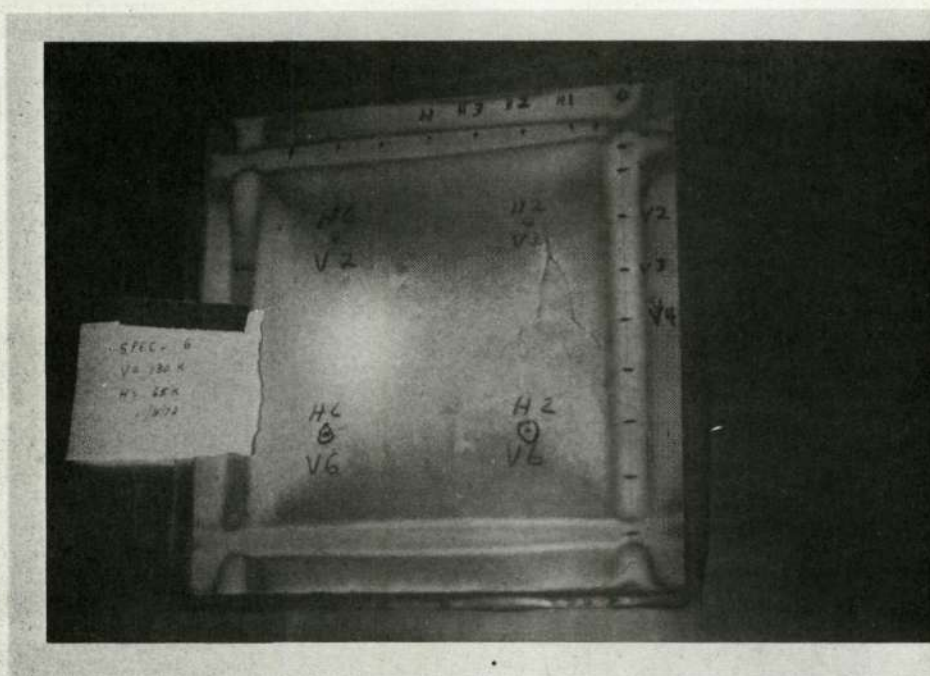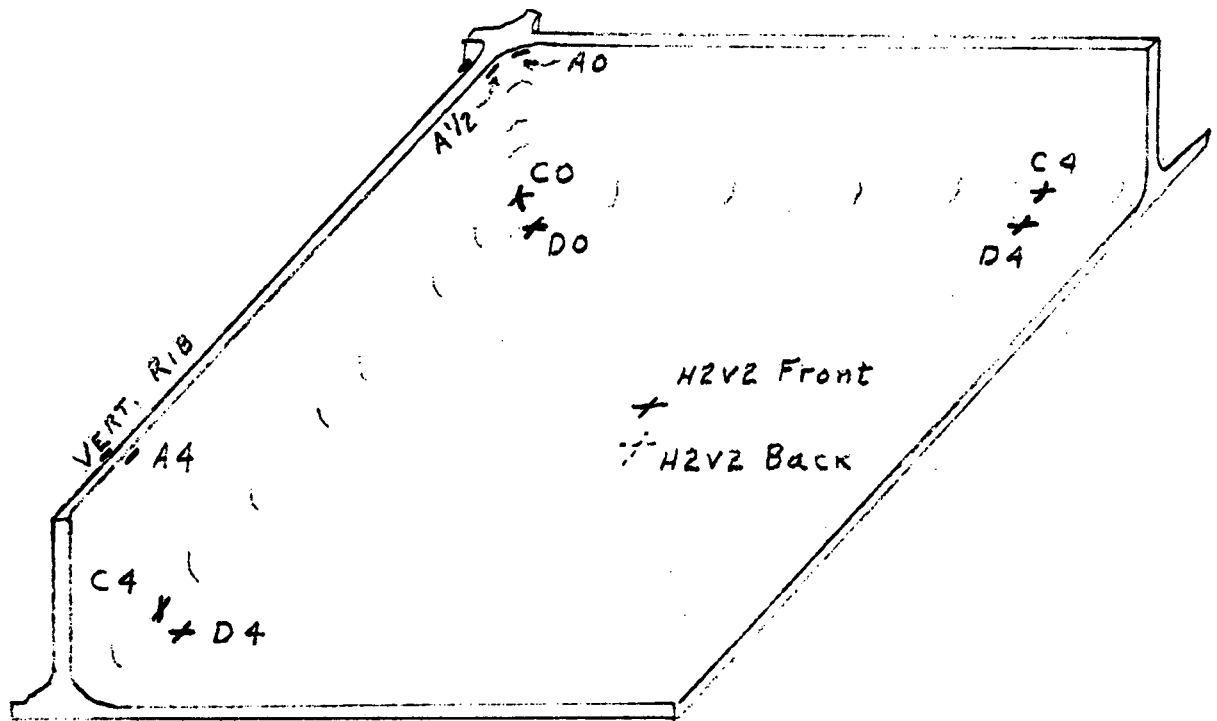FIGURE 22A-PANEL 6 BIAXIAL LOAD (2:1)
FRONT SURFACE

FIGURE 22B-PANEL 6 BIAXIAL LOAD (2:1)
REAR SURFACE

AO

A½

CO

DO

C4

D4

VERT. RIB

A4

H2V2 Front

H2V2 Back

C4

D4

VERT RIB		HORIZ. RIB	
C-4	2 GAGES	C-4	2 GAGES
D-4	"	D-4	"
C-0	"		
D-0	"		

FRONT FACE

A-½*	1 Gage
A-0	"
A-4*	"

FRONT FACE	
H2V2	2 GAGES

BACK FACE

BACK FACE	
HOVO	2 GAGES
H4V0	"
HOV4	"

*BOTH SIDES OF RIB

FIGURE 23 - STRAIN GAGE CHECK POINTS